PROGRESS IN RESEARCH

April 1, 2002 – March 31, 2003

Cyclotron Institute
Texas A&M University
College Station, Texas

TABLE OF CONTENTS

SECTION II: HEAVY ION REACTIONS

SECTION III: NUCLEAR THEORY

SECTION IV: ATOMIC AND MOLECULAR SCIENCE

SECTION V: SUPERCONDUCTING CYCLOTRON AND INSTRUMENTATION

SECTION VI: PUBLICATIONS

SECTION VII: APPENDIX

Introduction
April 1, 2002 - March 31, 2003

This document summarizes the progress in research and operations at the Texas A&M Cyclotron Institute for the period April, 1, 2002 through March 31, 2003. Sections I through IV contain reports from individual research projects. Operation and technical developments are given in Section V. Section VI lists the publications with Cyclotron Institute authors and the Appendix gives additional information including talks presented by members of the Institute during the past year. *Since most of the contributions presented here are truly reports on progress in research, results and conclusions should not be quoted from the report without the consent of the authors.*

In September, 2002, Professor J. Natowitz was appointed to the Cyclotron Institute Bright Chair in Nuclear Science. At that time, Joe indicated that he planned to step down as Director of the Institute by the end of December, 2002. During the past eleven years, Joe was instrumental in developing the scientific program at the Institute. All of us are indebted to him for the outstanding job that he did. Fortunately for us, he has returned to research with much enthusiasm. This Progress in Research is a result of Joe's effort.

With new leadership comes change. This volume of Progress in Research is the first one that will be available solely from our web site (http://cyclotron.tamu.edu). The format of the report also has changed. But the science accomplishments by Institute researchers are as impressive as in the past. Some of the recent achievements are noted here.

(1) First experiments have been carried out with BigSol.

(2) An improved understanding of the Deep Inelastic Transfer (DIT) process and its potential usefulness for producing neutron-rich rare beams is resulting from measurement of projectile fragmentation events detected by FAUST and heavy residues selected in MARS, where higher than expected cross sections for neutron-rich nuclides have been observed.

(3) Experimental and theoretical investigations of reactions of 26, 35 and 47 MeV/A ^{64}Zn projectiles with ^{58}Ni, ^{92}Mo and ^{197}Au provide evidence for a multi-fragmentation process in which a hot gas of nucleons and light clusters co-exists with relatively cold intermediate mass fragments.

(4) Nearly all of the isoscalar dipole resonance strength has been located in several heavy nuclei and the position of the compression-mode peak is in better agreement with calculations that use compressibilities obtained from giant monopole resonance positions.

(5) The first precision measurements have been completed in our program to sharpen the test of CKM unitarity via superallowed nuclear beta decay; these measurements utilized the recently completed "precision on-line decay facility", with which we can currently obtain half-lives accurate to 0.04% and beta branching ratios to 0.2%.

(6) A new way to relate direct stellar proton-capture reactions to cross-section measurements with stable beams has been proposed, which employs asymptotic normalization coefficients and charge symmetry; it was used to obtain the rate for ^{7}Be(p,γ)^{8}B from the ^{13}C(^{7}Li,^{8}Li)^{12}C reaction.

(7) Measurements of cross sections for electron loss by U^{28+} ions, in combination with n-body classical-trajectory Monte Carlo calculations, have been used to assess the vacuum requirements for the planned SIS ring at GSI-Darmstadt.

(8) Maximal fluctuations and apparent critical behavior in the disassembly of A ~ 36 nuclei have been found to occur at an excitation energy of 5.6 +- 0.5 MeV/u and a temperature of 8.3 +- 0.5 MeV.

(9) Coalescence of mini-jet partons with those from the quark-gluon plasma produced in relativistic heavy ion collisions is found to be important in understanding the enhanced production of antiprotons and the elliptic flow of various hadrons at intermediate transverse momenta.

Cyclotron Institute scientists remain active in a number of collaborative research efforts around the world. Major programs include: experiments at TRIUMF laboratory to measure heavy (A > 60) superallowed β decays and a measurement of Michel parameters in normal μ^+ decay; new mass measurements using the Canadian Penning Trap (CPT) at Argonne National Laboratory; and continued work with both the BRAHMS and STAR collaborations at RHIC. It is particularly noteworthy that Institute scientists played key roles in the analysis of the d-Au data from the last RHIC run which verified jet quenching in Au-Au collisions.

The K500 cyclotron continues to serve the broader community through testing of radiation effects on electronics components. This past year a bit over 20% of the scheduled accelerator time was devoted to single-event-upset testing. Both U.S. and foreign companies have utilized our facility this past year.

During the past year, two students have completed PhD's at the Institute. They are Tiegang Di and Changhui Li.

As in the previous years, the contributions of Cathy Heaslet and Y.-W. Lui have been invaluable in putting together this report.

R.E. Tribble
September 3, 2003

SECTION I

NUCLEAR STRUCTURE, FUNDAMENTAL INTERACTIONS, AND ASTROPHYSICS

Isoscalar giant dipole resonance for several nuclei with A ≥ 90

Y. –W. Lui, X. Chen, H. L. Clark, B. John,* Y. Tokimoto, D. H. Youngblood

Although evidence for the isoscalar giant dipole resonance (ISGDR) in ^{208}Pb has been reported by several groups [1-4], details of the ISGDR were not known until recent years [5,6]. In 2001, Clark *et al*. [5] reported that the isoscalar E1 strength distribution in ^{90}Zr, ^{116}Sn and ^{208}Pb consisted of two components, containing a total of more than 100% energy-weighted sum rule (EWSR). This discovery confirms the predictions from microscopic calculation that there are two components in E1 distribution, however, the large difference in the energy of the ISGDR between the experiment and theory was puzzling. The discrepancy found later [7] in the formula for the ISGDR transition density given by Harakeh and Dieprink [8] reduced the E1 EWSR strength located in those nuclei to ~ 40%. This suggests that there could be some missing E1 strength in the higher excitation region and a re-investigation of the E1 strength distribution with more sensitive data to the ISGDR angular distribution is necessary.

In these measurements, the horizontal and vertical acceptance of the spectrometer was set to minimize spurious scattering in the spectra and ray tracing was used to reconstruct the scattering angle. The focal plane detector contains two parts: the horizontal part covered approximately 50 MeV of excitation and measured position and angle θ in the scattering plane, and the vertical part measured the out-of-plane scattering angle ϕ [9]. The experimental technique has been described thoroughly in Ref. [10]. Sample spectra for ^{144}Sm at θ_{avg} = 0.4^o and 0.9^o are shown in Fig. 1. The giant resonance peak can be seen extending up past E_x=35 MeV with excellent peak to continuum ratio. The spectrum was divided into a peak and a continuum where the shape of the continuum was described in detail in Ref. [7]. The multipole decomposition analysis and the DWBA calculations were described in detail in Ref. [7,10].

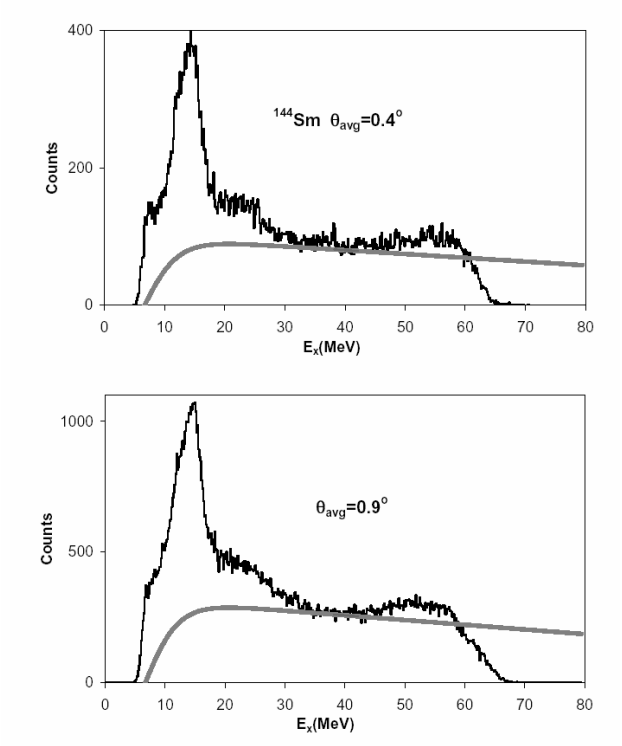

Figure 1. Inelastic alpha spectra for ^{144}Sm at θ_{avg} = 0.4^o and at 0.9^o. The solid lines show the continuum chosen for the analysis.

The E1 strength distributions obtained for ^{90}Zr, ^{144}Sm and ^{208}Pb are shown in Fig. 2. There are two components in each distribution, a broad component at E_x ~ 125MeV/$A^{1/3}$ containing approximately 70% of the E1 EWSR and a narrower component at E_x ~ 74MeV/$A^{1/3}$ containing 11 to 28% of the E1 EWSR. Two calculated Gaussian peaks are superimposed on each distribution. The estimated uncertainty in

each centroid is about 0.6 MeV. With the new data, the high energy component is much stronger than the low energy component and extends to higher excitation energy. The centroids of the high energy components are about 1 to 2 MeV higher than those given in Ref. [8].

The centroid energies for both components are compared to the calculated values of Colo *et al.* [20,23] in Table I. The centroids of the upper component are about 1 MeV less than the theoretical values in ^{208}Pb and ^{144}Sm and about 2.7 MeV lower than the predicted value in ^{90}Zr. The calculated centroids of the lower component locate 2-3 MeV below the experimental values in ^{208}Pb and ^{90}Zr and it is in good agreement with the experimental value in ^{144}Sm. The experimental E1 strength distributions were converted to ISGDR response functions and are shown with the calculation from Colo *et al.* for ^{144}Sm is shown in Fig. 3.

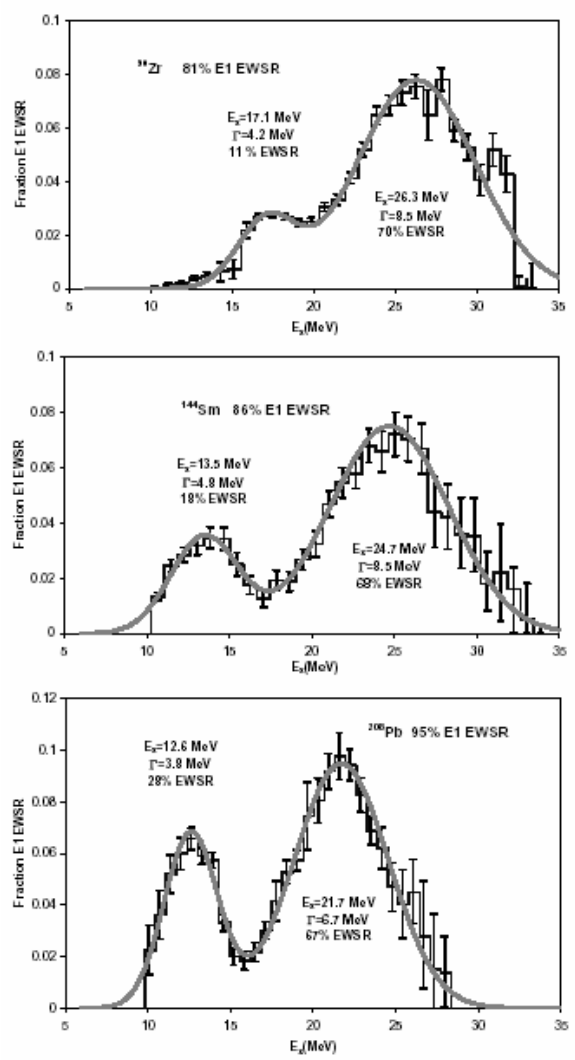

Figure 2. ISGDR strength distributions for ^{90}Zr, ^{144}Sm and ^{208}Pb are shown by the histogram. Error bars represent the uncertainty due to the fitting of the angular distributions. The solid lines are Gaussian peaks calculated with parameters labeled near the peak.

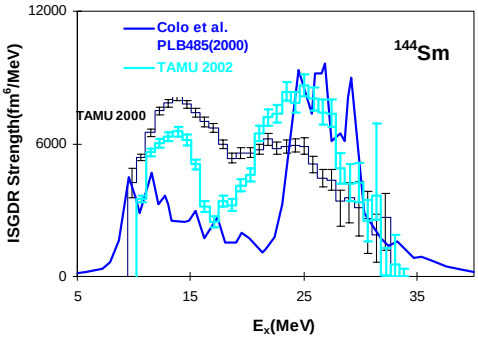

Figure 3. E1 response functions obtained from two different experiments, the dark color histogram is from experiment without measuring vertical angle and the light color histogram is from experiment with vertical angle information. The solid line is the calculation from Colo *et al.* [11].

The dark color data are from experiment without vertical angle information and the light blue data are from recent experiment with vertical angle information. The present results are in closer agreement with calculated values on the two components of the E1 distribution. However, the splitting of the ISGDR from the present data is still 3-5 MeV less than that predicated in calculations.

Table 1. Comparison of centroids to Colo *et al.*, [11, 12] calculations.

	Lower Component			Upper Component		
A	Exp. (MeV)	Colo *et al.* (MeV)	Diff. (MeV)	Exp. (MeV)	Colo *et al.* (MeV)	Diff. (MeV)
^{208}Pb	12.6	10.9	1.7	21.7	23.9 (22.9[a])	-1.8 (-0.8)
^{144}Sm	13.5	13.5	0.0	24.7	26.6 (25.6[a])	-1.9 (-0.9)
^{90}Zr	17.1	14.5	2.6	26.3	30.0 (29.0[a])	-3.7 (-2.7)

[a]Ref. 12

*Present address: Nuclear Physics Division, Bhabha Atomic Research Center, Mumbai-400085, India

References

[1] H. P. Morsch, M. Rogge, C. Mayer-Boricke, Phys. Rev. Lett. **45**, 337 (1980).
[2] H. P. Morsch *et al.*, Phys. Rev C **28**, 1947 (1983).
[3] G. S. Adams *et al.*, Phys. Rev. C **33**, 2054 (1986).
[4] B. F. Davis *et al.*, Phys. Rev. Lett. **79**, 609 (1997).
[5] H. L. Clark, Y. –W. Lui, D. H. Youngblood, Phys. Rev. C **63**, 031301 (2001).
[6] M. Uchida *et al.*, Phys. Lett. B **557**, 12 (2003).
[7] D. H. Youngblood, Y. –W. Lui, H. L. Clark, Phys. Rev. C **65**, 034302 (2002).
[8] M. N. Harakeh, A. E. L. Dieperink, Phys. Rev. C **23**, 2329 (1981).
[9] Y. –W. Lui, H. L. Clark, D. H. Youngblood, *Progress in Research*, Cyclotron Institute, Texas A&M University, (1999-2000), p. I-15.
[10] D. H. Youngblood, Y. –W. Lui, H. L. Clark, Phys. Rev. C **60**, 014304 (1999).
[11] G. Colo, N. Van Giai, P. F. Bortignon, M. R. Quaglia, Phys. Lett. B **485**, 362 (2000).
[12] G. Colo, private communication.

Giant Resonances in 46, 48Ti

Y. Tokimoto, B. John*, X. Chen, H. L. Clark, Y. –W. Lui and D. H. Youngblood

The study of the isoscalar giant monopole resonance (GMR) is important because its energy (E_{GMR}) is related to the compressibility of nuclear matter (K_{nm}) [1]. In the scaling model, the nuclear compressibility is described with $E_{GMR} = (m_3/m_1)^{1/2}$, where $m_k = \sum E_n^2 |\langle n|r^2|0\rangle|^2$ [1]. An investigation of the GMR in $^{46, 48}$Ti has been made to check the mass dependence of GMR energies in the mass region between ^{40}Ca [2] and ^{58}Ni [3].

The experimental technique and the detail of the method of the analysis have been described in Refs. [4, 5]. Elastic scattering from ^{46}Ti and ^{48}Ti were measured at spectrometer angles from 4° to 35° and 4° to 8°, respectively. Giant resonance data in ^{46}Ti was measured at 0° and 3.5° and that in ^{48}Ti at 0°, 4° and 6°. Uncertainties of the differential cross section including both statistical errors and systematic errors are approximately 10%.

Table 1 shows the potential parameters obtained for both targets. Both parameter sets successfully reproduced the angular distributions of the differential cross sections for the elastics and the first excited states for each target. The strength distributions of E0, E1 and E2 components are shown in Fig. 1. Energies and EWSR strengths of GMR for each target were listed in Table 2.

Table 1. Folding model parameters obtained from fits to elastic scattering.

	V (MeV)	VI (MeV)	RI (fm)	AI (fm)
^{46}Ti	44.187	29.656	4.871	0.859
^{48}Ti	33.699	32.913	4.920	0.862

Table 2. E_{GMR}s and strengths obtained for the distributions shown in Fig. 1 for the excitation energy up to 40 MeV.

		^{46}Ti	^{48}Ti
E_{GMR} (MeV)	E0	23.06+1.34/-0.44	22.75+1.03/-0.23
EWSR (%)	E0	80+16/-12	85+15/-12
	E1	12+11/-12	17±11
	E2	51±11	69±11

E0 Strengths in ^{46}Ti and ^{48}Ti are at 80+16/-12% and 85+15/-12% of E0 EWSR, respectively. In general E0 strengths in both nuclei are not affected very much by the choice of continuum, however, E1 strength distributions are found to be very sensitive to the choice of the continuum.

Figure 2 shows the mass dependence of E_{GMR} between ^{16}O and ^{208}Pb. $^{46, 48}$Ti and ^{58}Ni GMR energies follow ~ $80/A^{1/3}$ MeV trend with the heavier nuclei while the GMR in lighter nuclei falls well below this. Theoretical calculation using parameters for the Leptodermous expansion obtained by Nayak [6] agrees with the heavier nuclei and with ^{40}Ca, but are substantially below the $^{46, 48}$Ti and ^{58}Ni results.

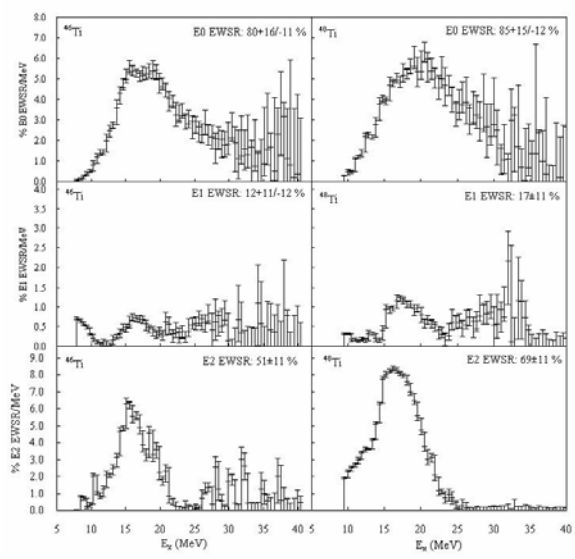

Figure 1. The solid lines show the fractions of the isoscalar EWSR obtained in present work for the multipolarities indicated. The error bars represent the uncertainty due to the fitting of the angular distributions.

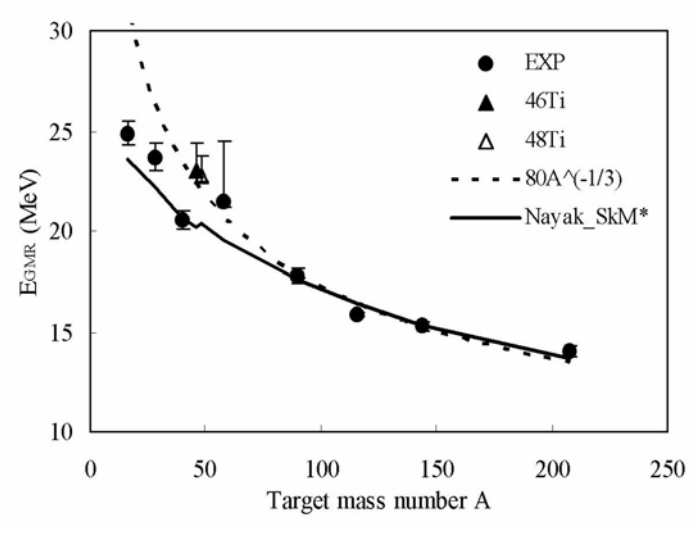

Figure 2. The target mass dependence of E_{GMR}. All experimental data points shown in the figure came from Texas A&M University group. The dotted line represents $E_{GMR} = 80A^{-1/3}$. The solid line shows a theoretical calculation with the SkM* interaction by Nayak [6].

*Present address: Nuclear Physics Division, Bhabha Atomic Research Center, Mumbai-400085, India.

References

[1] J. P. Blaizot, Phys. Rep. 64, 171 (1980).

[2] D. H. Youngblood, Y. –W. Lui, and H. L. Clark, Phys. Rev. C **63**, 067301 (2001).

[3] Y. –W. Lui, H. L. Clark, and D. H. Youngblood, Phys. Rev. C **61**, 067307 (2000).

[4] D. H. Youngblood, Y. –W. Lui, and H. L. Clark, Phys. Rev. C **60**, 014304 (1999).

[5] D. H. Youngblood, Y. –W. Lui, and H. L. Clark, Phys. Rev. C **65**, 034302 (2002).

[6] R. C. Nayak, J. M. Pearson, M. Farine, P. Gleissl, and M. Brack, Nucl. Phys. **A516**, 62 (1990).

Determination of the direct capture contribution for ^{13}N(p,γ)^{14}O from the ^{14}O →^{13}N + p asymptotic normalization coefficient

X. Tang, A. Azhari, C. Fu, C. A. Gagliardi, A. M. Mukhamedzhanov, F. Pirlepesov, L. Trache, R. E. Tribble, V. Burjan[1], V. Kroha[1] and F. Carstoiu[2]

[1]*Insitute of Nuclear Physics, Czech Academy of Sciences, Prague-Rez, Czech Republic*

[2]*Institute of Physics and Nuclear Engineering, H. Hulubei, Bucharest, Romania*

The hot CNO cycle is the main energy source for novae. A rapid change of the temperature dependent energy generation rate occurs when the CNO cycle transits from the cold to hot cycle. ^{13}N(p,γ)^{14}O is one of the important reactions which controls this transition [1]. For T_9=0.2, the Gamow window for this reaction is located at 148 keV with a width of 117 keV, where this reaction is dominated by the low energy tail of the s-wave capture on the broad 1^- resonance (E_r=0.529 MeV, total width of 37.3±0.9 keV) [2]. Within the Gamow window the direct capture is significantly smaller than the resonance contribution. But the interference between these two components will enhance or reduce the tail of the resonance dramatically. We have used a peripheral transfer reaction, ^{14}N(^{13}N,^{14}O)^{13}C at 11.8 MeV/nucleon, to study the direct capture process via the asymptotic normalization coefficient (ANC) technique.

The ^{13}N radioactive beam was produced via the inverse kinematics reaction ^{1}H(^{13}C,^{13}N)n, using ~600 enA of 15 MeV/nucleon ^{13}C from the K500 superconducting cyclotron bombarding a 10-cm long, LN_2-cooled H_2 gas cell with 12.7 μm Havar windows. ^{13}N recoils at 11.8 MeV/nucleon were collected and separated by MARS at 0º. Two secondary reaction targets, 1.50 mg/cm^2 melamine ($C_3H_6N_6$) and 1.90 mg/cm^2 C, were used. The reaction products were detected in two Si telescopes covering 4°-19° and the beam was counted by a scintillation detector at 0° [3]. Reaction channels were identified using the particle identification (PID) vs. Q value spectrum.

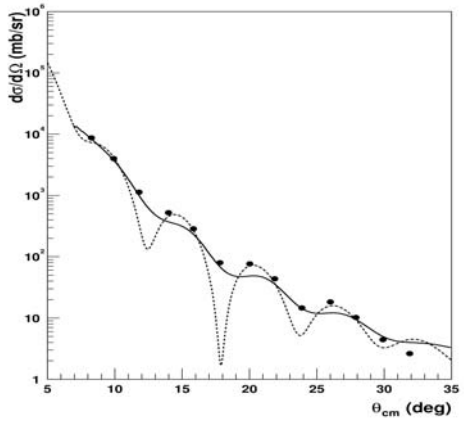

Figure 1. The elastic scattering angular distribution for ^{13}N on melamine. The experimental result is shown as dots with statistical uncertainties only. The dashed curve is the summed prediction for ^{13}N elastic scattering off C and N in the melamine target. The solid curve is the smeared result of the prediction.

The cross section for the elastic scattering of ^{13}N on melamine target is shown in Fig. 1 together with the optical model prediction. Since we cannot distinguish ^{13}N+^{12}C elastic scattering from ^{13}N+^{14}N, the predicted elastic angular distribution shown is the sum of the two elastic scattering channels in the target according to their atomic ratio. The prediction for ^{13}N+^{12}C elastic scattering was checked with the ^{12}C target.

The angular distribution for the proton transfer reaction ^{14}N(^{13}N,^{14}O)^{13}C$_{g.s.}$ is shown in Fig. 2 together with DWBA calculation. By normalizing the smeared prediction to the experimental data, the value of the ANC for ^{14}O→^{13}N + p was found to be $C^2_{1/2} = 29\, fm^{-1}$. The evaluation of the uncertainty is in progress. With the new ANCs, the S factor for ^{13}N(p,γ)^{14}O will be updated.

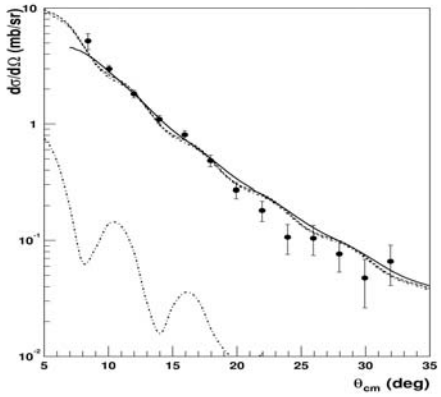

Figure 2. Transfer reaction angular distributions for $^{14}N(^{13}N,^{14}O)^{13}C$g.s. The dashed curve is the DWBA prediction. The solid curve is smeared prediction. The two dash-dotted curves show the two separate contributions to the proton transfer reaction (top to bottom): $p_{1/2} \rightarrow p_{1/2}$ and $p_{3/2} \rightarrow p_{1/2}$.

References:

[1] M. Wiescher, J. Gorres and H Schatz, J. Phys. G **25**, R133 (1999).

[2] P. V. Magnus, E. G. Adelberger and A. Garcia, Phys. Rev. C **49**, R1755 (1994).

[3] X. Tang *et al.*, Phys. Rev. C **67**, 015804 (1994).

Breakup of loosely bound nuclei at intermediate energies as indirect method in nuclear astrophysics: ^{8}B and the S_{17} astrophysical factor

F. Carstoiu[1], L. Trache, C. A. Gagliardi, and R. E. Tribble

[1]*Institute of Physics and Nuclear Engineering Horia Hulubei, Bucharest, Romania*

Recent results from the SuperK and SNO collaborations provide strong evidence for neutrino oscillations. A precise determination of the number of neutrinos produced in the Sun is crucial now to select between the various explanations proposed. The major source of high energy neutrinos observed by solar neutrino detectors is ^{8}B, produced in the ^{7}Be(p,γ)^{8}B reaction. But, in spite of much work in the past and a flurry of recent results of direct and indirect determinations of the astrophysical factor $S_{17}(0)$, there is no full agreement on a value. In the previous year we proposed the use of one-nucleon breakup reactions of loosely bound nuclei at intermediate energies as an indirect method in nuclear astrophysics [1] via ANC method. We found S_{17}= 17.4±1.5 eVb using data from the breakup of ^{8}B at energies between 28 and 285 MeV/u on targets from C to Pb and extended Glauber model calculations with one effective interaction (JLM). Like for all indirect methods, the precision of this one is subject not only to the experimental uncertainties, but also to the uncertainties in the calculations used. In order to check further the reliability of this method, we extended and improved the calculations. We improved the Glauber model. Final state interaction has been included in the Coulomb dissociation component. More experimental data were considered, for energies from 30 to 1000 MeV/u on light through heavy targets. The predictions of the model are in excellent agreement with independent reaction data (reaction cross sections and parallel momentum distributions for core like fragments). We show that there exists a favorable kinematical window (30 to 150 MeV/u) in which breakup reactions are highly peripheral and dominated by the external part of the wave function and that in this regime it is better to extract the ANC than a spectroscopic factor. For energies above 50 MeV/u Glauber model calculations in the eikonal approximation and the optical limit using different effective interactions were made. They give consistent, though slightly different results. These results are summarized in Fig. 1.

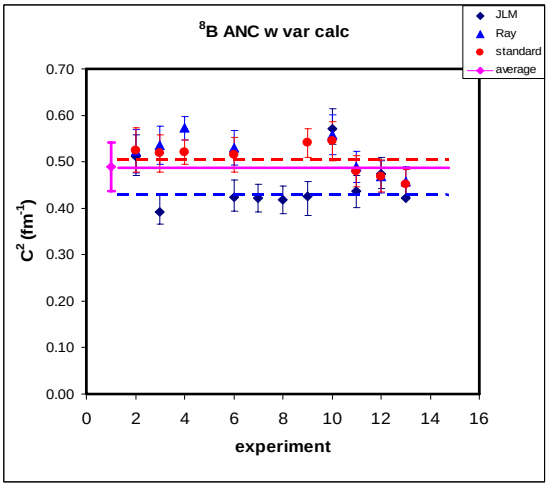

Figure 1. Summary of ANC results: The calculations with 3 different effective nucleon-nucleon interactions are shown: JLM (diamonds), standard μ=1.5 fm (red circles) and Ray (blue triangles). Data are from Blank *et al.*, Nucl. Phys. **A624** (1997), Negoita *et al.*, Phys. Rev. C **54** (1996) and Cortina-Gil *et al.*, Eur. Phys. J. A **10** (2001).

We can see that for one effective interaction, we obtain the same ANC from all experimental data considered, but the average

values depend slightly on the interaction used. The spreading of these average values gives a reasonable account of the precision we can expect from this method. The ^{8}B ANC extracted, lead to the astrophysical factor $S_{17}(0)$=17.4±1.5 eV·b when using the JLM interaction, $S_{17}(0)$=19.6±1.2 eV·b for the standard finite range interaction [2], $S_{17}(0)$=20.0±1.6 eV·b for the interaction of Ray [3] and $S_{17}(0)$=20.7±2.2 eV·b for the Franey-Love interaction [4]. The overall average obtained is $S_{17}(0)$=18.9±2.0 eV·b. This is in very good agreement with the latest values obtained from averaging all direct and indirect measurements [5,6] and new energy dependence for the radiative capture.

References

[1] L. Trache *et al.*, Phys. Rev. Lett. **87**, 271102 (2001).

[2] G. F. Bertsch, B. A. Brown and H. Sagawa, Phys. Rev. C **39**, 1154 (2001).

[3] L. Ray, Phys. Rev. C **20**, 1857 (1979).

[4] W. G. Love and M. A. Franey, Phys. Rev. C **24**, 1073 (1981); *ibid*. **31**, 488 (1988).

[5] F. Schumann *et al*., nucl-ex/0304011.

[6] B. Davids and S. Typel, nucl-th/03040.

Elastic Scattering of ^{8}B on ^{12}C and ^{14}N

A. Azhari, V. Burjan[1], F. Carstoiu[2], C. A. Gagliardi, X. Tang, L. Trache, R. E. Tribble
[1]*Insitute of Nuclear Physics, Czech Academy of Sciences, Prague-Rez, Czech Republic*
[2]*Institute of Physics and Nuclear Engineering Horia Hulubei, Bucharest, Romania*

As part of an ongoing program to better determine the astrophysical factor $S_{17}(0)$ [1,2], we studied the elastic scattering reaction of ^{8}B on ^{14}N. This is needed to check the optical potential used in the outgoing channel of the DWBA calculations for the reaction ^{14}N(^{7}Be,^{8}B)^{13}C [2]. The experiment was performed at the Cyclotron Institute where a primary beam of 27 MeV/A ^{10}B impinged upon a cryogenic Hydrogen gas target to produce the radioactive beam of ^{8}B at 11.8 MeV/n. The radioactive beam was separated using the Momentum Achromat Recoil Spectrometer (MARS) resulting in better than 95% purity and 8000 part/sec.

A 1.9 mg/cm^2 Melamine target and a 3.3 mg/cm^2 ^{12}C target were placed at the focal plane of MARS, as secondary targets. Particle detection was achieved using Silicon detector telescopes; each consisting of a 16 strip position sensitive ΔE Silicon detector backed by a thick Silicon detector to stop the particles. This allowed us to measure position and ΔE-E information for incoming particles, allowing for particle identification and kinematic reconstruction for each event.

A complete Monte-Carlo simulation of the experimental setup was used to obtain the experimental solid angles used to determine the differential cross sections for the elastic scattering of ^{8}B on Melamine and ^{12}C. Subtracting the contribution of ^{12}C from the Melamine target allowed us to obtain the differential cross section for the elastic scattering of ^{8}B on ^{14}N, shown in Fig. 1.

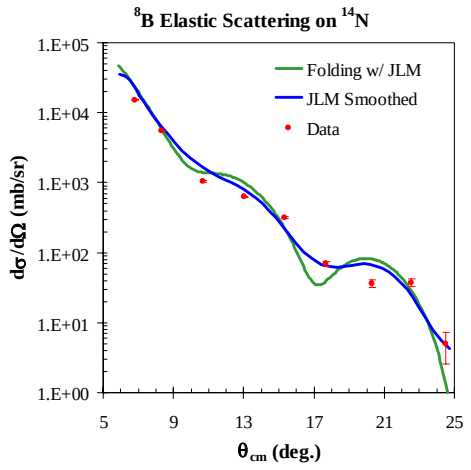

Figure 1. Comparison of theoretical angular distribution (solid lines) to data (points).

Double folded potentials using the JLM effective interaction and the procedure of ref. [3] were used to calculate theoretical cross sections. These were smoothed with experimental resolutions and are compared, not fitted, to the data in Fig. 1. The high degree of agreement between data and prediction indicates that our method for obtaining the theoretical distributions works well for these types of reactions.

References

[1] A. Azhari *et al.*, Phys. Rev. Lett. **82**, 1149 (1999).
[2] A. Azhari *et al.*, Phys. Rev. C **60**, 055803 (1999).
[3] L. Trache *et al.*, Phys. Rev. C **61**, 024612 (2000).

Study of ^{8}Li and the astrophysical $S_{17}(0)$ factor

L. Trache, A. Azhari, F. Carstoiu[1], H. L. Clark, C. A. Gagliardi, Y.-W. Lui, A. M. Mukhamedzhanov, X. D. Tang, N. Timofeyuk[2] and R.E. Tribble

[1]*Institute of Physics and Nuclear Engineering Horia Hulubei, Bucharest, Romania*

[2]*Department of Physics, University of Surrey, Guildford, Surrey, England, UK*

In the framework of our nuclear astrophysics program we extended our search for the astrophysical S-factor for the reaction ^{7}Be(p,γ)^{8}B – the main source of solar neutrinos - using indirect methods [1,2] with a new approach. Asymptotic normalization coefficients (ANCs) for ^{8}Li → ^{7}Li + n have been extracted from the neutron transfer reaction ^{13}C(^{7}Li,^{8}Li)^{12}C at 63 MeV. The experiment was carried out earlier using the MDM spectrometer and was described in [3]. This year we determined the absolute normalization of the ANCs extracted, extended the DWBA analysis and were able to relate the information about the structure of ^{8}Li to that of ^{8}B, and from there to S_{17}. Also we were able to separate the $p_{3/2}$ and $p_{1/2}$ components in the wave function of the g.s. and of the first excited state of ^{8}Li. The ANCs of the former were related to the ANCs in ^{8}B → ^{7}Be + p using charge symmetry, and from there to S_{17}. We studied, through extended DWBA calculations using 11 combinations of optical model potentials in the incoming/outgoing channels (including phenomenological Woods-Saxon and double folded potentials), the peripheral nature of the neutron transfer reaction and the uncertainties we expect due to calculations. We found for ^{8}Li g.s. the ANCs $C^2_{p3/2} = 0.384 \pm 0.038$ fm^{-1} and $C^2_{p1/2} = 0.048 \pm 0.006$ fm^{-1} for the two components. It was first suggested in Ref. [4] that the ANCs in ^{8}Li and ^{8}B could be connected. For mirror nuclei it is usually accepted that their spectroscopic factors are very similar, a statement supported by all microscopic calculations referring specifically to the ^{8}Li and ^{8}B case (see 10 references quoted in [5]). Using this equality and the relation between ANCs, spectroscopic factors and the single particle ANCs $C^2_{nlj} = S_{nlj} b^2_{nlj}$ [6], we find the ANCs for the g.s. of ^{8}B: $C^2_{p3/2}(^8B) = 0.405 \pm 0.041$ fm^{-1} and $C^2_{p1/2}(^8B) = 0.050 \pm 0.006$ fm^{-1}. They are in very good agreement with those extracted from the "mirror" proton transfer reaction (^{7}Be,^{8}B) on ^{10}B and ^{14}N targets [1] and using data from breakup experiments [2].

We find the astrophysical factor for the ^{7}Be(p,γ)^{8}B reaction to be $S_{17}(0)$=17.6±1.7 eV b. This is the first time that the rate of a direct capture reaction of astrophysical interest has been determined through a measurement of the ANCs in the mirror system. The method will be extended to other systems in the future.

References

[1] A. Azhari *et al*., Phys. Rev. C **63**, 055803 (2001).

[2] L. Trache *et al*., Phys. Rev. Lett. **97**, 271102 (2001).

[3] L. Trache *et al*., *Progress in Research*, Cyclotron Institute Texas A&M University (1999-2000), p. I-6.

[4] N. Timofeyuk, Nucl. Phys. **A632**, 19 (1998).

[5] L. Trache *et al*., submitted to Phys. Rev. C.

[6] A. M. Mukhamedzhanov *et al*., Phys. Rev. C **56**, 1302 (1997).

Remeasurement of $^{14}N+^{7}Be$ for the astrophysical $S_{17}(0)$ factor

G. Tabacaru, A. Azhari, J. Brinkley, V. Burjan[1], C. Fu, C. A. Gagliardi, X. Tang, L. Trache, R. E. Tribble
[1]*Insitute of Nuclear Physics, Czech Academy of Sciences, Prague-Rez, Czech Republic*

The first experiment where we have used the new detector assembly described in detail in reference [1] was performed to check the asymptotic normalization coefficient (ANC) for the $^{7}Be+p \rightarrow ^{8}B$ using the transfer reaction $^{14}N(^{7}Be,^{8}B)^{13}C$. Two improvements were made to our earlier experiment [2]: a better monitoring of the secondary beam intensity and extension of the angular range for the detection of the products from elastic scattering and transfer reaction. In the earlier experiment, monitoring of the beam intensity was done by measuring the primary beam intensities with a Faraday cup (FC) placed in the Momentum Achromat Recoil Spectrometer's (MARS) coffin. In experiments following [2], a drop of isotope production rate per nA beam current was observed when the intensity of the beam was increased, presumably due to a "tunneling" effect in the gas target. We suspected that this problem had an influence on the results obtained in [2]. The new beam monitoring system [1] consisted of a screen to reduce the ^{7}Be beam intensity by 88% and a scintillator coupled with a photo-multiplier. The advantage of this system is the direct counting of the beam secondary particles at the back of MARS.

The primary beam used was ^{7}Li at 18.6 MeV/A from the K500 cyclotron. The beam was transported to the H_2 liquid nitrogen cooled primary target at the MARS target chamber. The pressure of the H_2 in the cooled cell was 2.0 atm and the cooling of the cell was done with an LN_2 Dewar refilled automatically by means of a valve - filling sensor system. Vertical and horizontal slits were used in order to remove any impurities and to define the emittance of the secondary ^{7}Be beam. Details of the ^{7}Be beam production can be found in reference [2]. The final energy of the radioactive ^{7}Be beam was 12.6 MeV/A with intensities ≅150 - 200 kHz.

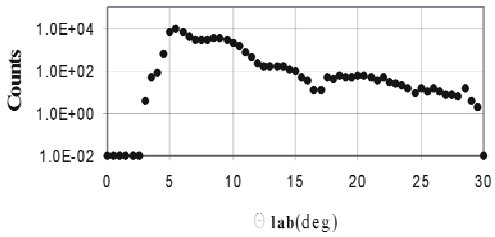

Figure 1. Experimental angular distribution (preliminary results) for the reaction $^{14}N(^{7}Be,^{7}Be)^{14}N$.

The position and spot size of the ^{7}Be beam were adjusted using a 900 mm position sensitive Si detector which was then removed and replaced by the secondary target 1.5 mg/cm^2 melamine. ^{7}Be elastic scattered events were detected by the new detector assembly. One of the most important results of this experiment is presented in Fig. 1, the extended angular distribution for the reaction $^{14}N(^{7}Be,^{7}Be)^{14}N$. We observe that we cover nearly four maxima which will be very important for future data analysis in order to obtain better agreement between the theoretical calculations and experimental data since elastic scattering provides a better check of the optical model potentials used for the calculation of the transfer reaction cross section.

References

[1] G. Tabacaru *et al.*, present *Progress in Research*, Cyclotron Institute, Texas A&M University (2002-2003) p. V-8.
[2] A. Azhari *et al.*, Phys. Rev. C **63**, 055803 (2001).

The Physics of STAR at RHIC

C. A. Gagliardi, T. W. Henry, R. E. Tribble, M. A. Vasiliev, and the STAR Collaboration

The role that our group is playing within the STAR Collaboration at RHIC has grown during the past year. In last year's progress report, we described the group activities within the STAR spin physics program and in construction of the STAR Endcap Electromagnetic Calorimeter (EEMC). Our work on STAR spin and the EEMC have continued this past year. But we have also become quite active within the STAR high-p_T physics program, and last December, one of us (CAG) was named co-convenor of the STAR High-p_T Physics Working Group, together with P. Jacobs of LBL. Below we give brief status reports on our efforts.

This past year the STAR spin program has focused on analysis of the data that were taken during the 2001-02 RHIC polarized proton run and on preparations for the '03 polarized proton run that is just beginning now. The ultimate goal of the STAR spin program is a determination of the polarization of the gluons within the proton as a function of Bjorken-x, through measurements of the longitudinal analyzing power A_{LL} for $p+p \rightarrow \gamma$ + jet. At the partonic level, this process is dominated by quark-gluon Compton scattering and has a large and well understood analyzing power. During the upcoming polarized proton run, we plan to get a first look at the gluon polarization through measurements of A_{LL} for inclusive jet and di-jet production. Over the past year, members of our group, in conjunction primarily with M. Miller of Yale University, have been active in the development of jet-finding algorithms for STAR. STAR now has several different algorithms available to reconstruct charged jets from the tracks that are seen in the TPC, each with its own characteristic strengths and biases. We have also developed tools to compare their performance event-by-event. The codes have already been used to analyze the existing '01-'02 *pp* data, and they are being used now to search for jets in the *d*+Au data that have just been taken. At present, we are working to integrate the neutral particle information from the STAR Barrel Electromagnetic Calorimeter (BEMC) into the jet finders. The jet codes will play a central role in the STAR gluon polarization studies over the next few years.

At present, the STAR high-p_T program is using observations of high-p_T hadron production and correlations in Au+Au, *p*+*p*, and *d*+Au collisions to search for evidence of jet quenching in relativistic heavy-ion collisions and to investigate changes in the gluon distribution of heavy nuclei relative to that in nucleons. This past year, STAR reported evidence for strong suppression of high-p_T inclusive hadron production and large azimuthal anisotropies in the production of high-p_T hadrons in Au+Au collisions at 130 GeV, for jet-like correlations of high-p_T hadrons at small relative angles in Au+Au collisions at 130 and 200 GeV, and for the disappearance of back-to-back high-p_T hadron pairs in Au+Au collisions at 200 GeV. All of these phenomena are consistent with the existence of large partonic energy loss in the hot, dense medium produced at RHIC. However, they can also be explained by an alternative model that attributes the effects to initial-state modifications of the gluon distribution in the Au nuclei due to saturation. The RHIC *d*+Au run which has just completed was intended to determine whether the striking phenomena that have been observed at high-p_T in Au+Au collisions are due to initial-state effects in the Au nuclei, final-state energy loss, or a combination of the two. STAR recorded over 30 million minimum-bias *d*+Au collisions during the run, together with over 1 million events triggered on the

presence of large (>2.5 or >4.5 GeV) energy deposition in a single BEMC tower. The minimum-bias data are being analyzed to determine the inclusive hadron production rate and to study di-hadron correlations. The results will be compared to the existing data from *pp* and Au+Au collisions.

Our group has also continued to work on the construction of the EEMC. At present, 1/3 of the EEMC is installed within STAR for use during the upcoming polarized proton run, and all of the towers within that third are instrumented. Construction has also continued for the rest of the detector. The remainder of the detector hardware will be installed during the RHIC shutdown this coming summer and fall. All of the PMTs for the detector and slightly under half of the multi-anode PMTs (MAPMTs), together with their associated electronics, will also be installed. The remainder of the MAPMTs will need to wait until the '04 RHIC shutdown due to budgetary constraints. We are responsible for the construction of the magnetic shielding boxes that house the PMTs and MAPMTs on the back of the west STAR pole tip. Approximately 70% of the PMT boxes for the entire EEMC have been completed, and the rest will be done within the next three months. This past year, we also built a prototype box to house the MAPMTs. It was tested at IUCF and found to meet the required specifications. However, construction of the MAPMT boxes has been delayed by changes in the front-end electronics cards that will be housed in the boxes with the MAPMTs. The IUCF group has only now provided us with the final modifications required to mount the electronics. Construction of the MAPMT boxes will begin shortly.

Finally, our group has carried a number of administrative responsibilities outside of the spin and high-p_T areas over the past year. These have included participation on god-parent committees for papers from the ultra-peripheral collisions and strangeness physics working groups and chairing the god-parent committee for a paper from the event structure physics working group. One of us is also a member of the STAR Trigger Board for the current RHIC run and was a member of the internal STAR committee to review the proposal for a multi-gap resistive plate chamber time-of-flight detector to provide STAR with large-acceptance particle identification capabilities. The TOF proposal has now been approved by STAR and forwarded to BNL management.

TWIST: Measuring the Space-Time Structure of Muon Decay

C. A. Gagliardi, J. R. Musser, R. E. Tribble, M. A. Vasiliev, and the TWIST Collaboration

TWIST had its first physics data run in Fall, 2002. The goal was to determine the Michel parameters ρ and δ in normal muon decay to 10^{-3}, factors of 3-4 improvement on the best previous measurements. This represents a significant step on our path toward ultimate determinations of the Michel parameters ρ, δ, and $P_\mu \xi$ to a few parts in 10^4. TWIST is a systematics dominated experiment, so most of the beam time was devoted to separate, independent measurements under a broad range of experimental conditions. The philosophy was to identify a potential systematic effect, then take a complete data set in which that effect was amplified many times compared to that expected in "standard" data sets. For example, muon decay data sets were taken under a range of beam conditions (different rates, steering, stopping locations, polarizations) and detector conditions (different high voltages, gas densities, magnetic fields, addition of extra material). Also, multiple data sets were taken under "standard" conditions in order to verify the long-term stability of the apparatus, a crucial consideration in an experiment that ultimately depends on data versus Monte Carlo comparisons. Each data set is large enough to determine ρ and δ with a statistical precision of ~6×10^{-4}. Therefore, comparisons between the data taken under "standard" and modified conditions will allow us to measure directly our sensitivity to the various systematic effects to a few parts in 10^4 or better. A broad range of ancillary measurements were also taken to provide dedicated data for tuning and verification of our GEANT-based Monte Carlo simulation of the experiment. Overall, approximately 6×10^9 muon decay events were recorded in over a dozen different data sets.

Since the run ended in December, most of the collaboration effort has been on analysis of the data and improvements and verification of the Monte Carlo. Our group has focused on improvements to the pattern recognition codes that are used to identify the drift chamber cells that were hit by the decay positron as it follows a helical trajectory through the detector, the proper introduction of multiple scattering effects into the track fitting procedure, and developing the tools necessary to perform the data versus data systematics comparisons. Our group, in conjunction with A. Olin of TRIUMF and B. Jamieson of University of British Columbia, has carried the primary responsibility for the pattern recognition code, which has been described in previous progress reports. Studies this past year of the code performance with both Monte Carlo and real data events have demonstrated that it successfully identifies nearly all clean decay positrons that fall within our fiducial energy and angle cuts. However, it often fails to reconstruct the ~5% of the events that include hard scatters or additional delta-ray tracks. Recently, we have been modifying the code to isolate and remove delta-ray tracks, while B. Jamieson has focused on identifying events that include hard scatters. Tests this past year of the tracking code, which fits a helix to the hits provided by the pattern recognition algorithms, demonstrated that multiple scattering of the decay positrons by the detector foils, gas and wires distorts the orbits substantially. This makes it essentially impossible to obtain good helical fits to the drift time measurements, and even introduces important biases as a function of decay energy and angle into fits that treat the drift chambers simply as coarse MWPCs. Recently, we have developed a technique, based on [1], that permits us to

include the multiple scattering explicitly in the helical fits. It has now been implemented into the MWPC fit. It increases the tracking efficiency within the fiducial region by 2-5%. It is being implemented into the drift time fit at present, where it is expected to have an even larger impact. Figure 1 shows decay energy and angle distributions from an analysis with the newly revised MWPC fitting code.

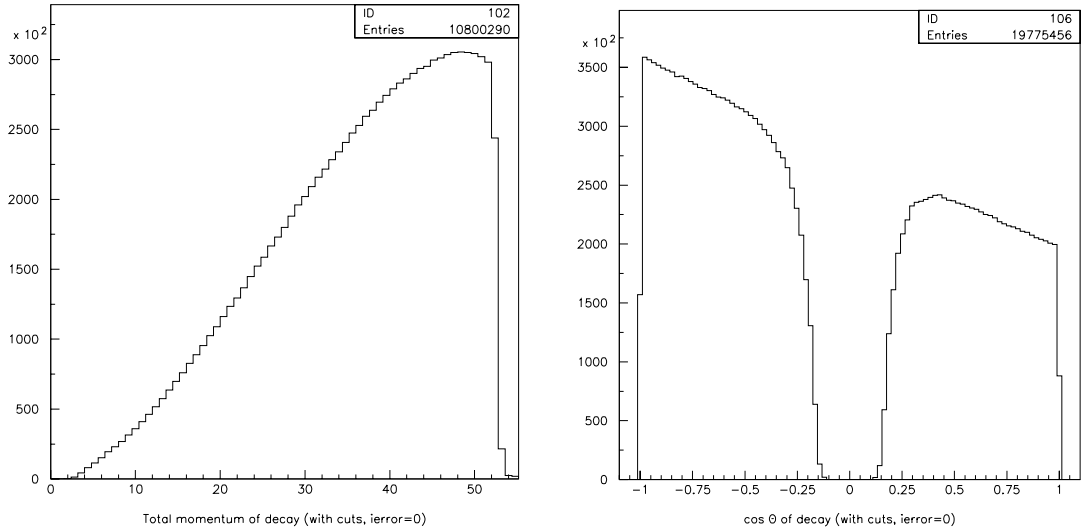

Figure 1. The decay energy and angle distributions from a recent analysis of ~1/3 of one of the "standard" data sets taken during Fall, 2002.

References

[1] G. Lutz, Nucl. Instrum. Methods Phys. Res. A **273**, 349 (1988).

Absolute Drell-Yan Dimuon Cross Sections in 800 GeV/c *pp* and *pd* Collisions

C. A. Gagliardi, E. A. Hawker, R. E. Tribble, M. A. Vasiliev, and the FNAL E866/NuSea Collaboration

During the past year, our efforts on FNAL E866 have focused on the determination of the absolute Drell-Yan dimuon cross sections in 800 GeV/c *pp* and *pd* collisions for dimuon effective masses in the range $4.2 < M < 16.85$ GeV and Feynman-*x* in the range $0.05 < x_F < 0.8$. These cross sections are sensitive to the magnitudes of the valence quark distributions in the proton beam at large Bjorken *x* (x_1) and the light antiquark distributions in the proton and deuteron targets at small *x* (x_2). Both of these kinematic regions are relatively poorly constrained by existing data in recent global parton distribution function (PDF) fits [1,2], and they both play important roles in searches for new physics at colliders. The analysis utilized the same FNAL E866 data that was previously analyzed to determine the $\bar{d}/\bar{u}$ ratio in the proton as a function of *x* [3]. This represents the Ph.D. dissertation of J. Webb of New Mexico State, who led the effort with assistance from collaborators at Argonne National Laboratory, Los Alamos National Laboratory, and Texas A&M.

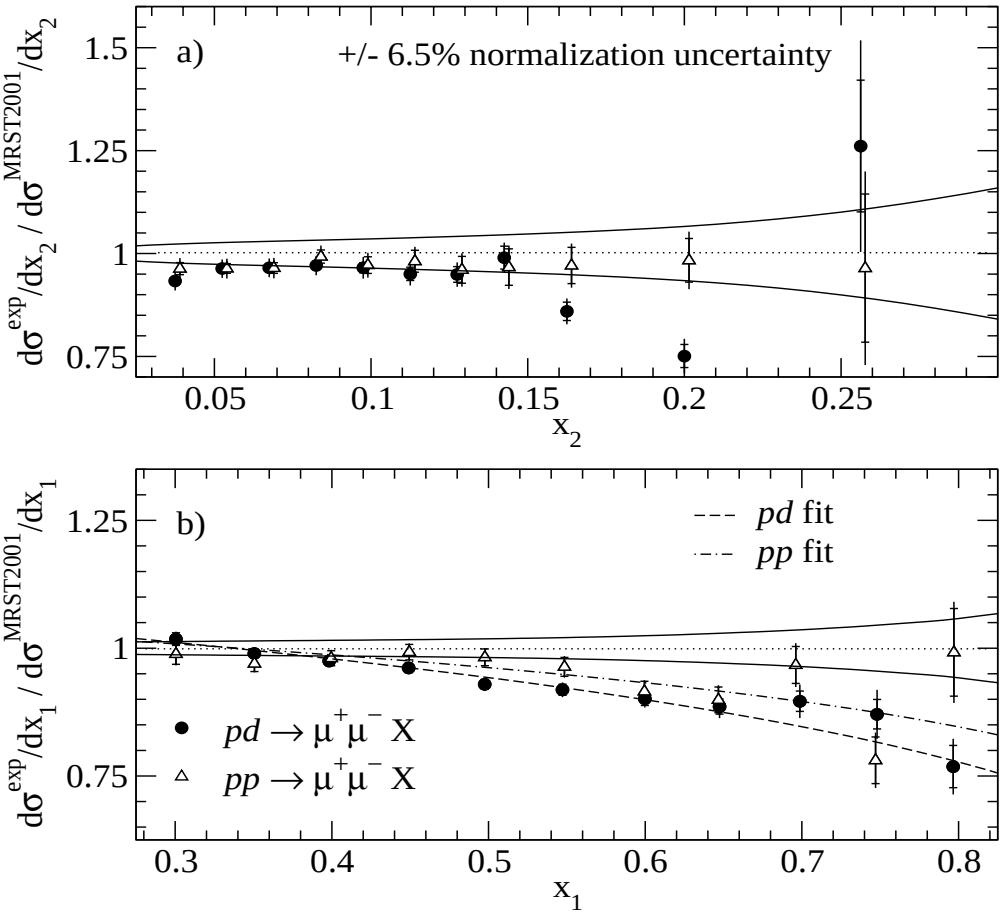

Figure 1. Ratios of the measured Drell-Yan cross sections to NLO calculations based on the MRST2001 PDF fit [1]. The solid curves represent the quoted uncertainties in the PDFs, and the dashed and dot-dashed lines represent phenomenological fits to the experimental results.

A description of the experiment and general analysis procedures may be found in Ref. [3]. That analysis was designed to minimize the systematic uncertainty in the cross section ratio $\sigma^{pd}/2\,\sigma^{pp}$. Several analysis details were changed in the present analysis in order to minimize the systematic uncertainties on absolute measurements of the cross sections.

Both doubly-differential ($M^3 d^2\sigma/dMdx_F$) and triply-differential ($E^3 d^3\sigma/dp^3$) cross sections were determined, and the former have been compared to next-to-leading-order calculations based on the current generation of global PDF fits [1,2]. In general, both global PDF fits provide a good description of the measured cross sections over the full kinematic region. However, there are small systematic differences between the measured cross sections and the predictions that are best understood by looking at the ratio of the measured to predicted cross sections separately as functions of x_1 and x_2. This comparison is shown for the MRST2001 PDF fit [1] in Fig. 1. The comparison for the CTEQ6M PDF fit [2] is similar. The PDFs provide a good description of the experimental results as a function of x_2 in the range $0.03 < x_2 < 0.15$, which was relatively unconstrained previously. In contrast, the PDFs overestimate the experimental cross sections at large x_1, indicating that the valence quark distributions in the PDFs are overestimated by 15-20% at large x. A letter describing these results has been submitted to *Physical Review Letters*, and a longer article is in preparation.

References

[1] A. D. Martin *et al.*, Eur. Phys. J. C **23**, 73 (2002); and hep-ph/0211080.

[2] J. Pumplin *et al.*, JHEP **0207**, 012 (2002).

[3] E. A. Hawker *et al.*, (FNAL E866/NuSea Collaboration), Phys. Rev. Lett. **80**, 3715 (1998); R. S. Towell *et al.*, (FNAL E866/NuSea Collaboration), Phys. Rev. D **64**, 052002 (2001).

High Precision Measurement of the Superallowed $0^+ \rightarrow 0^+$ Beta Decay of ^{22}Mg

J. C. Hardy, V. E. Iacob, M. Sanchez-Vega, R. G. Neilson, A. Azhari, C. A. Gagliardi, V. E. Mayes, X. Tang, L. Trache and R. E. Tribble

The first precision measurements in our program to sharpen the test of CKM unitarity are complete and a manuscript has been submitted for publication [1]. We have obtained the half-life, 3.8755(12) s, and superallowed branching ratio, 0.5315(12), for the ^{22}Mg beta decay. The resulting *Ft*-value provides an important test and confirmation of our new structure-dependent corrections [2] used to extract the vector coupling constant, G_V.

We produced ^{22}Mg using a 28*A*-MeV ^{23}Na beam from the K500 cyclotron to initiate the ^{1}H(^{23}Na, 2n)^{22}Mg reaction on an LN_2-cooled hydrogen gas target. The ejectiles were separated in the MARS spectrometer, leaving a >99.6% pure ^{22}Mg beam at the extraction slits in the MARS focal plane. This beam, containing ~10^4 atoms/s at 23*A* MeV, then exited the vacuum system and passed through a stack of aluminum degraders, finally stopping in the 75-μm-thick aluminized mylar tape of a tape transport system. Since the few impurities remaining in the beam had different ranges from ^{22}Mg, most were not collected on the tape; residual collected impurities were found to be substantially less than 0.1% of the ^{22}Mg content.

In a typical measurement, we collected ^{22}Mg on the tape for 5 s, then interrupted the accelerator beam in a few μs, and triggered the tape-transport system to move the sample in 180 ms to a shielded counting station located 90 cm away. There, data were recorded for a predetermined counting period while the beam remained off. This cycle was clock-controlled and repeated continuously. For the branching-ratio measurement, each counting period was 5 s, during which the sample was positioned between our precisely calibrated 70% HPGe γ-ray detector [3] and a 1-mm-thick BC404 plastic scintillator used to detect β particles. The former was located 15 cm from the sample, while the latter was 3 mm away. Time-tagged coincidence (or singles) data were stored event by event.

For the half-life measurement, the tape instead moved the collected sample to the center of a 4π proportional gas counter, where the β particles were detected and recorded for 80 s, more than 20 half-lives of ^{22}Mg. A separate decay spectrum was thus recorded for each cycle, ~60 cycles constituting a single measurement. The electronics included a deliberately introduced, dominant dead-time, which was pre-set and monitored continuously during the measurement and later used during analysis to correct the data cycle-by-cycle. Some 50 separate measurements were made, each with more than one million events but with a different combination of detector high-voltage, discriminator and dominant dead-time settings.

The decay scheme of ^{22}Mg appears in the figure. The β transition feeding the ground state must be second-forbidden unique and, being suppressed by some ten orders of magnitude, can be neglected. Thus, branching ratios to the excited states can be obtained from the *relative* intensities of γ-rays observed following the decay of ^{22}Mg. Our results for the relative γ-ray intensities, I_γ, and the deduced β-decay branching ratios, I_β, are shown in the table. The results agree with, but are an order of magnitude more precise, than any previous measurements [4].

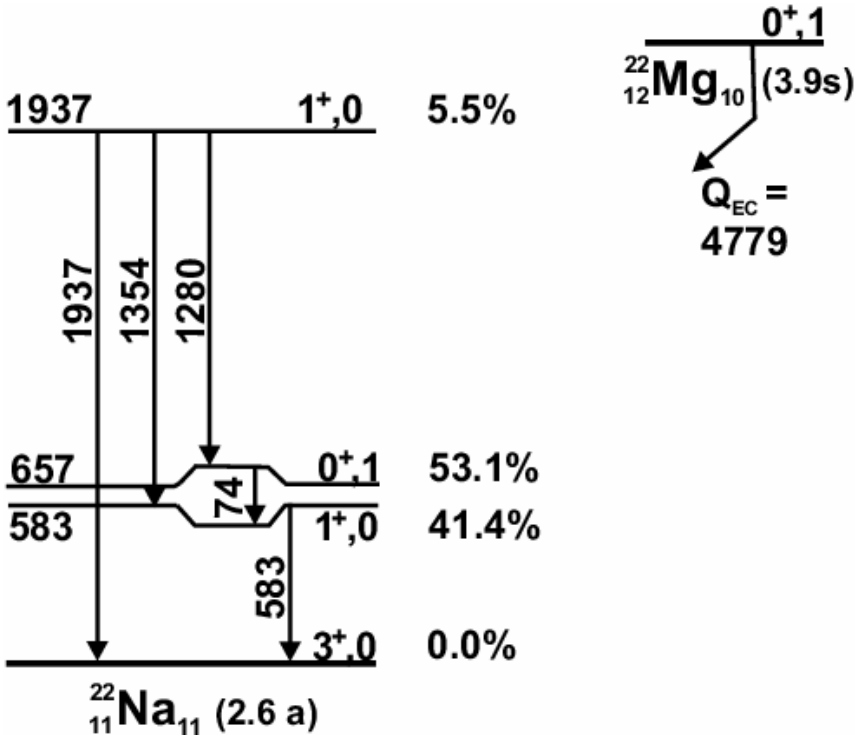

Figure 1. Decay scheme for the β decay of ^{22}Mg.

Table 1. Measured relative intensities of β-delayed γ rays, and deduced branching ratios for the β decay of ^{22}Mg.

E_γ (keV)	I_γ (%)	E_x (^{22}Na) (keV)	I_β (%)
74	58.36 (6)	583	41.40 (13)
583	100.00 (19)	657	53.15 (12)
1280	5.40 (7)	1937	5.45 (5)
1354	0.015 (3)		
1937	0.032 (3)		

The half-life data were analyzed with two different fitting procedures: (i) a maximum-likelihood fit to the sum of all dead-time corrected decay spectra; and (ii) a global fit of individual cycle spectra, with a common half-life but with amplitudes and dead-times correctly matched to each cycle. The second procedure contains no approximation but both yielded concordant results. To further consolidate the results, both fitting procedures and all tests were repeated on a parallel set of Monte-Carlo generated spectra, mimicking the trend of the real data, but with known half-life and background. No systematic experimental effects were observed, the results from all 50 individual measurements being statistically consistent with one another. Our final result for the ^{22}Mg half-life is 3.8755(12) s.

With these branching-ratio and half-life results, together with an updated value [1] of Q_{EC} = 4122.1(13), we obtain a corrected *Ft*-value for the superallowed transition of 3071(9) s. This is in

excellent agreement with 3072.2(8) s, the average *F*t-value for the nine well-known cases studied to date. This agreement provides important confirmation of our new structure-dependent corrections [2], which are used in all cases. If such agreement continues to be found in our future measurements on other light $T_Z = -1$ superallowed emitters, the uncertainties conventionally introduced with the structure-dependent corrections can be reduced and the CKM unitarity test sharpened appreciably.

References

[1] J. C. Hardy, V. E. Iacob, M. Sanchez-Vega, R. G. Neilson, A. Azhari, C. A. Gagliardi, V. E. Nayes, X. Tang, L. Trache and R. E. Tribble, Phys. Rev. Lett., in press.

[2] I. S. Towner and J. C. Hardy, Phys. Rev. C **66**, 035501 (2002).

[3] J. C. Hardy, V. E. Iacob, M. Sanchez-Vega, R. T. Effinger, P. Lipnik, V. E. Mayes, D. K. Willis and R. G. Helmer, Applied Radiation and Isotopes, **56**, 65 (2002); R. G. Helmer, J. C. Hardy, V. E. Iacob, M. Sanchez-Vega, R. G. Neilson and J. Nelson, Nucl. Instrum. Methods Phys. Res., to be published.

[4] J. C. Hardy *et al.*, Nucl. Phys. **A246**, 61 (1975) and references therein.

The Use of Monte Carlo Calculations in the Determination of a Ge Detector Efficiency Curve between 50 and 1400 keV

J. C. Hardy, V. E. Iacob, M. Sanchez-Vega, R. G. Neilson, J. Nelson and R. G. Helmer[1]
[1]*Idaho National Engineering and Environmental Laboratory, Idaho Falls, Idah*o

For our measurement of the superallowed β decay of ^{22}Mg [1], we required unprecedented precision in the calibration of our 280 cm^3 Ge detector between 50 and 1400 keV. Our work over this energy range, combining precise source measurements with an extensive set of Monte Carlo calculations, is now complete and a manuscript has been submitted for publication [2]. We have obtained 0.15% relative and 0.2% absolute precision over the entire energy range.

The quality of measured photon emission rates and the corresponding deduced relative efficiencies depend on several factors. These include the reproducibility of the source positions, determination of precise and reproducible peak areas, proper handling of coincident and random summing, knowledge of attenuation in the source, and accurate primary decay data. The source-detector distance was carefully measured from the source to a convenient reference point on the detector cap. Our main calibration was taken at a source-detector distance of 15.1 cm, but we also took some measurements at 100.1 cm. The source-detector distance was measured with a micrometer caliper, yielding a 0.2-mm uncertainty at 15.1 cm, and 0.3 mm at 100.1 cm.

In all, we have measured thirteen individual sources of ten radionuclides – ^{48}Cr, ^{60}Co, ^{88}Y, ^{108m}Ag, ^{109}Cd, ^{120m}Sb, ^{133}Ba, ^{134}Cs, ^{137}Cs and ^{180m}Hf – with activities between 2 and 47 kBq. We prepared three of these sources ourselves, ^{180m}Hf ($t_{1/2}$ = 5.5 h) with the Texas A&M reactor, and ^{48}Cr(21.6h) and ^{120m}Sb(5.8d) with the K500 Cyclotron. Two ^{60}Co sources were specially provided by the Physikalisch-Technische Bundasanstalt, PTB, Braunschweig, Germany and have quoted uncertainties in their activities of 0.06%. The remaining eight sources were purchased commercially and have activities quoted to 3%. Only the precisely known ^{60}Co sources were used to determine absolute efficiencies; all the others provided relative efficiencies that covered overlapping energy regions, which interconnected to one another and to the absolute ^{60}Co points.

For each source, we determined the relative efficiencies of its γ-ray lines by comparing the measured peak areas, determined with GF2, a least-squares peak-fitting program in the RADware series, with the corresponding known intensities. The sources of greatest importance to a precision calibration are those exhibiting simple γ-ray cascades uncomplicated by large conversion-electron components or by any possible β side feeding. Except for the calculable effects of electron conversion, the intensities of such cascaded γ-ray transitions are unambiguously equal. Of particular value to this work were the following sources (and cascaded γ-ray energies in keV): ^{48}Cr (112.4, 308.3), ^{108m}Ag (433.9, 614.28, 722.9), ^{120m}Sb (89.8, 197.3, 1023.1, 1171.3) and ^{180m}Hf (215.3, 332.2).

At our source-detector distance of 15.1 cm, the detector efficiency was between 0.2 and 1.0% over the energy region of interest. Thus, coincidence summing – the simultaneous detection of two γ-rays from the same decay event – could not be neglected. This summing results in a loss of counts from the peak of any γ-ray that is in cascade with another γ-ray, and an increase in peak counts for any crossover γ-

ray. In making these corrections, we took full account of any angular correlations between the summing γ-rays and, where necessary, used the detector's total efficiency (peak plus Compton), which we determined as a function of γ-ray energy in a separate set of measurements with sources selected for their relatively uncomplicated spectra. The sources used (and their relevant γ-ray energies in keV) were: ^{109}Cd (88.0), ^{48}Cr (112.4), ^{57}Co (123.7), ^{22}Na (511.0 and 1274.5), ^{137}Cs (661.7), ^{54}Mn (834.8) and ^{60}Co (average of 1253). The results appear in Fig. 1.

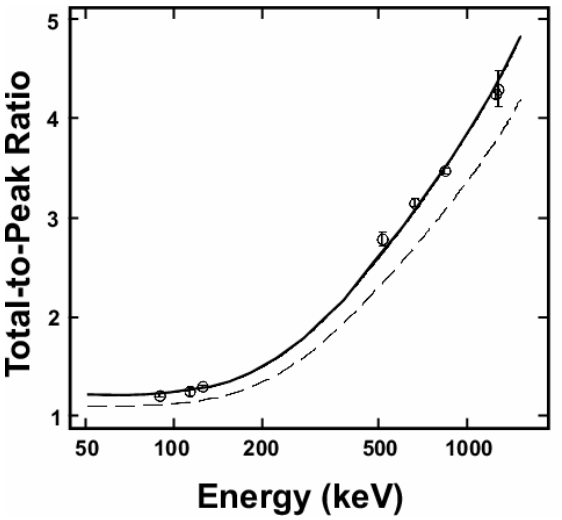

Figure 1. The ratio of the total efficiency to the full-energy-peak efficiency – the total-to-peak ratio – plotted as a function of γ-ray energy. The open circles with uncertainties are our measured data. The dashed curve is a smoothed representation of the Monte Carlo calculated results. The solid curve is a modification of the Monte Carlo result in which the non-peak efficiency has been increased by an energy-independent constant to account for scattering from external objects not included in the Monte Carlo input specifications.

In addition to acquiring calibration spectra, we also made a number of measurements designed to reveal the physical dimensions and location of the detector's Ge crystal in its housing. These measurements included a scan of the side of the detector with a tightly collimated ^{133}Ba source, to determine the crystal length; a pair of ^{57}Co spectra recorded at 4- and 20-cm source-detector distances, to locate the front surface of the crystal; and an overall x-ray picture of the crystal in its housing, to establish its exact orientation. This information was then used as input to Monte Carlo calculations performed with the electron and photon transport code CYLTRAN.

One further complication arose when we compared the Monte Carlo calculations with measurements at energies below ~80 keV: the former did not exactly reproduce the strengths of the measured Ge X-ray escape peaks, presumably because we had, of necessity, assumed that the detector has a uniform front deadlayer. In reality, this region of the detector is probably not uniform and, furthermore, it likely has only partial charge collection. Therefore, it is quite reasonable that the simple representation in the Monte Carlo calculations does not completely represent the measured data. Accordingly we undertook another separate study, of X-ray escape from our detector, with the following sources (and their relevant γ-, or X-ray energies in keV): ^{109}Cd (22.1, 24.9), ^{120m}Sb (25.2, 28.6), ^{137}Cs (32.0), ^{152}Eu (39.9), ^{180m}Hf (93.3) and ^{48}Cr (112.4). The results appear in Fig. 2. In subsequent comparisons with efficiency data, we added the Monte-Carlo calculated full-energy and X-ray-escape peaks together and used the experiment-based escape-to-full-energy function (Fig. 2) to derive the full-energy peak area from that sum. It is this result that we refer to as the "Monte-Carlo calculated" efficiency for peaks below 120 keV.

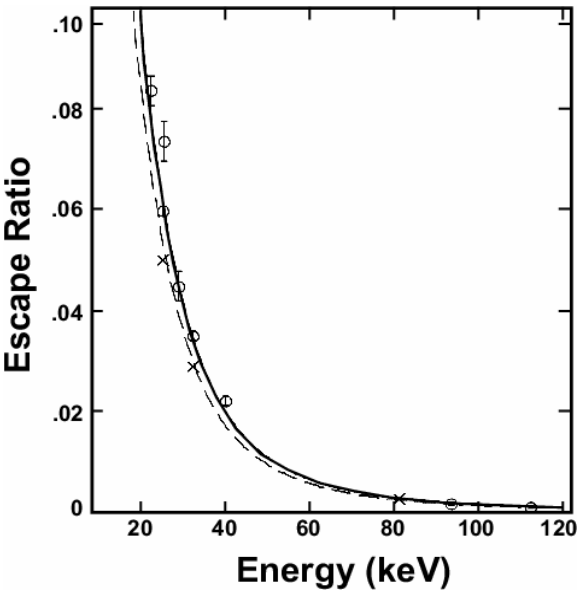

Figure 2. The ratio of the summed x-ray escape-peak areas to the full-energy peak area, plotted as a function of incident photon energy. The open circles with uncertainties are our measured data; the three points marked with an X are Monte Carlo calculated. The dashed curve is calculated with an expression due to Hansen *et al* [3]; the solid curve is the same calculation scaled upwards by 16%.

Now, with only the detector's two dead-layers as adjustable parameters, we achieved excellent agreement (χ^2/N = 0.8) between the Monte Carlo efficiency results and our 40 measured data points between 22 and 1836 keV. The results are shown in Fig. 3, where they are plotted as differences between the measured efficiencies and the Monte Carlo calculated values, expressed in percent. Each source is separately identified to make clear how the energy ranges overlap one another. We also compared calculation and experiment at a source-detector distance of 100.1 cm with no further parameter adjustment. They differed by a mere (energy independent) 0.8%.

Our data show that a well-determined set of Monte Carlo calculations can be used to interpolate with high precision between measured relative (or absolute) Ge-detector efficiencies. In our case, with 10 sources that included one whose activity was known to 0.06%, we have obtained an efficiency curve with relative uncertainties of 0.15% and absolute uncertainties of 0.2% from 50 to 1400 keV. Although the curves only strictly apply to a source distance of 15.1 cm, the distance for which we actually require the calibration, it is evident from our results at 100.1 cm that one could expect similar uncertainties if the Monte Carlo calculations were used to obtain efficiencies at distances substantially different from 15 cm.

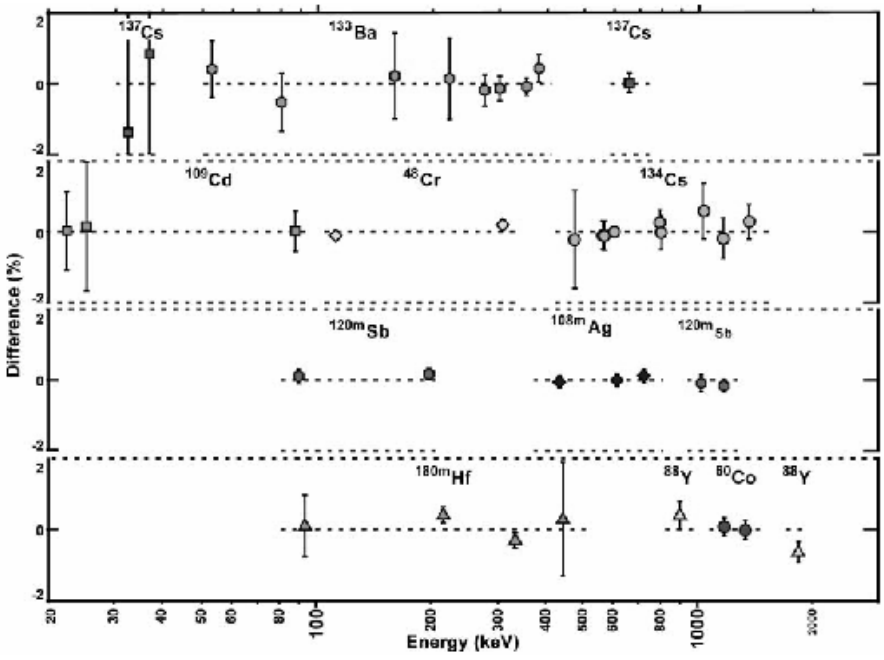

Figure 3. Differences between the measured efficiencies (points) and Monte Carlo calculated values (line at 0) plotted for the individual sources.

References

[1] J. C. Hardy *et al.*, *Progress in Research*, Cyclotron Institute, Texas A&M University (2002-2003) p. I-19.

[2] R. G. Helmer, J. C. Hardy, V. E. Iacob, M. Sanchez-Vega, R. G. Neilson and J. Nelson, Nucl. Instrum. Methods Phys. Res. A, in press.

[3] J. S. Hansem *et al.*, Nucl. Instrum. Methods Phys. Res. A **106**, 365 (1973).

TRIUMF E-823: High precision branching ratio measurement for the superallowed β decay of ^{74}Rb: a prerequisite for exacting tests of the standard model

J. C. Hardy and V. I. Iacob

The goal of the E-823 experimental program is to measure precise half-lives and branching ratios for superallowed 0^+-to-0^+ beta emitters in medium-mass (A > 60) nuclei produced by the new ISAC1 radioactive-beam facility at TRIUMF. This is an important adjunct to our program at the Cyclotron Institute to probe CKM unitarity via superallowed beta decay. In addition to the TAMU participants, the E-823 collaboration now includes members from TRIUMF, Simon Fraser University, Lawrence Berkeley National Laboratory, Queen's University, Argonne National Laboratory, Oak Ridge National Laboratory, Louisiana State University, University of Surrey, McMaster University, Georgia Institute of Technology and the University of Guelph.

During this past year, the collaboration has completed the first detailed and precise study of the superallowed β decay of ^{74}Rb, employing γ-ray and conversion-electron spectroscopy. We have experimentally identified a total non-superallowed feeding of 336(20) × 10^{-5} per ^{74}Rb decay. A partial decay scheme appears in Figure 1. From a comparison of these data with recent shell-model predictions

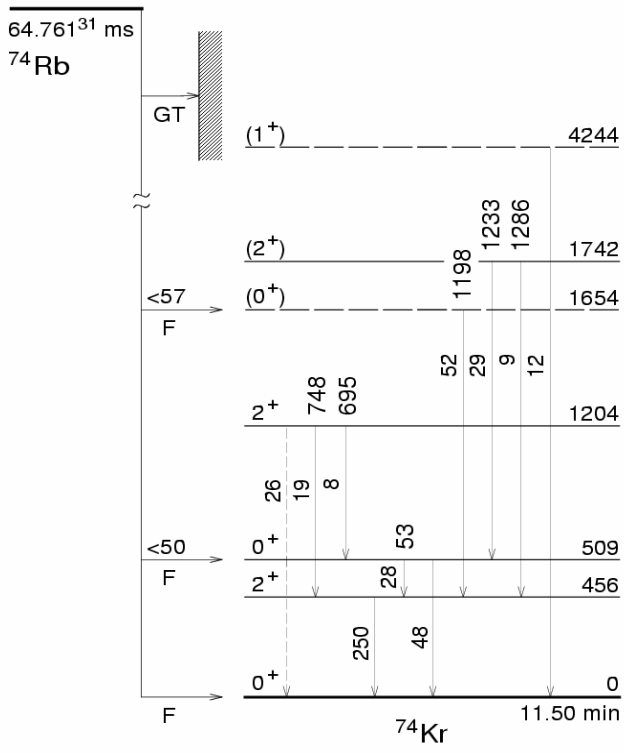

Figure 1. Partial decay scheme of ^{74}Rb. Intensities of transitions are given in units of 10^{-5} per ^{74}Rb decay.

[1] we estimate the unobserved non-superallowed feeding to be 50-250 $\times$ 10^{-5}, resulting in a deduced ground-state (superallowed) β branch of 99.5(1)%. A paper describing this work has been published [2].

Our results show that the precise determination of a superallowed branching ratio in the presence of non-negligible, strongly fragmented Gamow-Teller branches is not a hopeless endeavor. It appears that the shell-model calculations of reference [1] reflect the experimental situation surprisingly well and, with refined experimental techniques, even more precise results should be obtainable. Such measurements are presently in preparation. The ISAC separator will be operated in isobaric-resolution mode, and the upgraded Canadian 8π spectrometer, equipped with Si(Li) detectors and plastic-scintillator trigger detectors, will serve for γ-ray and conversion-electron detection. This spectrometer system will enable us to identify additional γ rays from the ^{74}Rb decay, especially those directly populating the ground state, and determine a more precise number for the ground-state branch and its error.

References

[1] J. C. Hardy and I. S. Towner, Phys. Rev. Lett. **88**, 252501 (2002).

[2] A. Piechaczek *et al.*, Phys. Rev. C **67**, 051305(R) (2003).

Precise efficiency calibration of an HPGe detector up to 3.5 MeV, with measurements and Monte Carlo calculations

N. Nica, J. C. Hardy, V. E. Iacob and R. G. Helmer[1]
[1]*Idaho National Engineering & Environmental Laboratory, Idaho Falls, Idaho*

In previous work [1], we determined the efficiency curve between 50 and 1400 keV for a coaxial, 280-cm^3 n-type Ge γ-ray detector, based on a combination of measured relative efficiencies for nine radionuclides, the measured absolute efficiency for the γ rays from ^{60}Co, and efficiencies calculated with CYLTRAN, a Monte Carlo photon and electron transport code. With the measured physical dimensions of the detector, only minor adjustments were required, well within tolerances, to obtain excellent agreement between the measured and calculated efficiency values [1]. From these results, we estimated the uncertainty in the final efficiency curve to be 0.15% relative and 0.2% absolute. Without changing the detector parameters in any way, we have now extended this work to 4.8 MeV by the continued use of both measured relative efficiencies and CYLTRAN-calculated efficiencies. This work is now complete and has been presented at the 14th International Conference on Radionuclide Metrology and its Applications in Dublin. A manuscript has been accepted for publication [2].

In this extension to 4.8 MeV, relative efficiencies for the full-energy (FE) peaks were measured for the strong γ rays from three additional sources: ^{24}Na, ^{56}Co, and ^{66}Ga. We produced 15-hour ^{24}Na by thermal neutron capture on Na_2CO_3 at the Texas A&M reactor, the source material being deposited on, and covered by 0.08-mm plastic foil. For 9.5-hour ^{66}Ga, we used a ^{66}Zn beam from the Texas A&M K500 Cyclotron to initiate the reaction ^{1}H(^{66}Zn, n)^{66}Ga, the recoiling ^{66}Ga nuclei being separated from other reaction products in the MARS recoil spectrometer, and then implanted into 0.08-mm plastic foil. The 77-day ^{56}Co source was purchased from Isotopes Products Laboratory. The efficiency measurements were made, and the spectra analyzed, as described in [1]. Since the γ rays from these nuclides are generally in cascade and the source-detector distance was 15.1 cm, corrections for coincidence summing were made: for most γ rays these corrections were less than 1% and were never larger than ~2%.

The relative FE efficiencies deduced from these measurements depend on the relative γ-ray emission probabilities used for these nuclides. On the one hand, the value for the two strong ^{24}Na γ rays is well known [3]. On the other, those for the more complex decays of ^{56}Co and ^{66}Ga have only recently become reasonably well determined; we used the values from reference [4]. We considered only those γ rays with emission probabilities known to 1% or better and, among those, we only retained the ones that were cleanly observed – uncontaminated by escape peaks, for example – with measured areas in our spectra determined to 1% or better. This left us with a total of 26 FE peaks between 834 and 4806 keV from the three sources.

Measured efficiencies for these peaks were compared with Monte Carlo calculations performed with the same CYLTRAN code and identical dimensions to those used in our earlier work between 50 and 1400 keV. The results appear in Fig. 1. In this comparison, there are only three free parameters – a single scaling factor for each nuclide. We determined these scaling factors by minimizing the weighted differences between the measured values and the Monte Carlo efficiency values: that is, by means of a

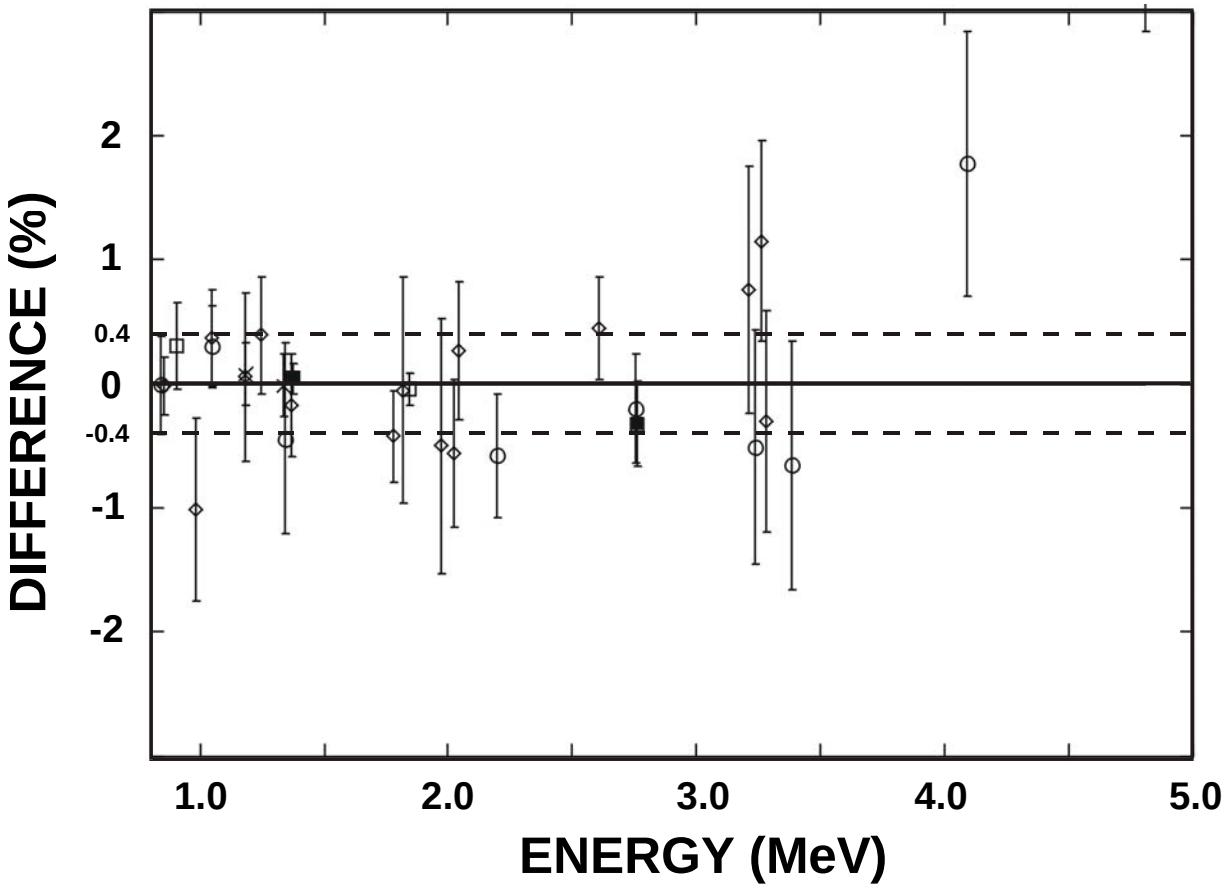

Figure 1. Differences between the measured efficiencies (points with uncertainties) and the corresponding Monte Carlo calculated values (line at 0). The differences are calculated as experiment minus calculation, divided by calculation, and are expressed as a percent. The points can be identified with individual sources as follows: ^{24}Na, solid squares; ^{56}Co, open diamonds; ^{60}Co, x's; ^{66}Ga, open circles; and ^{88}Y, open squares.

least-squares fit. Each of these nuclides has one or more γ rays below 1400 keV where the FE efficiency curve has already been determined precisely [1]. Therefore, the efficiencies at the higher energies presented here are completely consistent with those at the lower energies reported in reference [1]. Note that the figure also includes the results of two measurements from our previous work [1], those of ^{60}Co and ^{88}Y. The former provides an *absolute* efficiency determination that anchors the overall efficiency curve, while the latter yields a useful efficiency ratio that overlaps the energy region of interest in the present work.

As indicated in Fig. 1, the agreement between measured and calculated efficiencies below 3500 keV is excellent. Over this energy region, the normalized chi-squared for the 24 points from ^{24}Na, ^{56}Co and ^{66}Ga (with 21 degrees of freedom) is 0.70. We suggest that the uncertainty in the deduced efficiencies is 0.4% between 1400 and 3500 keV. Above 3500 keV there are two ^{66}Ga γ rays with emission probabilities claimed to better than 1%, both of which deviate significantly from the Monte Carlo calculations. Whether these represent real discrepancies between experimental and theoretical efficiencies or a systematic error in the accepted emission probabilities can only be decided by further experiments. For now, we forego any estimation of the uncertainty in our calibration curve above 3500 keV.

For many of the γ rays, our measured spectra also yielded single-escape (SE) and double-escape

(DE) peak relative efficiencies. We compared them with Monte Carlo calculations as well and, in doing so, we have found it most useful to express them as ratios of escape-peak areas to that of the corresponding FE peak. These ratios are independent of the γ-ray emission probabilities and of any coincidence summing corrections. However, when the measured SE/FE and DE/FE ratios were first compared with the Monte Carlo calculations, they were found to be consistently lower than the calculated ratios by up to 7%. We then learned from an author of the CYLTRAN code [5] that the program takes no account of positron annihilation-in-flight (AIF). Clearly, since the pair-produced positrons that do annihilate in flight produce photons with energies that are significantly different from 511 keV, the SE and DE peak areas calculated by the code need to be reduced by the known probabilities for AIF [6]. For each particular γ ray of energy E_γ, we reduced the SE and DE efficiency values from the Monte Carlo calculation by the AIF probability determined for a positron with energy ½ (E_γ - 1022 keV). As shown in Fig. 2, this produced excellent agreement with the measured escape ratios.

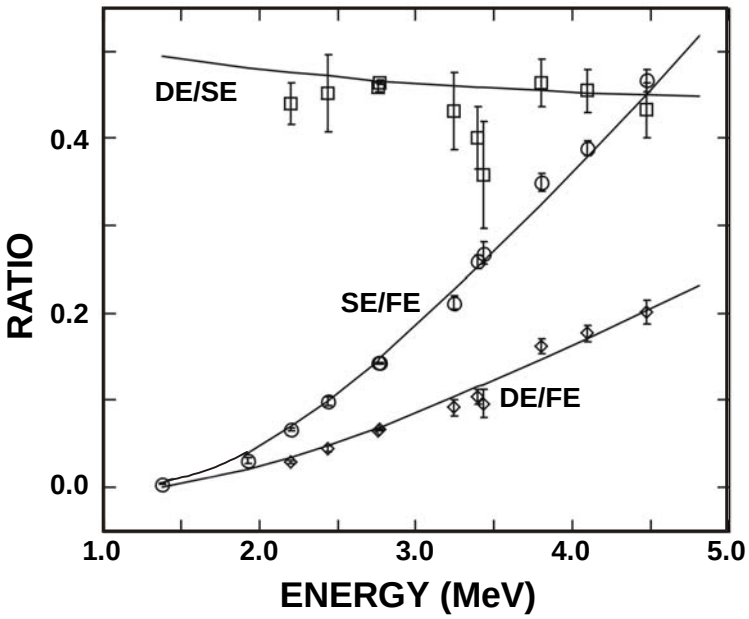

Figure 2. Measured escape ratios (points with uncertainties) compared with CYLTRAN Monte Carlo calculations (curves) that have been corrected for positron annihilation in flight.

With completion of this work, we have demonstrated that we can determine absolute γ-ray intensities to about 0.2% from 50 to 1400 keV and to about 0.4% from there to 3500 keV. This meets our requirements in measuring precise β-branching ratios for superallowed decays.

References

[1] J. C. Hardy *et al*., *Progress in Research*, Cyclotron Institute, Texas A&M University (2002-2003) p. I-22; R. G. Helmer, J. C. Hardy, V. E. Iacob, M. Sanchez-Vega, R. G. Neilson and J. Nelson, Nucl. Instrum. Methods Phys. Res. A, in press.

[2] R. G. Helmer, N. Nica, J. C. Hardy and V. E. Iacob, Int. J. Appl. Radiat. Isot., to be published.

[3] IAEA Coordinated Research Program, 1991, *X-ray and gamma-ray standards for detector calibration*, IAEA-TECDOC-619.

[4] C. M. Baglin, E. Browne, E. B. Norman, G. L. Molnár, T. Belgya, Zs. Révay, F. Szelecsényi, Nucl. Instrum. Methods Phys. Res. A **481**, 365 (2002).

[5] R. P. Kensek, private communication (2003).

[6] E. Browne, R. B. Firestone, *Table of Radioactive Isotopes*, John Wiley & Sons (New York, 1986), p. D-6.

Beta decay of ^{62}Ga

B. C. Hyman, V. E. Iacob, A. Azhari, C. A. Gagliardi, J. C. Hardy, V. E. Mayes, R. G. Neilson, M. Sanchez-Vega, X. Tang, L. Trache and R. E. Tribble

We have completed our study of the beta decay of ^{62}Ga, whose dominant branch is a superallowed 0^+-to-0^+ transition to the ground state of ^{62}Zn. A manuscript has been submitted for publication [1].

We produced ^{62}Ga with the ^{1}H(^{64}Zn, 3n)^{62}Ga reaction, using 41 and 42*A* MeV ^{64}Zn beams from the K500 cyclotron on an LN_2-cooled hydrogen gas target. A 1.5-mg/cm^2 Al stripper foil was placed immediately after the gas cell so that most of the outgoing ^{62}Ga ions were in the 31+ charge state. Reaction products entered the MARS spectrometer at 0^o and exited as an 80-94% pure 37*A*-MeV ^{62}Ga beam in the focal plane with a typical intensity of 1000-1500 Hz. The remaining background nuclei consisted of other N=Z, fully stripped nuclei that had the same magnetic rigidity. When required for the lifetime measurement, the impurities in this beam were further reduced by another order of magnitude without any loss of ^{62}Ga intensity: the beam was degraded and collected on the thin tape of our tape-transport system. Since impurities have different ranges, the collected ^{62}Ga samples were ~ 99% pure.

For the half-life measurement, approximately 3 x 10^6 β-decay events were recorded. Collected activity was conveyed via tape transport to a 4π proportional gas counter. See reference [2] for a description of the methods we use for lifetime measurements. As always, data were taken under a broad range of experimental conditions: different combinations of counter high voltage, discriminator threshold, fixed event-by-event deadtime, and channel dwell time. In addition, a run was taken with a much longer decay time in order to expose longer-lived impurities. This latter run indicated that 1.1(1)% of the observed activity arose from 3.21-s ^{58}Cu. Based on detector measurements in the MARS focal plane, we also expected 1.46-min ^{54}Co^g to be a possible impurity at the 0.1% level.

We performed five-parameter maximum-likelihood fits on the data. The five parameters represented the yield and half-life of ^{62}Ga, the yields of the ^{58}Cu and ^{54}Co^g impurities, and an additional constant background. The half-lives of the ^{58}Cu and ^{54}Co^g impurities were fixed at their accepted values. The fitted result for the magnitude of the ^{58}Cu impurity was consistent with the yield observed during the run specially timed to expose it. The fits also indicated that ^{54}Co^g contributed a maximum of 0.05% of the measured decays. The maximum effect that these decays could have on the measured ^{62}Ga lifetime was 0.04%. We find that the ^{62}Ga half-life is 115.84(25) ms.

Two different procedures were used to determine the branching ratios of ^{62}Ga to excited states in ^{62}Zn. The primary goal of the first measurement was to observe any Gamow-Teller branches and either to observe or to set an upper limit on the forbidden Fermi transition to the first 0^+ excited state in ^{62}Zn at 2.33 MeV. The ^{62}Ga beam was stopped in a 0.66-mm thick Al target placed in air beyond the MARS focal plane. The Al target was surrounded on four sides by 2-mm-thick plastic-scintillator beta detectors, as shown in Fig. 1. Gamma rays were detected by 70% HPGe detectors placed behind three of the four plastic scintillators. A 5-cm-thick graphite cone was attached to the front of each Ge detector to shield it from decay positrons, while exposing it to a minimum of Bremsstrahlung radiation. Events were recorded if they contained a β-γ coincidence. Since we maximized the yield by implanting the ^{62}Ga in the

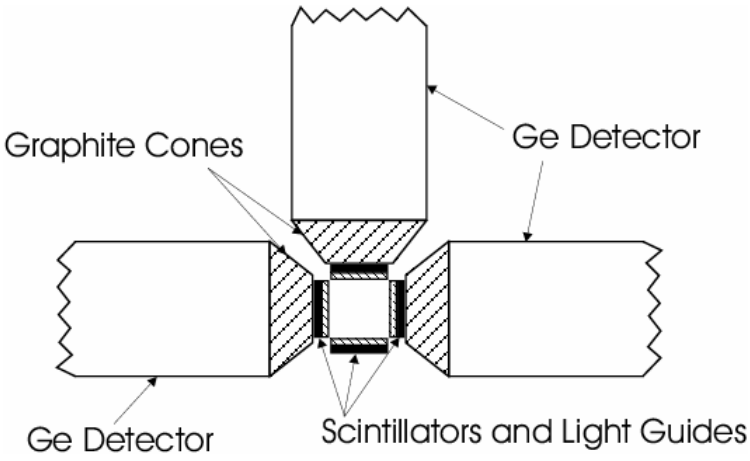

Figure 1. Detector configuration during the first branching-ratio measurement, as seen by looking into the ^{62}Ga beam. The aluminum stopping target was located in the center of the four-sided box formed by the scintillators and the light guides.

Al target and making the decay measurements simultaneously, the half-lives for the observed γ decays could not be determined.

Most of the ^{62}Ga decays go to the ^{62}Zn ground state. Thus, to infer branching ratios from the observed β-γ coincidence yields, one must know both the strength of the ^{62}Ga source and the absolute efficiency of the β and γ detectors. The ^{62}Ga yield was calibrated relative to the integrated ^{64}Zn beam intensity in dedicated runs with a Si strip detector in the MARS focal plane. The Ge-detector efficiencies were measured *in situ* with a ^{152}Eu source that was calibrated to 5%. The β-detector efficiencies were calculated to 5% with a Monte Carlo simulation. They were nearly independent of endpoint energy.

Figure 2 shows one of the γ-ray spectra in the vicinity of the 0.954 MeV γ ray from the decay of the 2^+ first-excited state in ^{62}Zn. This decay was clearly visible in all three β-γ coincidence spectra and corresponds to an apparent β-decay branching ratio to the 0.954 MeV state of 0.120(21)%. If these γ rays were the result of β decays directly to the 2^+ state, they would represent a log *ft* of 6.2. This is far too small for a second-forbidden β decay, so these γ rays must be the result of cascade γ decays following Gamow-Teller transitions to higher lying 1^+ states in ^{62}Zn. A systematic search was performed of the measured γ–ray spectra for evidence of transitions that might populate the 2^+ state. None were found with γ–ray energies below 2.5 MeV. There was no evidence either for a 1.376 MeV γ ray, which would indicate population of the first 0^+ excited state in ^{62}Zn at 2.33

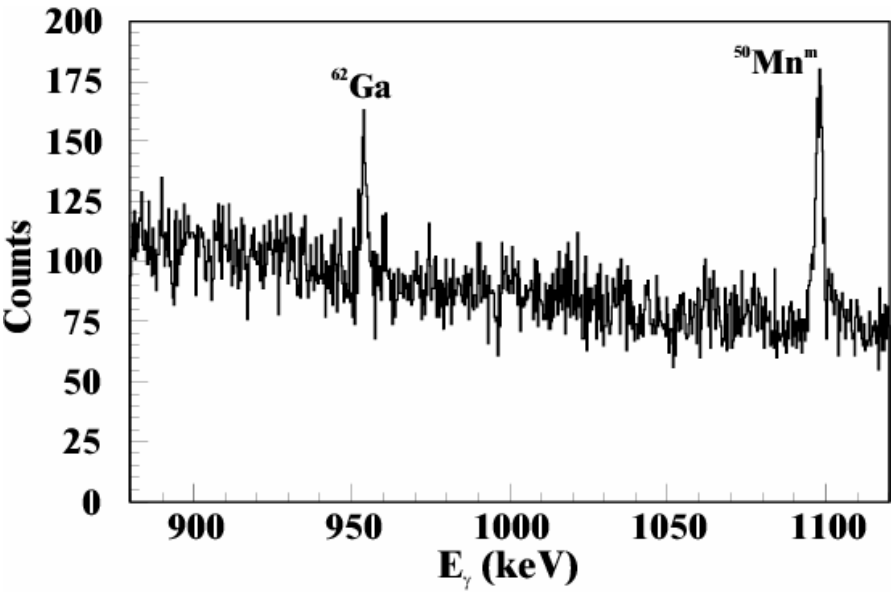

Figure 2. Gamma-ray spectrum from one of the Ge detectors in the vicinity of the ^{62}Zn first-excited state at 954 keV. The transitions are labeled according to the parent nucleus.

MeV. After accounting for statistical and systematic uncertainties, we conclude that the branching ratio for the forbidden Fermi decay from ^{62}Ga to ^{62}Zn(0+,2.33) is <0.043%, consistent with predictions [3].

A second branching-ratio measurement was performed with the tape transport system so that the decay of 0.954-MeV γ ray could be measured, albeit with lower statistics. We found its half-life to be 110(65) ms, thus confirming that it follows the β decay of the ^{62}Ga ground state.

Our measured γ-ray yields from the decay of ^{62}Ga would have been puzzling indeed without the recent calculations [4] of competing Gamow-Teller decays in superallowed emitters with A > 60. There, it is estimated that more than 100 such branches exist and, although their total strength is predicted to be significant (~0.3%), the individual branches themselves are considerably weaker and could well be unobservable. The calculations also predict the fraction of such branches that de-excite through the 0.954-MeV first-excited state and we can use that result, together with our measured intensity of the 0.954-MeV γ ray, to set limits on the total non-superallowed decay branches from ^{62}Ga. We thus find the superallowed branching ratio for ^{62}Ga decay to be 99.85(+5,-15)% and the corresponding corrected *Ft*-value to be 3050(47) s, in good agreement with 3072.2(8) s, the average *Ft*-value for the nine well-known cases studied to date. If the uncertainty on the Q_{EC}-value could be reduced to 1.7 keV – probably within the grasp of current technology – the uncertainty on the resulting *F*t-value would become 9 s. That would be sufficient to provide a demanding test of the structure-dependent corrections [3] used in obtaining the ^{62}Ga *Ft*-value.

References

[1] B. C. Hyman, V. E. Iacob, A. Azhari, C. A. Gagliardi, J. C. Hardy, V. E. Mayes, R. G. Neilson, M. Sanchez-Vega, X. Tang, L. Trache and R. E. Tribble, Phys. Rev. C **68**, 015501 (2003).

[2] J. C. Hardy *et al.*, *Progress in Research,* Cyclotron Institute, Texas A&M University (2002-2003) p. 19.

[3] I. S. Towner and J. C. Hardy, Phys. Rev. C **66**, 035501 (2002).

[4] J. C. Hardy and I. S. Towner, Phys. Rev. Lett. **88**, 252501 (2002).

T=5/2 states in ^{9}Li: Isobaric analog states of ^{9}He

G. Chubarian, V. Z. Goldberg, G. V. Rogachev, J. J. Kolata, D. Aleksandrov, A. Fomichev, M. S. Golovkov, Yu. Ts. Oganessian, A. Rodin, B. Skorodumov, R. S. Slepnev, G. Ter-Akopian, W. H. Trzaska, R. Wolski

The first study of isobar analog states of a neutron rich nucleus, ^{9}He, which is beyond the nuclear stability region, was made by means of resonance scattering using ^{8}He beam. The experiment was made along the ideas given in [1].

The experiment was performed with radioactive beams of ^{8}He at laboratory energies of 51 and 59 MeV having an intensity of about 1000/s, produced in the Flerov Laboratory (Dubna). The experimental setup is shown in Fig. 1 A primary beam of 32 MeV/A^{11}B ions was incident on a very thick beryllium target. A magnetic spectrometer was used to separate ^{8}He from all other reaction products. Two thin plastic detectors in the flight path, upstream of the experimental area, provided an event-by-event identification of the incoming particles. The scattering of ^{8}He on p was performed in a 50 cm scattering chamber filled with methane gas.

The excitation function for ^{8}He+p elastic scattering is presented in Fig.2 together with the fit based on two channel multi-level R-matrix theory. The R-matrix calculation, assuming $1/2^{-}$ spin for the first resonance, $3/2^{-}$ for the second, and $5/2^{+}$ for the third is shown in Fig. 2 by a dashed line. Energies and widths of the resonances are as follows: 16.1±0.1 MeV Γ<100 keV; 17.1(2) MeV Γ=800 keV; 18.9(1) MeV Γ=240 keV). The convolution of this calculation with the experimental resolution function is shown by the bold dot-dashed line.

The T=5/2 levels in ^{9}Li are directly related with the lowest levels in ^{9}He.Therefore, two main conclusion can be made on the basis of the results obtained: (i) predictions based on calculations for the nuclei on the stability line are made for ^{9}He [2,3] should be reconsidered, and (ii) there is a fruitful field of studies of analog states in neutron rich nuclei by the thick target inverse kinematics method.

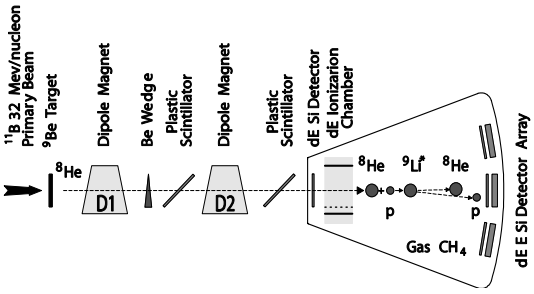

Figure 1. Experimental setup.

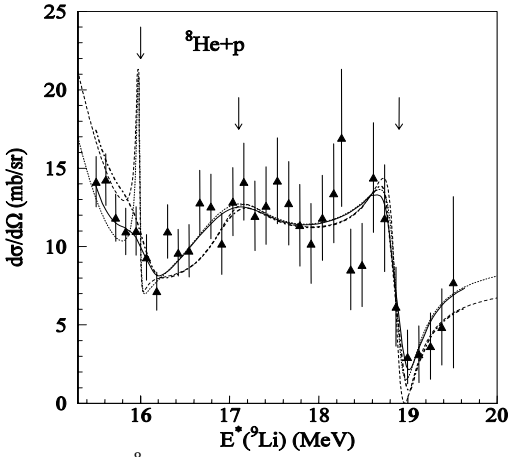

Figure 2. ^{8}He+p elastic scattering excitation function measured in the zero-degree telescope. Resonance energies are indicated with arrows.

References

[1] V. Z. Goldberg, Proc. of Exotic Nuclei and Atomic Masses (ENAM98) Conf. (1998).
[2] K. K. Seth, *et al.*, Phys. Rev. Lett. **58**, (1987).
[3] L. Chen, *et al.*, Phys. Lett. B **505**, 21 (2001).

α -Structure in ^{22}Ne by the resonance ^{18}O+^{4}He scattering

G. Chubarian, V. Z. Goldberg, G. V. Rogachev, M. V. Rozhkov and B. B. Skorodumov, W. H. Trzaska, K.-M. Kallman, T. Lönnroth, M. Mutterer

Knowledge of α-cluster structure is mainly based on investigations of light N=Z nuclei [1]. Many difficulties of experimental investigations of the α-cluster structure in N≠Z nuclei can be overcome using Thick Target Inverse Kinematics (TTIK) method [2]. However, while high efficiency and reasonably good resolution makes the method attractive (and the only possible one for nuclei far off the line of stability), the data, which correspond to the end of the heavy ions range in the TTIK method, might be less reliable due to the large spread of the beam in the end of its range. The aim of this work was a detailed comparison of the available data for the states in ^{22}Ne near the ^{18}O+α threshold, obtained by the conventional method with these, obtained by the TTIK method [3].

Broad region excitation functions for ^{18}O+α elastic scattering were measured at the Jyvaskyla University cyclotron, and part of the data (high energy) has been published [3].

The analysis showed that the energy and space spread of the beam must be taken into account in the TTIK method to provide for reliable data on level parameters for levels widths of few keV. Simultaneously, differences were found in the quality of the fit and in the parameters of the levels, which cannot be related with differences in the experimental methods or with the details of a somewhat different theoretical approach. These differences are the result of the restricted energy regions, which were under analysis in the former experiments [4,5]; it appears that strong higher energy resonances influence the low energy region. This fact can be an important issue for many studies of low energy region resonances of astrophysical importance.

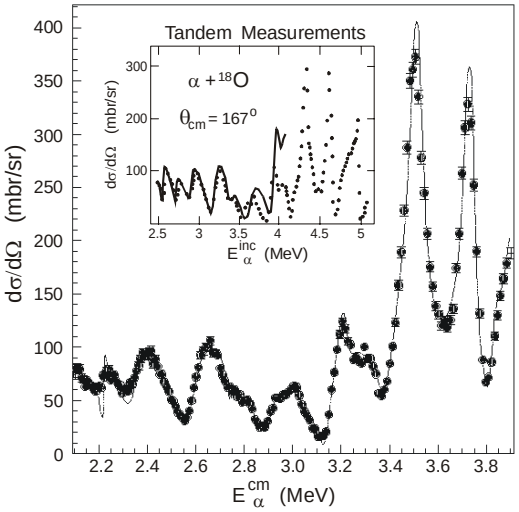

Figure 1. Excitation function for ^{18}O+α scattering at 180°. The spectrum was obtained in a single run. A comparison with the tandem data for low energy region is given in the inset.

References:

[1] P. A. Butler and W. Nazarewicz, Rev. Mod. Phys. **68**, 349 (1996).

[2] V. Z. Goldberg, in *Clustering Phenomena in Atoms and Nuclei*, eds. M. Brenner, T. Lonnroth, and F. B. Malik (Springer Ser. in Nucl. and Part. Phys., Springer Verlag, Heidelberg, 336 (1992).

[3] G. V. Rogachev, *et al.*, Phys. Rev. C **64**, 051302(R) (2001).

[4] D. Powers, H. T. Bair, J. L. C. Ford, and H. B. Willard, Phys. Rev. **134**, B1237 (1964).

[5] S. Gorodetzky, *et al.*, J. Phys. **29**, 271 (1968).

Recent Results in the Studies of Nuclear Structure by Resonance Scattering with Radioactive Beams

G. Chubarian, V. Z. Goldberg, W. H. Trzaska, G. V. Rogachev, J. J. Kolata, A. Andreyev, C. Angulo, M. J. G. Borge, S. Cherubini, G. Crowley, A. Fomichev, M. Gorska, M. Gulino, M. S. Golovkov, M. Huyse, K. -M. Källman, M. Lattuada, T. Lönnroth, M. Mutterer, R. Raabe, A. Rodin, S. Romano, M. V. Rozhkov, B. B. Skorodumov, C. Spitaleri, O. Tengblad, G. Ter-Akopian, A. Tumino, P. Van Duppen, R. Wolski

This work is related to the review talk, which was presented by V. Goldberg at the XXVI Symposium on Nuclear Physics, January 6-9, 2003, Mexico.

A new role of resonance scattering in the studies of drip line nuclei as well as in some other applications is based on the following.

1. The binding energies of drip line nuclei are small by definition (or even positive); it means that lowest states can be populated in resonant elastic scattering.

2. The inverse kinematics thick target method gives the possibility to use a great variety of available radioactive beams for resonance investigations. The method provides for very high efficiency of measurements, so that even intensities of 1000 /s can be used, together with high resolution especially around 180 degrees (cm).

3. The resonance interaction of proton rich species on hydrogen touches the proton rich border of nuclear stability, while interaction of neutron rich nuclei with hydrogen provides a means to investigate even more neutron rich nuclei through their analog states.

4. An investigation of resonance states in proton rich nuclei gives the possibility to study states, which are below the threshold for nuclear decay due to the difference in the Coulomb interaction in the mirror neutron rich ones.

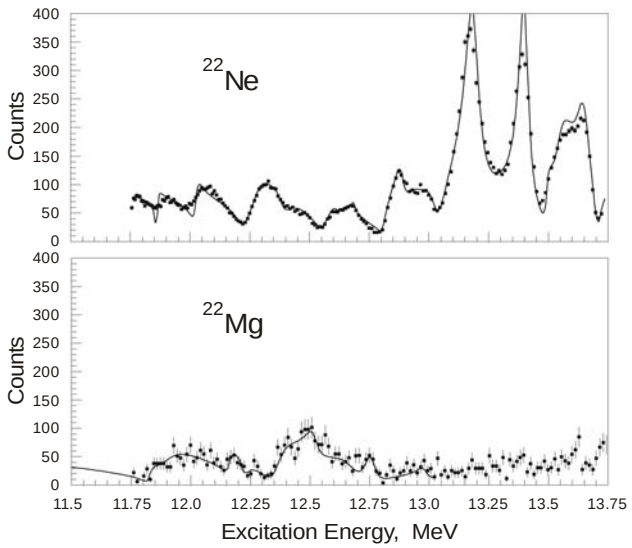

5. The observation of scattering at 180 degrees, where the Rutherford scattering is minimal, together with high energy of the recoils in the inverse kinematics, is an important issue for many studies of astrophysical interest.

Fig. 1 gives an example of investigation of the cluster structure in the mirror ^{22}Ne and ^{22}Mg nuclei. The disappearance of the intensive double stsructure of the ^{22}Ne spectrum in the ^{22}Mg spectrum gives some basis for the speculation of observation of the nuclear analog of the Josephson effect.

Evolution of Shell Structure to Drip Lines Near 1P Shell

V. Z. Goldberg

Investigation of T=5/2 levels in ^{9}Li [1] brought evidence for a surprisingly narrow width of the lowest ½$^{-}$ state. According to the single particle model the state should have the structure of one particle in the $p_{1/2}$ sub shell. This finding (as many others, see for example [2]) makes us consider a reason for changes of the conventional shell model structure near the neutron drip line.

High N/Z ratios result in low binding of the outermost neutrons. In ^{9}He the protons are bound by many MeV: the last neutron is unbound. Hence the wave functions of the outermost neutrons will extend far beyond the conventional nuclear radius. The spatial extent should correspond to a diffuse density distribution, and to a diffuse shell model potential.

Fig. 1 illustrates drastic changes in the shell model structure induced by a diffuse potential. (The specific example is given for A=13.) It can be seen in Fig. 1 (middle) that while a large energy gap still exists between 1s and 1p shells, the $1p_{3/2}$, $1p_{1/2}$, 2s and $d_{5/2}$ levels are almost degenerate in the diffuse potential. Since the spin-orbit potential has the radial form of a derivative of the central potential, it will be reduced in the strength, decreasing the gap between $p_{3/2}$ and $p_{1/2}$ levels in a diffuse potential (Fig.1c). In its turn, the enhanced density of the nearby continuum states increases the role of the pairing interaction.

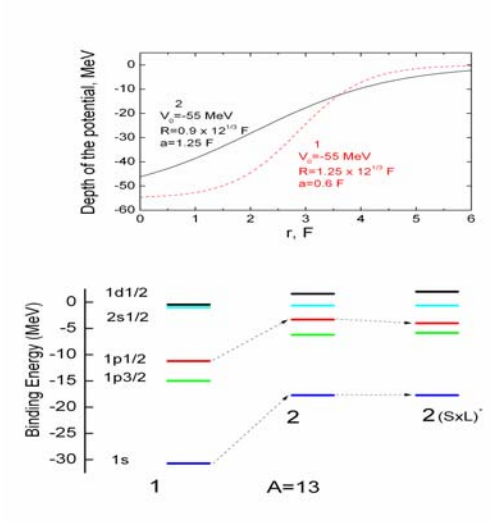

Figure 1. Left-levels in conventional potential; middle-levels in a diffused potential, right-(SL) potential decreased in accordance with r-dependence of the diffused potential.

Hence, the structure of the ground state in ^{8}He might be a complicated mixture of $p_{3/2}$, $p_{1/2}$, 2s, and $d_{5/2}$ configurations, quite different from the naïve picture of the closed $p_{3/2}$ sub shell. Therefore only part of the wave function of the ½- state in ^{9}He could be related with the nucleon decay to the ground state in ^{8}He resulting in the narrow width of this state.

In spite of the very qualitative character of the above considerations, it looks evident that in a diffuse potential 2s state appeared to be so close to the p1/2 state, that a small residual interaction can change the order of the levels without severely disturbing the single particle nature of the states. That is the situation, which is characteristic for the lowest states in ^{11}Be [3] and ^{11}N [4]. The s state is only 0.3 MeV below the $p_{1/2}$ state in ^{11}Be, and the low-lying 2+ level in ^{10}Be can be considered as a sign to take residual interaction into account. On other hand, the results [5] showed much larger descending of the s state in ^{9}He, and simultaneously it is known that a first excited state in ^{8}He is lying much higher than in ^{10}Be. All these make the results in [5] even more surprising.

References

[1] G. Chubarian, *et al.*, *Progress in Research*, Cyclotron Institute, Texas A&M University (2002-2003) p. I-34.

[2] R. F. Carsten, B. M. Sherrill, Prog. Part. Nucl. Phys. **43**, S171 (2000).

[3] F. Ajezenberg-Selove Nucl. Phys. **A433**, 1 (1985).

[4] L. Axelsson *et al*. Phys. Rev. C **54**, 1511(R) (1996).

[5] L. Chen *et al*. Phys. Lett. B **505**, 21 (2001).

Final State Interaction or a ^{3}H excited state?

V. Z. Goldberg, G. V. Rogachev, J. J. Kolata, L. V. Grigorenko, F. D. Becchetti, P. A. DeYoung, J. D. Hinnefeld, L. O. Lamm, J. Lupton, T. W. O'Donnell, D. A. Roberts, and S. Shaheen

Recently, resonance-like structure observed in the ^{1}H(^{6}He,α) reaction [1] was interpreted as an excited state of ^{3}H. After that, it was claimed [2], that low energy n-d scattering can be interpreted in terms of a virtual state in the vicinity of the n-d threshold. Another interesting idea was suggested in [4], that the existence of a previously unknown excited state of tritium would not be in contradiction with the available experimental data if a special structure was assumed for the resonance. Specifically, it must primarily consist of a "dineutron' bound to a proton. The importance of the main conclusion in [1], *viz.* the existence of an unknown state in a three nucleon system, cannot be overestimated.

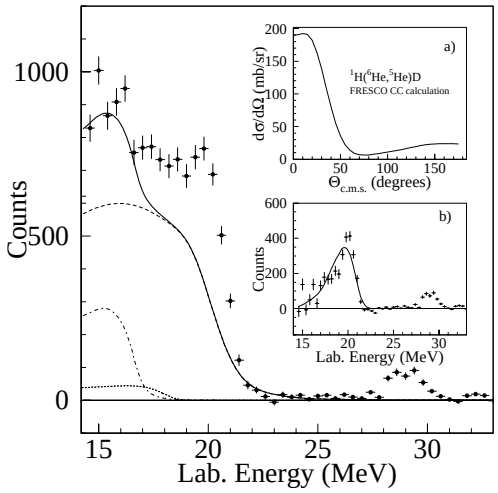

Figure 1. Description of the experimental α-particle spectra by different processes. The inset shows the α-particle spectrum after subtraction of the background (solid line). The curve in the inset shows the effect of three particle FSI.

The aim of this work was (i) to confirm the results, with a better experimental set up, because the experiment [1] was not without problems, and (ii)to consider, whether aspects of the reaction dynamics other than the interaction in the n-d channel can lead to resonance like behavior.

The main results of the present work are as follows: (i) the measured spectrum is in agreement with the results[1] (there is a peak in the α-particle spectrum corresponding to low energy in the n-d channel); (ii) none of the individual pair final state interactions in the system, except for the hypothetical state in the triton, can describe the experimental data; and (iii), the peak can however be explained by three body final state interactions together with the fact that total energy available for three particles (α, n, d) is rather low.

The latter explanation is of importance as a novel and unexpected effect of final state interactions for weakly bound nuclear systems.

References

[1] D.V. Alexandrov *et al.*, JETP Lett. **59,** 320 (1994).
[2] A. Csoto and G. M. Hale, Phys. Rev. C **59,** 1207 (1999).
[3] A. L. Barabanov, JETP Lett. **61**, 7 (1995)**.**

SECTION II

HEAVY ION REACTIONS

Temperature Dependence of the Isospin Distillation in Nuclear Fragmentation

D. V. Shetty for The NIMROD Collaboration

Temperature dependence of the isospin distillation in asymmetric nuclear matter was studied for ^{124}Sn + ^{124}Sn reaction at 28 MeV/A. Double isotope ratios were used to determine the temperature for fragments emitted along various laboratory angles. The bottom panels of the figure show temperatures extracted for the three emission angles of θ_{lab} = 4^o, 9.4^o and 32^o. The temperature is seen to evolve from 3.9 MeV at θ_{lab} = 4^o to 5.4 MeV for θ_{lab} = 32^o. Beyond θ_{lab} = 32^o, the temperature remains fairly constant indicating a unique thermalized source. The emission source was also characterized by performing a moving source fit on the kinetic energy spectra of the emitted particles. The top panels show isobaric ratios as a function of N/Z of the composite system for the two emission angles of θ_{lab} = 9.4^o and θ_{lab} = 32^o. It is observed that the isobaric ratios for the light clusters are comparatively higher for lower emission angle than those obtained for higher angles. The increase in isobaric ratio with decreasing emission angle indicates a significant enhancement of neutrons in the gas phase with decreasing temperature.

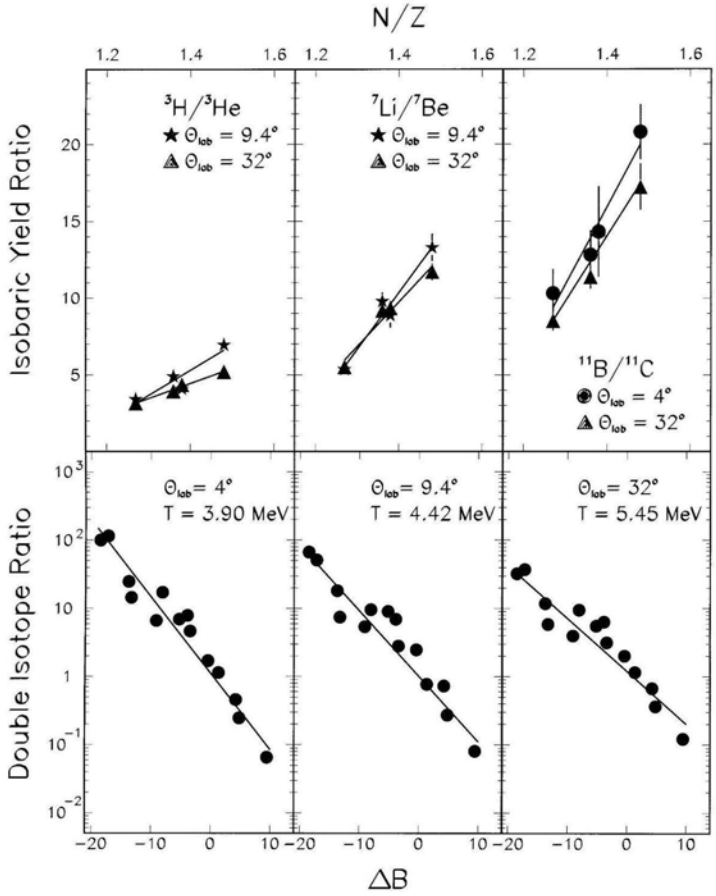

Figure 1. Double isotope ratio as a function of difference in binding energy at various laboratory angles (bottom panels). Isobaric ratio as a function of N/Z of the composite system at two different emission angles (top panels).

Midrapidity Emission in Nuclear Fragmentation

D. V. Shetty for The NIMROD Collaboration

Charged particle and their source of emission was studied in ^{124}Sn + ^{124}Sn reaction at 28 MeV/A by investigating the rapidity distribution. Figure 1 shows the rapidity distribution for ^{3}He, ^{4}He and ^{6}He isotopes for various charged particle multiplicity bins. While the rapidity distribution for all the He isotopes are observed to evolve identically as a function of multiplicity bin, the peak position of the distribution for the highest multiplicity bin are different for different He isotopes. The ^{3}He isotope for the highest multiplicity is observed to be centered closer to the projectile-like source velocity than the distributions for the ^{4}He and ^{6}He isotopes, which appear to evolve slowly towards midrapidity (dotted line). This indicates that the heavier isotopes of He may have different emission pattern. A similar evolution of the distribution with multiplicity bin is also observed when comparing the ^{4}He with heavier fragments like ^{7}Li and ^{11}B (right panels). However, here it is observed that for the highest multiplicity bin the fragments tend to localize closer to the midrapidity region with increasing fragment charge, Z. This suggests that the midrapidity region becomes increasingly favorable for fragments with higher charge Z. Also, a relative increase in the emission of heavy fragments with increasing centrality was observed in the yield ratios of the fragments (Z = 3 – 7) emitted in the forward and backward angles. The heavy fragments show a steep rise in their yields, compared to a gradual increase for the lighter fragments, as the centrality of the collision increases. The midrapidity region seems to be not only a neutron rich source but also a rich source of heavy fragment formation.

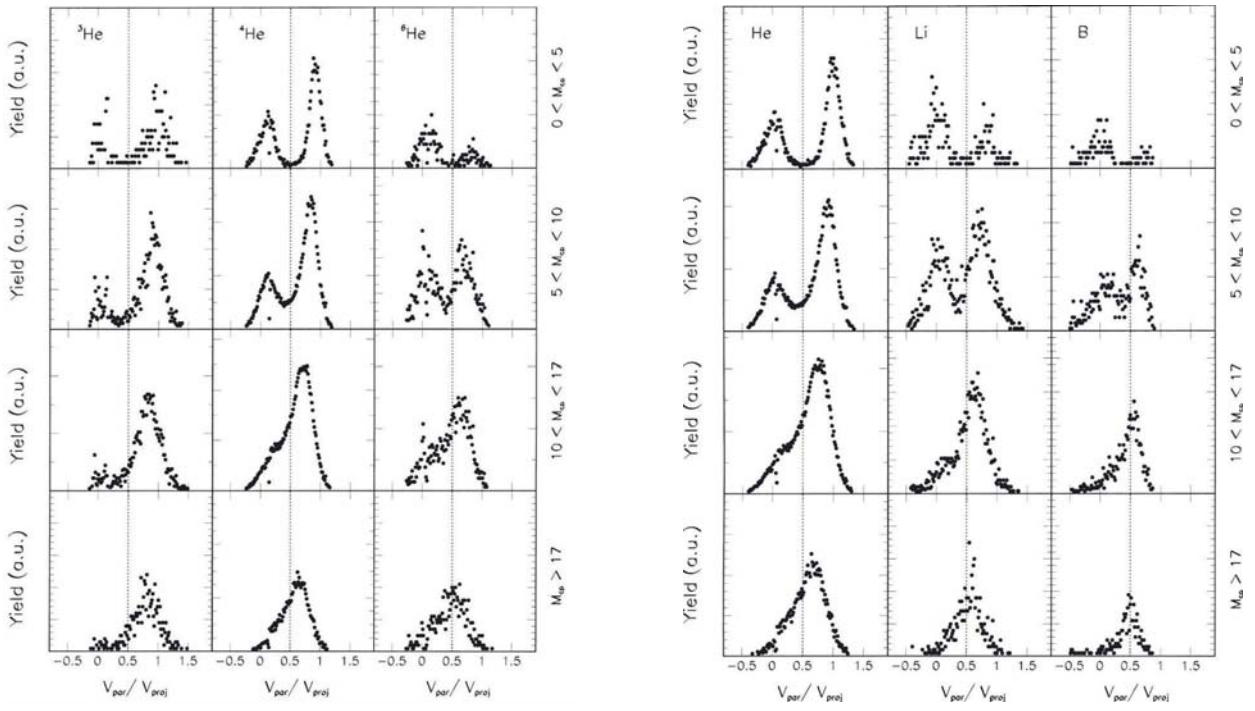

Figure 1. Rapidity distribution for the ^{3}He, ^{4}He and ^{6}He isotopes as a function of charged particle multiplicity bin in ^{124}Sn + ^{124}Sn reaction (left). (Right) same as the left, but for He, Li and B fragments.

Isospin Dependence of the <N/Z> in Nuclear Fragmentation

D. V. Shetty, for The NIMROD Collaboration

Fractionation of nuclear matter into a neutron rich gas composing of light clusters and a symmetric liquid phase consisting of heavy fragments has been predicted for isospin asymmetric nuclear matter [1]. This separation of excited nuclear matter into two phases affects the fragmentation process and can be studied by looking at the neutron content of the emitted fragments and how they differ between light and heavy fragments. If excited nuclear matter is separating into two phases, differing in isospin content, then light fragments may condense from the neutron rich gas, and heavy fragments may evaporate off of the more symmetric liquid. This would result in light fragments being more neutron rich than heavier fragments. Figure 1 shows the <N/Z> ratio of various intermediate mass fragments observed in four reactions having different neutron to proton content. The increase in <N/Z> of the fragments with

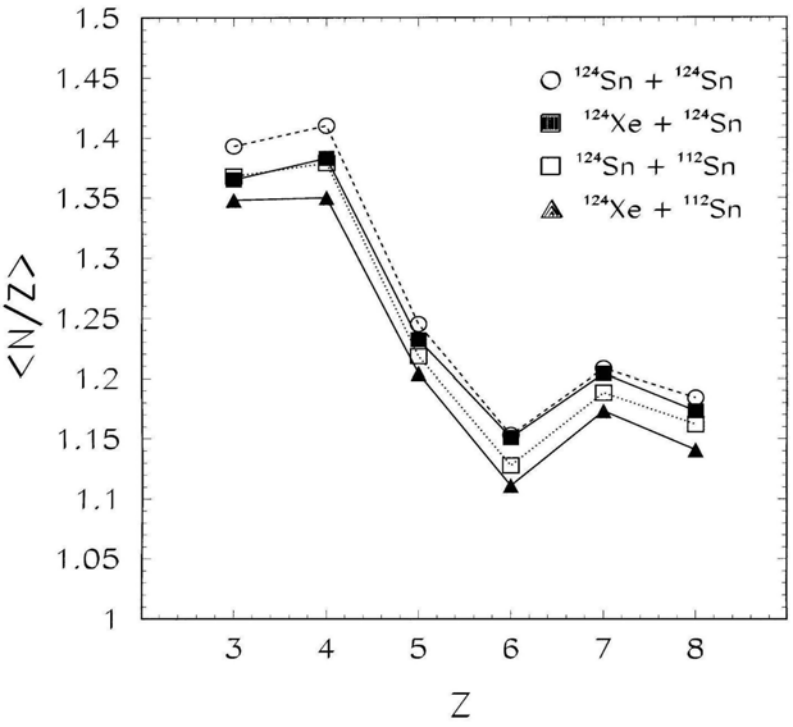

Figure 1. <N/Z> as a function of fragment charge, Z, for the ^{124}Sn, ^{124}Xe + ^{124}Sn, ^{112}Sn reactions at 28 MeV/nucleon. The lines through the symbols are drawn to guide the eye.

increasing isospin of the system and an overall decrease with increasing Z is clearly evident. The observation indicates that the excess neutrons in the composite system become available in the form of light neutron rich clusters, leaving the heavy fragments with relatively lower neutron content.

References

[1] H. Muller and B. Serot, Phys. Rev. C **52**, 2072 (1995).

Isospin Dependence of the Charge Distribution in Nuclear Fragmentation

D. V. Shetty, S. J. Yennello, E. Martin, A. Keksis, and G. Souliotis

The clusterization of nucleons into fragments in the fragmentation process of highly excited nuclei at intermediate energy is a subject of significant importance. It has been known that the yield distribution of the light cluster is characterized by a simple power law relation of the form, $P(Z) \alpha Z^{-\tau}$. This observation is believed to be a manifestation of phase transition in a system at equilibrium near it's critical temperature [1]. The distribution has been studied in the past as a function of both, the size and the excitation energy of the system. A very preliminary attempt has been made to study the isospin dependence of this yield distribution in ^{58}Ni + ^{58}Ni, ^{58}Fe + ^{58}Ni, ^{58}Ni + ^{58}Fe and ^{58}Fe + ^{58}Fe reactions at beam energies of 30, 40 and 47 MeV/nucleon. These reactions populate system of equal size but different excitation energy and isospin (N/Z). Figure 1 shows the rising steepness of the yield distribution with increasing bombarding energy, indicating a rise in the light cluster production with increasing temperature. However, the rise in the steepness also appears to depend on the isospin (N/Z) of the system. Attempts are being made to investigate this effect further.

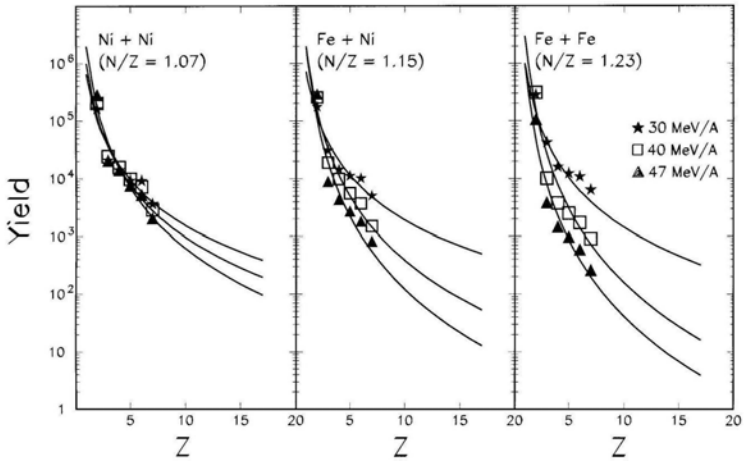

Figure 1. Charge distribution for the reactions ^{58}Ni + ^{58}Ni, ^{58}Fe + ^{58}Ni, and ^{58}Fe + ^{58}Fe at 30, 40 and 47 MeV/nucleon. The solid curves are the power law fit to the data.

References

[1] J. P. Bondorf, A. S. Botvina, A. S. Iljinov, I. N. Mishustin, and K. Sneppen, Phys. Rep. **257**, 133 (1995).

Isotopic Scaling of Heavy Projectile Residues from Deep-Inelastic Collisions at Fermi Energies

G. A. Souliotis, D. V. Shetty, M. Veselsky, G. Chubarian, L. Trache, A. Keksis, E. Martin, S. J. Yennello

The scaling of the yields of heavy projectile residue from the reactions of 25 MeV/nucleon ^{86}Kr projectiles with ^{124}Sn, ^{112}Sn and ^{64}Ni, ^{58}Ni targets is studied [1].

Isotopically resolved yield distributions of projectile fragments in the range Z=10-36 from these reaction pairs were measured with the MARS recoil separator in the angular range 2.7^o-5.3^o. For these deep inelastic collisions, the velocities of the residues, monotonically decreasing with Z down to Z~26-28, are employed to characterize the excitation energy. The yield ratios R_{21}(N,Z) for each pair of systems are found to exhibit isoscaling, namely, an exponential dependence on the fragment atomic number Z and neutron number N (e.g. Fig. 1). The isoscaling is found to occur in the residue Z range characterized by (almost) constant velocities, on average, implying constant excitation energies. The corresponding isoscaling parameters are α=0.43 and = –0.50 for the Kr+Sn system and α=0.27 and β=–0.34 for the Kr+Ni system (Fig. 2). These parameters are in general agreement with values reported recently in the literature [2,3].

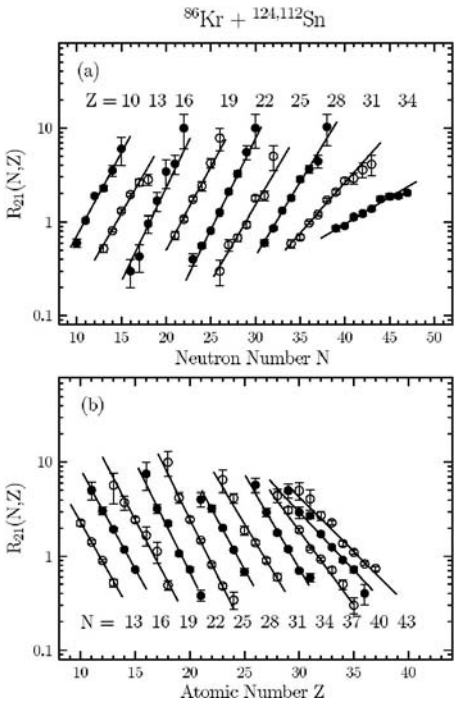

Figure 1. Yield ratios R_{21} (N,Z) = Y_2 (N,Z)/Y_1 (N,Z) of projectile residues from the reactions of ^{86}Kr (25MeV/nucleon) with ^{124,112}Sn (a) with respect to N for the Z's indicated, and (b) with respect to Z for the N's indicated. The data are given by alternating filled and open circles, whereas the lines are exponential fits.

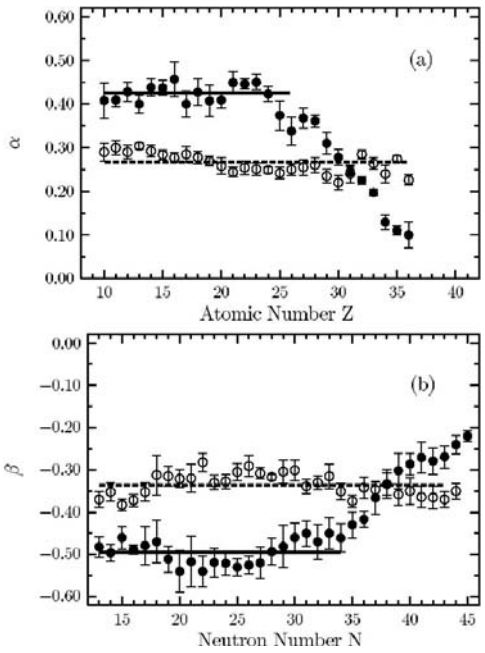

Figure 2. (a) Isoscaling parameter as a function of Z for projectile residues from the reactions ^{86}Kr(25MeV/nucleon)+^{124,112}Sn (closed circles) and ^{86}Kr(25MeV/nucleon) + ^{64,58}Ni (open circles). The straight lines are constant value fits for each system (see text). (b) Isocaling parameter as a function of N for ^{86}Kr (25 MeV/nucleon) +^{124,112}Sn (closed circles) and ^{86}Kr (25MeV/nucleon) +^{64,58}Ni (open circles). The straight lines are again constant value fits for each system.

For the Kr+Sn system, for which the experimental angular acceptance range lies inside the grazing angle, isoscaling was found to occur for Z<26 and N<34. The extracted values of the isoscaling parameters are used to

extract the neutron and proton chemical potentials, as well as obtain an estimate of the symmetry energy coefficient of highly excited primary fragments. For heavier fragments from Kr+Sn, the parameters vary monotonically, α decreasing with Z and β increasing with N (Fig. 2). This variation is found to be related to the evolution towards isospin equilibration and, as such, it can serve as a tracer of the N/Z equilibration process.

The present heavy-residue data demonstrate the occurrence of isotopic scaling from the intermediate mass fragment region to the heavy-residue region. Interestingly, such high-resolution mass spectrometric data may provide important information on the role of isospin and isospin equilibration in peripheral and mid-peripheral collisions, complementary to that accessible from large acceptance multidetector devices. Continuation of the present studies employing the newly commissioned Superconducting Solenoid Line (BigSol) is currently underway.

References

[1] G. A. Souliotis *et al*., nucl-ex/(May 2003).
[2] M. B. Tsang *et al*., Phys. Rev. Lett. **86**, 5023 (2001).
[3] A. Botvina *et al*., Phys. Rev. C **65**, 044610 (2002).

Enhanced Production of Neutron-Rich Rare Isotopes in Peripheral Collisions at Fermi Energies

G. A. Souliotis, M. Veselsky, G. Chubarian, L. Trache, A. Keksis, E. Martin, D. V. Shetty, S. J. Yennello

The cross sections and velocity distributions of projectile-like fragments from the reactions of 25 MeV/nucleon ^{86}Kr + ^{124}Sn,^{112}Sn have been measured using the MARS recoil separator at Texas A&M, with special emphasis on the neutron rich isotopes [1]. This work is an extension of our previous work on the reaction 25 MeV/nucleon ^{86}Kr + ^{64}Ni reported elsewhere [2]. Proton-removal and neutron pick-up isotopes have been observed with large cross sections. A model of deep-inelastic transfer (DIT) [3] for the primary interaction stage and the statistical evaporation code GEMINI [4] for the deexcitation stage have been used to describe the properties of the product distributions. The results have also been compared with the EPAX [5] parametrization of high-energy fragmentation yields.

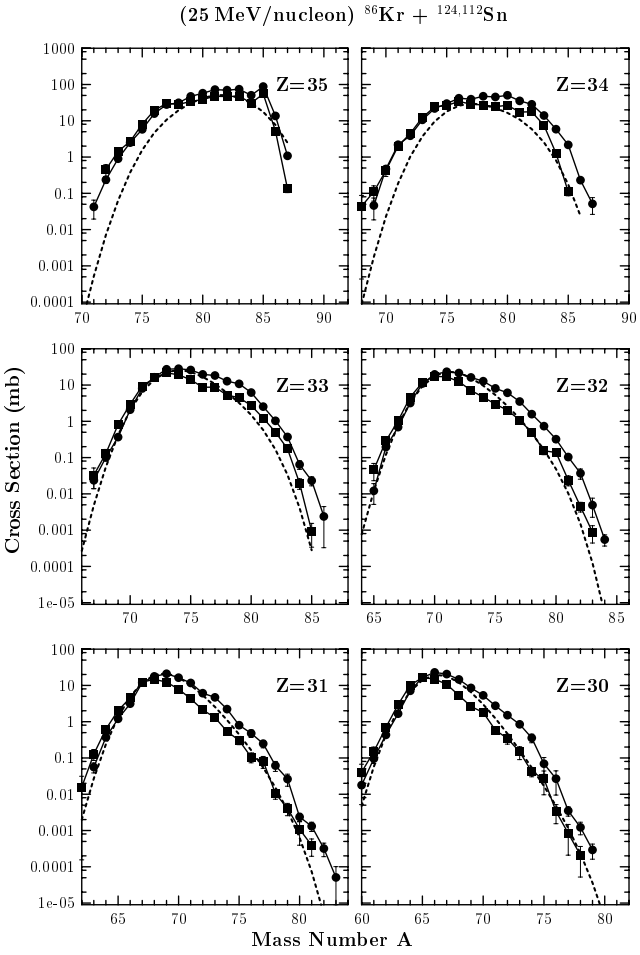

Figure 1. Mass distributions of elements Z=30-35 from the reaction of ^{86}Kr (25MeV/nucleon) with ^{124}Sn and ^{112}Sn. The data are shown by full circles for ^{86}Kr+^{124}Sn and full squares for ^{86}Kr+^{112}Sn. The dotted lines are EPAX expectations [5].

A large enhancement in the production of neutron-rich projectile residues is observed in the reaction of the ^{86}Kr beam with the neutron rich ^{124}Sn target relative to the predictions of the EPAX parametrization of high-energy fragmentation, as well as relative to the reaction with the less neutron-rich ^{112}Sn target (Fig. 1). The data demonstrate the significant effect of the target neutron-to-proton ratio (N/Z) in peripheral collisions at Fermi energies.

The hybrid DIT/GEMINI model appears to account for part of the observed large cross sections. The DIT simulation indicates that the production of neutron-rich nuclides in these reactions is associated with peripheral nucleon exchange in which the neutron skin of the neutron-rich ^{124}Sn target nucleus may play an important role. Similar conclusions have been drawn from recent calculations for the 25 MeV/nucleon ^{86}Kr + ^{64}Ni reaction [1,2].

From a practical viewpoint, such reactions between massive neutron-rich nuclei offer a novel and attractive synthetic avenue to access extremely neutron-rich rare isotopes towards the neutron-drip line.

Applications are investigated for the Texas A&M Cyclotron Institute upgrade and, in the far future, for the Rare Isotope Accelerator Facility (RIA).

References

[1] G. A. Souliotis *et al*., nucl-ex/0302011 (2003).
[2] G. A. Souliotis *et al*., Phys. Lett. B **543**, 163 (2002).
[3] L. Tassan-Got and C. Stefan, Nucl. Phys. **A524**, 121 (1991).
[4] R. Charity *et al*., Nucl. Phys. **A483** 371, (1988).
[5] K. Summerer and B. Blank, Phys. Rev. C **61**, 034607 (2000).

Energy Dependence of the Isotopic Composition in Nuclear Fragmentation

D. V. Shetty, S. J. Yennello, E. Martin, A. Keksis, and G. Souliotis

Theoretical studies based on isospin dependent interaction and nuclear equation of state predict drastic changes in the nature of liquid gas phase transition for isospin asymmetric nuclear matter [1]. Isotopic composition of the fragments emitted in ^{58}Ni + ^{58}Ni, ^{58}Fe + ^{58}Ni, ^{58}Ni + ^{58}Fe and ^{58}Fe + ^{58}Fe reactions were studied at beam energies of 30, 40 and 47 MeV/nucleon. The relative free neutron and proton density in the vapor phase was extracted from the measured isotope and isotone yield ratios as a function of N/Z of the composite system. It is observed that the neutron content of the vapor phase is sensitive to, both, the isospin (N/Z) of the initial colliding nuclei and the excitation energy. The asymmetry of the nucleons in the gase phase increases with the isospin, (N/Z), of the composite nuclei and decreases with increasing beam energy. The present observations indicate a temperature dependence of the isotopic composition consistent with those predicted by the isospin dependent calculation.

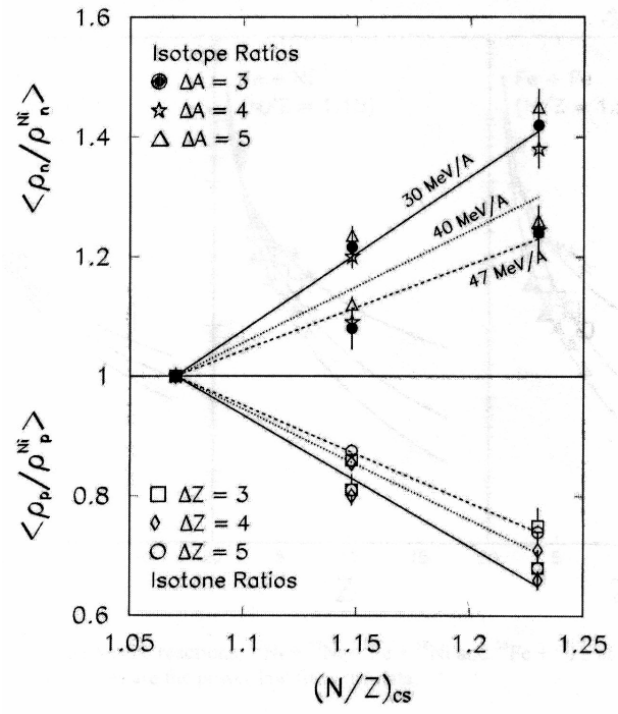

Figure 1. Relative free neutron (top) and proton density (bottom) as a function of N/Z of the composite system for various beam energies.

References

[1] B. A. Li and W. Schroder, eds., Isospin Physics in Heavy Ion Collisions at Intermediate Energies (Nova Science, New York, 2001).

Progress in Research of Isospin Equilibration

E. Martin for the NIMROD Collaboration

Many studies of isospin dependence of nuclear phenomena related to fragmentation from heavy-ion collisions have been conducted in recent times. NIMROD was used to examine the reactions of 35 and 45 MeV/nucleon $^{54, 58}$Fe and $^{58, 64}$Ni on $^{54, 58}$Fe and $^{58, 64}$Ni in order to study isospin equilibration. The beams were produced by the K500 Superconducting Cyclotron at the Cyclotron Institute of Texas A&M University using NIMROD, or the Neutron Ion Multidetector for Reaction Oriented Dynamics.

Figure 1 shows isotopic ratios for 35 and 45 MeV/nucleon ^{58}Fe, ^{58}Ni + ^{58}Fe, ^{58}Ni plotted as function of the (N/Z) content of the compound system. The error bars shown are statistical errors and the lines are meant to guide the eye. When two systems having differing entrance channel (N/Z) content but the same compound system (N/Z) content show isobaric or isotopic ratios with similar values, the systems are said to have reached isospin equilibrium [1]. Within the error bars, the data in Figure 1 show that isospin equilibrium had been reached prior to fragment emission. An error-weighted linear fit was put to the isobaric data in Figure 1.

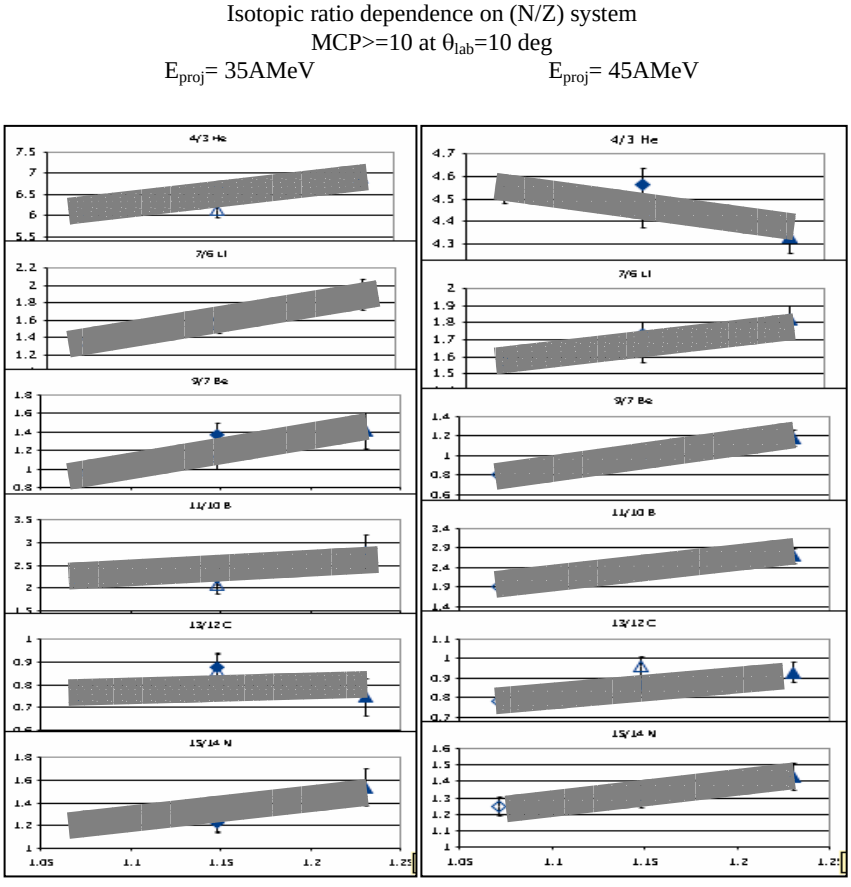

Figure 1. Isotopic ratios are shown plotted as a function of compound system (N/Z) content for four systems (^{58}Fe, ^{58}Ni + ^{58}Fe, ^{58}Ni) at two energies, 35 and 45 MeV/nucleon. The error bars show statistical errors and the lines are to guide the eye.

In future data analysis, the systems shown here will increase in statistics and more systems and angles will be added as the calibrations continue. The N/Z tracer method, as cited in ref. [2], will be used to gauge the amount of isospin equilibration that had occurred in the system prior to fragment emission, but at a more intermediate energy than in ref. [2].

References

[1] H. Johnston, *et al.*, Phys. Lett. B **371**, 186 (1996).

[2] F. Rami, *et al.*, Phys. Rev. Lett. **84**, 1120 (2002).

Isospin Dependence of Quasiprojectile Fragmentation using Mass 40 Isobars on $^{112, 124}$Sn Using FAUST

A. L. Keksis, M. Veselsky, G. A. Souliotis, E. Martin, D. Shetty, and S. J. Yennello

The isospin asymmetry term in the nuclear equation of state, EOS, can be studied using isobaric nuclei. The EOS is important for understanding astrophysical processes, such as neutron star cooling and the r-process [1, 2]. Increasing the isospin asymmetry produces new phenomena such as proton and neutron halos, and changes nuclear properties such as the nuclear density [3, 4].

This research was performed at Texas A&M University's Cyclotron Institute using FAUST [5, 6], the Forward Array Using Silicon Technology (FAUST) shown in Figure 1. The calibration and gating procedures were previously described [7]. During this period the decoding and analysis procedures have been under development. There are two paths that are being pursued. One focuses on adapting the new lab standard, CycApps, which was developed for NIMROD data, to handle FAUST data. The other focuses on another NIMROD analysis program, which was used successfully by Veselsky to analyze FAUST data.

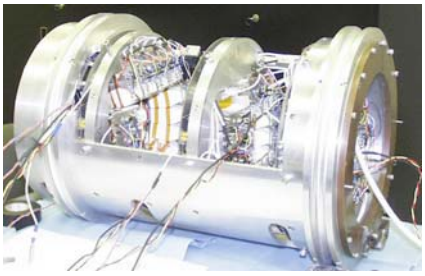

Figure 1: The FAUST forward array.

As of this writing systematic measurements with stable beams of ^{40}Ca, ^{40}Ar and ^{48}Ca at 32 and 45 MeV/u are underway. Then using the Superconducting Solenoid Rare Isotope Beam Line [8] rare ion beams such as ^{40}Sc ($t_{1/2}$ 0.1823 sec.), ^{40}Cl ($t_{1/2}$ 1.35 min.) and possibly ^{40}S ($t_{1/2}$ 8.8 sec.) will be produced and identified with TOF techniques. Rare ion beams allow for greater isospin asymmetric nuclei to be studied, which is one area that is of great interest since a plethora of beams will be available when RIA, the **R**are **I**sotope **A**ccelerator, comes online early next decade.

References

[1] B. A. Li *et al.*, Int. J. Mod. Phys. E **7**, 147 (1998).
[2] B. A. Li., Phys. Rev. Lett. **85**, 4221 (2000).
[3] J. Symons (Chair) *et al.*, *Opportunities in Nuclear Science: A Long-Range Plan for the Next Decade*, (April 2002).
[4] M. Colonna *et al.*, Phys. Rev. C **57**, 1410 (1998).
[5] F. Gimeno-Nogues *et al.*, Nucl. Instrum. Methods Phys. Res. A **399**, 94 (1997).
[6] R. Laforest *et al.*, Nucl. Instrum. Methods Phys. Res. A **404**, 470 (1998).
[7] A. L. Keksis *et al.*, *Progress in Research*, Cyclotron Institute, Texas A&M University (2001-2002), p. II-38.
[8] T. W. O'Donnell *et al.*, Nucl. Instrum. Methods Phys. Res. A **422**, 513 (1999) and **353**, 215 (1994).

Evidence of Critical Behavior in the Disassembly of Nuclei with A ~ 36

Y. G. Ma, R. Wada, K. Hagel, J. Wang, T. Keutgen,[1] Z. Majka,[2] M. Murray, L. Qin, P. Smith, J. B. Natowitz, R. Alfarro,[3] J. Cibor,[2] M. Cinausero,[4] Y. El Masri,[1] D. Fabris,[5] E. Fioretto,[4] A. Keksis, M. Lunardon,[5] A. Makeev, E. Martin, Martinez-Davalos,[3] A. Menchaca-Rocha,[3] G. Nebbia,[5] G. Prete,[4] V. Rizzi,[5] A. Ruangma, D. V. Shetty, G. Souliotis, P. Staszel,[2] M. Veselsky, G. Viesti,[5] E. M. Winchester, S. J. Yennello

[1]*UCL, Louvain-la-Neuve, Belgium,* [2]*Jagellonian University, Krakow, Poland,* [3]*UNAM, Mexico City, Mexico,* [4]*INFN Laboratori Nazionali di Legnaro, Legnaro, Italy,* [5]*INFN Dipartimento di Fisica, Padova, Italy*

Most efforts to determine the critical point for the expected liquid gas-phase transition in finite nucleonic matter have focused on examinations of the temperature and excitation energy region where maximal fluctuations in the disassembly of highly excited nuclei are observed. Data from the EOS and ISiS collaborations have been employed to construct a co-existence curve for nucleonic matter [1]. Those analyses have proceeded under the assumption that the point of apparent critical behavior was the true critical point of the system. However, some recent theoretical treatments suggest that apparent critical behavior may be encountered well away from the actual critical point [2] that excited lighter nuclei provide the most favorable venue for investigation of the critical point in finite nuclei. In this work we report results of an extensive investigation of nuclear disassembly in nuclei of A ~ 36, excited to excitation energies as high as 9 MeV/nucleon.

Using the TAMU NIMROD detector and beams from the TAMU K500 super-conducting cyclotron, we have probed the properties of excited projectile-like fragments produced in the reactions of ^{40}Ar + ^{27}Al, ^{48}Ti and ^{58}Ni at 47 MeV/nucleon. Earlier work on the reaction mechanisms of near symmetric collisions of nuclei in the 20<A<64 mass region at energies near the Fermi energy have demonstrated the essential binary nature of the collisions, even at relatively small impact parameters [3]. As a result, these collisions prove to be very useful in preparing highly excited light nuclei with kinematic properties which greatly simplify the detection and identification of the products of their subsequent de-excitation.

A wide variety of observables indicate that maximal fluctuations in the disassembly of hot nuclei with A~36 occur at an excitation energy of 5.6 ± 0.5 MeV and temperature of 8.3 ± 0.5 MeV.

Associated with this point of maximal fluctuations are a number of quantitative indicators of apparent critical behavior. First, the charge distribution shows a minimum power-law parameter ~2.2 which is consistent with the critical behavior predicted by Fisher's Droplet Model. Second, a number of indicators show the largest fluctuation, for instance, a Campi scatter plot shows that equal branches for the liquid and gas phases, the charge distribution of the largest fragment (Z_{max}) and the total kinetic energy show the maximum fluctuations, the behavior of the Δ-scaling of Z_{max} [4] shows a change from Δ=1/2 to

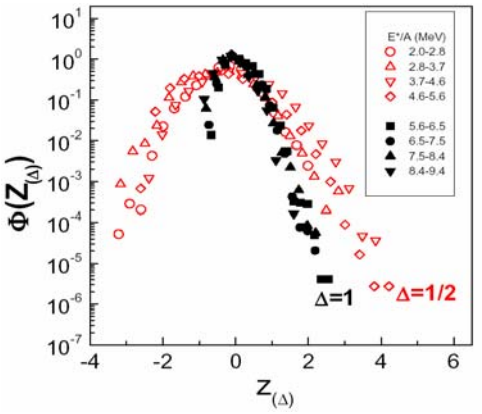

Figure 1. The Δ-scaling of Zmax.

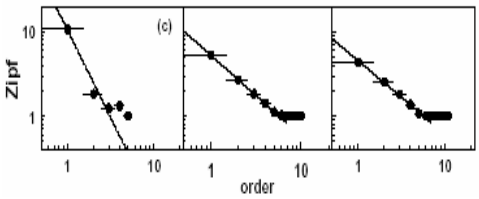

Figure 2. The Zipf-plot in three E*/A window (left: 2.0-2.8, middle: 5.6-6.5, right: 7.5-8.5).

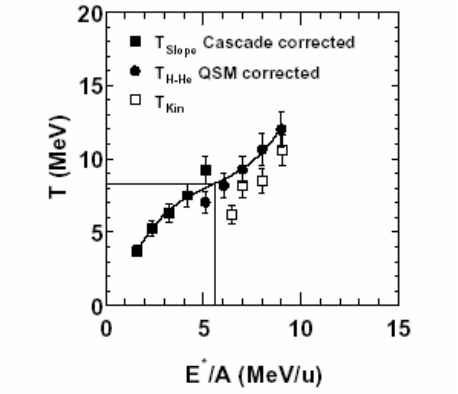

Figure 3. The caloric curves. The filled squares present the initial temperature deduced from the correction from cascade assumption (liquid phase), the filled circles how the initial temperature with the quantum statistical model correction (gas phase), and the open squares depict the thermal kinetic temperature.

Δ=1 scaling around the critical point (see Fig.1). Third, the fragment topological structure also indicates critical behavior, for instance, the Zipf law, which describes the mean sizes of the rank-ordered fragments as a function of the rank, is satisfied in the critical point [5] (see Fig.2), the charge correlation between the heaviest fragment and the second heaviest fragment also display behavior change around the critical point. Moreover, analysis of bimodality and critical exponent are consistent with the phase change at that point. The associated caloric curve does not appear to show a plateau such as that seen for heavier systems (see Fig.3). This may indicate that, in contrast to quasi-plateauing of caloric curves in heavier nuclei, the observed behavior in these very light nuclei may well be associated with a phase change in an equilibrated system at, or extremely close to, the critical point.

References

[1] R. Botet *et al*., Phys. Rev. Lett. **86**, 3514 (2001).
[2] J. B. Natowitz *et al*., ArXiv nucl-ex / 0206010.
[3] J. Peter *et al*., Nucl. Phys. **A593**, 95 (1995).
[4] R. Botet *et al.*, Phys. Rev. Lett. **86**, 3514.
[5] Y. G.. Ma, Phys. Rev. Lett. **83**, 3617 (1999).

Multifragmentation and Cold Fragment Emission

R. Wada, T. Keutgen, K. Hagel, M. Murray, Y. G. Ma, L. Qin, J. S. Wang, P. Smith, J. B. Natowitz, A. Makeev, A. Ono[1] and the NIMROD Collaboration

[1]*Tohoku University, Sendai, Japan*

A detailed study of the multifragmentation mechanism has been performed using the calculated central collision events of ^{64}Zn + ^{58}Ni, ^{92}Mo, ^{197}Au, at 26A, 35A and 47A MeV. The events are generated by Antisymmetrized Molecular Dynamics Model (AMD-V) with a Gogny type interaction of the stiff equation of state (EOS). This parameter set describes best the recent NIMROD results. In these calculated events multifragment production is observed in all cases and two features are commonly observed. One is that preequilibrium light particle emissions occur from the overlap zone of the projectile and the target. Another feature observed is that fragments are emitted rather cold. In Fig. 1 the excitation energy and emission time of fragments are plotted for ^{197}Au at 47A MeV. It is clearly seen that the excitation energies

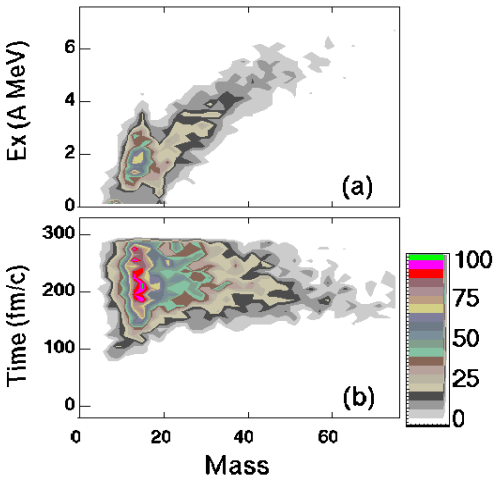

Figure 1. Excitation energy and emission time of fragments as a function of fragment mass from ^{64}Zn+^{197}Au at 47A MeV. The values are evaluated when the fragments are identified at the first time.

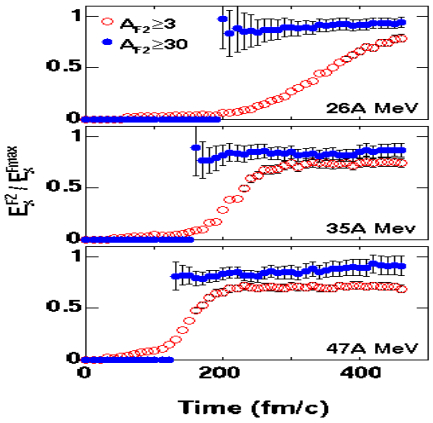

Figure 2. Ratio of the excitation energies of the largest fragment (F_{max}) and the second largest fragment (F_2) for ^{64}Zn+^{197}Au. Results for F_2 with all fragments (Z > 2) are shown by circles and those for F_2 with A ≥ 30 are shown by dots.

of light fragments are much lower than that of the maximum mass fragment. These fragments are not necessarily emitted at early stages as seen in (b). In order to elucidate the equilibration time of the system, the ratio of the excitation energies of the largest fragment (F_{max}) and the second largest fragment (F_2) is plotted in Fig. 2. When fragments with A < 30 are excluded from F_2, the ratio stays constant from the earliest time when F_2 is first identified. This indicates that the system reaches a thermal equilibrium before this time. These calculated results indicate that, after the emission of preequilibrium particles, smaller fragments are formed relatively cold and the system reaches a thermal equilibrium. In this environment these small fragments behave like nucleons and share the excitation energy of the system mainly as kinetic energy and little as internal energy. When the system undergoes multifragmentation, rather cold fragments are emitted.

Neutron Ball Efficiency Calculation for NIMROD

M. Murray, R. Wada, T. Keutgen, K. Hagel, Y. G. Ma, J. B. Natowitz, J. Cibor, L. Qin, C. Hamilton, A. Makeev, A. Ono[1] and the NIMROD Collaboration

[1]*Tohoku University, Sendai, Japan*

The neutron ball efficiency in NIMROD has been evaluated using the GCalor code coupled to the GEANT-3 simulation package. The geometry and material of the Neutron Ball and the charged particle array have been taken into account in detail in the program. Calculations were made for neutrons emitted isotropically from the target with energies from 2 to 100 MeV in 2 MeV steps. Each neutron was followed until either it escaped from the neutron ball or became thermalized (E <0.03 eV). If it is thermalized inside the liquid scintillator, we assumed the neutron was captured by the Gadolinium. The program was run in two modes, i.e., with the charged particle array and without the array to specify different contributions to the efficiency. In Fig.1 the calculated results are shown both without and with the charged particle array. For comparison the results calculated from the program DENIS are also shown by a solid line for the case without the charged particle array [1]. Since DENIS does not include neutron generation by materials inside, a significant discrepancy appears above 20 MeV.

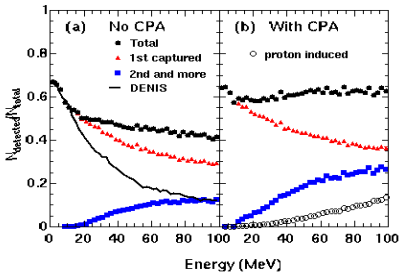

Figure 1. Calculated neutron ball efficiency without the charged particle array (a) and with the charged particle array (b). Neutron efficiency at a given neutron energy is shown by dots. The contribution for the first detected neutrons is shown by triangles and that for the second and higher order detected is shown by squares. The solid line in the left figure shows results from the DENIS code. The open circles neutrons in the right figure indicates the detection efficiency of the neutrons when a proton of an initial energy given on x-axis is emitted at the target.

The above calculated results have been applied to actual reactions of 64Zn + 58Ni, 92Mo and 197Au at 47A MeV. In Fig.2 the experimental neutron multiplicities are compared to the results of AMD-V calculations, filtered through the above calculated efficiencies. For lighter targets, reasonable agreements are obtained whereas for 197Au the calculation overpredicts by about 3 neutrons.

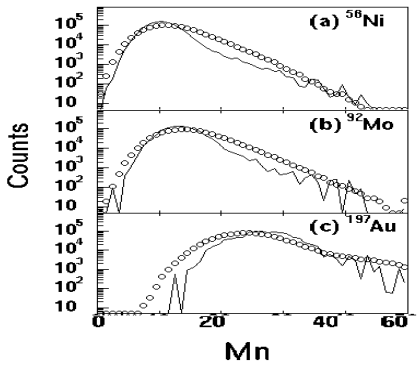

Figure 2. Neutron Ball multiplicities for ^{64}Zn + ^{58}Ni, ^{92}Mo and ^{197}Au at 47A MeV. Observed experimental results are shown by circles. Solid lines are the calculated results. The calculations are made using AMD-V with the standard Gogny interaction (soft EOS) and filtered through the calculated Neutron Ball efficiencies.

References:

[1] R. P. Schmitt *et al.*, Nucl. Instrum. Methods Phys. Res. A **354**, 487 (1995).

Reaction Dynamics and Equation of State in Fermi Energy Heavy Ion Reactions

R. Wada, T. Keutgen, K. Hagel, M. Murray, Y. G. Ma, L. Qin, J. S. Wang, P. Smith, J. B. Natowitz, A. Makeev, A. Ono[1] and the NIMROD Collaboration

[1]*Tohoku University, Sendai, Japan*

Three reaction systems, ^{64}Zn + ^{58}Ni, ^{92}Mo, ^{197}Au, at 26A, 35A and 47A MeV have been studied using a 4π detector array NIMROD. The analysis has now been completed. The observed results have been compared with Antisymmetrized Molecular Dynamics model (AMD-V) calculations [1] employing Gogny type effective interactions corresponding to soft (K=228 MeV) and stiff (K=360 MeV) equations of state (EOS). Effects of different in-medium NN cross sections, an empirical formulation [2] (NN_{emp}) and those from Li-Machleidt [3](NN_{LM}), were also examined. Direct observables, such as multiplicity distributions, charge distributions, energy spectra and velocity spectra, have been compared in detail with those of the calculations.

General trends of the experimental results are well reproduced by all calculations. In Fig.1 typical experimental multiplicity distribution of charged particles are compared with the AMD-V calculated results with different parameter sets. Energy spectra and charge distributions are also reproduced reasonably by all calculations and no significant preference for the parameters is observed from these comparisons.

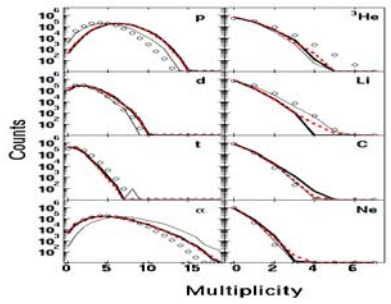

Figure 1. Multiplicity distributions of selected charged particles. Symbols show experimental data. Thin, dashed and thick lines correspond to the calculated results for soft EOS +NNemp, stiff EOS +NNemp and stiff EOS+NNemp, respectively.

However, the velocity distribution of alpha particles and heavier fragments shows a distinct difference for the soft EOS and the stiff EOS. In Fig.2 Gallilean invariant velocity distributions for Z=7 and 8 are compared with the calculated results for the soft EOS and the stiff EOS at 47A MeV. For ^{58}Ni the experimental distribution clearly favors the stiff EOS. A similar result is obtained for the velocity distribution of alpha particles.

None of the observables studied in the present work is sensitive enough to choose between the different formulations of the in-medium NN cross section, employed here.

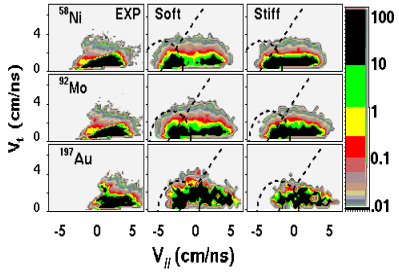

Figure 2. Gallilean invariant velocity distributions for fragments with Z=7 and 8. Experimental results are shown on the left column, the calculated results for soft EOS +NNemp, stiff EOS +NNLM are shown in the middle and right column. Dashed lines indicate the detection limit.

References

[1] A. Ono *et al.*, Phys. Rev. C **53**, 2958, (1996); Phys. Rev. C **59**, 853 (1999).

[2] A. Ono *et al.*, Phys. Rev. C **48**, 2946 (1993).

[3] G. Q. Li *et al.*, Phys. Rev. C **48**, 1702 (1993); Phys. Rev. C **49**, 566 (1994).

Nuclear Expansion and Cooling in Heavy Ion Reactions at Intermediate Energy

J. S. Wang, R. Wada, K. Hagel, Y. Ma, T. Keutgen, L. Qin, M. Murray, A. Makeev, P. Smith, J. B. Natowitz, J. Cibor, C. Hamilton, E. Martin, S. Liddick, D. Rowland, A. Ruangma, M. Veselsky, E. Winchester, G. Souliotis, S. J. Yennello, A. Samant[1], M. Cinausero[1], D. Fabris[1], E. Fioretto[1], M. Lunardon[1], G. Nebbia[1], G. Prete[1], G. Viesti[1], Z. Majka[2], P. Staszel[2]; S. Kowalski[3], W. Zipper[3], M. E. Brandan[4], A. Martinez-Rocha[4], A. Menchaca-Rocha[4] and Y. El Masri[5]

[1]*INFN-Legnaro, Padova, Italy,* [2]*Jagiellonian University, Krakov, Poland,* [3]*Silesian University, Katowice, Poland,* [4]*IFUNAM, Mexico,* [5]*UCL, Louvain-la-Neuve, Belgium*

Studies of dynamic processes in heavy ion nuclear reactions at intermediate energy have been extensively performed. The phenomenon of expansion and cooling has been observed [1,2] but the detailed process is still an open question. With the recently developed method of coalescence model analysis, employing the relationship between surface velocity and emission time from AMD calculations, it becomes possible to study the evolution of nuclear expansion and cooling during the process of heavy ion reactions in more detail.

Our studies were done for four reactions with entrance channel mass around 150, 47A MeV ^{64}Zn + ^{92}Mo, 35A MeV ^{64}Zn + ^{92}Mo, 40A MeV ^{40}Ar + ^{112}Sn and 55A MeV ^{27}Al + ^{124}Sn, performed using the 4pi detector(NIMROD) at TAMU. About 10% of the most central collision events were selected except for 47AMeV ^{64}Zn + ^{92}Mo for which mid-central collision events were selected in order to match the excitation energy for 35AMeV ^{64}Zn + ^{92}Mo. The excitation energies for all four reactions are matched by constraining to same mean neutron ball and charged particle multiplicity.

It has been pointed out that the surface velocity can be related to the particle emission time in QMD calculations [3,4]. The linear relation between the surface velocity at 60~120 degrees in the NN frame and the emission time is shown in Fig. 1. These were obtained for all four systems from AMD simulations that well reproduce the multiplicity and energy spectra of light charged particles [5].

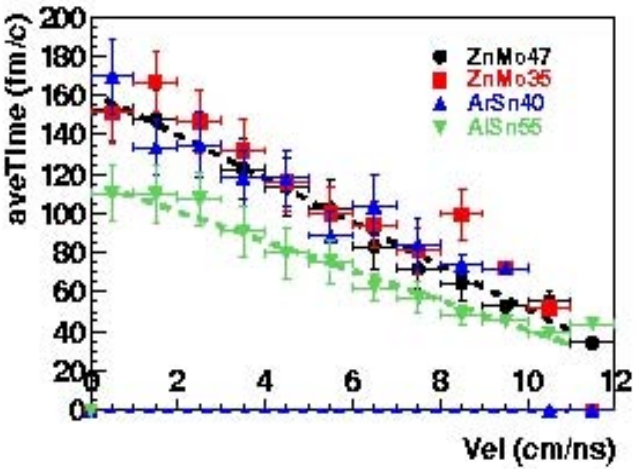

Figure 1. Average emission time of proton as a function of surface velocity at 60~120 degrees in the NN frame (from AMD simulations).

After applying three source fits to energy spectra from 3.6^{o} to 170^{o} in the laboratory frame, we extract the energy spectra of the NN source (coulomb energies and the TLF component are subtracted using Monte Carlo methods in an event-by-event analysis. Then the double isotope ratio temperatures T_{HHe} with surface velocity at 70~80 degrees in the NN frame are derived (Fig. 2).

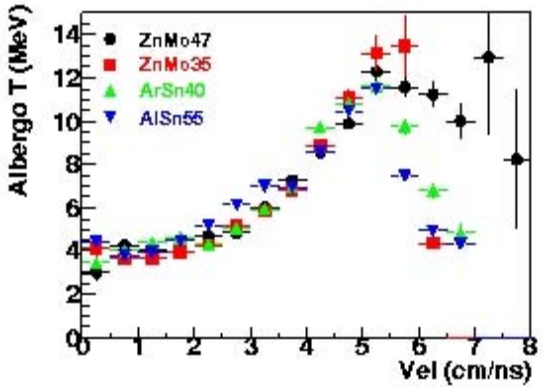

Figure 2. Double isotope temperature T_{HHe} vs surface velocity at 70~80 degrees in NN frame (from experimental data).

The coalescence radii P0 are obtained from the coalescence formula [6]. The source volumes are extracted using the Mekjian thermal model [6],

$$V\left[\left(\frac{Z!N!A^3}{2^A}\right)(2s+1)e^{E_0/T}\right]^{\frac{1}{(A-1)}}\frac{3h^3}{4\pi\rho_0^3}$$

The relative densities shown in Fig. 2 are normalized to the point with velocity about 4.25cm/ns at that point the normal density is assumed.

In Fig. 3, the fluctuation of temperature seen in the early stage (large surface velocity) appears to reflect non-equilibration of the source. The double isotope ratio temperature may not be applicable in that case. The temperature changes smoothly with surface velocity from 5.5 to 0 cm/nc. This means that chemical and thermal equilibration may be reached at about 5.5 cm/ns of surface velocity. The equilibration time is about 100fm/c.

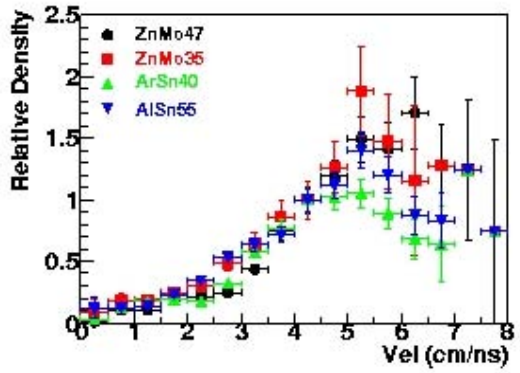

Figure 3. Relative density vs surface velocity at 70~80 degrees in the NN frame.

References

[1] K. Hagel, M. Gonin, R. Wada *et al*., Phys. Rev. Lett. **68**, 2141 (1992).

[2] H. Xi *et al*., Phys. Rev. C **57**, R462 (1998).

[3] K. Hagel *et al*., Phys. Rev. C **62**, 034607 (2000).

[4] J. Cibor *et al.*, Phys. Lett. B **473**, 29 (2000).

[5] R. Wada *et al*., Reaction Dynamic.

[6] A. Mekjian, Phys. Rev. Lett. **12**, 640 (1977).

Study of the Sensitivity of Coalescence Analyses to Impact Parameter Selection

J. S. Wang, R. Wada, K. Hagel, Y. Ma, T. Keutgen, L. Qin, M. Murray, A. Makeev, P. Smith, J. B. Natowitz, J. Cibor, C. Hamilton, E. Martin, S. Liddick, D. Rowland, A. Ruangma, M. Veselsky, E. Winchester, G. Souliotis, S. J. Yennello, A. Samant,[1] M. Cinausero,[1] D.Fabris,[1] E. Fioretto,[1] M. Lunardon[1], G. Nebbia[1], G. Prete[1], G. Viesti[1], Z. Majka[2], P. Staszel[2]; S. Kowalski[3], W. Zipper[3], M. E. Brandan,[4] A. Martinez-Rocha,[4] A. Menchaca-Rocha,[4] and Y. El Masri[5]

[1]*INFN-Legnaro, Padova, Italy,* [2]*Jagiellonian University, Krakov, Poland,* [3]*Silesian University, Katowice, Poland,* [4]*IFUNAM, Mexico,* [5]*UCL, Louvain-la-Neuve, Belgium*

Our previous coalescence analyses show that at $\theta_{1ab} \sim 60^0$, the radius of emission sources decrease with increasing impact parameter [1]. Here, we show that the radius from the coalescence analysis is well correlated with the impact parameter.

The total events observed in four different reactions, 47A MeV ^{64}Zn + ^{92}Mo, 35A MeV ^{64}Zn + ^{92}Mo, 40A MeV ^{40}Ar + ^{112}Sn and 55A MeV ^{27}Al + ^{124}Sn, were divided into four bins using the total particle multiplicity (including neutron and charged particles). Three-source fits were done for light charged particles of all four bins. After subtraction of the TLF components by Monte Carlo methods, we obtained the charged particle energy spectra in the NN frame.

The Albergo temperatures are presented in Fig. 1 for these four reactions. The similar behavior of temperature evolution with surface velocity for different bins indicates that the thermal and chemical properties of the participant zones are very similar from the most peripheral to the most central collisions. The radii of the participant zones were extracted from coalescence analyses as in ref [2]. These radii are compared with the radii from Glauber model simulations as shown in Fig. 2.

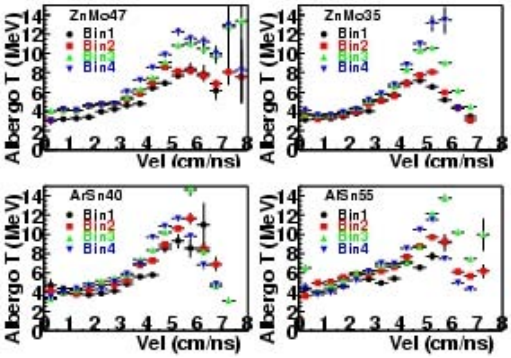

Figure 1. Albergo temperature as a function of surface velocity at 70~80 degree in NN frame for 4 bins of 4 reactions.

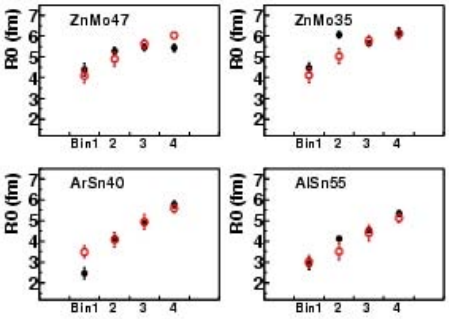

Figure 2. Comparison of radii from coalescence analyses for experimental data (solid circles) and Monte Carlo simulations in Glauber model (open circles).

In the Glauber model simulations, the events are divided into four bins from large to small impact parameter (bin1 to bin4). The cross section of each bin was matched to experimental bin selections. For each bin, the radius of the participant zone is evaluated from the average number of participants with the

simple radii formula, $r = r_0 \cdot A^{1/3}$ where r_0 is 1.2fm. The agreement of these radii is a strong indication of coalescence method analyses.

References

[1] Y. G. Ma *et al*., *Progress in Research*, Cyclotron Institute, Texas A&M University (2001-2002), p. II-11.

[2] J. S. Wang *et al.*, *Progress in Research*, Cyclotron Institute, Texas A&M University (2002-2003), p. II-17.

BRAHMS p+p Analysis

K. Hagel, M. Murray, R. Wada, J. Natowitz and the BRAHMS Collaboration

The analysis at the Cyclotron Institute of the BRAHMS p + p data taken at the end of RHIC run-II is currently focusing on extracting antihadron to hadron ratios. Some preliminary results are now beginning to appear.

The motivation for performing the p + p experiment at RHIC is to provide baseline points for the A + A analysis from the other RHIC experiments. This will aid the understanding of the A + A data as to whether those reactions are simply a superposition of many nucleon-nucleon collisions and/or what role collective effects might play.

To this end we have performed a similar analysis to that reported in [1]. We compare ratios extracted from p + p collisions at 200 GeV and compare those extracted from Au + Au at 200 GeV. Figure 1 shows the pt dependence of ratios extracted for a number of different rapidities. We note that the ratios of pions, kaons and protons from mid-rapidity to rapidity 1 exhibit fairly constant ratios within error bars. For the largest rapidity, y = 2.9, we observe a strong pt dependence of the ratios. Poor statistics in the 12o angle setting (y=2) make it difficult to decide whether a strong pt dependence is observed at that point. The compilation of the forward and backward spectrometer data show that this pt dependence might be starting to appear at this value of rapidity.

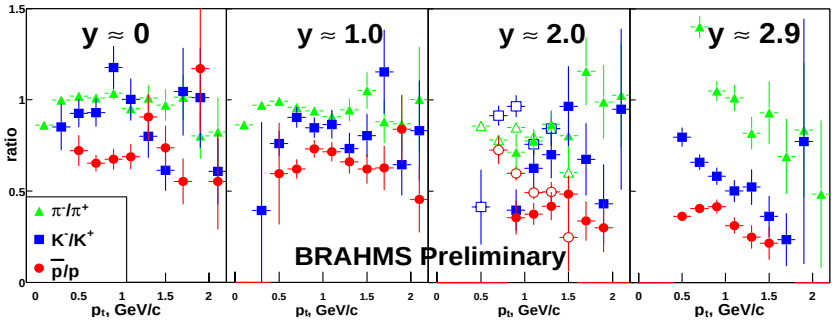

Figure 1. pt dependence of ratios for selected rapidity bins from the back part of the forward spectrometer. The open symbols at y=2 represent results from the Forward spectrometer data.

Figure 2 shows the behavior of the ratios as a function of rapidity when integrated between 1 and 1.5, the only region in pt where we have overlapping pt coverage. There is a fairly constant ratio for each of the particles from mid rapidity to y=1 and then it begins to drop off. This is very similar to the dependence observed in the Au + Au data[1]. However, no pt dependence of the ratios was observed. This dependence will be studied in the coming months. The new p + p data in RHIC run-III will certainly aid in the understanding of these interesting data.

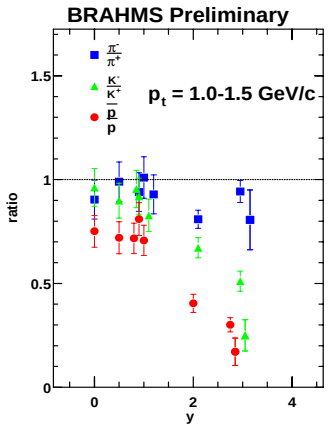

Figure 2. Ratios as a function of y.

References

[1] I. G. Bearden *et al.*, Phys. Rev. Lett. **90**, 102301 (2003).

BRAHMS Results

K. Hagel, M. Murray, R. Wada, J. Natowitz and the BRAHMS Collaboration

The BRAHMS experiment at RHIC made substantial progress in the data analysis of the RHIC run-II Au + Au which ended at the end of January, 2002. Data on the *Pseudorapidity Distributions of Charged Particles from Au + Au Collisions at the Maximum RHIC Energy* [1] and *Rapidity Dependence of Charged Antihadron to Hadron Ratios in Au + Au Collisions at 200 GeV* [2] have been published. In the meantime substantial progress in the data analysis continues to move forward.

The focus of the data analysis has been the effort to extract spectra and yields. A net-proton dN/dy preliminary result for 10% central collisions is shown in Fig. 1. The solid data points show the results extracted and the open open points show reflections of the data about y=0. In the data we observe a flat dN/dy distribution from mid-rapidity to about y=2 followed by a fairly sharp rise.

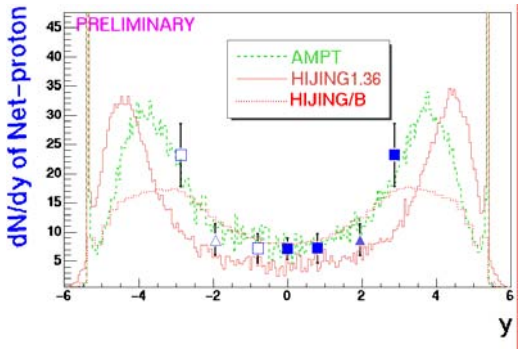

Figure 1. Net proton dN/dy. The solid points show the data extracted and the open symbols show reflections about y=0. Also shown are results of model calculations.

Shown also in Fig. 1 are the predictions of various models. The Hijing model in the default mode underpredicts the data at all rapidities. If baryon-junctions are added to the model, substantial agreement is achieved at mid-rapidity. At higher rapidity, however, the model begins to deviate from the data reaching only the edge of the error bars.

The AMPT model [3] appears to predict the data very well. This model extends a parton cascade model (ZPC) to include the quark-gluon–to–hadronic-matter transition as well as final-state hadronic interactions based on a relativistic transport (ART) model. It shows approximately the same behavior as Hijing/B at y<3, but then increases much faster. The error bars on the data do not yet allow for a definite conclusion to be drawn, but the agreement is intriguing.

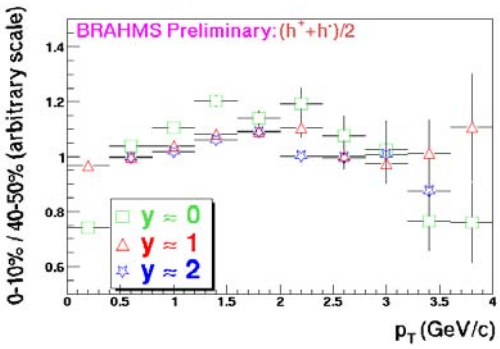

Figure 2. High pt suppression of hadrons for different rapidities.

Fig. 2 shows another example of analysis where high p_t suppression was studied. The figure shows the p_t dependence of the ratios of the yield of central to peripheral collisions for different rapidities. No substantial dependence on rapidity is observed. Results of many other analyzes from BRAHMS data will be forthcoming in the very near future.

References

[1] I. G. Bearden *et al.*, Phys. Rev. Lett. **88**, 202301 (2002).
[2] I. G. Bearden *et al.*, Phys. Rev. Lett. **90,** 102301 (2003).
[3] B. Zhang *et al.*, Phys. Rev. C **61**, 067901 (2000).

SECTION III

NUCLEAR THEORY

Superallowed Fermi Beta Decay: the accuracy of the phase-space integral

I. S. Towner[1] and J. C. Hardy

[1]*Queen's University, Kingston, Ontario, Canada, and Cyclotron Institute, Texas A&M University, College Station, TX*

The *ft*-value for a superallowed nuclear beta-decay transition between analogue 0+, *T*=1 states is given by

$$ft = \frac{2\pi^3\hbar^7 c^6 \ln 2/(m_e c^2)^5}{2G_F^2 V_{ud}^2} \quad (1)$$

where *f* is the statistical rate function, *t* the partial half-life, G_F the weak-interaction coupling constant (determined from the muon-decay lifetime), and V_{ud} the up-down quark-mixing matrix element of the Cabibbo-Kobayashi-Maskawa (CKM) matrix. Observe that the *ft*-value is a constant. (Eq. (1) is modified at the few percent level by radiative and isospin-symmetry breaking corrections. Since these corrections are not relevant to the substance of this report, we will not display them explicitly.) The study of superallowed transitions is aimed firstly at showing that the *ft*-values for a series of different nuclei, all of the same isospin $T = 1$, are indeed constant (a verification of the conserved vector current hypothesis), and secondly at determining the value of the CKM matrix element, V_{ud} (a test of the unitarity of the CKM matrix) .The goal of the current experimental program is to measure the lifetimes, branching ratios and Q-values with sufficient precision that Eq. (1) can be tested at the 0.1% accuracy. This report addresses the question of whether the statistical rate function, *f*, is free of uncertainties at the 0.1% level of accuracy.

The statistical rate function is an integral over the phase space

$$f = \int_1^{W_0} pW\,(W_0 - W)^2\, F(Z,W)\, S(Z,W)\, dW, \quad (2)$$

where *W* is the electron total energy in electron rest-mass units, W_0 the maximum value of *W*, *p* the electron momentum, *Z* the charge number of the daughter nucleus, *F(Z, W)* the Fermi function, and *S(Z, W)* the shape-correction factor. If the shape-correction factor is put to unity, the integral becomes the customarily defined one for beta decay, which we will denote as f_{stat}. The exact evaluation of *f* differs from f_{stat} by 0.2% at $A = 10$ to 5.7% at $A = 74$. Thus to maintain a 0.1% accuracy for *f* up to $A = 74$ requires the shape-correction factor to be determined with a 2% accuracy. To obtain this accuracy requires consideration of the following issues:

The electron wave functions can no longer be simply those of the lowest partial wave ($j = 1/2$) generated by a point nuclear charge and evaluated at the nuclear surface, but must be the exact functions for some chosen nuclear charge density distribution;

The atomic electrons cannot be ignored, but must be accommodated approximately in a screening correction;

The lepton wavefunctions exhibit some mild r^2 dependence over the nuclear volume, leading to what are called second-forbidden corrections. Further, a more accurate treatment of the weak interaction leads to relativistic and induced-current corrections. All

these effects impact on the nuclear matrix elements and inject some mild nuclear-structure dependence into the evaluation of *f*.

In the past year, we have been writing a new computer code to evaluate *f* based on the formalism given in the book of Behrens and Bühring [1]. The key ingredient for the computation of exact electron wave functions is the charge-density distribution of the daughter nucleus. Where possible these distributions are determined from experimental data on elastic electron scattering. A compilation of charge-density distributions is given by De Vries *et al.* [2]. We have assessed these data and selected what we believe is the 'best' value of the rms radius, $\left\langle r^2 \right\rangle^{1/2}$, and its probable error. In cases where data are not available on the isotope of interest, we have examined the nearest isotope available and applied a modest isotope shift to the value of $\left\langle r^2 \right\rangle^{1/2}$. In all cases the uncertainty in *f* due to the uncertainty in $\left\langle r^2 \right\rangle^{1/2}$ is less than or comparable to 0.01 %. Clearly, the uncertainty in the charge-density distribution is not a factor in the determination of *f* to 0.1% accuracy.

Another impact on the evaluation of exact electron wavefunctions is the effect of the screening from the other atomic electrons. Rose [3] gives a simple analytic prescription for how the Fermi function is modified by the screening. The correction to *f* is of order 0.2%. In this correction there is one parameter that quantifies the strength of the effective potential due to the atomic electrons. In past work this parameter has been kept fixed at $N = 1.45$ for all nuclei. Behrens and Bühring [1], however, give a table of *N* showing it varying smoothly from 1.42 at $Z = 8$ to 1.56 at $Z = 29$. The correction to *f* due to changing the screening parameter from a fixed average value to these more recent values ranges from 0.01% to 0.03%, again much less than our accuracy criterion of 0.1%.

Finally, we consider a true nuclear-structure impact by including relativistic and induced-current matrix elements (principally the weak magnetism term). For this a detailed shell-model calculation is required for the appropriate matrix elements. Thus, we are currently working on linking this *f*-value code with a shell-model code so that spectroscopic amplitudes produced in the latter could be used in the former. For the heavier nuclei, say $A = 74$, we believe the impact on *f* will be at the 0.05% to 0.1% level, but much less than this in lighter-mass cases. This issue is still under investigation.

In conclusion, we believe our computed *f*-values will be free of uncertainties at the required 0.1% level.

References

[1] H. Behrens and W. Bühring, *Electron Radial Wave Functions and Nuclear Beta-decay* (Clarendon Press, Oxford, 1982).

[2] H. De Vries, C. W. De Jager and C. De Vries, Atomic Data and Nucl. Data Tables **36**, 495 (1987).

[3] M. E. Rose, Phys. Rev. **49**, 727 (1936).

The evaluation of V_{ud}, experiment and theory

I. S. Towner[1] and J. C. Hardy
[1]*Queen's University, Kingston, Ontario, Canada and Texas A&M University, College Station, TX*

The Cabibbo-Kobayashi-Maskawa matrix relates the quark eigenstates of the weak interaction with the quark-mass eigenstates. The matrix is unitarity, so the squares of the elements in the first row should sum to one:

$$V_{ud}^2 + V_{us}^2 + V_{ub}^2 = 1. \quad (1)$$

In examining this test, we will adopt the Particle Data Group (PDG02) [1] recommendations for V_{us} and V_{ub}. We note that for V_{us} PDG02 recommends only the value determined from K_{e3} decay, $|V_{us}| = 0.2196 \pm 0.0023$, arguing that the value obtained from hyperon decays suffers from theoretical uncertainties due to first-order SU(3) symmetry-breaking effects in the axial-vector couplings. It now appears, though, from preliminary results [2] that the experimental result for the e3 branch of the $K+$ decay may also be in doubt. As to V_{ub}, its value is small, $|V_{ub}| = 0.0036 \pm 0.0010$, and, consequently, it has a negligible impact on the unitarity test, Eq. (1).

The value of the V_{ud} matrix element of the CKM matrix can be derived from nuclear superallowed beta decays, neutron decay, and pion beta decay. We comment on each in turn.

Nuclei have the singular advantage that transitions with specific characteristics can be selected and then isolated for study. One example is the superallowed $0+ \rightarrow 0+$ beta transitions, which depend uniquely on the vector part of the weak interaction. Furthermore, in the allowed approximation, the nuclear matrix element for these transitions is given by the expectation value of the isospin ladder operator, which is independent of any details of nuclear structure and is given simply as an SU(2) Clebsch-Gordan coefficient. Thus, the experimentally determined *ft*-values are expected to be very nearly the same for all $0+ \rightarrow 0+$ transitions between states of a particular isospin, regardless of the nuclei involved. Naturally, there are corrections to this simple picture coming from electromagnetic effects, but these corrections are small--of order 1%--and calculable.

The value of V_{ud} is obtained [3] from the average *ft*-values for a series of superallowed nuclear decays yielding

$$|V_{ud}| = 0.9740 \pm 0.0005, \quad \text{[Nuclear]} \quad (2)$$

and the unitarity sum, Eq. (1), becomes

$$\sum_i V_{ui}^2 = 0.9968 \pm 0.0014, \quad \text{[Nuclear]} \quad (3)$$

which fails to meet unity by 2.2 standard deviations. In connection with this result, we note the following two points:

(a) The error bar associated with $|V_{ud}|$ in Eq. (2) is *not* predominantly experimental in origin. In fact, if experiment were the sole contributor, the uncertainty would be only ± 0.0001.

(b) The unitarity result in Eq. (3) depends on the values of nuclear- structure dependent corrections. We have examined [4] the required theoretical corrections and find no evident defects in the calculated radiative and isospin symmetry-breaking corrections that could remove the problem. So, if any progress is to be made in firmly establishing (or eliminating) the discrepancy with unitarity, additional experiments are required.

Free neutron decay has an advantage over nuclear decays since there are no nuclear-structure dependent corrections to be calculated. However, it has the disadvantage that it is not purely vector-like but has a mix of vector and axial-vector contributions. Thus, in addition to a lifetime measurement, a correlation experiment is also required to separate the vector and axial-vector pieces. The current best value of V_{ud} from neutron decay is

$$|V_{ud}| = 0.9745 \pm 0.0016, \qquad \text{[Neutron]} \qquad (4)$$

and the unitarity sum is

$$\sum_i V_{ui}^2 = 0.9978 \pm 0.0033, \qquad \text{[Neutron]} \qquad (5)$$

a value that agrees with unitarity *and* with the nuclear result, Eq. (3). We note the following two points:

(a) For neutron decay, the error bar associated with $|V_{ud}|$ in Eq. (4) is some three times larger than the error bar obtained from nuclear decays, Eq. (2); however, in contrast with the latter case, it is predominantly experimental in origin.

(b) Currently, the theoretical uncertainty on the inner radiative correction dominates the nuclear result for $|V_{ud}|$. As experimental results for the neutron improve, the uncertainty in the inner radiative correction will eventually dominate the neutron result too.

Like neutron decay, pion beta decay has an advantage over nuclear decays in that there are no nuclear structure-dependent corrections to be made. It also has the same advantage as the nuclear decays in being a purely vector transition, in its case, $0^- \to 0^-$ so no separation of vector and axial-vector components is required. Its major disadvantage, however, is that pion beta decay, $\pi^+ \to \pi^0 e^+ \nu_e$, is a very weak branch, of the order of 10^{-8}. The value of V_{ud} from pion decay is

$$|V_{ud}| = 0.9670 \pm 0.0161, \qquad \text{[Pion]} \qquad (6)$$

and the unitarity sum

$$\sum_i V_{ui}^2 = 0.9833 \pm 0.0311, \qquad \text{[Pion]} \qquad (7)$$

satisfying the unitarity condition but with comparatively large uncertainty. The error on $|V_{ud}|$ is entirely due to the uncertainty in the pion branching ratio.

Clearly, there is strong motivation to pursue experiments, not only on the neutron and nuclear front but also in revisiting the K_{e3} decay, since, if firmly established, a discrepancy with

unitarity would indicate the need for important new physics. A review by us on this topic was published [3] earlier this year.

References

[1] K. Hagiwara *et al.*, Phys. Rev. D **66**, 010001 (2002).
[2] A. Sher *et al.*, arXiv:hep-ex/0305042 (2003).
[3] I. S. Towner and J. C. Hardy, J. Phys. G **29**, 197 (2003).
[4] I. S. Towner and J. C. Hardy, Phys. Rev. C **66**, 035501 (2002).

Asymptotic wavefunction for three charged particles in the continuum

A. M. Mukhamedzhanov, F. Pirlepesov, A. Kadyrov

We present preliminary results for an extended version of the wave function derived in [1,2] that satisfies the Shroedinger equation up to terms of order $O(1/\rho_\alpha^3)$ in the region where the pair $\alpha=(\beta,\gamma)$ remains close, while the third particle α moves to infinity $(\rho_\alpha\to\infty)$. Consider a system of three particles with mass m_α and charge e_α, $\alpha=1,2,3,$ in the continuum. The Schroedinger equation describing this system is

$$(E-T_{\vec r_\alpha}-T_{\vec\rho_\alpha}-V)\Psi^{(+)}_{\vec k_\alpha,\vec q_\alpha}(\vec r_\alpha,\vec\rho_\alpha)=0 \tag{1}$$

An improved wave function contains all the terms of orders of $O(1)$, $O(1/\rho_\alpha)$, $O(1/\rho_\alpha^2)$ and satisfies the Shroedinger equation in Ω_α up to terms of order $O(1/\rho_\alpha^3)$. The derived wave function is the asymptotic term (up to order of $O(1/\rho_\alpha^3)$) of the exact three-body wave function in Ω_α which should match smoothly with the leading asymptotics of the exact three body wave function in the region Ω_0. We seek the solution of equation (1) in Ω_α up to terms of order $O(1/\rho_\alpha^3)$ in the following form:

$$\Psi^{(as)(+)}_{\vec k_\alpha,\vec q_\alpha}(\vec r_\alpha,\vec\rho_\alpha)=e^{i\vec q_\alpha\cdot\vec\rho_\alpha}e^{i\vec k_\alpha\cdot\vec r_\alpha}\sum_{i,j=1,2}F^{(i)}_\beta(i\varsigma_\beta)F^{(j)}_\gamma(i\varsigma_\gamma)\varphi^{(ij)}_\alpha(\vec r_\alpha,\vec\rho_\alpha), \tag{2}$$

where $F^{(1)}_\nu(i\varsigma_\nu)+F^{(2)}_\nu(i\varsigma_\nu)=N_\nu F(-i\eta_\nu,1;i\varsigma)$, $F(-i\eta_\nu,1;i\varsigma)$ is the confluent hypergeometric function and $\varsigma_\nu=k_\nu r_\nu-\vec k_\nu\cdot\vec r_\nu$. When substituting Eq. (2) into (1) we assume that each term of the sum in Eq. (2) satisfies this equation. Then we derive four independent equations. For the first term in (2) we arrive at the equation

$$\begin{aligned}&F^{(1)}_\beta(i\varsigma_\beta)F^{(1)}_\gamma(i\varsigma_\gamma)\Big[\frac{1}{2\mu_\alpha}\Delta_{\vec r_\alpha}+\frac{1}{2M_\alpha}\Delta_{\vec\rho_\alpha}+i\frac{1}{\mu_\alpha}\vec k_\alpha\vec\nabla_{\vec r_\alpha}+i\frac{1}{M_\alpha}\vec q_\alpha\vec\nabla_{\vec\rho_\alpha}+\\&\frac{1}{\mu_\alpha}\sum_{\nu=\beta,\gamma}\vec\nabla_{\vec r_\alpha}\ln F^{(1)}_\nu(i\varsigma_\nu)\cdot\vec\nabla_{\vec r_\alpha}+\frac{1}{M_\alpha}\sum_{\nu=\beta,\gamma}\vec\nabla_{\vec\rho_\alpha}\ln F^{(1)}_\nu(i\varsigma_\nu)\cdot\vec\nabla_{\vec\rho_\alpha}\quad V_\alpha+\\&\frac{1}{\mu_\alpha}\vec\nabla_{\vec r_\alpha}\ln F^{(1)}_\beta(i\varsigma_\beta)\cdot\vec\nabla_{\vec r_\alpha}\ln F^{(1)}_\gamma(i\varsigma_\gamma)+\frac{1}{M_\alpha}\vec\nabla_{\vec\rho_\alpha}\ln F^{(1)}_\beta(i\varsigma_\beta)\cdot\vec\nabla_{\vec\rho_\alpha}\ln F^{(1)}_\gamma(i\varsigma_\gamma)\Big]\ {}^{(11)}_{\alpha}=0\end{aligned} \tag{3}$$

Keeping all the terms up to order $O(1/\rho_\alpha^3)$ we look for a solution in the form

$${}^{(11)}_{\alpha}(\vec r_\alpha\vec\rho_\alpha)={}^{(11)}_{\alpha(0)}(\vec r_\alpha,\vec\rho_\alpha)[1+\chi(\vec\rho_\alpha)]+{}^{(11)}_{\alpha(1)}(\vec r_\alpha,\vec\rho_\alpha). \tag{4}$$

Here $\varphi^{(11)}_{\alpha(0)}(\vec r_\alpha,\vec\rho_\alpha)$ is the solution found in [1,2]. Eq. (4) is our main result. Both unknown functions can be found after substitution (4) into (3).

References

[1] E. O. Alt and A. M. Mukhamedzhanov, Phys. Rev. A **47**, 2004 (1993).
[2] A. M. Mukamedzhanov and M. Lieber, Phys. Rev. A **54**, 3078 (1996).

Asymptotic normalization coefficients from the $^{14}N(^{3}He,d)^{15}O^{*}$ reaction and astrophysical factor for $^{14}N + p \rightarrow ^{15}O^{*} + \gamma$

A. M. Mukhamedzhanov, P. Bém, B. A. Brown, V. Burjan, C. A. Gagliardi, V. Kroha, J. Novák, F. M. Nunes, Š. Piskoř, F. Pirlepesov, E. Šimečkova, R. E. Tribble and J. Vincour

The $^{14}N(p,\gamma)^{15}O$ reaction is one of the most important reactions in the CNO cycle. As the slowest reaction in the cycle, it defines the rate of energy production and, hence, the lifetime of stars that are governed by hydrogen burning via CNO processing. There are controversial reports in the literature about S-factor for the $^{14}N + p \rightarrow ^{15}O + \gamma$ capture at stellar energies (see [1] and the references therein). The latest measurements of the capture cross section at energies E > 0.187 MeV showed that at low energies the capture is dominated by a combination of direct and resonant capture and interference from the tails of the subthreshold and first resonances [1]. Taking into account that the absolute normalization for the direct capture S factor to the subthreshold state can be determined by its asymptotic normalization coefficient (ANC), we measured this ANC and, simultaneously, the ANCs for the ground and five other excited states in ^{15}O to determine more accurately the S factors for transitions to the subthreshold and other states. In order to determine the ANCs for $^{14}N + p \rightarrow ^{15}O$, the $^{14}N(^{3}He,d)^{15}O$ proton transfer reaction has been measured at an incident energy of 26.3 MeV. Angular distributions for proton transfer to the ground and five excited states were obtained. ANCs were then extracted from comparison with both DWBA and CCBA calculations. Our measured ANCs are in a very good agreement with those reported in [2]. Using the measured ANCs, we fit the astrophysical S factors for transitions to the ground and excited states and the total S factor using the R-matrix method. In our analysis, we accurately account for interference effects by splitting the resonance amplitudes into the internal and channel terms. We find that for captures to all the states except for the ground state, the $S(0)$ factors are almost entirely determined by the corresponding ANCs. Here we report the final results of our analysis. The astrophysical factor for the capture to the ground state, $1/2^{-},\ 0.00\,MeV$, is $S(0) = 0.15 \pm 0.07\,keVb$, which is significantly lower than the value $S(0) = 1.55 \pm 0.34\,keVb$ found in [1]. The calculated $S(0)$ astrophysical factor for the capture to the third excited state, $3/2^{-},\ 6.18\,MeV$, is $S(0) = 0.13 \pm 0.02\,keVb$. The capture to the fourth excited state, $3/2^{+},\ 6.79\,MeV$, dominates all others and the calculated astrophysical factor is $S(0) = 1.4 \pm 0.20\ keVb$. According to [1] the captures to other states contribute about 3% to the total $S(0)$ factor and have been neglected here. The total calculated astrophysical factor at zero energy is $S(0) = 1.70 \pm 0.22\ keVb$. Correspondingly our calculated production rate of ^{15}O is significantly lower than was previously calculated [1].

References

[1] U. Schroeder *et al.*, Nucl. Phys. **A467**, 240 (1987).

[2] P. F. Bertone *et al.*, Phys. Rev. C **66**, 055804 (2002).

Asymptotic form of the electron-hydrogen scattered wave

A. S. Kadyrov, A. M. Mukhamedzhanov and A. T. Stelbovics

Despite the success of different modern practical approaches in providing accurate cross sections, formal theory of breakup with charged particles remains incomplete. The formal theory given over thirty years ago [1] is still considered state of the art. Within the framework of this theory there is no, and cannot be, an exact algorithm, e.g., similar to the one below the breakup threshold, for solution of the Schroedinger and differential Faddeev equations with correct boundary conditions above the breakup threshold. Though an asymptotic form of the scattered wave for electron-impact ionization of hydrogen for the case when all interparticle distances are large was obtained by Peterkop [1] four decades ago, it has not been successfully implemented in the aforementioned approaches. One reason is that direct numerical solution of the Schroedinger equation for the full hydrogen-ionization problem requires partial-wave analysis of the asymptotic wave function which doesn't exist because the Peterkop's asymptotic wave function is invalid when the two electrons are close to each other. Another problem of the Peterkop's approach is amplitude-phase ambiguity which comes from the Hamilton-Jacobi equation used by him. This amplitude-phase ambiguity has caused problems in the formal theory of breakup at a very fundamental level. Finally, full knowledge of the asymptotic behavior of the scattered wave forms the basis for the Kohn variational approach to breakup processes [2]. In this work a relationship between the total wave function describing ionization in the electron-hydrogen system and the one representing scattering of three particles of the system in the continuum is established. On the basis of this relationship, forms of the scattered wave for ionization valid in all asymptotic domains relevant to ionization are obtained and the amplitude-phase ambiguity of the Peterkop wave function is resolved. This removed the above-mentioned problems in practical calculations and made the correct extraction of observables possible. In this work the scattered waves for electron-impact ionization of hydrogen valid in all asymptotic domains are derived. The wave functions are obtained directly from a formal solution of the Schroedinger equation. When all interparticle distances become large, the new wave functions reduce to the well known Peterkop asymptotics obtained from solution of the semiclassical Hamilton-Jacobi equation. We identified the failure of the Peterkop's asymptotics when two electrons are at the same distance from the proton as the result of using of the Coulomb three-body plane (Redmond asymptotics). The replacement of this three-body plane-wave by a Coulomb three-particle wave function valid in all the asymptotic regions [3] allows one to obtain a new scattered wave which is valid in the entire domain including the domain where all particles are wide apart. Simultaneously, for the first time, we resolve the amplitude-phase ambiguity problem which was an artifact of the hypersperical approach to the ionization process.

References

[1] R. K. Peterkop, Zh. Eksp. Teor. Fiz. **43**, 616 (1962).
[2] A. Kievsky *et al.*, Phys. Rev. C **64**, 024002 (2001).
[3] A. M Mukhamedzhanov and M. Lieber, Phys. Rev. A **54**, 3078 (1996).

The $^{17}F(p,\gamma)^{18}Ne$ direct capture cross section

J. C. Blackmon, D. W. Bardayan, C. R. Brune, A. E. Champagne, R. Crespo, T. Davinson, J. C. Fernandes, C. A. Gagliardi, U. Greife, C. J. Gross, P. A. Hausladen, C. Iliadis, C. C. Jewett, R. L. Kozub, T. A. Lewis, F. Liang, B. H. Moazen, A. M. Mukhamedzhanov, C. D. Nesarja, F. M. Nunes, P. D. Parker, D. C. Radford, L. Sahin, J. P. Scott, D. Shapira, M. S. Smith, J. S. Smith, L. Trache, R. E. Tribble, P. J. Woods, C.-H. Yu

The ^{17}F isotope is copiously produced in novae when hydrogen-rich gas accretes onto a white dwarf and burns explosively with the dwarf's abundant ^{16}O. The decay of ^{17}F produced in novae helps power the expansion and is possibly the dominant source in the Galaxy of the fragile ^{17}F isotope. However, the $^{17}F(p,\gamma)^{18}Ne$ reaction bypasses ^{17}O production and instead leads to ^{18}F, a primary target of gamma-astronomy. The ratio of the $^{17}F(p,\gamma)^{18}Ne$ reaction rate to the ^{17}F β decay rate is important for understanding of nucleosynthesis in novae, especially the production of ^{18}O and ^{18}F. The $^{17}F(p,\gamma)^{18}Ne$ cross section is dominated at the energies of interest in novae by direct capture to bound excited states in ^{18}Ne ($\sigma \approx nb$) [1]. This contribution is unmeasured, and the rate estimation is based on properties of states in the mirror nucleus [2]. The dominant transition is to the subthreshold 4^+,3.376 MeV state. The overall normalization of the S factor for the direct radiative capture to this state is entirely determined by its asymptotic normalization coefficient (ANC). The aim of this work is to determine the $^{17}F(p,\gamma)^{18}Ne$ direct capture S factor using the ANCs determined from the proton-transfer reaction $^{14}Ne(^{17}F,\ ^{18}Ne)^{13}C$. A 170-MeV beam of isototpically-pure ^{17}F from the Holifield Radioactive Ion Beam Facility bombarded a 1-mg/cm melamine target. Charged particles were detected by position-sensitive silicon-strip detectors covering $\theta_{lab} = 2^\circ - 9^\circ$. The Z of the charged particles was identified by their energy loss in a $65-\mu m$-thick ΔE detector. The energy resolution was not sufficient to distinguish transfer to individual states of interest in ^{18}Ne by detecting only charged particles, so gamma rays emitted by the recoiling ^{18}Ne were detected in coincidence by CLARION, an array of 11 clover germanium detectors. Prominent transitions in ^{18}Ne are identified. Strongest transition is to the subthreshold state 4^+, 3.376 MeV. Detailed analysis of the data is currently in progress. The optical model parameters were determined by fitting the $^{14}Ne(^{17}F,\ ^{17}F)^{14}Ne$ elastic scattering cross sections in the entry channel that were also measured over $\theta_{cm} = 8^\circ - 40°$. By extracting ANCs from differential cross sections for each state, we can accurately determine the $^{17}F(p,\gamma)^{18}Ne$ reaction rates at nova temperatures.

References

[1] D. W. Bardayan *et al.*, Phys. Rev. C **62**, 055804 (2000).
[2] A. Garcia *et al.*, Phys. Rev. C **43**, 2012 (1991).
[3] C. A. Gagliardi *et al.*, Phys. Rev. C **59**, 1149 (1999).

Coulomb breakup of ^8B in the framework of three-body theory

E. O. Alt, B. F. Irgaziev, and A. M. Mukhamedzhanov

Knowledge of the astrophysical S-factor for the capture reaction $^7Be + p \to {}^8B + \gamma$ is *important* for many problems in nuclear astrophysics, in particular for the estimation of the solar neutrino flux. But information on it at the required low energies is very hard to obtain via observation of the direct capture. It has, therefore, been suggested to extract this quantity from the indirect reaction, namely the breakup of ^8B in the Coulomb field of a heavy target. Indeed, for this purpose four ^8B Coulomb breakup experiments have been performed recently using the $^{208}Pb(^8B, ^7Be\, p)^{208}Pb$ reaction. However, the value of the astrophysical factor extracted from these reactions is affected by several uncertainties. One of the most interesting effects contributing to this uncertainty is the so-called post-decay acceleration (PDA) of the fragments in the Coulomb field of the target. This can be understood as follows: the target nucleus does not only act as a source of the photons to induce the breakup of ^8B, but after the breakup it will continue to influence the motion of the ejectiles depending on their charge-over-mass ratio. Conventional approaches eliminate all PDA effects. In our work, for the first time, we treat the PDA effects for the Coulomb breakup reactions in a genuine three-body approach. The Coulomb breakup amplitude for $a + A \to b + c + A$ is given by $M = \langle \Psi_f^{(-)} | V_b^C + V_c^C - U^C | \varphi \Phi_i^{(+)} \rangle$.

Here, V_j^C is the Coulomb potential acting between particle $j = b, c$ and the target A and U^C is the Coulomb optical potential responsible for scattering of a and A. Moreover, φ_a is the (bc) bound state wave function, $\Psi_f^{(-)}$ the exact final state wave function describing the three mutually interacting charged particles b, c and A in the continuum, $\Phi_i^{(+)}$ the $a + A$ Coulomb scattering wave function in the initial channel. For small scattering angles the leading contribution to the breakup amplitude comes from large impact parameters allowing us to approximate $\Psi_f^{(-)}$ by its correct three-body asymptotic terms in the region where two fragments b and c are close to each other and far away from A [1]. In Table 1 we present the ratio of the single differential cross sections (SDCS) for the $^{208}Pb(^8B, ^7Be\, p)^{208}Pb$ Coulomb breakup calculated with and without final-state three-body effects for two incidents energies.

Table 1. The ratio of the SDCS calculated with and without final-state three-body Coulomb effects.

$E_{^7Be-p}$ [MeV]	0.20	0.40	0.60	0.80	1.00
Ratio ($E_i = 46.5$ MeV/A)	1.10	0.92	0.96	0.99	1.00
Ratio ($E_i = 83$ MeV/A)	1.01	0.99	0.99	1.00	1.00

From our calculations we conclude that in order to minimize post-decay Coulomb acceleration effects, experiments should be performed at as small as possible scattering angles, not to low relative energies of the fragments and high incident energies [1].

References

[1] E. O. Alt, B. F. Irgaziev and A. M. Mukhamedzhanov, Phys. Rev. Lett. **90**, 122701 (2003).

Coulomb breakup problem and asymptotic behaviour of the three-body scattered wave

A. S. Kadyrov, A. M. Mukhamedzhanov, A. T. Stelbovics, I. Bray, and F. Pirlepesov

With the progress in high-performance computing, the direct numerical integration of the Schroedinger equation has emerged as a powerful method to study scattering processes with three charged particles. Such a method, in principle, requires the knowledge of the asymptotic behavior of the scattered wave function in all asymptotic regions of the configuration space. The most studied system is that of electron-hydrogen scattering. Lack of knowledge of the complete asymptotic behavior of the scattered wave function has lead to different approaches, aimed at "avoiding" the true three-body asymptotic state, including exterior complex scaling [1] and other approaches. These approaches provide an accurate three-body scattered wave function in an "internal" region in coordinate space and the ionization amplitude is extracted by matching to ionization boundary conditions in the asymptotic region. However, the extraction process relies on approximate ionization boundary conditions. This yields an ionization amplitude with divergent phase as a function of matching radius although its magnitude converges. Despite the success of these approaches in providing accurate cross sections, formal theory of breakup with charged particles remains incomplete. Within the conventional theory there is no algorithm toward solution of the Schroedinger equation with correct boundary conditions above the breakup threshold. An asymptotic form of the scattered wave for electron-impact ionization of hydrogen obtained by Peterkop [2] is invalid when the two electrons are close to each other. For full-scale numerical calculations a representation of the wave function describing ionization in this region as well is necessary. We propose a new representation for the breakup amplitude

$$f(\vec{k}_\alpha,\vec{q}_\alpha)=\langle \Psi^{(-)}_{\vec{k}_\alpha,\vec{q}_\alpha} \,|\overleftarrow{H}_0-\overrightarrow{H}_0|\Phi^{(sc)(+)}_{\vec{k}_\alpha,\vec{q}_\alpha}\rangle,$$

Here $\Psi^{(-)}_{\vec{k}_\alpha,\vec{q}_\alpha}$ is the exact final-state 3-body scattering wave function, $\Phi^{(sc)(+)}_{\vec{k}_\alpha,\vec{q}_\alpha}$ is the three-body scattered wave function, $\vec{k}_\alpha,\vec{q}_\alpha$ are the Jacobian momenta describing the relative momentum of two particles and the relative momentum of the their c.m. and the third particle . This new representation can easily be transformed into an integral over an infinitely large surface, so that the result depends solely on the asymptotic behavior of the wave functions $\Psi^{(-)}_{\vec{k}_\alpha,\vec{q}_\alpha}$ and $\Phi^{(sc)(+)}_{\vec{k}_\alpha,\vec{q}_\alpha}$. The asymptotic form for $\Psi^{(-)}_{\vec{k}_\alpha,\vec{q}_\alpha}$ in all domains relevant for breakup has been obtained in [3]. Recently we derived an analytical expression for the asymptotic form of $\Phi^{(sc)(+)}_{\vec{k}_\alpha,\vec{q}_\alpha}$ valid in all the asymptotic domains. We demonstrate that new representation for the breakup/ionization amplitude is exact, free of divergence and suitable for numerical calculations.

References

[1] M. Baertschy *et al*, Phys. Rev. A **64**, 022709 (2001).
[2] R. K. Peterkop, Izv. Akad. Nauk Latv. SSR, Ser. Fiz. Tekh. **9**, 79 (1960).
[3] A. M. Mukhamedzhanov and M. Lieber, Phys. Rev. A **54**, 3078 (1997).

Coulomb breakup of light nuclei in the field of a heavy ion at relativistic energies

B. F. Irgaziev, Sh. Kalandarov, and A. M. Mukhamedzhanov

A simple method for calculating the amplitude and the cross section for the Coulomb breakup of light nuclei into two fragments in the field of a heavy target at relativistic energies is proposed. The method is based on the time-dependent perturbation theory. The double differential cross section of $a+A\to A+b+c$ of the breakup of a light nucleus a into fragments b and c in the Coulomb field of a heavy ion A at the relativistic energies for $E1$ in our approach is given by

$$\frac{d^2\sigma}{dE_{bc}d\Omega_a}=\frac{1}{3}\left[\frac{8\pi Z_A Z_{eff}e^2\omega}{\gamma v^2 k_{bc}}\right]^2\frac{d\sigma_R}{d\Omega_a}\sum_{l_f}\left(\langle l_f\,|r|l_i\rangle C^{l_f\,0}_{l_i\,0\,1\,0}\right)^2\left[K_1^2\left(\frac{\omega b}{\gamma v}\right)+\frac{1}{\gamma}K_0^2\left(\frac{\omega b}{\gamma v}\right)\right]\frac{\mu_{bc}k_{bc}}{(2\pi)^3}$$

Here, Z_Ae^2 is the charge of the ion, $Z_{eff}e$ is the effective charge, ω is the excitation energy of the projectile, k_{bc} and μ_{bc} are the relative momentum and reduced mass of the fragments b and c in the final state, v is the speed of the projectile a, $d\sigma_R/d\Omega_a$ is the Rutherford $a+A$ elastic cross section, K_i is the Bessel function of the order i, γ is the Lorentz factor. The second term is the contribution of a longitudinal component of the Coulomb field which goes to zero at the ultrarelativistic limit. Our cross section has correct relativistic and nonrelativistic limits. The contribution of the longitudinal component, as expected, tends to zero in the ultrarelativistic limit. The concrete realization of the suggested method is carried out for $^{208}Pb(^8B,^7Be\,p)^{208}Pb$ Coulomb breakup at two different collision energies, 46.5 and 254 MeV/A. We have not yet included the magnetic dipole transition what causes the disagreement with the experimental data at relative kinetic energy of the fragments $E_{bc}\approx 0.6\,MeV$. Electric quadrupole and magnetic dipole transitions can be easily taken into account in our formalism and it will be done in future. We are planning also to take into account correctly the final-state three-body interaction where the relative motion of two fragments can be described in the nonrelativistic approach while the relative motion of the c.m. of the fragments and the target needs the relativistic consideration.

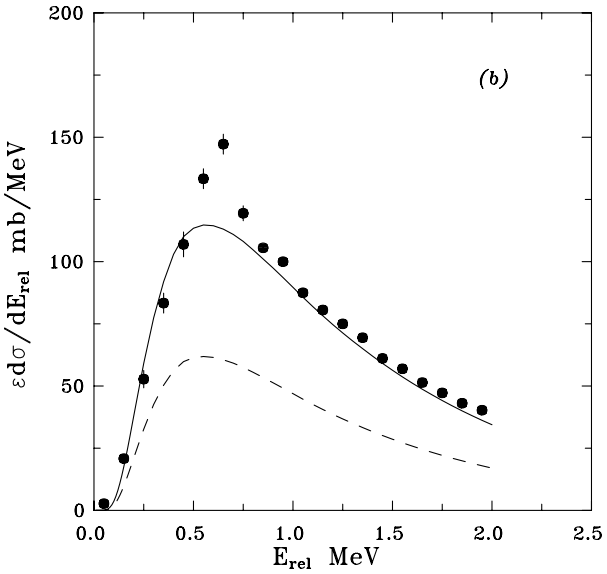

Figure 1.

Asymptotic normalization coefficients from the $^{20}Ne(^{3}He,d)^{21}Na$ reaction

P. Bém, V. Burjan, C. A. Gagliardi, V. Kroha, A. M. Mukhamedzhanov, J. Novák, Š. Piskoř, E. Šimečková, R. E. Tribble and J. Vincour

Besides the p-p chain and the CNO cycle, the Ne-Na cycle may play an important role in hydrogen burning in stars with masses larger than the mass of the sun. The $^{20}Ne(p,\gamma)^{21}Na$ reaction is the first one among the reactions of the Ne-Na cycle. The final nucleus ^{21}Na has a sub-threshold bound state with the binding energy of 7.1 ± 0.6 keV. This state gives the most significant contribution to the stellar production of ^{21}Na. So far direct measurements of the S factor for $^{20}Ne(p,\gamma)^{21}Na$ were done at proton energies ≥ 300 keV [1]. As a part of the collaboration between the Cyclotron Institute and the Nuclear Physics Institute of the Czech Academy of Sciences the method of the asymptotic normalization coefficients (ANC) is applied to determine the astrophysical factor for the $^{20}Ne(p,\gamma)^{21}Na$ reaction. In this approach the ANCs extracted from the $^{20}Ne(^{3}He,d)^{21}Na$ reaction are used to determine the overall normalization of the direct capture processes $^{20}Ne(p,\gamma)^{21}Na$ leading to the ground and excited states of ^{21}Na and capture through the subthreshold resonance at $E_R=-(7.1\pm0.6)$ keV. The measured ANC for the subthreshold state also determines the proton partial width and the channel (external) part of the radiative width of the subthreshold resonance. The experiment was carried out using a momentum analyzed 25.8 MeV ^{3}He beam from the U-120M isochronous cyclotron of the Nuclear Physics Institute of the Czech Academy of Sciences incident on a neon gas target. The target gas chamber contained high purity ^{20}Ne. Input and output gas cell windows were made from 3.05 μm thick havar foils. A control system also enabled continuous feed of ^{20}Ne gas into the gas chamber in case of leakage during long term measurements. Reaction products were registered by a pair of ΔE-E telescopes consisting of 250-μm and 3-mm thick Si(Li) surface barrier detectors. Both detectors were equipped with a pair of collimating slits of dimension 2 x 3 mm^2. One telescope was fixed at an angle of 19° as a monitor and the second one was adjusted at different laboratory angles in the range between 6.5° and 70°. All measured data, including the charge from the Faraday cup, were collected in an on-line computer for later analysis. By comparison of the experimental and DWBA angular distributions we determined the ANCs for the ground and three excited states in ^{21}Na. In Fig. 1 we present the experimental and DWBA angular distributions for the subthreshold bound state in ^{21}Na.

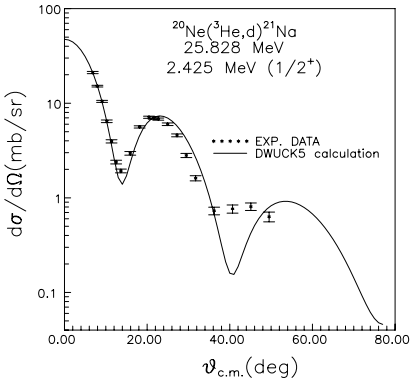

Figure 1. The experimental and calculated angular distributions for the reaction $^{20}Ne(^{3}He,d)^{21}Na(1/2^{+},2.425$ MeV). The points are experimental data. The solid line is the DWBA cross section.

References

[1] Rolfs C. *et al.*, Nucl. Phys. **A241**, 460 (1975).

Charm production from photon-proton reactions in a hadronic model

W. Liu, S. H. Lee[1], and C. M. Ko

[1]*Yonsei University, Seoul, Korea*

Reliable estimates of the production and scattering cross sections of open and/or hidden charmed hadrons in hadronic matter are important for understanding many phenomena in relativistic heavy ion collisions and hadron-nucleus reactions. In a recent work [1], we have generalized the effective hadronic Lagrangian, which has been previously used to study charmed meson scattering by hadrons [2] and charmed meson production from meson-nucleon scattering [3], to include the photon and to study charmed hadron production from photon-proton reactions near threshold. With cutoff parameters in the form factors adjusted to fit measured total cross section at center-of-mass energy of 6 GeV, we find that the relative contribution of two-body ($\bar{D}\Lambda_c$, $\bar{D}^*\Lambda_c$) to three-body ($\bar{D}$ DN, $\bar{D}^*$DN) final states is consistent with that seen in experimental data. As expected, two-body final states dominate near threshold while three-body final states become important at high energies. Our results at high energies are much smaller than those measured experimentally or given by the LO perturbative QCD as more complicated final states are not included in the hadronic approach. The present study thus provides an independent test and confirmation of the usefulness of hadronic models for studying the production and scattering cross sections of charmed hadrons at low energies.

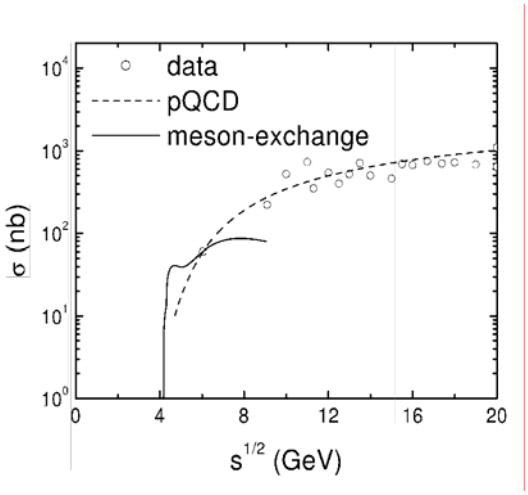

Figure 1. Cross sections for charm production from photon-proton reactions in the hadronic model (solid curve) and the pQCD approach (dashed curve). Experimental data are shown by open circles.

References

[1] W. Liu, S. H. Lee, and C. M. Ko, Nucl. Phys. A **724**, 375 (2003).

[2] W. Liu, C. M. Ko and Z. W. Lin, Phys. Rev. C **65**, 015203 (2002).

[3] W. Liu and C. M. Ko, Phys. Lett. B **533**, 259 (2002).

Charmonium mass in nuclear matter

S. H. Lee[1] and C. M. Ko

[1]*Yonsei University, Seoul, Korea*

Understanding hadron mass changes in nuclear medium and/or at finite temperature can provide valuable information about the QCD vacuum [1]. Using either QCD sum rules [2] or the quark-meson coupling model [3], it has been found that the mass of D meson, which is made of a charm quark and a light quark, is reduced significantly in nuclear medium as a result of decrease of light quark condensate. For J/, which consists of a charm and anticharm quark pair, both the QCD sum rules analysis and the leading-order (LO) perturbative QCD calculation show that its mass is reduced slightly in nuclear matter mainly due to the reduction of the gluon condensate. In our recent work [4], we have evaluated the mass shift of $\Psi(3686)$ and $\Psi(3770)$ due to changes in the gluon and quark condensates in nuclear medium. While the effect of gluon condensate can be determined using the LO QCD formula, that due to change in quark condensates is difficult to calculate using the quark and gluon degrees of freedom as they appear as higher twist effects in the operator product expansion. We have therefore studied the effect of changing quark condensate on the charmonium states at finite density by using a hadronic model to calculate their mass shifts due to change of D meson mass in nuclear medium. We find that masses of charmonium states are modified by the following amount at normal nuclear matter density:

$$\Delta m_{J/\Psi} = -8 \quad +3 \quad \text{MeV},$$
$$\Delta m_{J/\Psi 3686} = -100 \quad -30 \quad \text{MeV},$$
$$\Delta m_{J/\Psi 3770} = -140 \quad +15 \quad \text{MeV},$$

where the first number represents mass shift from the LO QCD while the second number is from the D meson loop. Our results thus show that masses of excited charmonium states are reduced significantly in nuclear matter, largely due to the non-trivial decrease of in-medium gluon condensate. The mass shifts of both $\Psi(3686)$ and $\Psi(3770)$ in nuclear medium are large enough to be observed in experiments involving antiproton-nucleus annihilation as proposed in future accelerator facility at the German Heavy Ion Accelerator Center (GSI).

References

[1] C. M. Ko, V. Koch, and G. Q. Li, Ann. Rev. Nucl. Part. Sci. **47**, 505 (1997).

[2] A. Hayashigahi, Phys. Lett. B **487**, 96 (2000).

[3] K. Tsushima, D. H. Lu, A. W. Thomas, K. Saito, and R. H. Landau, Phys. Rev. C **59**, 2824 (1999).

[4] S. H. Lee and C. M. Ko, Phys. Rev. C **67**, 038202 (2003).

Deuteron-gold collisions at RHIC

Z. W. Lin[1] and C. M. Ko

[1]*Ohio State University, Columbus, OH*

Using a multi-phase transport (AMPT) model that includes both initial partonic and final hadronic interactions [1], we have studied the pseudo-rapidity distribution of charged particles and its centrality dependence in deuteron-gold collisions at 200 AGeV [2]. Due to asymmetry of the collisions, the centrality dependence of charged particle multiplicity per participant is very different at different pseudo-rapidities as shown in Fig. 1. It increases with centrality at backward pseudo-rapidity region. i.e., the fragmentation region of gold nuclei, but decreases with centrality at forward region. Using several methods for centrality selection, we have found that, while using the impact parameter or the number of participant N_{part} to determine the centrality gives a similar centrality dependence for $dN_{ch}/d\eta/N_{part}$ at various pseudo-rapidities, using N_{ch} for the centrality selection leads to very different results. We further find that although the charged particle multiplicity distribution in central deuteron-gold collisions is not sensitive to nuclear shadowing effect, it is affected significantly by the values of the parameters used in the string fragmentation function. Comparisons of these predictions with experimental data will thus help us to learn whether the string fragmentation is modified in deuteron-gold collisions as in central heavy ion collisions. This will in turn provide useful information on the impact parameter dependence of the string fragmentation function in heavy ion collisions.

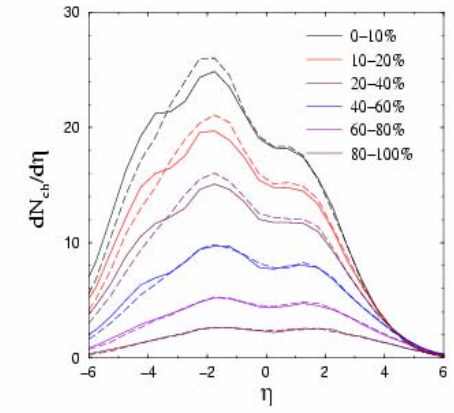

Figure 1. Pseudo-rapidity distributions of charged particles in d+Au collisions at 200 AGeV with centralities determined from N_{part}.

References

[1] B. Zhang, C. M. Ko, B. A. Li and Z. W. Lin, Phys. Rev. C **61**, 067901 (2000); Z. W. Lin, S. Pal, C. M. Ko, B. A. Li, and B. Zhang, *ibid*. **64**, 011902 (2001); Nucl. Phys. **A698**, 375 (2002).

[2] Z. W. Lin and C. M. Ko, nucl-th/0301025.

Isospin effects on two-nucleon correlation functions in heavy ion collisions at intermediate energies

L. W. Chen[1], V. Greco, C. M. Ko, and B. A. Li[2]

[1]*Shanghai Jiao Tung University, Shanghai, China,* [2]*Arkansas State University, Jonesboro, AR*

Using an isospin-dependent transport model (IBUU), we have studied the effects of nuclear symmetry energy $E_{sym}(\rho)$ on two-nucleon correlation functions in heavy-ion collisions induced by neutron-rich nuclei at intermediate energies [1]. With $E_{sym}(\rho)=E_{sym}(\rho_0)(\rho/\rho_0)^{\gamma}$, where $E_{sym}(\rho_0)\approx$ 30 MeV is the symmetry energy at normal nuclear matter density ρ_0, we find that strengths of the correlation functions for nucleon pairs with high total momentum are stronger for a stiffer $E_{sym}(\rho)$, corresponding to a larger value of γ, as shown in Fig.1. This is due to the fact that a stiff density dependence of nuclear symmetry energy leads to earlier and nearly simultaneous emissions of high momentum neutrons and protons. The two-nucleon correlation functions are, on the other hand, insensitive to the incompressibility of symmetric nuclear matter and in-medium N-N cross sections. Although the symmetry energy effect becomes weaker with increasing impact parameter, incident energy, and masses of colliding systems, studies of two-nucleon correlation functions in heavy ion collisions provides a possible tool for extracting useful information about the density dependence of nuclear symmetry energy, which is essential for understanding the structures of radioactive nuclei and many important issues in astrophysics [2].

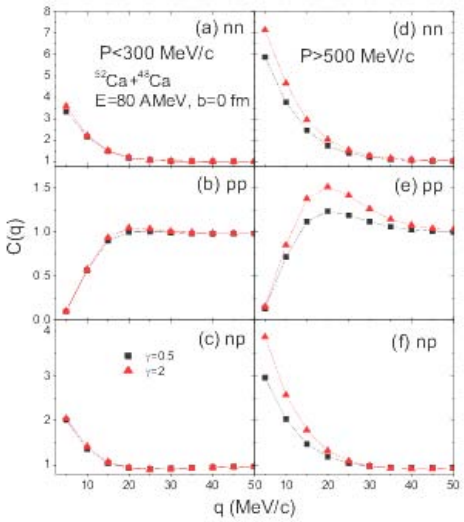

Figure 1. Two-nucleon correlation functions gated on the total momentum P of nucleon pairs using the soft (filled squares) or stiff (filled triangles) symmetry energy. Left panels are for P<300 MeV/c while right panels are for P>500 MeV/c.

References

[1] L. W. Chen, V. Greco, C. M. Ko, and B. A. Li, Phys. Rev. Lett. **90**, 162701 (2003); nucl-th/0305036, Phys. Rev. C (in press).

[2] B. A. Li, C. M. Ko, and W. Bauer, Int. Jour. Phys. E **7**, 147 (1998).

Kaon interferometry at RHIC

Z. W. Lin[1] and C. M. Ko

[1]*Ohio State University, Columbus, OH*

Using a multiphase transport model (AMPT) that includes both initial partonic and final hadronic interactions [1], we have studied the interferometry of two identical kaons at RHIC [2]. Very different correlation functions are obtained for the cases with and without melting of initial strings. Unlike the case for pions [3], the two-kaon correlation function in the scenario of string melting is not very sensitive to the parton scattering cross section as shown in Fig. 1, where the two-kaon correlation function is shown as a function of various projections of the total momentum of kaon pairs. We also find that the kaon source radii extracted directly from the emission function are close to the fitted radius parameters extracted from a Gaussian fit to the three-dimensional correlation function. However, the ratio R_{out}/R_{side} extracted from a Gaussian fit to the correlation function is close to one, and is much smaller than that obtained from the emission function. Our results further show that the kaon emission source has a large positive correlation between the freezeout time and the freezeout position along the out-direction, similar to the pion emission source.

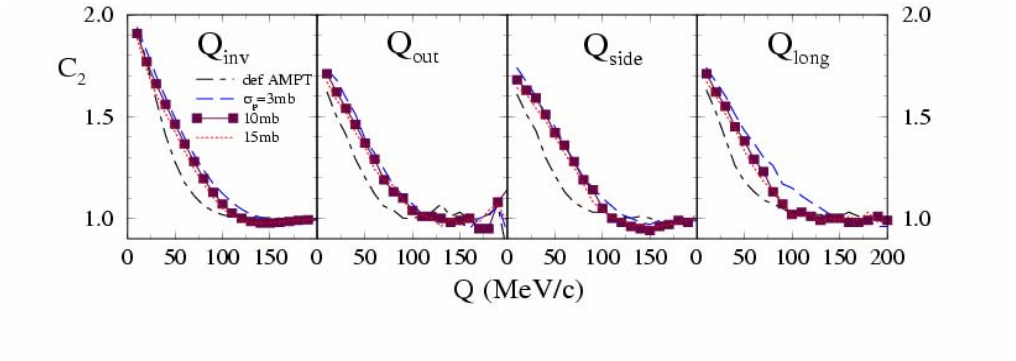

Figure 1. Correlation function for K_0 with $200<p_t<400$ MeV/c and $-1<y<1$ for different values of parton scattering cross section in central Au+Au collisions at 130 AGeV.

References

[1] B. Zhang, C. M. Ko, B. A. Li and Z. W. Lin, Phys. Rev. C **61**, 067901 (2000); Z. W. Lin, S. Pal, C. M. Ko, B. A. Li, and B. Zhang, ibid. **64**, 011902 (2001); Nucl. Phys. **A698**, 375 (2002).

[2] Z. W. Lin and C. M. Ko, nucl-th/0305069; J. Phys. G, in press.

[3] Z. W. Lin, C. M. Ko, and S. Pal, Phys. Rev. Lett. **89**, 152301 (2002).

Light clusters production as a probe to the nuclear symmetry energy

L. W. Chen[1], C. M. Ko, and B. A. Li[2]

[1]*Shanghai Jiao Tung University, Shanghai, China,* [2]*Arkansas State University, Jonesboro, AR*

Although the nuclear symmetry energy $E_{sym}(\rho)$ at normal nuclear matter density ρ_0 is known to be around 30 MeV from the empirical liquid-drop mass formula, its values at other densities are poorly known. Using the coalescence model based on nucleon distribution functions from an isospin-dependent transport model, we have studied the effect of nuclear symmetry energy on the production of light clusters such as deuteron, triton, and ^{3}He in heavy-ion collisions induced by neutron-rich nuclei at intermediate energies [1]. Assuming $E_{sym}(\rho)=E_{sym}(\rho_0)(\rho/\rho_0)^\gamma$, we find that both the yield and energy spectrum of light clusters are sensitive to the value of γ, with more light clusters produced for γ=2, corresponding to a stiff symmetry energy as shown in Fig. 1. On the other hand, effects due to the stiffness of the isoscalar part of nuclear equation of state and the medium dependence of nucleon-nucleon cross sections are unimportant. We have also studied the correlation functions of light clusters, and they are affected by the density dependence of nuclear symmetry energy as well, with the stiff symmetry energy giving a stronger anticorrelation of light clusters.

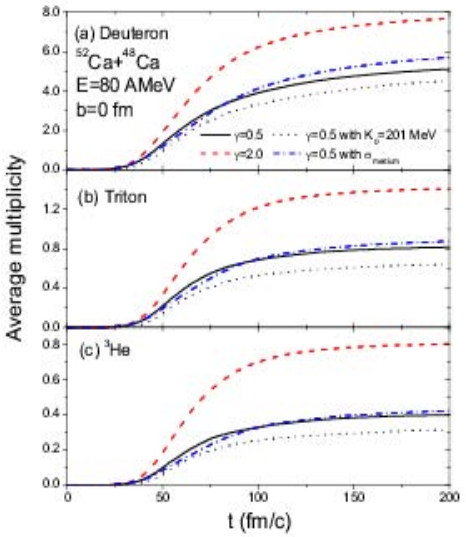

Figure 1. Time evolution of average multiplicities of (a) deuterons, (b) tritons, and (c) ^{3}He from central collisions of ^{52}Ca+^{48}Ca at E=80 MeV/nucleon by using the soft (solid curves) or stiff (dashed curves) symmetry energy with a stiff EOS of K_0=380 MeV and free N-N cross sections. Results using soft symmetry energy and free N-N cross sections but K_0=201 MeV are shown by dotted curves, while those from soft symmetry energy and K_0=380 MeV but in-medium N-N cross sections are given by dash-dotted curves.

References

[1] L. W. Chen, C. M. Ko, and B. A. Li, nucl-th/0305036, Phys. Rev. C (in press); nucl-th/0306032.

Partonic coalescence at RHIC

V. Greco, C. M. Ko, and P. Lévai[1]

[1]*KFKI Research Institute for Particle and Nuclear Physics, Budapest, Hungary*

Using a covariant coalescence model, we have studied hadron production in relativistic heavy ion collisions from both soft partons in the quark-gluon plasma and hard partons in minijets [1]. Including transverse flow of soft partons and independent fragmentation of minijet partons, the model is able to describe available experimental data on pion, kaon, and antiproton transverse momentum spectra. As shown in Fig. 1, the resulting antiproton to pion ratio increases at low transverse momenta and reaches a value of about one at intermediate transverse momenta, as observed in experimental data at RHIC. At high transverse momenta, this ratio decreases and approaches that given by the perturbative QCD. Elliptic flows of phi mesons and baryons such as protons, lambdas, cascades, and omegas have also been evaluated from partons with elliptic flows extracted from fitting measured pion and kaon elliptic flows. The predicted proton and lambda elliptic flows are consistent with available experimental data as shown in Fig. 2 for protons.

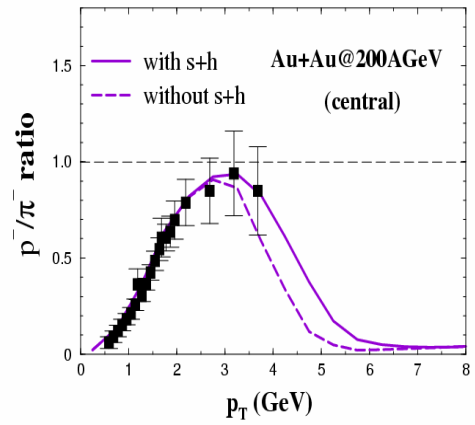

Figure 1. Antiproton to pion ratio with (solid curve) and without (dashed curve) coalescence of minijet and quark-gluon plasma partons. Filled squares are experimental data from PHENIX.

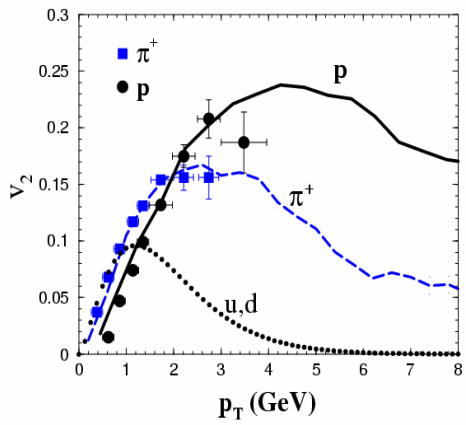

Figure 2. Elliptc flows of partons (dotted curve), protons (solid curve), and pions (dashed curve). Experimental data from STAR are shown by filled circles for protons and squares for pions.

References

[1] V. Greco, C. M. Ko and P. Lévai, Phys. Rev. Lett. **90**, 0202302 (2003); nucl-th/0305024; Phys. Rev. C, in press.

Ξ production at AGS

S. Pal* and C. M. Ko

Using a relativistic hadronic transport (ART) model [1], we have investigated the enhancement of doubly strange baryon (Ξ) production as a signature for quark-gluon plasma formation in high density nuclear matter formed in heavy ion collisions at AGS energies [2]. We find that the strangeness-exchange reactions between antikaons and hyperons lead to substantial production of Ξ in Au+Au collisions at 6 AGeV. Within a phase transition scenario in which the Ξ production cross section is taken to be ten times its value in free space when the energy density exceeds a critical value, the calculated Ξ yield exhibits a nonlinear centrality dependence. For peripheral collisions, the relatively small volume occupied by the QGP phase leads to only a slightly enhanced production of Ξ's that are destroyed in the subsequent hadronic scattering phase. In contrast, the pronounced Ξ yield in central collisions is essentially driven by the QGP phase as it undergoes a smaller reduction by hadronic scattering. On the other hand, the Λ hyperons from the QGP phase suffer stronger rescattering, and their final yield is essentially the value obtained without a phase transition. The enhanced Ξ formation in the QGP scenario, in conjunction with the smaller growth of Λ for central collisions results in a large Ξ/Λ ratio. Similar behavior is predicted for the excitation function where the Ξ yield shows a sudden rise at a beam energy E_{beam}~ 4 AGeV, indicating the onset of the phase transition. This suggests that a measurement of the Ξ excitation function and its centrality dependence at AGS energies may provide valuable insight into the formation of the quark-gluon plasma at high baryon densities.

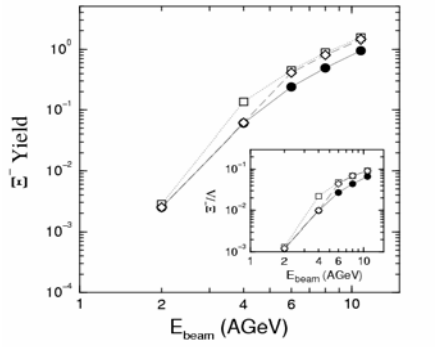

Figure 1. Excitation function from the ART model for the Ξ yield and Ξ/Λ ratio (inset) in central (b=0-3 fm) Au+Au collisions. The solid circles give results without any transition. The squares and diamonds show results for a transition above critical energy densities of 1 and 2 GeV/fm^3, respectively.

*Present address: Michigan State University, East Lansing, MI

References

[1] B. A. Li and C. M. Ko, Phys. Rev. C **52**, 2037 (1995).

[2] S. Pal, C. M. Ko, J. M. Alexander, P. Chung, and R. A. Lacey, nucl-th/0211020.

Excitation of nuclear isoscalar giant dipole resonance by inelastic scattering of 240 and 400 MeV α particles

O. G. Pochivalov, S. Shlomo, B. K. Agrawal

The main experimental tool for studying Isoscalar Giant Dipole Resonance (ISGDR) is inelastic α-particle scattering. This type of reactions is selective to excitation of the isoscalar modes in which the interference of the other excitations can be either eliminated or greatly reduced. Until now in the experiments with the 240 MeV α particles there existed a problem in the identification the high-energy component of the ISGDR. New data on the 400 MeV α-particles allows analysis of the high laying component of the ISGDR in nuclei with much greater precision.

In the current work the analysis of the dependence of the maximal inelastic differential cross-section of the ISGDR with the energy of the inelastic scattering of α particle is presented. For the analysis we use the experimental data for the scattering of α-particle of energy 240 and 400 MeV.

For α-particles of energy 240 MeV we used the Folding Model Distorted Wave Born Approximation (FM-DWBA) for the evaluation of the optical potential from the ground state density and a density dependent nucleon-α interaction (*Vαn*). The parameters of *Vαn* are determined by fitting the experimentally measured angular distributions for the case of elastic scattering cross section. Angular distributions of inelastic scattered α-particles for ISGDR excitation of the target nucleus are obtained by using the FM-DWBA with the collective model transition density [1]. Experimental data for elastic scattering of α-particles of energy 400 MeV is not currently available. Therefore for the analysis of this case we use a ground state density of the nucleus in form of Woods-Saxon distribution with the parameters a_n = 0.5 fm, and half density radius R_n = 6.82 fm. The corresponding (*Vαn*) parameters are taken from Ref. [2].

Using the methods described above we are able to predict the maximal cross-section for the ISGDR for α particle of both energies.

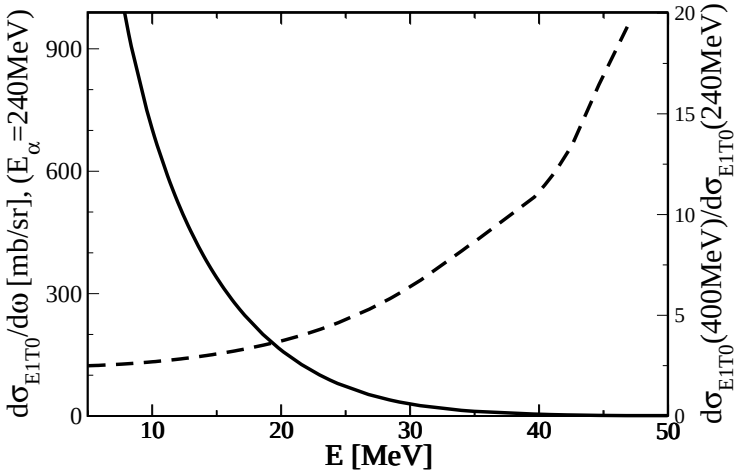

Figure 1. The solid line is the differential cross-sections for ISGDR for the experiments with α particle energy E_α=240 MeV. The dashed line is the ratio between differential cross-sections of the ISGDR modes in the experiments with α particle energies E_α=400 and 240MeV.

As it is seen from Fig.1, with the increase of energy of the α-particles we expect to have increase in the differential cross-section that would allow us to study high-energy component of the ISGDR in greater details.

References

[1] Kolomiets, A., Pochivalov, O., and Shlomo, S., Phys. Rev. C **61**, 034312 (2000).

[2] M. Uchida *et al.*, Phys. Lett. B **557**, 12 (2003).

Direct emission of particles from the isoscalar giant monopole resonance

B. Dobrescu and S. Shlomo

Highly complex many-body systems are often described in macroscopic terms. For example, the time evolution of the nuclear surface and the corresponding geometrical shape provides a very useful parameter to help organize experimental data and numerous evolutionary models, based on this approach, have been developed. However, guessing the correct degrees of freedom without a full understanding of the dynamics can sometimes be misleading. Furthermore, it is most often not possible to connect these macroscopic classical parameters, describing excitation and rearrangement in nuclei, with the more fundamental properties of the nuclear force. Such difficulties can only be overcome within a fully microscopic theory. The time-dependent Hartree-Fock (TDHF) theory is the only fully microscopic description of nuclear dynamics, which has proven applicable in a meaningful fashion to phenomena ranging from the small amplitude domain, where it provides a useful description of collective states, to the large amplitude dynamics of heavy-ion collisions.

Decay properties play an essential role in the study of giant resonances since they are intimately connected with their microscopic structure. Having an excitation energy above the particle emission threshold, giant resonances generally decay by particle emission and consequently the particle decay rates provide an important source of information on the particle-hole (p-h) structure of these collective excitations.

Our main focus in this report is the understanding of lifetimes of giant resonances within the TDHF approach rather than a realistic comparison with experiment. Therefore we restrict ourselves to the isoscalar monopole mode (ISGMR) in spherical nuclei and carry this study with the same simplified Skyrme interaction of ref. [1]. Our TDHF numerical codes have been developed anew and put to the test of the well-known conservation laws preserved by the TDHF formalism ([2], [3]). The time evolution of the root-mean square (rms) radius and the distribution of monopole strength in oxygen-16 presented in ref. [1] have been numerically tested with these codes and a very good agreement has been found.

At the initial time a monopole constraint is imposed on the system and the ground state is approximated by a Slater determinant obtained by minimizing the expectation value of the constrained Hamiltonian. Having set the initial condition, the constraint is switched off and the system is evolved in time within TDHF formalism, governed by its original (unconstrained) Hamiltonian.

As an example we report the results obtained for calcium-40. The Lagrange parameter (i.e. the "strength") of the monopole constraint has been chosen to be $\lambda = 1.134$ MeV/fm^2, which corresponds to an excitation energy of 23.976 MeV, in agreement with the empirical relation $82/A^{1/3}$ MeV that gives the energy centroid for ISGMR. When integrating the TDHF equations we assume the single-particle wave functions (s.p.w.f.) to be zero beyond the edge of a spherical box. The radial mesh size was chosen $\Delta r = 0.1$ fm and the time step $\Delta t = 0.3\times10^{-26}$ sec. The total time interval over which the system was evolved is $T = 5.175\times10^{-22}$ sec. In order to avoid spurious variations in the s.p.w.f. over the time T, due to reflections by the edge of the box, we chose the radius of this sphere to be very large, R = 90 fm. The flux of particles as a function of time, through a sphere of radius $\rho = 20$ fm, increases smoothly, reaching its

maximum of 2.3 particles/10^{-21} sec at t = 3.9× 10^{-22} sec and then decreases. This behavior is that characteristic of a wave packet that clears the chosen spherical enclosure of radius ρ over the time T. The time average of the particle flux was found to be 0.872 particles/10^{-21}sec, corresponding to a life-time of 1.147×10^{-21} sec.

References

[1] S. Stringari and D. Vautherin, Phys. Lett. **88B**, 1 (1979).

[2] P. Bonche, S. E. Koonin and J. W. Negele, Phys. Rev. C **13**, 1226 (1976).

[3] J. W. Negele, Rev. Mod. Phys. **54**, 913 (1982).

Comparison of the continuum and discretized HF-RPA calculations for the isoscalar giant resonances

B. K. Agrawal and S. Shlomo

Recently, precise measurement of the centroid energy for the isoscalar giant resonances (ISGR) has triggered the need for highly accurate microscopic calculations of the response functions for the ISGR. The most accurate response functions for the ISGR are obtained using the Hartree-Fock (HF) based continuum random phase approximation (CRPA). For numerical tractability, one often discretizes the continuum using a box of finite size. To mimic the continuum appropriately, one must use a very large box for the discretization. Furthermore, the RPA calculations should be performed using sufficiently large cut-off for the particle-hole excitation energy ($E_{ph}^{\max}$) and a reasonable value for the smearing width ($\Gamma/2$). We have investigated the influence of the nature of discretization on the response functions and the centroid energies of the ISGR with multipolarities L = 0, 1, and 2. To illustrate this, we present here the discretized (D) and continuum HF-RPA results obtained using a two-body interaction given by

$$V_{12} = \delta(r_1 - r_2)[t_0 + \frac{1}{6} t_3 \rho^{\alpha}(\frac{r_1 + r_2}{2})],$$

with $\alpha = 1/3$, t_0 = -1800 MeV fm^3, and $t_3 = 12871$ MeV fm^4. For these values of the interaction parameters, the nuclear matter equation of state $E(\rho)/A$, has a minimum at $E/A = -15.99$ MeV, $\rho_0 = 0.157$ fm^{-3} with $K_{nm} = 226$ MeV, where $E/A, \rho$ and K_{nm} are the binding energy per nucleon, matter saturation density, and incompressibility coefficient for symmetric nuclear matter, respectively. In Fig. 1, we show the response functions for the isoscalar giant dipole resonance (ISGDR) obtained by using the box size of 12 and 72 fm, together with the corresponding results obtained in HF-CRPA. We see that the DRPA results obtained for the large box coincide with the results obtained within the CRPA. The transition strength gets fragmented if the discretization is carried out using a small box. To avoid a misleading interpretation of the fragmentation and obtain agreement with the CRPA results, one needs to use a large enough value of the smearing parameter consistent with the size of the box. Therefore, one can satisfactorily reproduce the CRPA results, provided the DRPA calculations are carried out using a box of very large size (i.e., dense discretization) and the $E_{ph}^{\max}$ is set to be sufficiently high. We see from Table 1 that as $E_{ph}^{\max}$ increases, the centroid energies for L = 0, 1 and 2 resonances, converge to their corresponding exact values obtained using HF-CRPA. However, this convergence is slower for the E_{ss}. For the low values of $E_{ph}^{\max}$ we observe that the centroid energy of the ISGR with L= 0 is overestimated by about 0.5 MeV, which can significantly affect the value determined for the nuclear incompressibility coefficient.

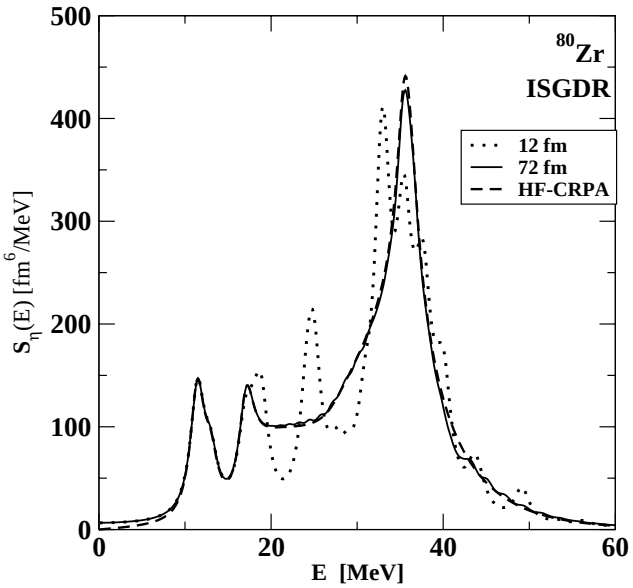

Figure 1. Discretized RPA results for the ISGDR response functions obtained using $E_{ph}^{\max} = 200$ MeV with the smearing parameter $\Gamma = 1.0$ MeV.

Table 1. Dependence of the spurious state energy (E_{ss}) and the centroid energies E_L ($L = 0,1,$ and 2), in MeV, on the value of $E_{ph}^{\max}$ (in MeV) used in HF-DRPA calculations together with the corresponding HF-CRPA results (last row). The HF calculation is performed using a box of 72 fm for the ^{80}Zr nucleus.

$E_{ph}^{\max}$	E_{ss}	E_0	E_1	E_2
50	4.7	23.92	35.34	16.11
75	3.3	23.51	35.76	15.51
100	2.9	23.25	35.66	15.14
200	1.5	23.09	35.55	14.82
400	1.0	23.02	35.51	14.73
600	0.9	23.02	35.51	14.72
∞	0.7	23.01	35.46	14.70

Nuclear matter incompressibility coefficient in relativistic and nonrelativistic microscopic models

B. K. Agrawal, S. Shlomo, and V. Kim Au

The nuclear matter incompressibility coefficient K_{nm} plays an important role in understanding a wide variety of phenomena ranging from giant resonances in finite nuclei to heavy-ion collisions and supernova explosion. Most recent microscopic calculations carried out using the nonrelativistic and the relativistic mean field based random phase approximation (RPA) yield the values for K_{nm} in the range of 210 – 220 and 250 – 270 MeV, respectively. It has been claimed [1,2] that these pronounce differences (~20%) in the value of K_{nm} are due to the model dependence. On the other hand, it has been pointed out in Ref. [3] that the differences in the values of K_{nm} obtained in the relativistic and the nonrelativistic models can be attributed, at least in part, to the differences in the density dependence of the symmetry energy in these models. However, in Ref. [3], the analysis was restricted to the single nucleus ^{208}Pb.

We have analyzed in detail the aforesaid claim. For a meaningful comparison, we have generated parameter sets for Skyrme interaction by a least square fitting procedure using exactly the same experimental data for the bulk properties of nuclei considered in Ref. [4] for determining the NL3 parameterization of an effective Lagrangian used in the relativistic mean field (RMF) models. We deal with the centre of mass correction to the total binding energy, finite size effects of the protons and Coulomb energy in the way similar to that employed in determining the NL3 parameter set in Ref. [4]. Further, we also demanded in our fitting procedure that the values of K_{nm}, symmetry energy coefficient (J) and the charge radius of the ^{208}Pb nucleus should be very close to 271.76 MeV, 37.4 MeV and 5.50 fm, respectively, as obtained with the NL3 interaction. The parameter sets thus obtained are used to calculate the centroid energy for the isoscalar giant resonance (ISGMR) for several nuclei. In Table 1 we give the results for the ISGMR centroid energy obtained using our new parameter sets SK272 and SK255 and compare them with the RMF based RPA results of Ref. [1] for the NL3 interaction. For the parameter set SK272 (K_{nm} = 272 MeV and J = 37.4 MeV), the calculated values of E_o are higher by about 5% compared to the corresponding NL3 results. This implies that the difference in the value of K_{nm} obtained in the relativistic and the nonrelativistic

Table 1. ISGMR centroid energy $E_o = m_1/m_o$ (in MeV, where m_o and m_1 correspond to the non-energy and energy weighted sums) obtained by integrating over the energy range ω_1-ω_2 MeV with the strength function smeared by using $\Gamma/2$ = 1 MeV.

Nucleus	ω_1-ω_2	Exp	NL3	SK272	SK255	SGII
^{90}Zr	0 – 60		18.7	20.0	18.9	18.3
	10 –26	17.89±0.2		19.3	18.4	17.9
^{116}Sn	0 – 60		17.1	18.0	17.5	16.6
	10 –26	16.07±0.12		17.4	16.9	16.3
^{144}Sm	0 – 60		16.1	17.1	16.4	15.6
	10 –26	15.39±0.28		16.5	15.9	15.2
^{208}Pb	0 – 60		14.2	14.7	14.2	13.9
	10 –26	14.17±0.28		14.2	13.8	13.6

microscopic models could be at most 10%. In view of this, we generate another parameter set SK255 having K_{nm} = 255 MeV with J = 37.4 MeV. As expected, the parameter set SK255, yields for the ISGMR centroid energies values which are quite close to the NL3 results. Moreover, for the SK255 parameter set, we find a good agreement with experimental data for E_o for all the nuclei considered, provided, the corresponding excitation energy ranges used in determining E_o are the same as those used in obtaining the experimental data. We have thus shown that the difference in the values of K_{nm} obtained in the relativistic and nonrelativistic models is rather small (less than 10%) and it mainly arises due to the difference in the value of the symmetry energy coefficient associated with these models.

References

[1] Nguyen Van Giai, P. F. Bortignon, G. Colo, Zhongyu Ma and M. Quaglia, Nucl. Phys. **A687**, 44c (2001).

[2] T. Niksic, D. Vretenar and P. Ring, Phys. Rev. C **66**, 064302 (2002).

[3] J. Piekarewicz, Phys. Rev. C **66**, 034305 (2002).

[4] G. A. Lalazissis, J. Konig and P. Ring, Phys. Rev. C **55**, 540 (1997).

Non-Markovian effects on the bubble dynamics in hot asymmetric nuclear matter

V .M. Kolomietz[l], A. I. Sanzhur[l] and S. Shlomo
[1]*Institute for Nuclear Research, Kiev 03680, Ukraine*

We study the conditions for the generation and the dynamical evolution of embryonic overcritical vapor bubbles in an overheated asymmetric nuclear matter. Using the temperature dependent Thomas-Fermi approximation [1] and the Skyrme-type forces as the effective nucleon- nucleon interaction, we have solved the equilibrium equations and evaluated the dependence of the critical radius R^* of the embryonic bubble on the overheating temperature δT. We have established that the critical radius R^* increases with the asymmetry parameter $X_{\rm liq}$ of the liquid phase. This is mainly due to the increase of the boiling temperature $T_{\rm o}$ with the decrease of the asymmetry parameter $X_{\rm liq}$.

The generation of the embryonic bubble of arbitrary radius R is subsidized by the variation of the free energy $\Delta\Phi\ (R)$. The maximum of $\Delta\Phi\ (R)$ is located at $R= R^*$. The bubble radius R^* is the critical point for the metastable phase with respect to the boiling process. To start up the boiling (cavitation), i.e., to start the infinite growth in the size of the bubbles, the system must pass through the barrier of $\Delta\Phi\ (R)$ to reach the region of R^*.

We have studied the problem of the dynamical evolution of the overcritical bubble with the radius R of the barrier at $R> R^*$. Starting from the collisional kinetic equation for the nuclear Fermi liquid, we have derived the non-Markovian equation of motion for the bubble radius $R(t)$ without restrictions on the amplitude of $\delta R(t)=R(t)- R^*$.

We have shown that the development of instability of the bubble near the barrier point $R= R^*$ is strongly influenced by the memory effects, if the relaxation time τ is large enough. In this case, an expansion of the bubble is accompanied by characteristic shape oscillations of the bubble radius (see Fig. 1) which depend on the structure of the memory kernel and on the relaxation time τ. Oscillations of the radius appear due to an elastic force induced by the memory integral. This elastic force acts against the adiabatic force and significantly hinders the growth of the bubble radius. The characteristic oscillations of $\delta R(t)$ disappear in the short relaxation time limit $\tau \to 0$.

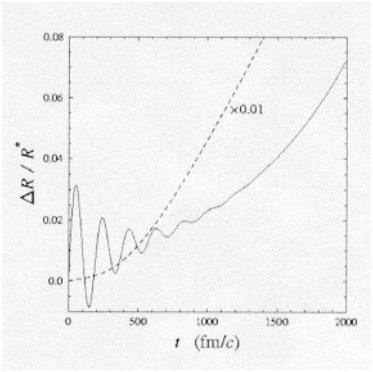

Figure 1. Time variation of the bubble shape parameter R near the barrier point $R=R^*$ for various values of the relaxation time τ. The dashed and solid curves correspond to the values of τ = 3 10^{-23} s and τ =4.5 10^{-23} s, respectively.

References

[1] V. M. Kolomietz, A. I. Sanzhur, S. Shlomo and S. A. Firin, Phys. Rev. C **64**, 024315 (2001).

Nuclear dissipativity effects on the nuclear friction

V. M. Kolomietz[1], S. V. Lukyanov[1] and S. Shlomo
[1]*Institute for Nuclear Research, Kiev 03680, Ukraine*

Starting from the collisional kinetic equation with a random force and using the p-moments technique, we have derived the equations of motion of viscous fluid dynamic for the local values of particle density, velocity field and pressure tensor. The important features of these equations of motion are due to the non-Markovian form of the pressure tensor caused by the relaxation on the distorted Fermi surface. In contrast to the commonly used τ-approximation, we take into account the higher orders of the variation of the collision integral with respect to the variation of the phase-space distribution function. Using the Abrikosov-Khalatnikov transformation we have then obtained the collision integral in the form of the extended τ-approximation.

Assuming the displacement field in a separable form, we have introduced the macroscopic collective variable β(t) and reduced the problem to a macroscopic equation of motion for β(t). The final macroscopic equation of motion includes both the memory effects and the nonlinear dissipativity terms. We have separated the description of the collective motion into two parts. The first (slow) one is related to the driving force and it is associated with a slow motion. The second (fast) one is due to the fast fluctuations of the random force. Using the correlation properties of the random force, we have performed the averaging of the macroscopic equation of motion over the fast fluctuations, reducing the nonlinear dissipativity terms to the form which is linear with respect to the slow collective motion.

Finally, assuming the periodic driving force ~exp ($i\omega t$), we have derived the macroscopic strength function S(ω). We show that the nonlinear dissipativity effect leads to an additional spreading $\Delta\gamma$ and a resonance shift $\Delta\omega_0$ in the strength function S(ω). The contribution $\Delta\gamma$ appears due to the thermodynamical fluctuations of the collective variable β. In contrast to the Fermi-liquid friction parameter $\gamma_0 \sim T^2$ (for high temperatures), the spreading width $\Delta\gamma$ is a linear function of the temperature *T*. This fact provides a non-monotonic behavior of the ratio $\Delta\gamma/\gamma_0$, see Fig. 1. As seen from Fig. 1, the nonlinear dissipativity effects are enhanced at moderate temperatures T≈ 2 MeV and do not exceed ≈20%.

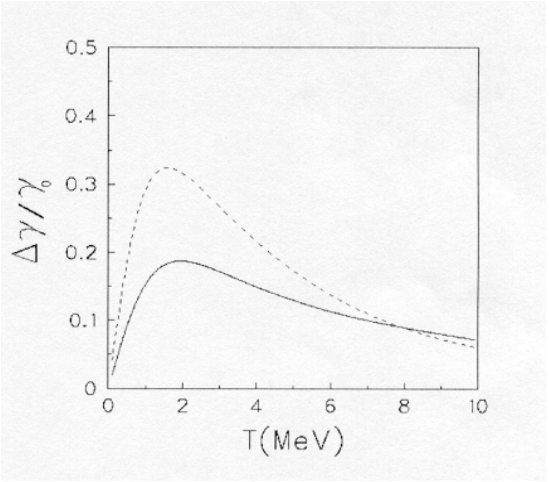

Figure 1. Temperature dependence of the ratio $\Delta\gamma/\gamma_0$ for the nucleus with A=224 for the giant quadrupole resonance (GQR). The solid curve was obtained from the strength function S(ω); the dashed line was obtained using the phenomenological parametrization of $E_R = 60A^{1/3}$MeV.

SECTION IV

ATOMIC, MOLECULAR AND MATERIALS SCIENCE

Projectile Ionization in Collisions of U^{28+} with Gases

R. E. Olson[1], R. L. Watson, V. Horvat, K. E. Zaharakis, and T. Stöhlker[2]
[1]*University of Missouri – Rolla,* [2]*Atomphysik, GSI-Darmstadt*

The n-CTMC method has been used to calculate the stripping cross sections for collisions of U^{28+} with several gases. The method numerically solves the classical Hamiltonian for an n-body collision [1]. The initial electronic state of the projectile ion and target atom are based on the experimental binding energies of the electrons and their radial expectation values. Both the electron-electron and electron-nucleus interactions are included between centers. In these calculations 36 electrons were used in the description of the U^{28+} ion, which consisted of the $4s^2 4p^6 4d^{10} 4f^{14} 5s^2 5p^2$ outer shell electrons. On the nitrogen target all 7 electrons were included, while for Ar we found only the L- and M-shells were active for a total of 16 electrons. Thus, at the maximum, 54 bodies were carried in the n-CTMC calculations, resulting in the solution of the time evolution of 324 first order differential equations for each trajectory.

As a benchmark, a comparison between calculated and experimental electron loss cross sections [1] for $Xe^{18+} + N_2$ collisions are displayed in Fig. 1. There is reasonable agreement in magnitude and energy dependence with the largest discrepancy being approximately 25% at the lowest energy of 2 Mev/amu. Both experiment and theory show an overall energy dependence of approximately $E^{-0.5}$ with the slope increasing slightly above 10 MeV/amu in the calculated values. The $E^{-0.5}$ dependence is contrary to the predictions of one-electron theories [3,4]. Such behavior appears to be associated with the fact that the ions studied are only partially stripped, so that there is always an electron shell whose cross section for ionization is near its maximum value. Presented on the same graph are the calculated stripping cross sections for U^{28+} on H_2, N_2, and Ar. The $U^{28+} + N_2$ cross sections are almost identical to those for $Xe^{18+} + N_2$. Note that the U^{28+} cross sections also have an energy dependence of approximately $E^{-0.5}$. This becomes important in the prediction of ion beam lifetimes in an accelerator structure. Experimental measurements of the stripping cross sections for U^{28+} in N_2 and Ar are currently in progress.

The calculated U^{28+} cross sections were used to predict ion loss due to charge changing in the GSI-Darmstadt SIS beam line. Very recently, measurements were made of the ion beam lifetime in the present SIS ring for energies from 10 to 150 MeV/amu [2]. The composition and the concentration of residual gas in the ring was determined at a background pressure of 7.7×10^{-11} mbar. The results deviated significantly from lifetimes deduced from stripping cross sections determined by one-electron Born calculations [3,4]. At the highest energies, the difference was on the order of a factor of three (Fig. 2).

The n-CTMC cross sections given in Fig. 1 were used to estimate the U^{28+} beam lifetime for the parameters given in the SIS measurements. The results are in reasonable accord with the data in both shape and magnitude (Fig. 2). The $E^{-0.5}$ dependence on the stripping cross sections of Fig. 1 yield an almost constant lifetime for all energies. The error bars on the calculations reflect the uncertainty in the H_2 target calculations whose contribution to the lifetime is calculated to be approximately 30% at the energies where the H_2 cross sections could be made. There is a slight increase in the calculated lifetime at the highest energy due to the relativistic correction to the collision velocity.

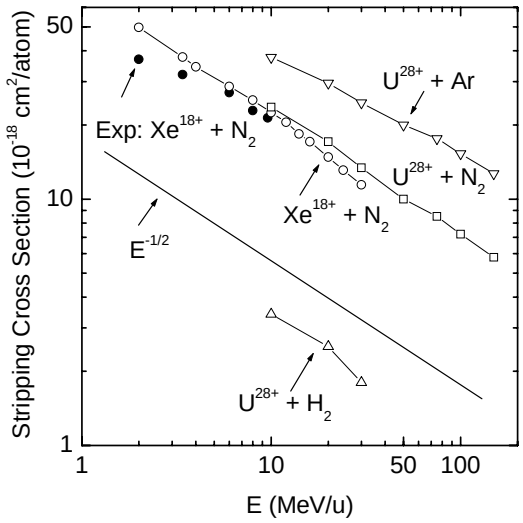

Figure 1. Total cross sections for electron removal from the projectile by various gases: solid circles are experimental data [1] for Xe^{18+} + N_2, the n-CTMC calculations are given by open symbols with circles – Xe^{18+} + N_2, triangles – U^{28+} + H_2, squares – U^{28+} + N_2, and inverted triangles – U^{28+} + Ar.

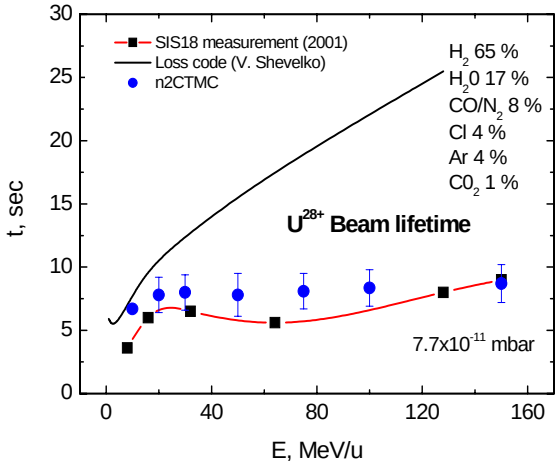

Figure 2. U^{28+} beam lifetime as a function of energy at $7.7x10^{-11}$ mbar. The solid line is from the work of Shevelko et al. [3,4], the solid circles are from the cross sections of Fig. 1 that were calculated by the n-CTMC method, and the solid squares are the measurements from GSI-Darmstadt [2].

References

[1] Olson, R. E., *et al.*, J. Phys B. **35**, 1893 (2002).

[2] Krämer A., *et al.*, Proc. of EPAC2002, Paris (2002).

[3] Shevelko V. P. *et al.*, Nucl. Instrum. Methods Phys. Res. A **415**, 609 (1998).

[4] Shevelko V. P., *et al.*, Nucl. Instrum. Methods Phys. Res. B **184**, 295 (2001).

Projectile and Target Electron Loss in Fast Ion-Atom Collisions

R. D. DuBois[1], A. C. F. Santos[1], R. Olson[1], V. Horvat, R. L. Watson, A. N. Perumal, and Y. Peng
[1]*University of Missouri-Rolla, Rolla, MO, USA*

As an extension of the work described previously [1], cross sections for projectile electron loss and target ionization were measured for 2.3 MeV/amu and 4.8 MeV/amu $Ne^{2,\,3,\,4+}$ ions interacting with Ar and Xe gas targets. The idea behind this method is to extend the measurements for "low" charge state heavy projectiles to higher energies by reversing the roles of the projectile and the target, i.e., by studying fast light ion impact ionization of heavy neutral targets. Thus, in the reverse collision, electron loss from neutral Ar and Xe "projectiles" occurs when they impact Ne "target" ions. Cross sections for the collisions involving a neutral projectile and a neutral target can be extrapolated based on the measured projectile charge dependence.

This work consisted of two parts. First, absolute cross sections for electron loss from $Ne^{2,\,3,\,4+}$ ions were measured. Then, ionization of the target (Ar or Xe) was detected in coincidence with the outgoing neon ions. In this part of the experiment, information about pure target ionization is obtained from coincidences with a projectile that has not changed its charge state, while information about simultaneous ionization of both collision partners is obtained from coincidences with projectiles which have lost 1,2,3, etc. electrons. Combining the measured yields with the absolute target density, the length of the target gas from which target ions are extracted, the extracted ion transmission and detection efficiencies, and the detection efficiencies for the projectile ions allows us to determine absolute cross sections.

Recoil ions produced in the gas cell were accelerated into a 15 cm long flight tube of a time-of-flight (TOF) spectrometer by an electric field directed perpendicular to the projectile ion beam. Two acceleration stages were used in order to provide space focusing. Upon reaching the end of the flight tube, the recoil ions were accelerated into a microchannel plate detector, 40 mm in diameter. Typically, the pressure inside the gas cell ranged between 2 and 4 mTorr and was maintained at a constant value by means of an automatic valve and a capacitance manometer. This pressure range was sufficiently low to effectively suppress double-collision events.

Signals from the recoil ion detector were used to start a time-to-amplitude converter (TAC), while delayed timing signals from the projectile ion detector were used to stop it. The TOF signals generated by the TAC were then digitized by a CAMAC analog-to-digital converter, along with the position signals derived from those generated by the projectile ion detector using a dual sum/inverter and position sensitive detector analyzer. The data were recorded event-by- event using a personal computer running customized data acquisition software.

Results for 4.8 MeV/amu Ne^{2+} - Ar collisions (shown in Fig. 1 below) indicate that collisions in which the projectile loses electrons are more efficient at removing large numbers of target electrons than collisions in which the projectile remains un-stripped (pure target ionization). Moreover, target and projectile ionization cross sections are found to be roughly identical. However, it should be noted that the target ionization cross section values presented here are *preliminary*, as the detection and transmission efficiencies are still under investigation. Based on the measurements with Ne^{2+}, Ne^{3+}, and Ne^{4+}, it was

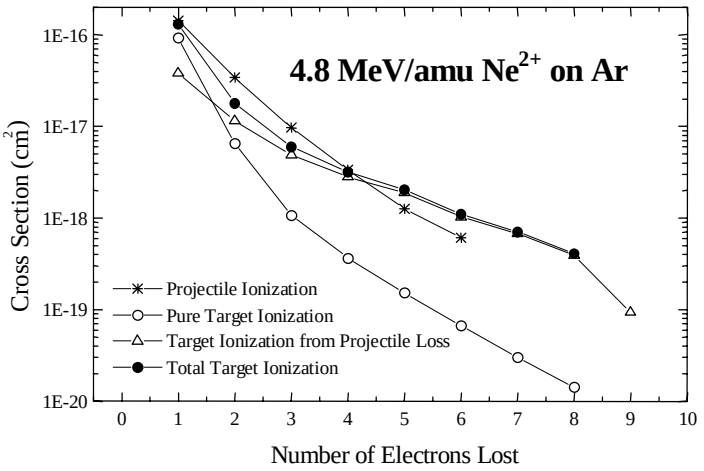

Figure 1. Dependence on the number of electrons lost of the cross sections for ionization of the 48.8 MeV/u Ne^{2+} projectile ions (stars) and Ar target atoms (solid circles). Also shown are the contributions to the latter from pure ionization (hollow circles) and ionization in coincidence with projectile electron loss (triangles).

found that with increasing projectile charge, target ionization cross sections increase while projectile electron loss cross sections decrease.

References

[1] R. L. Watson, Y. Peng, V. Horvat, G. Kim, and R. E. Olson, Phys. Rev. A **67**, 022706 (2003).

Electron Loss by 6 MeV/amu Xe^{18+} in Ne and SF_6

Y. Peng, R. L. Watson, V. Horvat, and A. N. Perumal

In an effort to investigate the possible influence of molecular structure on fast ion collisions, electron loss cross sections were measured for 6 MeV/amu Xe^{18+} ions in thin (gas) targets of Ne and SF_6. The choice of SF_6 as the molecular target was dictated by the fact that its average atomic number (10) is the same as the atomic number of Ne. The results are shown in Fig. 1 where cross sections (per atom) for the loss of one to eight electrons (n=1 to 8) are compared. It is apparent that the cross sections for the loss of one through five electrons are nearly identical for the two targets, while differences between the cross sections for electron loss in the two gases begin to appear at n = 5 and steadily increase with n. Nevertheless, the effect is surprisingly weak.

A possible explanation for the insensitivity of the electron loss cross sections to the molecular nature of the target is that the average impact parameters for electron loss might be much smaller than the molecular bond lengths. If this were the case, then a molecular target would act simply as a collection of independent atoms. In order to test this idea, a semiempirical representation of the impact parameter dependence of electron loss based on the independent electron approximation [1] was used to estimate the most probable impact parameters b_n. The differential cross section for electron loss may be expressed as

$$d\sigma_n = 2\pi P_n(b)db$$

where the P_n is the probability of removing n out of a total of N electrons, given by

$$P_n(b) = \frac{N!}{n!(N-n)!}\, p(b)^n [1 - p(b)]^{N-n}.$$

The probability for single electron loss was represented by a Gaussian;

$$p(b) = p_0 e^{-b^2/2\delta^2}.$$

The probability (p_0) and width (δ) parameters were previously determined by fitting the calculated cross sections to measured cross sections for electron loss in the noble gas targets He through Xe [2]. The most probable impact parameters obtained by finding the maxima in the distribution functions $2\pi bP_n(b)$ are listed in Table 1 for F, Ne, and S atoms.

A comparison of the bond lengths, atomic radii, and most probable impact parameters for one-electron loss collisions of Xe^{18+} ions with SF_6 molecules is shown in Fig. 2. (Only four of the six fluorine atoms are shown). The solid circles represent the average radii of the outermost shells of the target atoms, the dotted circles represent the most probable impact parameters, and the dashed circles represent the outer shell radius of the Xe^{18+} ion when it is centered on the dotted circles. Since the sum of the most probable impact parameters for one-electron loss collisions with S and F atoms (0.60 Å) is much less than the S-F bond length (1.56 Å), it is unlikely that the projectile will undergo an electron loss collision with more than one atom in the molecule. Therefore, the original hypothesis appears to be correct.

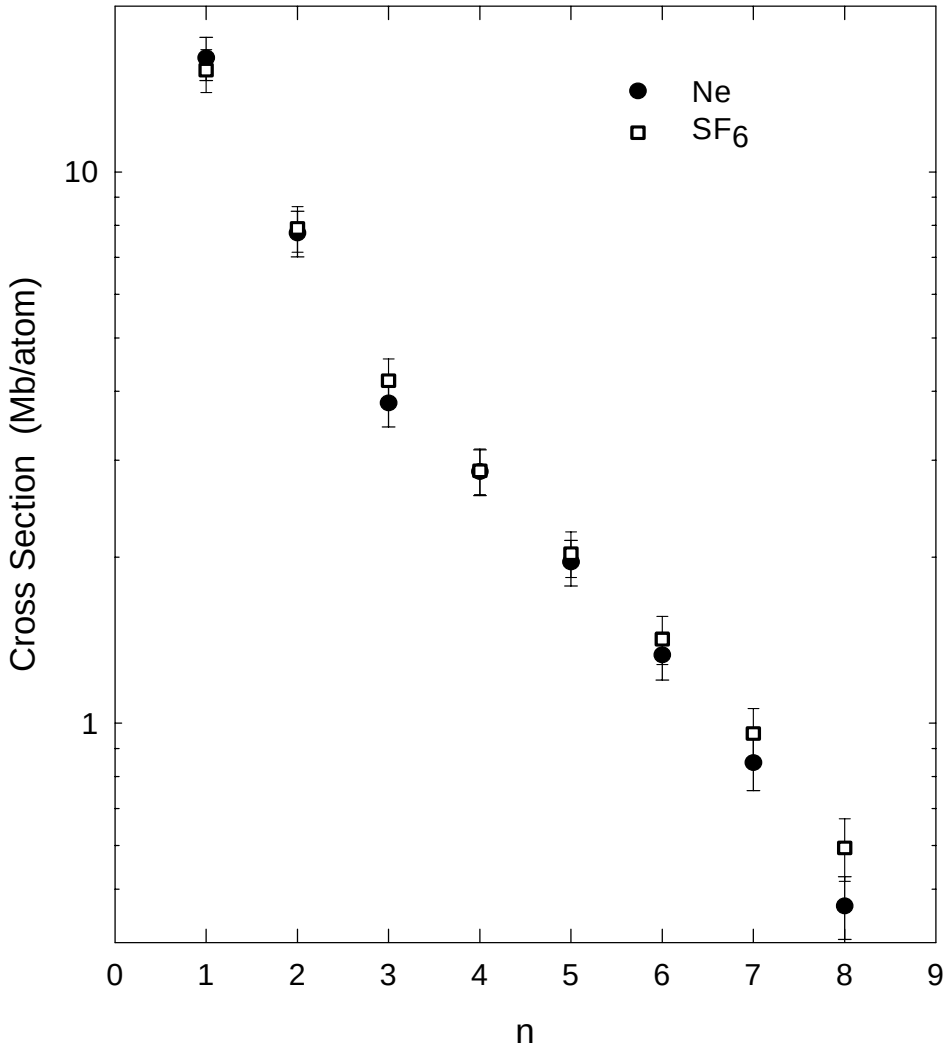

Figure 1. Comparison of cross sections for the loss of one to eight electrons in the atomic target Ne and the molecular target SF_6.

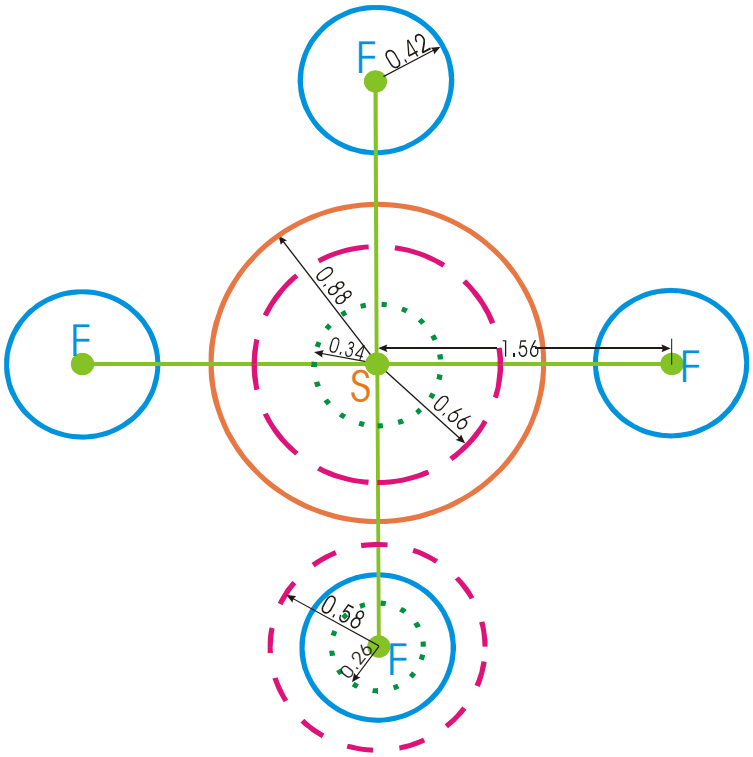

Figure 2. Diagram comparing the S-F bond length in SF_6 to the calculated most probable impact parameters (dotted circles) for one-electron loss collisions of 6 MeV/u Xe^{18+} ions with S and F atoms.

Table 1. Calculated most probable impact parameters (Å) for electron loss from 6 MeV/amu Xe^{18+} ions in collisions with fluorine, neon, and sulfur atoms.

Number of electrons	Most probable impact parameter		
Lost	Fluorine	Neon	Sulfur
1	0.259	0.271	0.337
2	0.206	0.218	0.271
3	0.168	0.181	0.228
4	0.137	0.147	0.193
5	0.109	0.118	0.159
6	0.081	0.090	0.128
7	0.059	0.066	0.090
8	0.044	0.047	0.056

References

[1] T. Tonuma, H. Shibata, S. H. Be, H. Kumagai, M. Kase, T. Kambera, I. Kohono, A. Ohsaki, and H. Tawara, Phys. Rev. A **33**, 3047 (1986).

[2] R. L. Watson, Y. Peng, V. Horvat, G. J. Kim, and R. E. Olson, Phys. Rev. A **67**, 022706 (2003).

Evaluation of Stripping Foils for the RIA Driver

E. Kanter[1], J. Nolan[1], D. H. Youngblood, Y. -W. Lui, H. L. Clark, Y. Tokimoto, X. Chen, and R. L. Watson

[1]*Argonne National Laboratory*

One of the continuing problems in the design of the RIA driver linac has been the reliability of predicting charge state distributions given by various computer codes which are currently available. For any heavy ion accelerator, one faces a tradeoff in selection of strippers between maximizing the mean charge, minimizing the width of the outgoing charge state distribution (to maximize efficiency), and minimizing transverse (angular) and lateral (energy) beam spreads. In the case of RIA, this means being able to calculate these quantities for 10- and 85-MeV/amu uranium ions. Because there is a paucity of experimental data available in the energy regimes of current interest, we have had to rely on computer codes which simulate the passage of fast ions through matter (e.g., ETACHA [1], SRIM [2], and GLOBAL). These codes, however, all employ numerous approximations in estimating various physical quantities (such as electron capture and loss cross sections, interaction potentials, etc.) and in the cases of interest, produce different results. Thus, it is crucial to test the predictions of such calculations with experimental data. Toward that end, the MDM spectrograph was used to measure the charge state distributions of 10.5-MeV/amu U^{38+} ions emerging from thin carbon and beryllium stripper foils of various thicknesses. The charge state distribution obtained with a 600 μg/cm^2 carbon foil is shown in Fig. 1. The lateral straggling was found to be significantly larger than predicted by SRIM and an interesting decrease in the apparent stopping power was observed with the thinnest foils. Further analysis of the data is in progress and there is hope of extracting angular information as well.

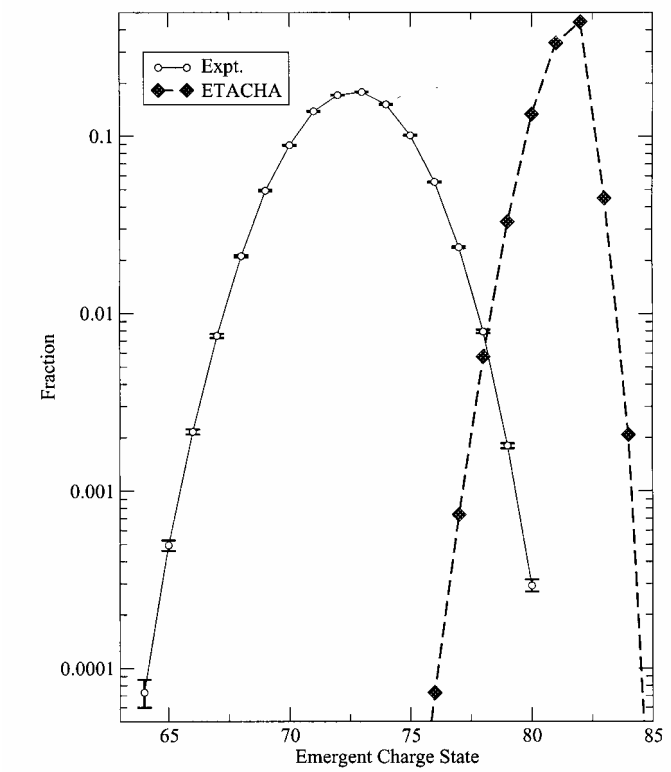

Figure 1. Emergent charge state distribution measured for 10.5-MeV/amu U^{38+} ions impinging on a 600 μg/cm^2 carbon foil. Also shown are predictions of the computer code ETACHA [1].

References

[1] J. P. Rozet, C. Stephan, and D. Vernhet, Nucl. Instrum. Methods Phys. Res. B **107**, 67 (1996).

[2] *The Stopping and Range of Ions in Matter*, J. F. Ziegler, J. P. Biersack, and U. Littmark, Pergamon Press,

New York, 1985; Program SRIM by J. P. Ziegler, IBM-Research, 28-0, Yorktown, NY.

Energy Dependence of the Average Equilibrium Charge of Uranium Ions

R. L. Watson, V. Horvat, Y. Peng, and A. N. Perumal

In addition to our work on cross sections for electron capture and loss by U^{28+} (mentioned in a preceding report) we have measured the charge distributions of 3.5 and 6.5 MeV/amu U^{28+}, exiting carbon foils, as a function of the foil thickness. This data has been used to determine the average equilibrium charges for uranium ions at these two energies. The results of the present measurements are presented in Table 1, along with the experimental average equilibrium charges obtained by others. In Fig. 1, the experimental average equilibrium charges are compared with the predictions of various semiempirical formulas over the energy range of 1.4 to 16.3 MeV/amu. The solid curve in Fig. 1 has been fit to the experimental data and is given by

$$\overline{Q}_{eq} = 23.90 + \frac{68.01\ E}{4.438 + E},$$

where E is in MeV/amu. The above equation reproduces the experimental $\overline{Q}_{eq}$ to within 1.4 charge units over the whole energy range from 1.5 to 200 MeV/amu, whereas the semiempirical formulas deviate from the experimental values by as much as 5.8 charge units over the restricted range of comparison.

Table 1. Experimental average equilibrium charges for uranium ions in carbon.

Energy (MeV/amu)	$\overline{Q}_{eq}$	**References**
1.4	40.9	B. Erb, GSI Rep. p-7-78 (unpublished); K. Shima *et al*., At. Data & Nucl. Data Tables **34**, 357 (1986).
3.5	52.5	Present work.
5.9	63.1	B, Franzke (unpublished); K. Shima *et al*., At. Data & Nucl. Data Tables **34**, 357 (1986).
6.5	64.0	Present work.
10.5	72.6	*Progress in Research*, Cyclotron Institute, Texas A&M University (2002-2003), p. IV-8.
16.3	77.9	A. Leon *et al*., At. Data & Nucl. Data Tables **69**, 217 (1998).
200.0	89.9	H. Gould *et al.*, Nucl. Instrum. Methods Phys. Res. B **10**, 32 (1985).

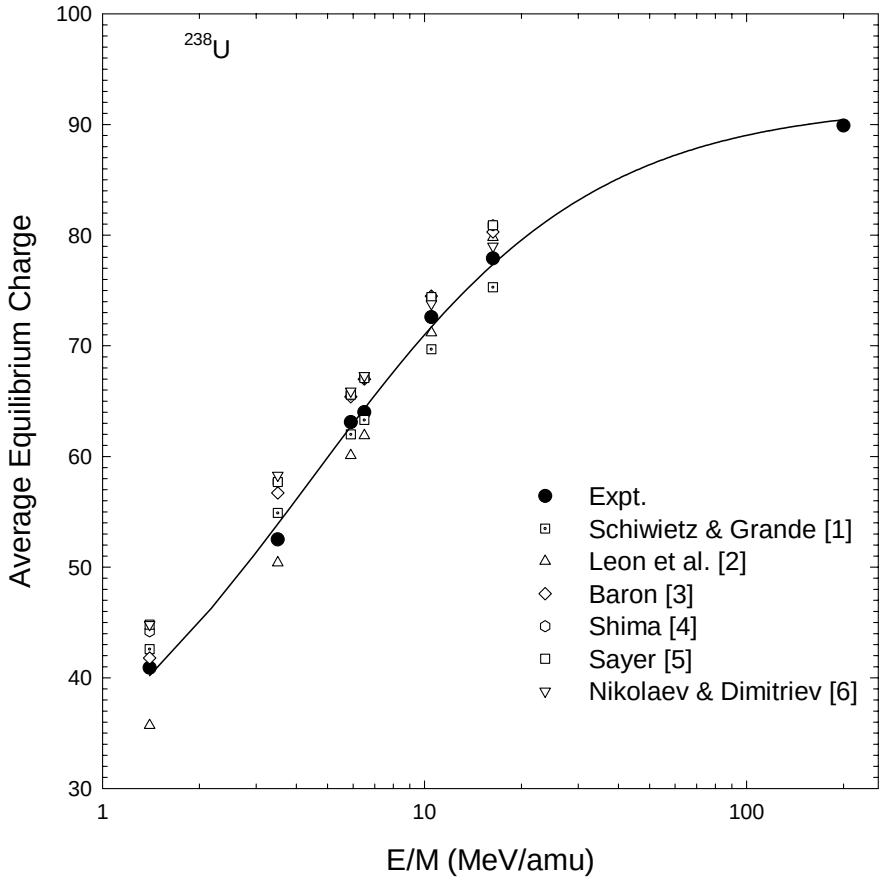

Figure 1. Average equilibrium charge of uranium ions in carbon as a function of energy.

References

[1] G. Schiwietz and P. L. Grande, Nucl. Instrum. Methods Phys. Res. B **175**, 125 (2001).

[2] A. Leon, S. Melki, D. Lisfi, J. P. Grandin, P. Jardin, M. G. Suraud, and A. Cassimi, At. Data and Nucl. Data Tables **69**, 217 (1998).

[3] E. Baron, IEEE Trans. Nucl. Sci. **NS-26**, 2411 (1979).

[4] K. Shima, T. Ishihara, and T. Mikumo, Nucl. Instrum. Methods Phys. Res. **200**, 605 (1982).

[5] O. Sayer, Rev. Phys. Appl. **12**, 1543 (1977).

[6] V. S. Nikolaev and I. S. Dimitriev, Phys. Lett. **28A**, 277 (1968).

Spectra of Ho Lα x rays emitted in collisions with 6 MeV/amu Heavy Ions

A. N. Perumal, V. Horvat, R. L. Watson, and Y. Peng

It is well known that fast heavy ions provide an efficient means for creating multiple inner-shell vacancies in small impact parameter atomic collisions. In general, the presence of multiple vacancies results in a complex and mostly unresolvable multiplet structure which appears above the diagram (single vacancy) lines in the x-ray spectrum. Over the past thirty years, numerous spectroscopic investigations of Kα x-ray satellites and hypersatellites have led to a detailed understanding of the L spectator vacancy states produced in K-shell ionizing collisions. However, comparatively little work has been devoted to the spectroscopy of L x-ray satellites arising from M spectator vacancies [1-3]. This is primarily due to the fact that the multiplet structure associated with L plus M vacancy states is much more complicated than that for K plus L vacancy states. In addition, the average energy separations between the diagram lines and the L x-ray satellites are smaller than those for the corresponding K x-ray satellites. For example, the $K\alpha_1$ transition energy in Co is 6930 eV and its energy separation from the KL^1 satellite is 30 eV, whereas the $L\alpha_1$ transition energy in Ho is 6722 eV and its energy separation from the LM^1 satellite is 21 eV.

In the present work, the Lα x-ray satellite structure of holmium has been examined using 6 MeV/amu C, Ne, Ar and Kr ions. Spectra for a metallic Ho target were obtained by means of a curved crystal (Johansson) spectrometer employing second order diffraction from a LiF crystal. The spectrometer energy resolution for the Ho $L\alpha_1$ line excited by 10 keV electron bombardment was determined to be 9.0 eV (FWHM). Spectra of Ho Lα x rays obtained with the three heavy ion projectiles are compared in Fig. 1. The spectra contain the single vacancy (diagram) $L\alpha_2$ and $L\alpha_1$ lines at 6679 eV and 6722 eV, respectively, and extensive satellite structure arising from Lα x-rays emitted in the presence of spectator M vacancies. The diagram lines originate from single L_3 vacancies produced both in ion-atom collisions and secondary ionization processes involving x rays and electrons. The diagram lines arising from ion-atom collisions are broadened and slightly shifted up in energy relative to those from secondary ionization. As the projectile atomic number increases, relative intensity of the ion-atom collision contribution decreases and the relative intensity of the secondary ionization contribution increases. In the spectrum obtained with Ar ions, for example, almost all of the $L\alpha_{1,2}$ intensity is attributable to secondary ionization.

A simplified preliminary analysis has been performed on the spectra shown in Fig. 1. In this analysis, the manifold of multiplet transitions for a specified number n of M vacancies was represented by two Voigt functions - one representing the $L_3M^n \rightarrow M_4M^n$ multiplet transitions ($L\alpha_2$ satellites) and one representing the $L_3M^n \rightarrow M_5M^n$ multiplet transitions ($L\alpha_1$ satellites). In the least-squares fitting process, the energy separation of the two peaks in each set was fixed at the diagram $L\alpha_1$-$L\alpha_2$ separation value, but the average energy of each set was allowed to vary. In addition, the intensity ratio of the two peaks in each set was assumed to be the same as that for the diagram lines and the total intensity contribution of each peak set to the spectrum was constrained to follow a binomial distribution, as predicted by the independent electron approximation. The results are shown by the thin solid curves in Fig. 1. Each contributing LM^n manifold is shown by a dashed curve and the secondary ionization diagram lines are shown by thick solid curves. It is evident from the fits shown in Fig. 1 that the highest contributing value

of n (the number of spectator M vacancies) is four for C ions, six for Ne ions, and nine for Ar ions. In the case of the Ar spectrum, additional components attributed to L hypersatellites (double L vacancy initial states) have been included in the fits. The fitted values of the energy centroids for the $L\alpha_1$ satellite peaks

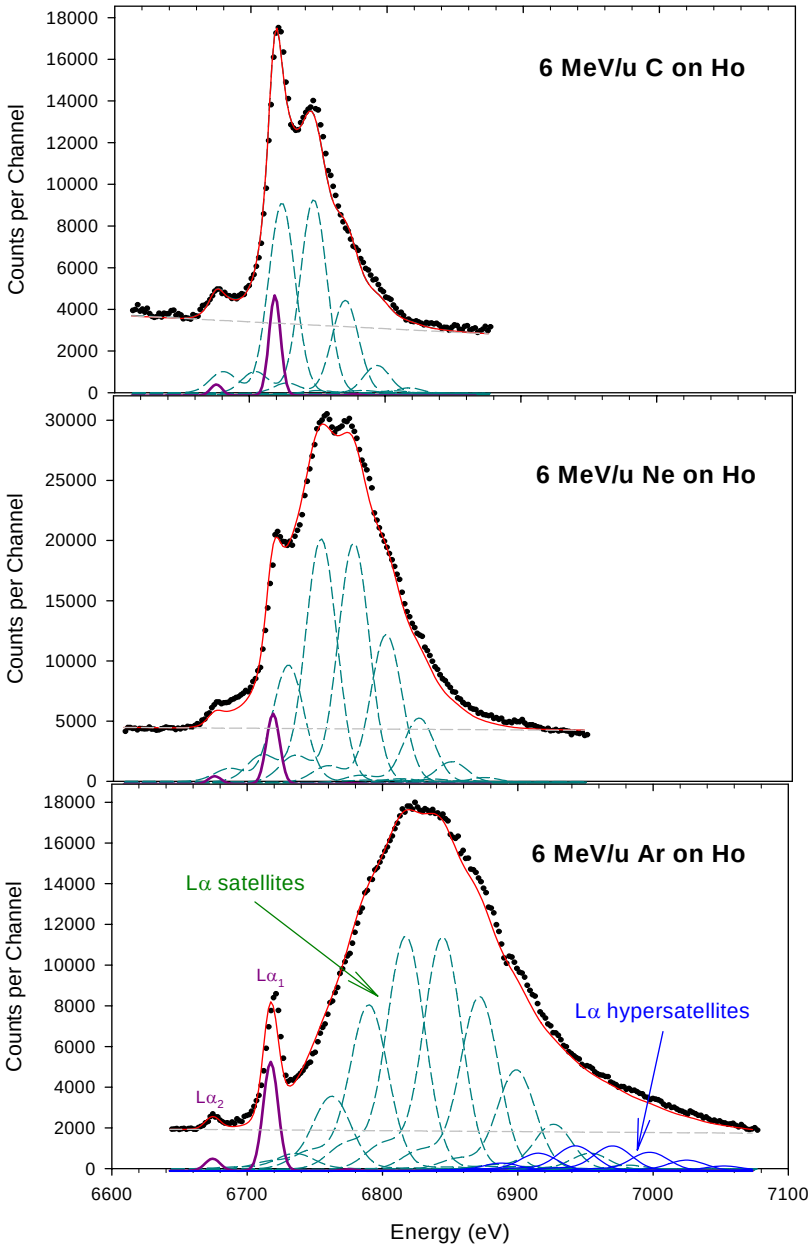

Figure 1. Spectra of Ho Lα x rays emitted under bombardment by 6 MeV/amu C, Ne, and Ar ions.

are in good agreement (within 3 eV on average) with the Dirac-Fock average of configurations energies (see preceding report) if additional energy shifts of 7 eV (C spectrum), 13 eV (Ne spectrum), and 21 eV (Ar spectrum) are assumed to be present due to N-shell vacancies.

The energy calibrations were performed by measuring the Kα x-ray spectra of Co, Ni, and Cu. These calibration spectra, which also contained the Kα satellites, provided an opportunity to compare the average probability of L vacancy production in K-shell ionizing collisions, P_L, with the average probability of M vacancy production in L-shell ionizing collisions, P_M, for atoms having similar x-ray transition energies. The average spectator vacancy probabilities were determined by dividing the average numbers of satellite vacancies (calculated from the satellite relative intensities) by the corresponding shell occupation numbers (i.e., eight for the L shell and 18 for the M shell). This comparison is shown in Fig. 2. It appears that the M spectator vacancy probability is systematically lower than the L spectator vacancy probability.

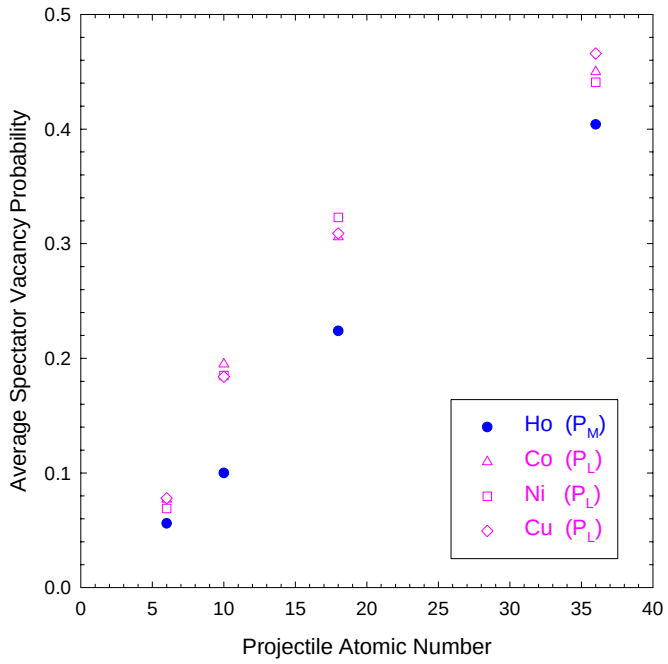

Figure 2. Comparison of the average probabilities of producing spectator L- and M-shell spectator vacancies in K- and L-shell ionizing collisions, respectively, for Co, Ni, Cu and Ho.

References

[1] D. K. Olsen, C. F. Moore, and P. Richard, Phys. Rev. A **7**, 1244 (1973).

[2] Ch. Heitz, J. Larcher, G. J. Costa, A. Pape, Y. El Masri, Th. Keutgen, I. Tilquin, F. Hanappe, and P. Duhamel, Z. Phys. D **42**, 15 (1997).

[3] J. M. Blackadar, Ph.D. dissertation, Texas A&M University (1999).

L X-ray satellite energies of Holmium

A. N. Perumal, V. Horvat, J. M. Blackadar, and R. L. Watson

The interpretation of ion induced L x-ray spectra of heavy elements is a challenging problem because of complications arising from the presence of numerous satellites associated with spectator vacancies in the M and higher shells. In order to understand the satellite structure, it is important to know the transition energy for each contributing configuration. Energies for multiple vacancy configurations are not generally available although the single vacancy energies are well known [1]. Calculating the transition energies for all the possible vacancy configurations is an extensive process and therefore, a simplified representation is desireable. In this report, we present (a) average of configurations energies of Holmium $L\alpha_1$, $L\alpha_2$, $L\beta_1$, and $L\beta_2$ transitions for initial state configurations having 0 to 17 M vacancies (0 to 18 in the case of $L\beta_2$), and (b) L-S multiplet transition energies for the case of one spectator vacancy.

In the average of configurations calculations, the following restrictions and simplifications have been adopted;

- At least one electron must be initially present in the M or N shell and one vacancy in the L shell in order to observe the transitions $L\alpha_1$, $L\alpha_2$, $L\beta_1$, and $L\beta_2$.
- The transition energy obtained for a given number of initial state M vacancies is an average of the transition energies between all the possible initial and final electron configurations having that number of M spectator vacancies statistically weighted for the subshell populations. For example, in the case of one spectator M vacancy, the $L\alpha_1$ transition energy is averaged over five initial and final state electron configurations.
- To reduce the number of calculations, a simple interpolation procedure is adopted which requires calculating average transition energies for configurations having 0, 1, 16 and 17 spectator M-shell vacancies (or 0, 1, 17 and 18 spectator vacancies in the case of $L\beta_2$). The transition energies for other numbers of spectator M vacancies may then be determined through interpolation using a polynomial fitting function.
- The N-and higher shells are considered in two ways. When the number of spectator M-shell vacancies is 0 or 1, then the N and higher shells are assumed to be full and when the number of spectator vacancies is 16 or 17 (17 or 18 in the case of $L\beta_2$), the N and higher shells are considered to be empty. However, the P-shell is always assumed to be empty.

The Multi-configuration Dirac-Fock (MCDF) atomic structure program [2] has been used to calculate the satellite energies for different vacancy configurations. The x-ray transition energy of an ion is calculated by taking the difference in the average of configurations total energies of the initial and final vacancy configurations. Figure 1 shows the calculated average $L\alpha_1$ and $L\alpha_2$ transition energies of Ho. The open circles are the calculated energies and the filled circles are determined through interpolation. The $L\alpha_1$, $L\alpha_2$, $L\beta_1$ and $L\beta_2$ average transition energies are listed in the Table 1. The first column indicates the number of M-shell spectator vacancies (n_M) and the energies are given in units of eV.

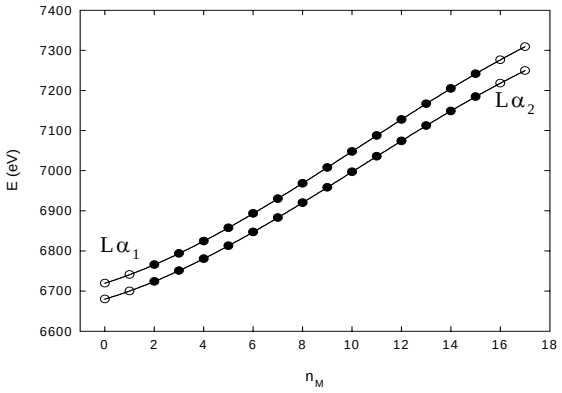

Figure 1. Calculated $L\alpha_1$ and $L\alpha_2$ x-ray average transition energies for Ho as a function of the number of spectator M-shell vacancies.

Table 1. The average x-ray satellite energies (eV) of Ho $L\alpha_1$, $L\alpha_2$, $L\beta_1$ and $L\beta_2$ for 0 to 17 M-shell spectator vacancies (0 to 18 in the case of $L\beta_2$), calculated using the Dirac-Fock program along with an interpolation procedure.

n_M	$L\alpha_1$	$L\alpha_2$	$L\beta_1$	$L\beta_2$
0	6719.525	6679.879	7525.57	7904.145
1	6740.660	6699.988	7546.96	7955.890
2	6765.425	6723.702	7572.17	8019.083
3	6793.432	6750.635	7600.80	8092.493
4	6824.295	6780.400	7632.44	8174.894
5	6857.624	6812.611	7666.68	8265.054
6	6893.032	6846.881	7703.12	8361.745
7	6930.132	6882.824	7741.35	8463.737
8	6968.535	6920.055	7780.97	8569.802
9	7007.855	6958.185	7821.58	8678.711
10	7047.703	6996.829	7862.75	8789.234
11	7087.703	7035.601	7904.10	8900.141
12	7127.433	7074.114	7945.22	9010.205
13	7166.540	7111.981	7985.69	9118.195
14	7204.625	7148.817	8025.11	9222.883
15	7241.299	7184.234	8063.09	9323.039
16	7276.176	7217.847	8099.21	9417.434
17	7308.867	7249.269	8133.06	9504.839
18	-	-	-	9584.025

Along with this simplified method of calculating average transition energies, an attempt has also been made to calculate all the possible transition energies for a single spectator M vacancy. Using the Dirac-Fock program, the multiplet energies for all possible values of total angular momentum (J) have been calculated. Then, using the L-S coupling scheme and Hund's rule, the corresponding L-S term symbols and energies were identified. Once the term symbols were known for the initial and final states, the energies of allowed transitions were determined by applying dipole selection rules. The energies of 113 allowed transitions for a single spectator M-vacancy are listed in table 2.

Table 2. Calculated L-S multiplet transition energies (eV) for a Ho atom having a single spectator M-shell vacancy.

Transition	Energy	Transition	Energy	Transition	Energy	Transition	Energy
$2s^{-1}3s^{-1} \rightarrow 3s^{-1}3p^{-1}$		$2s^{-1}3d^{-1} \rightarrow 3d^{-2}$		$^3F_2 \rightarrow {}^3D_3$	5968.406	$^3D_3 \rightarrow {}^3F_4$	6751.224
$^3S_1 \rightarrow {}^3P_0$	7525.357	$^3D_3 \rightarrow {}^3P_2$	8043.283	$^3F_3 \rightarrow {}^3D_2$	5969.043	$^3D_2 \rightarrow {}^3F_2$	6759.899
$^1S_0 \rightarrow {}^1P_1$	7542.677	$^3D_2 \rightarrow {}^3P_1$	8050.701	$^3P_1 \rightarrow {}^3D_1$	5977.349	$^3P_2 \rightarrow {}^3D_3$	6889.493
$^3S_1 \rightarrow {}^3P_1$	7667.826	$^3D_3 \rightarrow {}^3F_3$	8053.042	$^3P_0 \rightarrow {}^3D_1$	5977.772	$^3P_1 \rightarrow {}^3D_2$	6898.433
$^3S_1 \rightarrow {}^3P_2$	7707.002	$^3D_2 \rightarrow {}^3P_2$	8053.100	$^3F_3 \rightarrow {}^3D_3$	5980.045	$^3P_2 \rightarrow {}^3D_2$	6901.032
$2s^{-1}3p^{-1} \rightarrow 3p^2$		$^3D_2 \rightarrow {}^3F_3$	8062.859	$^3P_1 \rightarrow {}^3D_2$	6005.108	$^3P_1 \rightarrow {}^3D_1$	6907.508
$^1P_1 \rightarrow {}^1S_0$	7515.145	$^3D_3 \rightarrow {}^3F_2$	8081.107	$^3P_2 \rightarrow {}^3D_2$	6736.069	$^3P_2 \rightarrow {}^3D_1$	6910.107
$^1P_1 \rightarrow {}^1D_2$	7700.792	$^3D_1 \rightarrow {}^3P_1$	8081.250	$^1F_3 \rightarrow {}^1D_2$	6775.175	$^1D_2 \rightarrow {}^1P_1$	7364.966
$2s^{-1}3d^{-1} \rightarrow 3p^{-1}3d^{-1}$		$^3D_1 \rightarrow {}^3P_2$	8083.649	$^3P_2 \rightarrow {}^3D_1$	6780.152	$^3S_1 \rightarrow {}^3P_2$	7412.750
$^1D_2 \rightarrow {}^1P_1$	7514.466	$^3D_3 \rightarrow {}^3F_4$	8086.318	$^3P_2 \rightarrow {}^3D_3$	6818.913	$^1D_2 \rightarrow {}^1F_3$	7418.855
$^3D_3 \rightarrow {}^3P_2$	7519.294	$^3D_2 \rightarrow {}^3F_2$	8090.924	$^1P_1 \rightarrow {}^1D_2$	6821.066	$^3S_1 \rightarrow {}^3P_0$	7552.683
$^3D_2 \rightarrow 3P_2$	7529.109	$^3D_1 \rightarrow {}^3P_0$	8106.101	$2p^{-1}3s^{-1} \rightarrow 3s^{-1}3d^{-1}$		$^3S_1 \rightarrow {}^3P_1$	7553.207
$^3D_1 \rightarrow {}^3P_2$	7559.660	$^3D_1 \rightarrow {}^3F_2$	8121.473	$^3P_2 \rightarrow {}^3D_1$	6708.310	$^1P_1 \rightarrow {}^1D_2$	7561.525
$^1D_2 \rightarrow {}^1F_3$	7568.355	$2p^{-1}3s^{-1} \rightarrow 3s^{-2}$		$^3P_1 \rightarrow {}^3D_1$	6714.439	$^1S_0 \rightarrow {}^1P_1$	7568.010
$^3D_2 \rightarrow {}^3P_1$	7669.568	$^1P_1 \rightarrow {}^1S_0$	6806.479	$^3P_2 \rightarrow {}^3D_2$	6736.069	$2p^{-1}3d^{-1} \rightarrow 3d^{-2}$	
$^3D_3 \rightarrow {}^3F_3$	7681.096	$2p^{-1}3p^{-1} \rightarrow 3s^{-1}3p^{-1}$		$^3P_1 \rightarrow {}^3D_2$	6742.198	$^3D_1 \rightarrow {}^3P_1$	6716.002
$^3D_2 \rightarrow {}^3F_3$	7690.913	$^3D_1 \rightarrow {}^3P_0$	5790.387	$^3P_2 \rightarrow {}^3D_3$	6747.071	$^3D_1 \rightarrow {}^3P_2$	6718.401
$^3D_1 \rightarrow {}^3P_0$	7699.599	$^3D_1 \rightarrow {}^3P_1$	5932.856	$^1P_1 \rightarrow {}^1D_2$	7551.673	$^3D_2 \rightarrow {}^3P_1$	6737.564
$^3D_1 \rightarrow {}^3P_1$	7700.117	$^3D_2 \rightarrow {}^3P_1$	5954.219	$^3P_0 \rightarrow {}^3D_1$	7555.828	$^3D_2 \rightarrow {}^3P_2$	6739.963
$^3D_3 \rightarrow {}^3F_2$	7702.855	$^3D_3 \rightarrow {}^3P_2$	5971.951	$2p^{-1}3p^{-1} \rightarrow 3d^{-1}3p^{-1}$		$^3D_1 \rightarrow {}^3P_0$	6740.853
$^3D_2 \rightarrow {}^3F_2$	7712.672	$^3D_1 \rightarrow {}^3P_2$	5972.032	$^3D_1 \rightarrow {}^3P_2$	6554.975	$^3D_3 \rightarrow {}^3P_2$	6746.772
$^3D_3 \rightarrow {}^3F_4$	7715.355	$^3D_2 \rightarrow {}^3P_2$	5993.395	$^3D_3 \rightarrow {}^3P_2$	6554.894	$^3D_2 \rightarrow {}^3F_3$	6749.722
$^3D_1 \rightarrow {}^3F_2$	7743.221	$^1D_2 \rightarrow {}^1P_1$	6643.034	$^3D_2 \rightarrow {}^3P_2$	6576.338	$^3D_1 \rightarrow {}^3F_2$	6756.225
$2s^{-1}3p^{-1} \rightarrow 3p^{-1}3d^{-1}$		$^3S_1 \rightarrow {}^3P_0$	6648.162	$^3D_1 \rightarrow {}^3P_0$	6694.908	$^3D_3 \rightarrow {}^3F_3$	6756.531
$^3P_2 \rightarrow {}^3D_3$	8042.877	$^3S_1 \rightarrow {}^3P_1$	6790.631	$^3D_1 \rightarrow {}^3P_1$	6695.432	$^3D_2 \rightarrow {}^3F_2$	6777.787
$^3P_0 \rightarrow {}^3D_1$	8248.205	$^3S_1 \rightarrow {}^3P_2$	6829.807	$^3D_3 \rightarrow {}^3F_3$	6716.696	$^3D_3 \rightarrow {}^3F_2$	6784.596
$^3P_2 \rightarrow {}^3D_2$	8054.416	$^1S_0 \rightarrow {}^1P_1$	6846.078	$^3D_2 \rightarrow {}^3P_1$	6716.795	$^3D_4 \rightarrow {}^3F_4$	6789.807
$^3P_1 \rightarrow {}^3D_2$	8059.148	$2p^{-1}3d^{-1} \rightarrow 3s^{-1}3d^{-1}$		$^3D_1 \rightarrow {}^3F_2$	6737.536	$^1F_3 \rightarrow {}^1D_2$	7522.098
$^3P_2 \rightarrow {}^3D_1$	8063.491	$^3F_2 \rightarrow {}^3D_1$	5929.645	$^3D_2 \rightarrow {}^3F_3$	6738.140	$^1F_3 \rightarrow {}^1G_4$	7522.535
$^3P_1 \rightarrow {}^3D_1$	8068.223	$^3F_2 \rightarrow {}^3D_2$	5957.404	$^3D_3 \rightarrow {}^3F_2$	6738.455	$^1P_1 \rightarrow {}^1S_0$	7544.236
$^1P_1 \rightarrow {}^1D_2$	8069.214	$^3F_4 \rightarrow {}^3D_3$	5961.212	$^3P_0 \rightarrow {}^3D_1$	6750.054	$^1P_1 \rightarrow {}^1D_2$	7567.989

References

[1] J. A. Bearden, Rev. Mod. Phys. **39**, 78 (1967).

[2] J. P. Desclaux, Comp. Phys. Commun. **9**, 31 (1975).

Target and Projectile K-vacancy Production by Fast Heavy Ions in the Molecular Orbital Regime

V. Horvat, Z. Smit[1], R. L. Watson, A. N. Perumal, and Y. Peng
[1]*Department of Physics, University of Ljubljana, Jadranska, and J. Stefan Institute, Jamova Ljubljana, Slovenia*

An increase in the K x-ray production cross section as the atomic number of the projectile (Z_1) approaches the atomic number of the target atom (Z_2) is a characteristic of the molecular-orbital (MO) mechanism. In this process, K vacancy production in the target atom and in the projectile ion is due to interactive level crossings that occur as the two collision partners dynamically combine to form a quasi-molecule. This mechanism is expected to be predominant when the projectile speed is significantly smaller than the orbital speed of the K electrons.

Cross sections for target atom and projectile ion K vacancy production have been measured using Mo, Ag, and Sn targets bombarded by 10 MeV/amu beams of H, Ne, Ar, Cr, Kr, Mo, Ag, Sn, Xe, Nd, Ho, Ta, Au, and Bi. The targets were self-supporting solid metallic foils, having thickness of ~2 mg/cm^2, positioned at 45^o relative to the beam. A plastic scintillator mounted on a photomultiplier tube was positioned directly behind the target and used to count the outgoing beam particles. Emitted x rays were measured with a Si(Li) detector, positioned at 90^o relative to the beam, viewing the beam-impact surface of the target at 45^o. The signals from the detector were fed into a pulse-height analyzer. Finer details of the experiment are essentially identical to those described in a previous publication [1].

Contributions from the MO mechanism were calculated using the diffusion model of Mittleman and Wilets [2] and the hidden crossing model of Janev [3]. Other processes may also contribute to target K-vacancy production. These include direct ionization of the target electron in a binary collision with the projectile (DI) and non-radiative capture of the target electron to a projectile bound state (NREC). For targets with large atomic numbers, significant contributions from the radiative electron capture mechanism (REC) can be expected. DI also contributes to projectile K-vacancy production.

The contributions from DI and NREC are typically calculated using the ECPSSR theory [4]. However, this theory is expected to be valid only when $0.03 \leq Z_1 / Z_2 \leq 0.3$, which means that it does not apply in the near-symmetric region. Indeed, the K-vacancy production cross sections for a Cu target bombarded by 10 MeV/amu projectiles with $Z_1 \geq Z_2$ (measured previously [5]), were found to be significantly smaller than the ECPSSR cross sections for DI alone. A theory of DI that would be valid for near-symmetric collisions involving heavy projectiles is not presently available.

The tentative contributions to target K-vacancy production from NREC were also calculated using the ECPSSR theory, taking into account the availability of projectile states for capture while the projectile is inside the target. It also found that these contributions alone overestimate the measured cross sections for the copper target, both in the near-symmetric collision region and also for heavier projectiles. The same was found for contributions from REC [6] involving Sm and Ta targets [7]. Therefore, the measured cross sections were compared with those calculated using the MO approach, assuming that all other contributing processes could be represented by a second-order polynomial in Z_1. The coefficients of this polynomial were determined in a least-squares fit to the difference between the measured and calculated cross sections.

K-vacancy production cross sections for Mo, Ag, and Sn targets are shown in Fig. 1 as a function of projectile atomic number. Good overall representations of the data are achieved. The shapes of the regions of enhanced cross sections are well reproduced by the MO contributions calculated using the hidden crossing model [3] in conjunction with vacancy sharing fractions obtained experimentally using the collected data. This mechanism contributes about 75% of the measured cross section at the peak of the enhancement. The agreement with the experimental data is almost as good when the diffusion model [2] is used to calculate the contributions from the MO effects under the same conditions. A comprehensive theory of K-vacancy production in near-symmetric regions is needed to describe the individual contributing mechanisms on a quantitative basis.

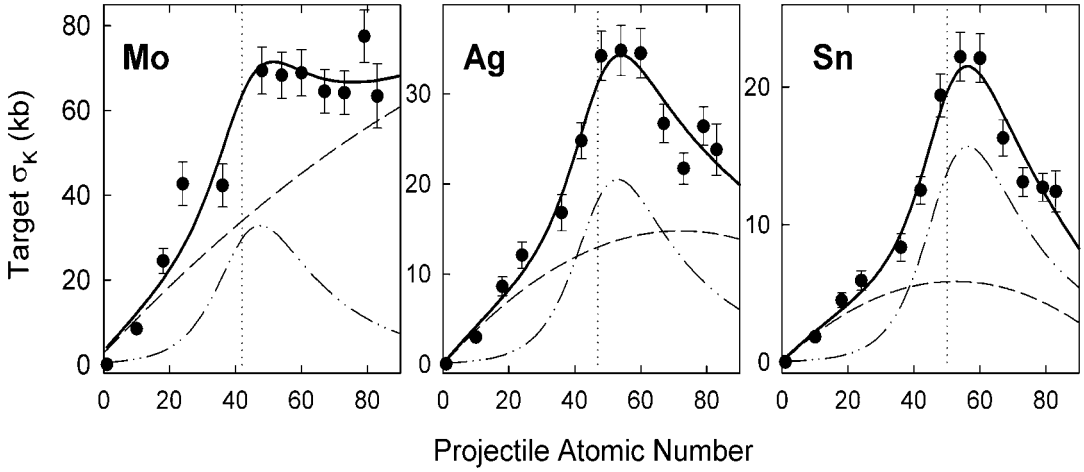

Figure 1. Cross sections for K-vacancy production in Mo, Ag, and Sn targets as a function of projectile atomic number. Solid circles represent the measured data. Calculations based on the theory of Janev [3], using measured vacancy sharing fractions, are represented by the dash-dotted line, a polynomial fit to the residuals is represented by the dashed line, and the total cross section is represented by the thick solid line. The vertical dotted lines denote the center of the symmetric region.

References

[1] R. L. Watson, V. Horvat, J. M. Blackadar and K. E. Zaharakis, Phys. Rev. A **62**, 052709 (2000).

[2] M. H. Mittleman and L. Wilets, Phys. Rev. **154**, 12 (1967).

[3] R. K. Janev, Nucl. Instrum. Methods Phys. Res. B **124**, 290 (1997); R. K. Janev, J. Phys. B **30**, 3019 (1997).

[4] W. Brandt and G. Lapicki, Phys. Rev. A **23**, 1717-1729 (1981); G. Lapicki and F. D. McDaniel, Phys. Rev. A **22**, 1896 (1980).

[5] R. L. Watson, V. Horvat, J. M. Blackadar and K. E. Zaharakis, Phys. Rev. A **60**, 2959 (1999).

[6] G. Raisebeck and F. Yiou, Phys. Rev. A **4**, 1858 (1971).

[7] R. L. Watson, V. Horvat and K. E. Zaharakis, *Projectile and Target Z-scaling of Target K- vacancy Production Cross Sections at 10 MeV/amu*, in Application of Accelerators in Research and Industry, edited by J. L. Duggan and I. L. Morgan, AIP Conference Proceedings, 576, New York, 2001, pp. 93.

SECTION V

SUPERCONDUCTING CYCLOTRON AND INSTRUMENTATION

K500 Operations and Development

D. P. May, G. J. Kim, H. L. Clark, F. P. Abegglen, G. J. Derrig, and W. H. Peeler

Introduction

During the 2002-2003 reporting period a total of 60 different beams were used for experiments. These included 26 newly developed beams. There were a total of 213 beam tunings not counting multiple tunes of beams during the same day for the SEE program. The beams for experiments included some new species and the highest E/Q beam to date. The SEE program will be treated in a separate contribution.

Ion Sources

The 14.5 GHz ECR2 ion source has not been used for experiments yet, due mainly to high vacuum in the plasma chamber caused by what are assumed to be water leaks. Even so, the source has produced 139 eμA of $^{16}O^{7+}$ and 400 eμA of $^{16}O^{6+}$ without any gas input, presumably from the oxygen in water. Meanwhile, more lead shielding has significantly cut down on the x-ray flux into areas surrounding the source, and some progress has been made in remoting the controls for both sources.

A new hexapole bar is being assembled from new NdFeB material to replace the damaged one in ECR1. When ECR2 can be operated for experiments, the switch will be made to ECR1 in an effort to return it to its original performance. Also coil-winding for the two new Glaser lenses has begun. Each will replace the first focussing solenoid in each injection line and should improve the injection efficiency.

Cyclotron Beams

Of the new beams developed, several are of note. Cadmium and molybdenum beams as well as two new uranium beams were developed at low energies for the atomic physics program and a praseodymium beam was developed for the SEE program. All of these elements were introduced into ECR1 via sputtering. Also a beam of 47 AMeV $^{3}He^{+}$ was developed. At an E/Q of 141, this is the beam requiring the highest dee-voltage to date and thus the one closest to the focussing limit. Before this beam could be developed, the rf had to be conditioned for two days.

Operations

For the period April 1, 2002 through March 31, 2001, the operational time is summarized in Table I, while Table II lists how the scheduled time was divided. The time spent in unscheduled maintenance was unusually low while the time scheduled for outside users, all for the SEE program, went up dramatically from last year. The idle time reported arose from the failure of some of the time devoted to SEE to be used.

Table 1. 2002-2003 Operational Time.

Time	Hrs.	%Time
Beam on target	4542.00	**60.1**
Tuning, optics, set-up	1034.25	**13.7**
Beam development	1271.75	**16.8**
Scheduled maint.	560.00	**7.4**
Unscheduled maint.	35.25	**0.5**
Idle time	113.75	**1.5**
Cool down	0.00	**0.0**
Total	**7557.00**	**100.0**

Table 2. Scheduled Beam Time.

Time	Hrs.	%Time
Nuclear physics	1654.75	**23.6**
Nuclear chemistry	773.75	**11.1**
Atomic physics	752.50	**10.7**
Outside collaboration	0.0	**0.0**
Outside users	2559.50	**36.5**
Beam development	1271.75	**18.1**
Total	**7012.25**	**100.0**

Radiation Effects Facility

H. L. Clark, V. Horvat, B. Hyman and D. Utley

The activity of the Radiation Effects Facility (REF) increased substantially over the previous reporting year. In this reporting period, the facility was used for 1851 hours, which is a ~40% increase over the 1327 hours used in the 2001-2002 reporting period. Users of the facility (and hours used) over the past year were: Boeing Satellite Systems (469), NASA JPL (206.5), NASA GSFC (204.5), Mitsubishi (164), Maxwell Technology (112.75), Prairie View A&M University (91), Aerospace Corp. (61.5), Xilinx (55), Innovative Concepts (49.75), Aeroflex UTMC (44.75), NAVSEA (44.5), Boeing-Seattle (41.25), United Space Alliance (40), BAE Systems (35.75), Harris (31), International Rectifier (30.5), ICS Radiation (25.75), Raytheon (23), Full Circle Research (21), SEAKR (19.75), Intersil (16), Air Force (15.5), Naval Research Laboratory (15.25), Honeywell (12), Johns Hopkins (10.5), General Dynamics (8) and Makel Engineering (2). From the list above, Mitsubishi, Boeing-Seattle, United Space Alliance, Johns Hopkins and Makel were all new customers of the facility.

Table I compares the facility usage by commercial and government customers. The ratio from this reporting year (67% to 33%) is close to the trend seen in previous years. Despite the lagging economy, the number of commercial hours actually increased substantially. Many commercial agencies are now testing for devices to be used in defense systems rather than in commercial telecommunication equipment. It is expected that the facility will remain as active in the future.

Table II lists the beams used this year and the number of times each was requested. In total, 360 beams were run this year, which is almost 200% higher than the previous year. Three new beams were developed--15A MeV ^{63}Cu, ^{109}Ag and ^{141}Pr. These beams "bridged" the LET gaps between Ar-Kr, Kr-Xe and Xe-Ho. 7A MeV ^{40}Ar was developed for ion implantation experiments for Full Circle Research.

Table 1. Radiation Effects Facility usage by commercial and government customers for this and previous reporting years.

Reporting Year	Total Hours	Commercial Hours (%)	Government Hours (%)
2002-2003	1851	1242 (67%)	609 (33%)
2001-2002	1327	757 (57%)	570 (43%)
2000-2001	1500	941 (63%)	559 (37%)
1999-2000	548	418 (76%)	131 (24%)
1998-1999	389	171 (44%)	218 (56%)
1997-1998	434	210 (48%)	224 (52%)
1996-1997	560	276 (49%)	284 (51%)
1995-1996	141	58 (41%)	83 (59%)

Table 2. Beams used and the number of times requested for this reporting year and previous years. 360 beams were run this year.

Particle Type	A MeV	Requests 2000-2001	Requests 2001-2002	Requests 2002-2003
^{40}Ar	7	N/A	N/A	2
^{197}Au	10.5	4	N/A	N/A
^{4}He	12.5	1	1	0
^{20}Ne	15	1	13	19
^{40}Ar	"	4	24	43
^{63}Cu	"	N/A	N/A	5
^{84}Kr	"	6	26	55
^{109}Ag	"	N/A	N/A	6
^{129}Xe	"	5	18	43
^{141}Pr	"	N/A	N/A	2
^{165}Ho	"	3	11	17
^{181}Ta	"	4	5	4
^{197}Au	"	12	9	23
H-D	25	1	0	N/A
^{22}Ne	"	27	13	19
^{40}Ar	"	31	20	32
^{84}Kr	"	32	20	35
^{129}Xe	"	25	18	24
H-D	40	1	8	10
^{20}Ne	"	5	3	5
^{40}Ar	"	12	8	10
^{78}Kr	"	13	9	6
H-H	55	2	N/A	N/A
^{16}O	"	1	0	0
^{36}Ar	"	2	1	0
Total		192	207	360

Cyclotron Data Acquisition

K. Hagel and R. Burch

Experimental data can be acquired at the Cyclotron Institute without the use of a VMS system for the first time since 1980. This marks a milestone in our data acquisition capabilities since the aging Vaxes were placing experiments in jeopardy by playing the critical role of loading frontend software.

The use of the Vaxes began to diminish several years ago as reported in [1] by using cheap linux boxes as the "backend" computer to monitor the progress of the experiment. But loading the data acquisition software in VME68040s still required the use of the VAX.

To eliminate even this necessity we utilize PCI-VME bridges installed on dual processor linux machines. The driver associated with the PCI-VME bridge allows VME memory mapping in much the same way as on the older VME Motorola 68040 processors. This has allowed us to rewrite our frontend software to take advantage of cheap computers, a free operating system (Linux) and free analysis software from CERN (ROOT) [2].

The frontend program is implemented as follows: It is built on ROOT[2] using the gui classes available for easy experiment control. A thread is generated which polls the VME trigger box to determine if an event trigger is present. If the event trigger is present, the event is read out using the users experiment specific event readout code. Each event is inserted into a buffer and once the buffer is full the main thread is notified and the buffer is taken, written to file and passed to analysis clients.

In order to facilitate writing the user event reading routines, a base class was constructed from which user classes inherit. The routines required to be written are simply the ones for initialization, run begin, run end and scaler readout. The scaler readout can be set according to the requirements of the experiment.

Further facilitation of writing is achieved by construction of CAMAC module class objects which encapsulate the BCNAFs required for the different operations of the modules. In this way the user has a consistent interface to the read and clear commands (among others) instead of constantly having to look up the BCNAF codes in the user manuals.

The program and hardware have been tested in several small blocks of time and a number of bugs were identified and corrected. It is in use in the first major experiment using FAUST and appears to be functioning well.

In the coming year we plan to return to an examination of the backend software. In particular we wish to examine the feasibility of implementing the go4 [3] backend software from GSI.

References

[1] R. Burch *et al., Progress in Research*, Cyclotron Institute, Texas A&M University (2000-2001) p V-11.

[2] Rene Brun and Fons Rademakers, ROOT - An Object Oriented Data Analysis Framework, Proceedings AIHENP '96 Workshop, Lausanne, September 1996, Nucl. Instrum. Methods Phys. Res. A **389**, 81 (1997); http://root.cern.ch/.

[3] http://go4.gsi.de/go4.htm.

Commissioning of the Superconducting Solenoid Rare Isotope Beamline

G. A. Souliotis, G. J. Derig, G. J. Kim, F. P. Abegglen, G. Chubarian, K. Hagel, R. Wada, J. Natowitz, G. Prete,[1] G. Viesti,[1] A. Keksis, D. V. Shetty, M. Veselsky[2] and S. J. Yennello

[1]*INFN Legnaro, Padova, Italy,* [2]*Institute of Physics, Slovak Academy of Sciences, Bratislava, Slovakia*

Initial tests of the Big Sol line

The description and installation of the Superconducting Solenoid Line and its characteristics have been reported previously [1]. The first part of the line (up to the intermediate focus, Fig. 1) was completed in Fall 2002 and first tests were performed in November 2002. The cooling procedures of the Big Sol magnet are also described in this report.

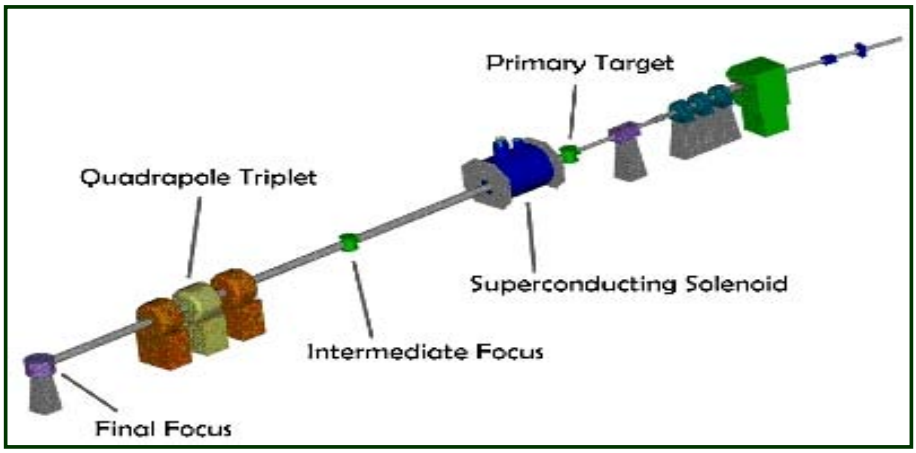

Figure 1. Schematic diagram of the Superconducting Solenoid Rare Isotope Beamline.

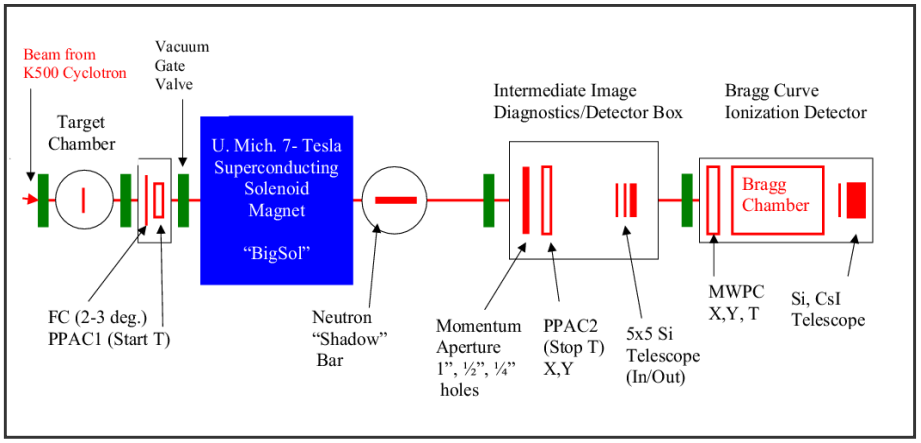

Figure 2. Schematic diagram of the experimental setup of the first part of the Big Sol Line.

A schematic diagram of the experimental setup used in the tests is given in Fig. 2. The primary beam was collected on a small cylindrical Faraday cup positioned approx. 30 cm after the target. With an additional circular aperture, fragments emitted in the range 2-3 degrees were allowed to enter the solenoid and were focused ~4 m after it (intermediate focus). At this location, groups of fragments were magnetically selected using a circular aperture. A simple identification scheme was implemented in these tests involving time-of flight and ΔE-E measurements. An example of a two-dimensional ΔE-E spectrum of fragments from a ^{40}Ar (40 MeV/nucleon) beam on a ^{64}Ni (6 mg/cm^2) target is shown in Fig. 3. The Big Sol line was set at Bρ=1.80 Tm (I_{BigSol}=96A). For the fully stripped ^{40}Ar (40 MeV/nucleon) beam the corresponding

value is 2.04 Tm (I_{BigSol}=110A). A circular aperture of 6 mm was used at the intermediate focus (corresponding to a Bρ window of roughly 2%). The separation of individual masses at various charge states is obvious in this figure.

During this phase of tests, the operation of a Bragg Curve gas ionization detector system [2] (Fig. 2) was also successfully conducted with ^{40}Ar (40 MeV/nucleon) and ^{197}Au (15 MeV/nucleon) beams.

Operation of the Big Sol Cryogenic System

For the initial cool down and operation, the cryogenic system was run in a trickle fill mode with LHe being constantly fed in to the magnet to maintain level and, most importantly, pressure in the magnet. The pressure was needed to maintain flow through the vapor-cooled electrical leads. When the magnet was run in this mode, the overall heat leak from the 186-ft.-long transfer line and the magnet was an estimated 23 L/Hr. and in excess of the approx. 20 L/Hr. excess capacity available from our CCI 200 watt helium refrigerator. Under these conditions the magnet could only be energized for about 12 hr. before it would be necessary to shut off the LHe supply and catch up on the LHe reserve.

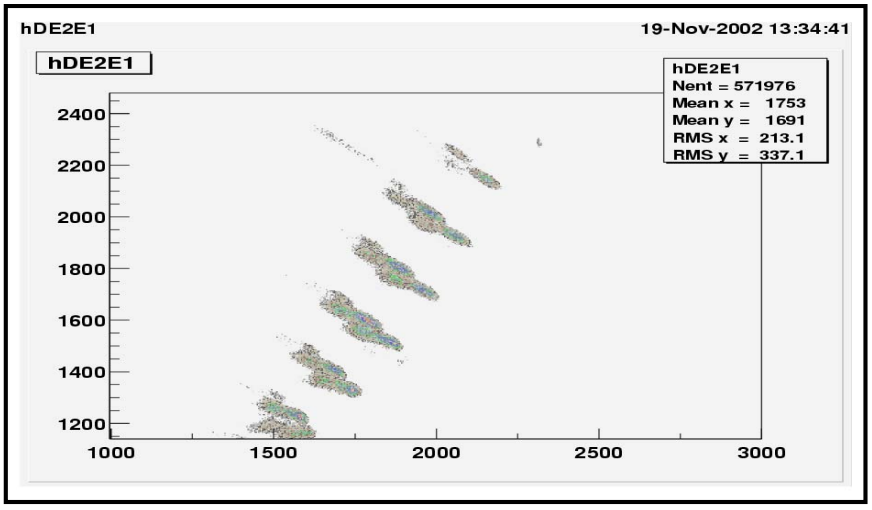

Figure 3. ΔE-E spectrum of fragments from a ^{40}Ar (40MeV/nucleon beam on a ^{64}Ni target [see text]).

In January 2003, the warm Helium gas return plumbing was reconfigured to include a back pressure regulator which maintains approx. 3.5 psig in the magnet. This valve solved two major problems; one was to maintain pressure in the magnet and as a result maintain flow through the vapor-cooled leads and, secondly, by maintaining a pressure head on the magnet, the boil-off rate of the LHe was reduced. As a result of these changes, we are now able to run in a batch fill mode with a cycle time of approx. 12 hr. where we do not need to maintain the transfer line constantly cold. In early March 2003, the system was operated continuously for several days and the boil-off rate of the magnet between batch fills was approx. 5 L/Hr.

Completion of the line and further plans

The second part of the line, namely the part from the intermediate focus to the final focus (Fig. 1) has been completed. A stand-alone mode of operation of the whole line (without operation of Big Sol) has already been tested and successfully employed, allowing the use of the line as a transfer line of primary beams.

Tests of the whole Big Sol line are planned for summer of 2003. As we have already shown (Fig 3), a first selection of fragment groups at the intermediate focus is provided by the use of an appropriate aperture. The second part of the line will provide a second selection stage and adequate flight path (~7m) to perform time-of-flight tagging of fragments. We plan to test the use of degraders at the intermediate image to enhance the selection ability of the line. In addition, we plan to use a multistage ionization chamber at this location, simultaneously functioning as degrader and as Z identifier. Simultaneous ΔE and TOF tagging of the produced rare isotope beam mixtures will enable reaction studies at the end of the line, where a number of reacting systems may be studied simultaneously. As a stand-alone device, the solenoid line will be used for rare isotope search and reaction dynamics studies. In addition to the various in-flight possibilities, the use the solenoid line as a separator to produce, separate, deccellerate (with degraders) and focus rare isotopes before a gas-cell to develop an Ion-Guide-based RIB concept at TAMU (see also [3]) will be investigated.

References

[1] G.A. Souliotis *et al*., *Progress in Research*, Cyclotron Institute, Texas A&M University (2001-2002) p. V-19.

[2] A. Moroni, I. Iori, L. Yu, G. Prete, G. Viesti, F. Gramegna, and A. Dainelli, Nucl. Instrum. Methods Phys. Res. **225**, 57 (1984).

[3] http://cyclotron.tamu.edu/facility_upgrade.htm.

New detector assembly for experiments with secondary RIBs

G. Tabacaru, L. Trache, C. Fu, R. Olsen and R. E. Tribble

We redesigned the detection system used for nuclear astrophysics experiments with secondary rare isotope beams produced with MARS. The aims were to:

- detect elastic scattering and transfer reaction products with higher efficiency over a larger angular range;
- increase the geometrical precision and the reproducibility of the geometry used in various experiments;
- use more compact electronics;
- achieve better cooling of the silicon detectors;
- produce more flexibility and provide the addition of multihit capability;
- have a better monitoring of the beam intensity.

The new detector assembly designed and built at our institute has a rectangular geometry: four 5x5 cm^2 Position Sensitive Silicon Detectors (PSSD) backed by four thick (typically 500 μm) silicon detectors are placed on an aluminum plate as shown in the figure. Two telescopes (no. 1 and no. 2) are positioned in a geometry quasi identical with the past one. They have a laboratory angular coverage of 4º to 19º. The detectors no. 3 and no. 4 have an angular coverage of 16º to 30º. The aluminum plate is seated on a XYZ optical table that provides an easy and precise (10 μm precision) fine positioning of the whole assembly. The optical table moves on two rails providing an easy coarse positioning of the detectors for position calibration with beam. In order to minimize the inverse current in the all silicon detectors, the whole assembly is cooled by two electric thermo-coolers of 80 W maximum power. The cold plate was glued on the aluminum plate and the hot one is water cooled. The number of incoming beam particles is monitored by a plastic scintillator located at the back of the detector chamber.

The 4x16 signals from the strips are collected by two compact 32 channel preamplifiers (RIS corp.) located in air as close as possible to the detector chamber feedthroughs. A relatively high noise level required careful shielding of the cabling and preamplifier boxes. Four CAEN 16 channel spectroscopy amplifiers are used for the shaping and these are fed into the ADCs of the acquisition system.

The new detection set-up can be very easily adapted for a multitude of experiments and it is an important tool for the investigation of the interesting nuclear astrophysics process.

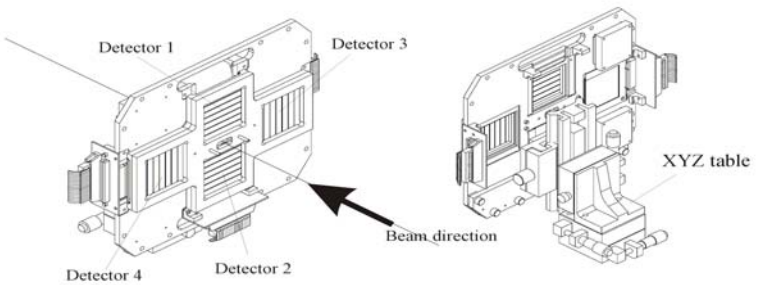

New Cryogenic Target Gas Cell for MARS Line

J. F. Brinkley, A. Azhari, B. Olsen, X. Tang, L. Trache and R. E. Tribble

Last year we designed a new cryogenic target gas cell, to go with the Target Chamber we installed last summer on the MARS Line. Several problems with previous designs were addressed: maintenance, window replacement, vacuum integrity, and changes in gas density due to increased beam current. We also had to interrupt experiments regularly in order to refill the dewar with LN2.

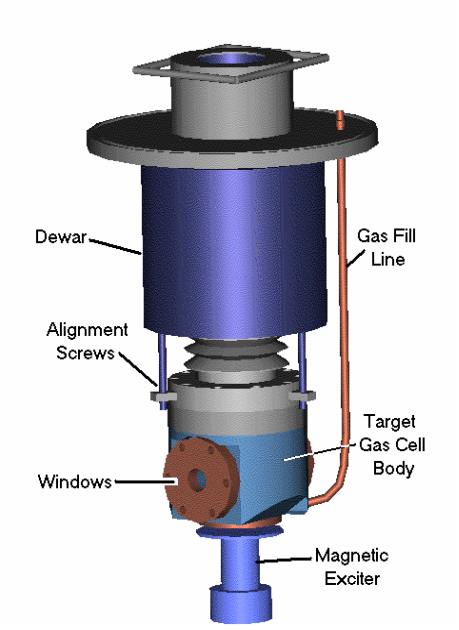

The current Cryogenic Gas Cell design is a single rigid piece approximately 32" tall with only the windows and the gas delivery system detachable. This layout makes it somewhat difficult to repair or modify any part of the assembly without risking damage to the sensitive lower components. Maintenance is also hampered by radioactive activation of the lower components, which is high enough to require special precautions. The new design, which is only 16" tall, addresses these issues by making the Gas Cell Body (the part that contains most of the radiation) detachable from the rest of the assembly as well as moving the gas delivery system to the lid of the chamber. This has the advantage of making maintenance operations much less cumbersome as well as simplifying future cryogenic target designs and modifications.

When replacing the windows on the gas cell one could easily damage gas lines causing vacuum problems, also it was difficult to maintain alignment of the cell. We addressed these problems by going to a three-point rigid alignment system that prevents misalignment and stress due to torque on the gas cell body during window changes.

There have been problems in the past with leaks developing around the feed through where the gas is injected into the gas cell. It was determined that this is due to damaging silver solder junctions during routine maintenance as well as stress during cryogenic cycling. We have addressed this issue by replacing the silver solder junctions with more reliable "VCR" type connections.

We have seen a noticeable drop in isotope production rate per nA of incoming beam as the current was increased. It was determined that this effect was due to a density gradient in the cylinder caused by "heating-up" the stagnant gas along the beam trajectory as intensity was increased. The new design addresses this issue by increasing the contact area with the LN2, in order to increase conductive cooling, as well as the addition of a "stirrer" inside the gas cell that will dramatically increase convective cooling. An external non-cryogenic exciter magnetically drives the stirrer.

In the new design we also eliminated the need for refilling the dewar every 4-6 hours by adapting a commercially available auto fill system. We now have the capability of running an entire experiment without opening the cave.

SECTION VI

PUBLICATIONS

PAPERS PUBLISHED
April 1, 2002 – March 31, 2003

Determination of the S_{18} astrophysical factor for $^{8}B(p,\gamma)^{9}C$ from the breakup of ^{9}C at intermediate energies

L. Trache, F. Carstoiu, A. M. Mukhamedzhanov and R. E. Tribble
Phys. Rev. C **66**, 035801 (2002).

Determination of the S_{17} and S_{18} astrophysical factors from the breakup of ^{8}B and ^{9}C at intermediate energies

L. Trache, F. Carstoiu, C. A. Gagliardi, A. M. Mukhamedzhanov and R. E. Tribble
Nucl. Phys. **A718**, 493 (2002).

New 0^{+} states in ^{158}Gd

S. R. Lesher, A. Aprahamian, L. Trache, A. Oros-Peusquens, S. Deyliz, A. Gollwitzer, R. Hertenberger, B. D. Valnion, and G. Graw
Phys. Rev. C **66**, 051305 (2002).

STAR Detector Overview

K. H. Ackermann *et al.* [STAR collaboration]
Nucl. Instrum. Methods Phys. Res. **A499**, 624 (2003).

The STAR endcap electromagnetic ealorimeter

C. E. Allgower, B. D. Anderson, A. R. Baldwin, J. Balewski, M. Belt-Tones, L. C. Bland, R. L. Brown, R. V. Cadman, W. Christie, I. Cyliax, V. Dunin, G. Eppley, C. A. Gagliardi, N. Gagunashvili, T. Hallman, W. Hunt, A. Ogawa, Y. Panebratsev, M. Planinic, J. Puskar-Pasewicz, G. Rakness, S. Razin, O. Rogachevski, S. Shimansky, K. A. Solberg, J. Sowinski, H. Spinka, E. J. Stephenson, V. Tikhomirov, M. Tokarev, R. E. Tribble, D. Underwood, A. M. Vander Molen, S. E. Vigdor, J. W. Watson, G. Westfall, S. W. Wissink, A. Yokosawa, V. Yurevich, W.-M. Zhang, A. Zubarev
Nucl. Instrum. Methods Phys. Res. **A499**, 740 (2003).

Direct capture S-factors from asymptotic normalization coefficients

R. E. Tribble, A. Azhari, H. L. Clark, C. A. Gagliardi, Y.-W. Lui, A. M. Mukhamedzhanov, A. Sattarov, X. Tang, L. Trache, V. Burjan, J. Cejpek, V. Kroha, S. Piskor, J. Vincour, and F. Carstoiu
Proceedings of OMEG2000, Tokyo, January, 2000 (World Scientific, Singapore, 2003), 107.

Disappearance of back-to-back high p_T hadron correlations in central Au+Au collisions at $(S_{NN})^{½}$ = 130 GeV

C. Adler *et al.* [STAR collaboration, including C. A. Gagliardi, T. W. Henry and R. E. Tribble]
Phys. Rev. Lett. **90**, 082302 (2003).

Azimuthal anisotropy and correlations in the hard scattering regime at RHIC
C. Adler *et al.* [STAR collaboration, including C. A. Gagliardi, T. W. Henry and R. E. Tribble]
Phys. Rev. Lett. **90**, 032301 (2003).

Centrality dependence of high p_T hadron suppresion in Au+Au collisions at $(S_{NN})^{½}$ = 130 GeV
C. Adler *et al.* [STAR collaboration, including C. A. Gagliardi, T. W. Henry and R. E. Tribble]
Phys. Rev. Lett. **89**, 202301 (2002).

Coherent ρ^0 production in ultra-peripheral heavy ion collisions
C. Adler *et al.* [STAR collaboration, including C. A. Gagliardi, T. W. Henry and R. E. Tribble]
Phys. Rev. Lett. **89**, 272302 (2002).

Elliptic flow from two- and four-particle correlations in Au+Au collisions at $(S_{NN})^{1/2}$ = 130 GeV
C. Adler *et al.* [STAR collaboration, including C. A. Gagliardi, T. W. Henry and R. E. Tribble]
Phys. Rev. C **66**, 034904 (2002).

$K^*(892)^0$ Production in relativistic heavy ion collisions at $(S_{NN})^{1/2}$ = 130 GeV
C. Adler *et al.* [STAR collaboration, including C. A. Gagliardi, T. W. Henry and R. E. Tribble]
Phys. Rev. C **66**, 061901(R) (2002).

Azimuthal anisotropy of K_s^0 and $\Lambda + \bar{\Lambda}$ production at mid-rapidity from Au+Au collisions at $(S_{NN})^{1/2}$ = 130 GeV
C. Adler *et al.* [STAR collaboration, including C. A. Gagliardi, T. W. Henry and R. E. Tribble]
Phys. Rev. Lett. **89**, 132301 (2002).

Mid-rapidity Λ and $\bar{\Lambda}$ production in Au+Au collisions at $(S_{NN})^{1/2}$ = 130 GeV
C. Adler *et al.* [STAR collaboration, including C. A. Gagliardi, T. W. Henry and R. E. Tribble]
Phys. Rev. Lett. **89**, 092301 (2002).

Asymptotic normalization coefficients in nuclear astrophysics and structure
C. A. Gagliardi, A. Azhari, V. Burjan, F. Carstoiu, V. Kroha, A. M. Mukhamedzhanov, A. Sattarov, X. Tang, L. Trache and R. E. Tribble
Eur. Phys. J. A **15**, 69 (2002).

Astrophysical S factors from asymptotic normalization coefficients

R. E. Tribble, A. Azhari, P. Bem, V. Burjan, F. Carstoiu, J. Cejpek, H. L. Clark, C. A. Gagliardi, V. Kroha, Y.-W. Lui, A. M. Mukhamedzhanov, J. Novak, S. Piskor, A. Sattarov, E. Simeckova, X. Tang, L. Trache, J. Vincour
Proc. of Nuclear Physics at the Border Lines, Lipari, Italy, May, 2001, World Scientific, Singapore, 340 (2002).

Radioactive beams at Texas A&M University
R. E. Tribble, A. Azhari, C. A. Gagliardi, J. C. Hardy, A. Mukhamedzhanov, X. Tang, L. Trache and S. J. Yennello
Nucl. Phys **A701**, 278 (2002).

Search for the lepton-family-number nonconserving decay $\mu^+ \rightarrow e^+ \gamma$
M. Ahmed *et al.* ,(MEGA Collaboration)
Phys. Rev. D **65**, 112002 (2002).

Astrophysical *S* factor for $^{13}C(p, \gamma)^{14}N$ and asymptotic normalization coefficients
M. Mukhamedzhanov, A. Azhari, V. Burjan, C. A. Gagliardi, V. Kroha, A. Sattarov, X. Tang, L. Trache, and R. E. Tribble
Phys. Rev. C **66**, 027602 (2002).

Midrapidity Λ and $\bar{\Lambda}$ production in *Au+Au* collisions at $\sqrt{S_{NN}}$ = 130 *GeV*
C. Adler *et al.*, (STAR Collaboration)
Phys. Rev. Lett. **89**, 092301 (2002).

Azimuthal anisotropy of K^0_S and Λ and $\bar{\Lambda}$ production at midrapidity from *Au+Au* collisions at $\sqrt{S_{NN}}$ = 130 *GeV*
C. Adler *et al.*, (STAR Collaboration)
Phys. Rev. Lett. **89**, 132301 (2002).

Elliptic flow from two- and four-particle correlations in Au+Au collisions at $\sqrt{S_{NN}}$ = 130 GeV
C. Adler *et al.*, (STAR Collaboration)
Phys. Rev. C **66**, 034904 (2002).

Centrality dependence of high-p_T hadron suppression in *Au+Au* collisions at $\sqrt{S_{NN}}$ = 130 *GeV*
C. Adler *et al.*, (STAR Collaboration)
Phys. Rev. Lett. **89**, 202301 (2002).

A precision measurement of muon decay

M. A. Quraan, A. Gaponenko, P. Green, P. Kitching, R. MacDonald, G. Price, N. L. Rodning, J. Schaapman, F. Sobratee, J. Soukup, G. Stinson, A. Khruchinsky, V. Selivanov, V. Torokhov, C. A. Gagliardi, J. C. Hardy, J. R. Musser, R. E. Tribble, M. A. Vasiliev, W. Anderson, M. Comyn, Yu. Davydov, J. Doornbos, W. Faszer, D. R. Gill, P. Gumplinger, R. Henderson, J. A. Macdonald, G. Marshall, A. Olin, D. Ottewell, R. Openshaw, J.-M. Poutissou, R. Poutissou, G. Sheffer, H. K. Walter, D. Wright, M. Hasinoff, D. Maas, P. Depommier, E. Korkmaz, Tracy Porcelli, T. Mathie, R. Tacik, Y. Shin, D. D. Koetke, R. Manweiler, P. Nord and T. D. S. Stanislaus

Int. J. Mod. Phys. A **16S1A**, 296 (2001).

The Canadian Penning Trap Spectrometer at Argonne

G. Savard, R. C. Barber, C. Boudreau, F. Buchinger, J. Caggiano, J. Clark, J. E. Crawford, H. Fukutani, S. Gulick, J. C. Hardy, A. Heinz, J. K. P. Lee, R. B. Moore, K. S. Sharma, J. Schwartz, D. Seweryniak, G. D. Sprouse and J. Vaz

Hyperfine Interactions, **132**, 223 (2001).

Production of ^{60}Co sources for high-accuracy efficiency calibrations of gamma-ray spectrometers

E Schoenfeld, H. Janssen, R. Klein, J. C. Hardy, V. Iacob, M. Sanchez-Vega, H. C. Griffin and M. A. Ludington

Radiation Applications and Isotopes **56**, 215 (2002).

Precise efficiency calibration of an HPGE detector: source measurements and Monte Carlo calculations with sub-percent precision

J. C. Hardy, V. E. Iacob, M. Sanchez-Vega, R. T. Effinger, P. Lipnik, V. E. Mayes, D. K. Willis and R. G. Helmer

Radiation Applications and Isotopes, **56**, 65 (2002).

Tests of the standard model from superallowed fermi beta-decay studies: the ^{74}Rb beta decay

E. F. Zganjar, A. Piechaczek, G. C. Ball, P. Bricault, J. M. D'Auria, J. C. Hardy, D. F. Hodgson, V. Iacob, P. Klages, W. D. Kulp, J. R. Leslie, M. Lipoglavsek, J. A. Macdonald, H.-B. Mak, D. M. Moltz, G. Savard, J. von Schwarzenberg, C. E. Svenson, I. S. Towner and J. L. Wood

Eur. Phys. J. **A15** (2002) 229.

Superallowed beta decay of nuclei with A $\geq$ 62: the limiting effect of weak Gamow-Teller branches

J. C. Hardy and I. S. Towner

Phys. Rev. Lett. **88**, 252501 (2002).

Superallowed $0^+ \rightarrow 0^+$ beta decay and CKM unitarity: recent results and future prospects

J. C. Hardy and I. S. Towner

Eur. Phys. J. A **15** (2002) 223.

Calculated corrections to superallowed fermi β-decay: new evaluation of the nuclear-structure-dependent terms

S. Towner and J. C. Hardy

Phys. Rev. C **66**, 035501 (2002).

The evaluation of v_{ud}, experiment and theory

I. S. Towner and J. C. Hardy

J. Phys. G: Nucl. Part. Phys. **29**, 197 (2003).

Cross section measurements of the ^{181}Ta(γ,n)^{180}Ta reaction near neutron threshold and the p-process nucleosynthesis

H. Utsunomiya, H. Akimune, S. Goko, M. Ohta, H. Ueda, T. Yamagata, K. Yamasaki, H. Ohgaki, H. Toyokawa, Y. –W. Lui, T. Hayakawa, T. Shizuma, E. Khan, S. Goriely

Phys. Rev. C **67**, 015807 (2003).

Enhanced production of neutron-rich rare isotopes in the reaction of 25 MeV/nucleon ^{86}Kr on ^{64}Ni

G. A. Souliotis, M. Veselsky, G. Chubarian, L. Trache, A. Keksis, E. Martin, A. Ruangma, E. Winchester and S. J. Yennello

Phys. Lett. B **543**, 163 (2002).

The liquid to vapor phase transition in excited nuclei

J. B. Elliott, L. G. Moretto, L. Phair, G. J. Wozniak, L. Beauliew, H. Breuer, R. G. Korteling, K. Kwiatkowski, T. Lefort, L. Pienkowski, A. Ruangma, V. E. Viola and S. J. Yennello

Phys. Rev. Lett. **88**, 042701 (2002).

Event-by-event analysis of proton-induced nuclear multifragmentation: determination of phase transition universality-class in system with extreme finite-size constraints

M. K. Berkenbusch, W. Bauer, K. Dillman, S. Pratt, T. Lefort, K. Kwiatkowski, V. E. Viola, L. Beaulieu, A. Ruangma, S. J. Yennello, R. G. Korteling, L. Pienkowski

Phys. Rev. Lett. **88**, 022701 (2002).

Breakup time scale studied in the 8 GeV/c π^- + ^{197}Au reaction

L. Pienkowski, K. Kwiatkowski, T. Lefort, L. Beaulieu, A. Botvina, B. Back, H. Breuer, S. Gushue, L. P. Remsberg, D. Rowland, A. Ruangma, V. E. Viola, E. Winchester, S. J. Yennello

Phys. Rev. C **65**, 064606 (2002).

Caloric curve of 8 GeV/c p, π+ ^{197}Au reactions

Ruangma, R. Laforest, E. Martin, E. Ramakrishnan, D. Rowland, M. Veselsky, E. Winchester, S. J. Yennello, L. Beaulieu, W.-c. Hsi, K. Kwiatkowski, T. Lefort, V. E. Viola, A. Botvina, R. G. Korteling, L. Pienkowski, H. Breuer, S. Gushue, L. P. Remsberg, B. Back
Phys. Rev. C **66**, 044603 (2002).

Tracking the phase-transition energy in the disassembly of hot nuclei

C. B. Das, S. Das Gupta, L. Beaulieu, T. Lefort, K. Kwiatkowski, V. E. Viola, S. J. Yennello, L. Pienkowski, R. G. Korteling, and H. Breuer
Phys. Rev. C, **66**, 044602 (2002).

Formation of excited systems with a wide range in N/Z

D. J. Rowland, R. Laforest, E. Ramakrishnan, M. Veselsky, E. M. Winchester, A. Ruangma, E. Martin and S. J. Yennello
Phys. Rev C, **67**, 064602 (2003).

Limiting temperatures and the equation of state of nuclear matter

J. B. Natowitz, K. Hagel, Y. Ma, M. Murray, L. Qin, R. Wada, and J. Wang
Phys. Rev. Lett. **89**, 212701 (2002).

Caloric curves and nuclear expansion

J. B. Natowitz, K. Hagel, Y. Ma, M. Murray, L. Qin, S. Shlomo, R. Wada, and J. Wang
Phys. Rev. C **66**, 031601 (2002).

Pseudorapidity distributions of charged particles from Au + Au collisions at the maximum RHIC energy, $\sqrt{S_{NN}}$ = 200 GeV

G. Bearden *et al*. The BRAHMS Collaboration
Phys. Rev. Lett. **88**, 202301 (2002).

Sequential decay distortion of Goldhaber model widths for spectator fragments

Y. G. Ma, R. Wada, K. Hagel, M. Murray, J. S. Wang, L. J. Qin, A. Makeev, P. Smith, J. B. Natowitz, and A. Ono
Phys. Rev. C **65**, 051602 (2002).

Experimental investigation of the level density in highly excited nuclei around Pb-208

M. Lunardon, G. Viesti, D. Bazzacco, D. Fabris, G. Nebbia, C. Ur, C. R. Alvarez, M. Cinausero, E. Farnea, E. Fioretto, G. Prete, G. de Angelis, D. R. Napoli, K. Hagel, J. B. Natowitz, and R. Wada
Eur. Phys. J. A **13**, 419 (2002).

Charged particle multiplicities at BRAHMS
S. J. Sanders *et al*., The BRAHMS Collaboration
Acta. Phys. Hung. NS-H **15** (3-4), 315 (2002).

Results from BRAHMS experiment at RHIC
P. Staszel *et al*., The BRAHMS Collaboration
Acta. Phys. Pol. B **33** (6), 1387 (2002).

Entrance channel dependence of particle and fragment emission
J. Wang, T. Keutgen, R. Wada, K. Hagel, Y. G. Ma, M. Murray, L. Qin, A. Makeev, P. Smith, and J. B. Natowitz, for the NIMROD Collaboration
Bulletin of the American Physical Society (2002).

Projectile and target ionization in MeV/u collisions of Xe ions with N_2
R. E. Olson, R. L. Watson, V. Horvat, and K. E. Zaharakis
J. Phys. B **35**, 1893 (2002).

Multiple electron stripping of heavy ion beams
D. Mueller, L. Grisham, I. Kaganovich, R. L. Watson, V. Horvat, K. E. Zaharakis, and Y. Peng
Laser and Part. Beams **20**, 551 (2002).

Target Z dependence and additivity of cross sections for electron loss by 6-MeV/amu Xe^{18+} Projectiles
R. L. Watson, Yong Peng, V. Horvat, G. J. Kim, and R. E. Olson
Phys. Rev. A **67** 022706 (2003).

J/ψ production in relativistic heavy ion collisions from a multiphase transport model
B. Zhang, C. M. Ko, Z. W. Lin, B. A. Li, and S. Pal
Phys. Rev. C **65**, 054909 (2002).

Charm meson production from meson-nucleon scattering
W. Liu and C. M. Ko
Phys. Lett. B **533**, 259 (2002).

Phi meson production in relativistic heavy ion collisions
S. Pal, C. M. Ko, and Z. W. Lin
Nucl. Phys. **A707**, 525 (2002).

Partonic effects on pion interferometry in relativistic heavy ion collisions
Z. W. Lin, C. M. Ko, and S. Pal
Phys. Rev. Lett. **89**, 152301 (2002).

Cascade production from antikaon induced reactions on lambda and sigma
C. H. Li and C. M. Ko
Nucl. Phys. **A712**, 110 (2002).

Flavor ordering of elliptic flows at high transverse momentum
Z. W. Lin and C. M. Ko
Phys. Rev. Lett. **89**, 202302 (2002).

Charmonium mass in nuclear matter
S. H. Lee and C. M. Ko
Phys. Rev. C **67**, 038202 (2003).

Charmonium absorption in the meson-exchange model
Z. W. Lin and C. M. Ko
Nucl. Phys. **A715**, 533c (2003).

Effects of symmetry energy on two-nucleon correlation functions in heavy ion collisions induced by neutron-rich nuclei
L. W. Chen, V. Greco, C. M. Ko, and B. A. Li
Phys. Rev. Lett. **90**, 162701 (2003).

Parton Coalescence and the Antiproton/Pion Anomaly at RHIC
V. Greco, C. M. Ko, and P. Lévai
Phys. Rev. Lett. **90**, 202302 (2003).

Charm production from photon-proton reactions in a hadronic model
W. Liu, S. H. Lee, and C. M. Ko
Nucl. Phys. **A724**, 375 (2003).

Final state three-body coulomb effects in the ^{208}Pb (^{8}B, ^{7}Bep)^{208}Pb coulomb breakup reaction
E. O. Alt, B. F. Irgaziev, A. M. Mukhamedzhanov
Phys. Rev. Lett. **90**, 122701 (2003).

Caloric curves and nuclear expansion
J. B. Natowitz, K. Hagel, Y. Ma, M. Murray, L. Qin, S. Shlomo, R. Wada and J. Wang
Phys. Rev. C **66**, 031601 (2002).

Self-consistent Hartree-Fock based random phase approximation and the spurious state mixing
B. K. Agrawal, S. Shlomo and A. I. Sanzhur
Phys. Rev. C **67**, 034314 (2003).

Determining the nuclear matter incompressibility coefficient from compression modes in nuclei

S. Shlomo and A. I. Sanzhur

Nuclear Physics in the 21st Century, American Institute of Physics, New York, 2002, p. 678.

Phase transitions in asymmetric nuclear matter

V. M. Kolomietz, A. I. Sanzhur, S. Shlomo and S. A. Firin

Nuclear Physics in the 21st Century, American Institute of Physics, New York (2002), p. 707.

Nuclear equation of state and compression modes

S. Shlomo and A. I. Sanzhur

Heavy Ion Physics **16**, 303 (2002).

Isoscalar giant monopole and dipole resonances and the nuclear matter incompressibility coefficient

S. Shlomo, A. I. Sanzhur and B. K. Agrawal

Nucl. Phys. **A719**, 225c (2003).

Current status of the nuclear matter incompressibility coefficient as deduced from data on compression modes

S. Shlomo and B. K. Agrawal

Nucl. Phys. **A722**, 98C, (2003).

Asymptotic form of the electron-hydrogen scattered wave

A.S. Kadyrov, A.M. Mukhamedzhanov, A.T. Stelbovics

Phys. Rev. A **67**, 024702 (2003)

Low energy behavior of the astrophysical S-factor in radiative captures to loosely bound final states

A. M. Mukhamedzhanov and F. M. Nunes

Nucl. Phys. **A708**, 437, (2002)

Proton-deuteron elastic scattering from 2.5 to 22.7 MeV

E.O. Alt, A.M. Mukhamedzhanov, M.M. Nishonov, A.I. Sattarov

Phys. Rev. C **65**, 064613 (2002)

Determination of the astrophysical S factor for $^{11}C(p,\gamma)^{12}N$ from the $^{12}N \rightarrow {}^{11}C + p$ asymptotic normalization coefficient

Xiaodong Tang, A. Azhari, C. A. Gagliardi, A. M. Mukhamedzhanov, F. Pirlepesov, L. Trache, R. E. Tribble, V. Burjan, V. Kroha, and F. Carstoiu

Phys. Rev. C **67**, 015804 (2003).

PAPERS PUBLISHED
April 1, 2002 – March 31, 2003

Determination of the S_{18} astrophysical factor for $^{8}B(p,\gamma)^{9}C$ from the breakup of ^{9}C at intermediate energies, L. Trache, F. Carstoiu, A. M. Mukhamedzhanov and R. E. Tribble, Phys. Rev. C **66**, 035801 (2002).

Determination of the S_{17} and S_{18} astrophysical factors from the breakup of ^{8}B and ^{9}C at intermediate energies, L. Trache, F. Carstoiu, C. A. Gagliardi, A. M. Mukhamedzhanov and R. E. Tribble, Nucl. Phys. **A718**, 493 (2002).

New 0^{+} states in ^{158}Gd, S. R. Lesher, A. Aprahamian, L. Trache, A. Oros-Peusquens, S. Deyliz, A. Gollwitzer, R. Hertenberger, B. D. Valnion, and G. Graw, Phys. Rev. C **66**, 051305 (2002).

STAR Detector Overview, K. H. Ackermann *et al.* [STAR collaboration], Nucl. Instrum. Methods Phys. Res. **A499**, 624 (2003).

The STAR endcap electromagnetic ealorimeter, C. E. Allgower, B. D. Anderson, A. R. Baldwin, J. Balewski, M. Belt-Tones, L. C. Bland, R. L. Brown, R. V. Cadman, W. Christie, I. Cyliax, V. Dunin, G. Eppley, C. A. Gagliardi, N. Gagunashvili, T. Hallman, W. Hunt, A. Ogawa, Y. Panebratsev, M. Planinic, J. Puskar-Pasewicz, G. Rakness, S. Razin, O. Rogachevski, S. Shimansky, K. A. Solberg, J. Sowinski, H. Spinka, E. J. Stephenson, V. Tikhomirov, M. Tokarev, R. E. Tribble, D. Underwood, A. M. Vander Molen, S. E. Vigdor, J. W. Watson, G. Westfall, S. W. Wissink, A. Yokosawa, V. Yurevich, W.-M. Zhang, A. Zubarev, Nucl. Instrum. Methods Phys. Res. **A499**, 740 (2003).

Direct capture S-factors from asymptotic normalization coefficients, R. E. Tribble, A. Azhari, H. L. Clark, C. A. Gagliardi, Y.-W. Lui, A. M. Mukhamedzhanov, A. Sattarov, X. Tang, L. Trache, V. Burjan, J. Cejpek, V. Kroha, S. Piskor, J. Vincour, and F. Carstoiu, Proceedings of OMEG2000, Tokyo, January, 2000 (World Scientific, Singapore, 2003), 107.

Disappearance of back-to-back high p_T hadron correlations in central Au+Au collisions at $(S_{NN})^{½}$ = 130 GeV, C. Adler *et al.* [STAR collaboration, including C. A. Gagliardi, T. W. Henry and R. E. Tribble], Phys. Rev. Lett. **90**, 082302 (2003).

Azimuthal anisotropy and correlations in the hard scattering regime at RHIC, C. Adler *et al.* [STAR collaboration, including C. A. Gagliardi, T. W. Henry and R. E. Tribble], Phys. Rev. Lett. **90**, 032301 (2003).

Centrality dependence of high p_T hadron suppresion in Au+Au collisions at $(S_{NN})^{½}$ = 130 GeV, C. Adler *et al.* [STAR collaboration, including C. A. Gagliardi, T. W. Henry and R. E. Tribble], Phys. Rev. Lett. **89**, 202301 (2002).

Coherent ρ^0 production in ultra-peripheral heavy ion collisions, C. Adler *et al.* [STAR collaboration, including C. A. Gagliardi, T. W. Henry and R. E. Tribble], Phys. Rev. Lett. **89**, 272302 (2002).

Elliptic flow from two- and four-particle correlations in Au+Au collisions at $(S_{NN})^{1/2}$ = 130 GeV, C. Adler *et al.* [STAR collaboration, including C. A. Gagliardi, T. W. Henry and R. E. Tribble], Phys. Rev. C **66**, 034904 (2002).

$K^*(892)^0$ Production in relativistic heavy ion collisions at $(S_{NN})^{1/2}$ = 130 GeV, C. Adler *et al.* [STAR collaboration, including C. A. Gagliardi, T. W. Henry and R. E. Tribble], Phys. Rev. C **66**, 061901(R) (2002).

Azimuthal anisotropy of K_s^0 and $\Lambda + \bar{\Lambda}$ production at mid-rapidity from Au+Au collisions at $(S_{NN})^{1/2}$ = 130 GeV, C. Adler *et al.* [STAR collaboration, including C. A. Gagliardi, T. W. Henry and R. E. Tribble], Phys. Rev. Lett. **89**, 132301 (2002).

Mid-rapidity Λ and $\bar{\Lambda}$ production in Au+Au collisions at $(S_{NN})^{1/2}$ = 130 GeV, C. Adler *et al.* [STAR collaboration, including C. A. Gagliardi, T. W. Henry and R. E. Tribble], Phys. Rev. Lett. **89**, 092301 (2002).

Asymptotic normalization coefficients in nuclear astrophysics and structure, C. A. Gagliardi, A. Azhari, V. Burjan, F. Carstoiu, V. Kroha, A. M. Mukhamedzhanov, A. Sattarov, X. Tang, L. Trache and R. E. Tribble, Eur. Phys. J. A **15**, 69 (2002).

Astrophysical S factors from asymptotic normalization coefficients, R. E. Tribble, A. Azhari, P. Bem, V. Burjan, F. Carstoiu, J. Cejpek, H. L. Clark, C. A. Gagliardi, V. Kroha, Y.-W. Lui, A. M. Mukhamedzhanov, J. Novak, S. Piskor, A. Sattarov, E. Simeckova, X. Tang, L. Trache, J. Vincour, Proc. of Nuclear Physics at the Border Lines, Lipari, Italy, May, 2001, World Scientific, Singapore, 340 (2002).

Radioactive beams at Texas A&M University, R. E. Tribble, A. Azhari, C. A. Gagliardi, J. C. Hardy, A. Mukhamedzhanov, X. Tang, L. Trache and S. J. Yennello, Nucl. Phys **A701**, 278 (2002).

Search for the lepton-family-number nonconserving decay $\mu^+ \rightarrow e^+ \gamma$, M. Ahmed *et al.* ,(MEGA Collaboration) Phys. Rev. D **65**, 112002 (2002).

Astrophysical *S* factor for $^{13}C(p, \gamma)^{14}N$ and asymptotic normalization coefficients, A. M. Mukhamedzhanov, A. Azhari, V. Burjan, C. A. Gagliardi, V. Kroha, A. Sattarov, X. Tang, L. Trache, and R. E. Tribble, Phys. Rev. C **66**, 027602 (2002).

Midrapidity Λ and $\bar{\Lambda}$ production in *Au+Au* collisions at $\sqrt{S_{NN}}$ = 130 *GeV* C. Adler *et al.*, (STAR Collaboration) Phys. Rev. Lett. **89**, 092301 (2002).

Azimuthal anisotropy of K^0_S and Λ and $\bar{\Lambda}$ production at midrapidity from *Au+Au* collisions at $\sqrt{S_{NN}}$ = 130 *GeV,* C. Adler *et al.*, (STAR Collaboration) Phys. Rev. Lett. **89**, 132301 (2002).

Elliptic flow from two- and four-particle correlations in Au+Au collisions at $\sqrt{S_{NN}}$ = 130 GeV, C. Adler *et al.*, (STAR Collaboration) Phys. Rev. C **66**, 034904 (2002).

Centrality dependence of high-p_T hadron suppression in *Au+Au* collisions at $\sqrt{S_{NN}}$ = 130 *GeV,* C. Adler *et al.*, (STAR Collaboration) Phys. Rev. Lett. **89**, 202301 (2002).

A precision measurement of muon decay, M. A. Quraan, A. Gaponenko, P. Green, P. Kitching, R. MacDonald, G. Price, N. L. Rodning, J. Schaapman, F. Sobratee, J. Soukup, G. Stinson, A. Khruchinsky, V. Selivanov, V. Torokhov, C. A. Gagliardi, J. C. Hardy, J. R. Musser, R. E. Tribble, M. A. Vasiliev, W. Anderson, M. Comyn, Yu. Davydov, J. Doornbos, W. Faszer, D. R. Gill, P. Gumplinger, R. Henderson, J. A. Macdonald, G. Marshall, A. Olin, D. Ottewell, R. Openshaw, J.-M. Poutissou, R. Poutissou, G. Sheffer, H. K. Walter, D. Wright, M. Hasinoff, D. Maas, P. Depommier, E. Korkmaz, Tracy Porcelli, T. Mathie, R. Tacik, Y. Shin, D. D. Koetke, R. Manweiler, P. Nord and T. D. S. Stanislaus, Int. J. Mod. Phys. A **16S1A**, 296 (2001).

The Canadian Penning Trap Spectrometer at Argonne, G. Savard, R. C. Barber, C. Boudreau, F. Buchinger, J. Caggiano, J. Clark, J. E. Crawford, H. Fukutani, S. Gulick, J. C. Hardy, A. Heinz, J. K. P. Lee, R. B. Moore, K. S. Sharma, J. Schwartz, D. Seweryniak, G. D. Sprouse and J. Vaz, Hyperfine Interactions, **132**, 223 (2001).

Production of ^{60}Co sources for high-accuracy efficiency calibrations of gamma-ray spectrometers, E Schoenfeld, H. Janssen, R. Klein, J. C. Hardy, V. Iacob, M. Sanchez-Vega, H. C. Griffin and M. A. Ludington, Radiation Applications and Isotopes **56**, 215 (2002).

Precise efficiency calibration of an HPGE detector: source measurements and Monte Carlo calculations with sub-percent precision, J. C. Hardy, V. E. Iacob, M. Sanchez-Vega, R. T. Effinger, P. Lipnik, V. E. Mayes, D. K. Willis and R. G. Helmer, Radiation Applications and Isotopes, **56**, 65 (2002).

Tests of the standard model from superallowed fermi beta-decay studies: the ^{74}Rb beta decay, E. F. Zganjar, A. Piechaczek, G. C. Ball, P. Bricault, J. M. D'Auria, J. C. Hardy, D. F. Hodgson, V. Iacob, P. Klages, W. D. Kulp, J. R. Leslie, M. Lipoglavsek, J. A. Macdonald, H.-B. Mak, D. M. Moltz, G. Savard, J. von Schwarzenberg, C. E. Svenson, I. S. Towner and J. L. Wood, Eur. Phys. J. **A15** (2002) 229.

Superallowed beta decay of nuclei with A $\geq$ 62: the limiting effect of weak Gamow-Teller branches, J. C. Hardy and I. S. Towner, Phys. Rev. Lett. **88**, 252501 (2002).

Superallowed $0^+ \rightarrow 0^+$ beta decay and CKM unitarity: recent results and future prospects, J. C. Hardy and I. S. Towner, Eur. Phys. J. A **15** (2002) 223.

Calculated corrections to superallowed fermi β-decay: new evaluation of the nuclear-structure-dependent terms, I. S. Towner and J. C. Hardy, Phys. Rev. C **66**, 035501 (2002).

The evaluation of v_{ud}, experiment and theory, I. S. Towner and J. C. Hardy, J. Phys. G: Nucl. Part. Phys. **29**, 197 (2003).

Cross section measurements of the ^{181}Ta(γ,n)^{180}Ta reaction near neutron threshold and the p-process nucleosynthesis, H. Utsunomiya, H. Akimune, S. Goko, M. Ohta, H. Ueda, T. Yamagata, K. Yamasaki, H. Ohgaki, H. Toyokawa, Y. –W. Lui, T. Hayakawa, T. Shizuma, E. Khan, S. Goriely, Phys. Rev. C **67**, 015807 (2003).

Enhanced production of neutron-rich rare isotopes in the reaction of 25 MeV/nucleon ^{86}Kr on ^{64}Ni, G. A. Souliotis, M. Veselsky, G. Chubarian, L. Trache, A. Keksis, E. Martin, A. Ruangma, E. Winchester and S. J. Yennello, Phys. Lett. B **543**, 163 (2002).

The liquid to vapor phase transition in excited nuclei, J. B. Elliott, L. G. Moretto, L. Phair, G. J. Wozniak, L. Beauliew, H. Breuer, R. G. Korteling, K. Kwiatkowski, T. Lefort, L. Pienkowski, A. Ruangma, V. E. Viola and S. J. Yennello, Phys. Rev. Lett. **88**, 042701 (2002).

Event-by-event analysis of proton-induced nuclear multifragmentation: determination of phase transition universality-class in system with extreme finite-size constraints, M. K. Berkenbusch, W. Bauer, K. Dillman, S. Pratt, T. Lefort, K. Kwiatkowski, V. E. Viola, L. Beaulieu, A. Ruangma, S. J. Yennello, R. G. Korteling, L. Pienkowski, Phys. Rev. Lett. **88**, 022701 (2002).

Breakup time scale studied in the 8 GeV/c π^- + ^{197}Au reaction, L. Pienkowski, K. Kwiatkowski, T. Lefort, L. Beaulieu, A. Botvina, B. Back, H. Breuer, S. Gushue, L. P. Remsberg, D. Rowland, A. Ruangma, V. E. Viola, E. Winchester, S. J. Yennello, Phys. Rev. C **65**, 064606 (2002).

Caloric curve of 8 GeV/c p, π+ ^{197}Au reactions, A. Ruangma, R. Laforest, E. Martin, E. Ramakrishnan, D. Rowland, M. Veselsky, E. Winchester, S. J. Yennello, L. Beaulieu, W.-c. Hsi, K. Kwiatkowski, T. Lefort, V. E. Viola, A. Botvina, R. G. Korteling, L. Pienkowski, H. Breuer, S. Gushue, L. P. Remsberg, B. Back, Phys. Rev. C **66**, 044603 (2002).

Tracking the phase-transition energy in the disassembly of hot nuclei, C. B. Das, S. Das Gupta, L. Beaulieu, T. Lefort, K. Kwiatkowski, V. E. Viola, S. J. Yennello, L. Pienkowski, R. G. Korteling, and H. Breuer, Phys. Rev. C, **66**, 044602 (2002).

Formation of excited systems with a wide range in N/Z, D. J. Rowland, R. Laforest, E. Ramakrishnan, M. Veselsky, E. M. Winchester, A. Ruangma, E. Martin and S. J. Yennello, Phys. Rev C, **67**, 064602 (2003).

Limiting temperatures and the equation of state of nuclear matter, J. B. Natowitz, K. Hagel, Y. Ma, M. Murray, L. Qin, R. Wada, and J. Wang, Phys. Rev. Lett. **89**, 212701 (2002).

Caloric curves and nuclear expansion, J. B. Natowitz, K. Hagel, Y. Ma, M. Murray, L. Qin, S. Shlomo, R. Wada, and J. Wang Phys. Rev. C **66**, 031601 (2002).

Pseudorapidity distributions of charged particles from Au + Au collisions at the maximum RHIC energy, $\sqrt{S_{NN}}$ **= 200 GeV,** I. G. Bearden *et al*. The BRAHMS Collaboration, Phys. Rev. Lett. **88**, 202301 (2002).

Sequential decay distortion of Goldhaber model widths for spectator fragments, Y. G. Ma, R. Wada, K. Hagel, M. Murray, J. S. Wang, L. J. Qin, A. Makeev, P. Smith, J. B. Natowitz, and A. Ono, Phys. Rev. C **65**, 051602 (2002).

Experimental investigation of the level density in highly excited nuclei around Pb-208, M. Lunardon, G. Viesti, D. Bazzacco, D. Fabris, G. Nebbia, C. Ur, C. R. Alvarez, M. Cinausero, E. Farnea, E. Fioretto, G. Prete, G. de Angelis, D. R. Napoli, K. Hagel, J. B. Natowitz, and R. Wada, Eur. Phys. J. A **13**, 419 (2002).

Charged particle multiplicities at BRAHMS, S. J. Sanders *et al*., The BRAHMS Collaboration, Acta. Phys. Hung. NS-H **15** (3-4), 315 (2002).

Results from BRAHMS experiment at RHIC, P. Staszel *et al*., The BRAHMS Collaboration Acta. Phys. Pol. B **33** (6), 1387 (2002).

Entrance channel dependence of particle and fragment emission, J. Wang, T. Keutgen, R. Wada, K. Hagel, Y. G. Ma, M. Murray, L. Qin, A. Makeev, P. Smith, and J. B. Natowitz, for the NIMROD Collaboration, Bulletin of the American Physical Society (2002).

Projectile and target ionization in MeV/u collisions of Xe ions with N_2, R. E. Olson, R. L. Watson, V. Horvat, and K. E. Zaharakis, J. Phys. B **35**, 1893 (2002).

Multiple electron stripping of heavy ion beams, D. Mueller, L. Grisham, I. Kaganovich, R. L. Watson, V. Horvat, K. E. Zaharakis, and Y. Peng, Laser and Part. Beams **20**, 551 (2002).

Target Z dependence and additivity of cross sections for electron loss by 6-MeV/amu Xe^{18+} Projectiles, R. L. Watson, Yong Peng, V. Horvat, G. J. Kim, and R. E. Olson, Phys. Rev. A **67** 022706 (2003).

J/ψ production in relativistic heavy ion collisions from a multiphase transport model, B. Zhang, C. M. Ko, Z. W. Lin, B. A. Li, and S. Pal, Phys. Rev. C **65**, 054909 (2002).

Charm meson production from meson-nucleon scattering, W. Liu and C. M. Ko, Phys. Lett. B **533**, 259 (2002).

Phi meson production in relativistic heavy ion collisions, S. Pal, C. M. Ko, and Z. W. Lin, Nucl. Phys. **A707**, 525 (2002).

Partonic effects on pion interferometry in relativistic heavy ion collisions, Z. W. Lin, C. M. Ko, and S. Pal, Phys. Rev. Lett. **89**, 152301 (2002).

Cascade production from antikaon induced reactions on lambda and sigma, C. H. Li and C. M. Ko, Nucl. Phys. **A712**, 110 (2002).

Flavor ordering of elliptic flows at high transverse momentum, Z. W. Lin and C. M. Ko, Phys. Rev. Lett. **89**, 202302 (2002).

Charmonium mass in nuclear matter, S. H. Lee and C. M. Ko, Phys. Rev. C **67**, 038202 (2003).

Charmonium absorption in the meson-exchange model, Z. W. Lin and C. M. Ko, Nucl. Phys. **A715**, 533c (2003).

Effects of symmetry energy on two-nucleon correlation functions in heavy ion collisions induced by neutron-rich nuclei, L. W. Chen, V. Greco, C. M. Ko, and B. A. Li, Phys. Rev. Lett. **90**, 162701 (2003).

Parton Coalescence and the Antiproton/Pion Anomaly at RHIC, V. Greco, C. M. Ko, and P. Lévai, Phys. Rev. Lett. **90**, 202302 (2003).

Charm production from photon-proton reactions in a hadronic model, W. Liu, S. H. Lee, and C. M. Ko, Nucl. Phys. **A724**, 375 (2003).

Final state three-body coulomb effects in the ^{208}Pb (^{8}B, ^{7}Bep)^{208}Pb coulomb breakup reaction, E. O. Alt, B. F. Irgaziev, A. M. Mukhamedzhanov, Phys. Rev. Lett. **90**, 122701 (2003).

Caloric curves and nuclear expansion, J. B. Natowitz, K. Hagel, Y. Ma, M. Murray, L. Qin, S. Shlomo, R. Wada and J. Wang, Phys. Rev. C **66**, 031601 (2002).

Self-consistent Hartree-Fock based random phase approximation and the spurious state mixing, B. K. Agrawal, S. Shlomo and A. I. Sanzhur, Phys. Rev. C **67**, 034314 (2003).

Determining the nuclear matter incompressibility coefficient from compression modes in nuclei, S. Shlomo and A. I. Sanzhur, *Nuclear Physics in the 21st Century*, American Institute of Physics, New York, 2002, p. 678.

Phase transitions in asymmetric nuclear matter, V. M. Kolomietz, A. I. Sanzhur, S. Shlomo and S. A. Firin, *Nuclear Physics in the 21st Century*, American Institute of Physics, New York (2002), p. 707.

Nuclear equation of state and compression modes, S. Shlomo and A. I. Sanzhur, Heavy Ion Physics **16**, 303 (2002).

Isoscalar giant monopole and dipole resonances and the nuclear matter incompressibility coefficient, S. Shlomo, A. I. Sanzhur and B. K. Agrawal, Nucl. Phys. **A719**, 225c (2003).

Current status of the nuclear matter incompressibility coefficient as deduced from data on compression modes, S. Shlomo and B. K. Agrawal, Nucl. Phys. **A722**, 98c, (2003).

SECTION VII

APPENDIX

TALKS PRESENTED
April 1, 2002 – March 31, 2003

Measurement of the Absolute Drell-Yan Dimuon Cross Section in 800 GeV/c pp and pd Collisions, **C. A. Gagliardi, Invited Talk**, (for the FNAL E866/NuSea Collaboration), XVIth Particles and Nuclei International Conference (PANIC02), referred, Osaka, Japan (September 2002).

Spin Physics and Ultra-Peripheral Collisions at STAR, **C. A. Gagliardi, Invited Talk,** (for the STAR Collaboration), 18th Lake Louise Winter Institute, Lake Louise, Alberta, Canada (February 2003).
Fragment Isospin as a Probe of Heavy-Ion Collisions, **S. J. Yennello,** Gordon Research Conference on Nuclear Chemistry, New London NH (June 2002).

Nuclear Reactions: Can they lead to Distillation?, **S. J. Yennello,** University of Maryland (February 2002).

What You Don't Know Can Hurt You: The Importance of a Nuclear Education, **S. J. Yennello,** American Chemical Society Meeting, Boston (August 2002).

Production and Deexcitation of Isotopically Diverse Nuclear Systems near the Fermi Energy, **S. J. Yennello,** American Chemical Society Meeting, Boston (August 2002).

Nuclear Reactions: Distillation on a Femtometer Scale?, **S. J. Yennello,** Union College, Schnectady, NY (January 2003).

Nuclear Reactions: Exploring Phase Transitions in Excited Nuclear Material, **S. J. Yennello,** Renselaer Polytechnic Institute, Troy, NY (January 2003).

Multi-detector Arrays for Reaction Studies at E/A<200 MeV, **S. J. Yennello,** RIA detector development workshop (March 2003).

Energy Dependence of the Isotopic Composition in Nuclear Fragmentation, **S. J. Yennello,** APS meeting (April 2003).

WECAN Encourage Women to Advance in Physics, **S. J. Yennello,** Keynote talk for the Committee on the Status of Women in Physics, Philadelphia (April 2003).

Science Society and Scientists: Looking Toward the Future, **S. J. Yennello,** Keynote talk for Sigma Xi, University of Denver (April 2003).

Separator systems for deep inelastic scattering with RIBs at RIA, **G. A. Souliotis**, Workshop on the Experimental Equipment for RIA, Oak Ridge, TN (March 2003).

Asymptotic Normalization Coefficients in Nuclear Astrophysics, **Akram Mukhamedzhanov, Invited Talk**, Catania National Lab, Catania, Italy (April 2002).

ANC and CNO Cycle Reactions $^{11}C(p,\gamma)^{12}N$, $^{13}C(p,\gamma)^{14}N$ *and* $^{14}N(p,\gamma)^{15}O$, **Akram Mukhamedzhanov, Invited Talk**, Catania National Lab, Catania, Italy (April 2002).

Astrophysical Factors **Akram Mukhamedzhanov, Invited Talk**, Catania National Lab, Catania, Italy (April 2002).

Three-body Coulomb Asymptotic Wave Function and Post-decay Coulomb, Acceleration Effects in the Coulomb Breakup Reactions, **Akram Mukhamedzhanov, Invited Talk**, Catania National Lab, Catania, Italy (April 2002).

Astrophysical Factors, **Akram Mukhamedzhanov, Invited Talk**, Instituto Superior Tecnico, Lisbon, Portugal (April 2002).

Low-energy Behavior of Direct Capture Astrophysical Factors, **Akram Mukhamedzhanov, Invited Talk**, University of Surrey, Guilford, UK (September 2002).

Asymptotic 3-body Coulomb Scattering Wave Function, **Akram Mukhamedzhanov, Invited Talk**, University of Surrey, Guilford, UK (September 2002).

Asymptotic Three-body Coulomb Scattering Wave Function and Final-state Interaction in Breakup, Reactions, **Akram Mukhamedzhanov, Invited Talk**, University of Lisbon, Portugal (September 2002).

Astrophysical Factors, **Akram Mukhamedzhanov, Invited Talk**, Institut fuer Physik, Mainz Universitat, Mainz, Germany (September 2002).

Astrophysical S Factors for CNO Reactions $^{11}C(p,\gamma)^{12}N$ *and* $^{14}N(p,\gamma)^{15}O$ *from Asymptotic normalization coefficients*, **Akram Mukhamedzhanov**, APS DNP meeting, East Lansing, Michigan (October 2002).

Final State Three-body Coulomb Effects in the $^{208}Pb(^{8}B,^{7}Be\,p)^{208}Pb$ *Coulomb Breakup Reaction*, **Akram Mukhamedzhanov**, APS DNP meeting, East Lansing, Michigan (October 2002).

Asymptotic normalization coefficient for $^{3}He + {}^{4}He \rightarrow {}^{7}Be$ *from the* $^{3}He({}^{6}Li, d)\,{}^{7}Be$ *transfer reaction*, **Akram Mukhamedzhanov**, PAC meeting, Catania National Lab, Catania, Italy (October 2002).

Determination of the S_{17} and S_{18} Astrophysical Factors from Transfer Reactions and from the Breakup of ^{8}B and ^{9}C at Intermediate Energies, **L. Trache, Invited Talk,** GANIL/LPC Caen, France (May 2002).

Determination of the S_{17} and S_{18} Astrophysical Factors from Transfer Reactions and the Breakup of ^{8}B and ^{9}C at Intermediate Energies, **L. Trache, Invited Talk**, HRIBF Workshop on Transfer Reactions, Oak Ridge, TN (June 2002).

Determination of the S_{18} Astrophysical Factor from the Breakup of ^{9}C at Intermediate Energies, **L. Trache, F. Carstoiu, A. M. Mukhamedzhanov and R. E. Tribble,** talk presented at the 2002 Fall Meeting of the Nuclear Physics Divisions of APS, East Lansing, MI (October 2002).

Experience and Lessons Learned with MARS, **L. Trache**, presented at the Workshop on the Experimental Equipment for RIA, Oak Ridge, TN (March 2003).

Target K-vacancy Production by Fast Heavy Ions in the Molecular Orbital Regime, **V. Horvat**, **Z. Smit, and R. L. Watson**, Seventeenth International Conference on the Application of Accelerators in Research and Industry, Denton, Texas (November 2002).

Systematics of Electron Capture and Loss by 2-6 MeV/u Xe Ions, **R. L. Watson, V. Horvat, Y. Peng, and R. E. Olson,** Seventeenth International Conference on the Application of Accelerators in Research and Industry, Denton, Texas (November 2002).

Projectile and Target Ionization in MeV/u Collisions of Xe-Ions with N_2, **R. E. Olson, R. L. Watson, V. Horvat, and K. E. Zaharakis,** Seventeenth International Conference on the Application of Accelerators in Research and Industry, Denton, Texas (November 2002).

Indirect Ways to Measure Stellar Reaction Rates, **R. E. Tribble,** Institute for Nuclear Theory, University of Washington, Seattle (June 2002).

New Results for $^{8}B(p,\gamma)^{9}C$, $^{11}C(p,\gamma)^{12}N$, $^{13}C(p,\gamma)^{14}N$, and $^{14}N(p,\gamma)^{15}O$ at Stellar Energies Nuclei in the Cosmos, **R. E. Tribble**, Fujikyu, Japan (July 2002).

Capture Gamma Reaction Rates at Stellar Energies by the Asymptotic Normalization Coefficient Method, **R. E. Tribble**, Capture Gamma Spectroscopy 11 (CGS11), Prague, Czech Republic (September 2002).

Radioactive Beams with MARS: Applications in Nuclear Astrophysics and Weak Interactions, **R. E. Tribble**, BIG DRAGON Workshop, TRIUMF, Vancouver, BC (July 2002).

Stellar Capture Rates from Measurements of Asymptotic Normalization Coefficients, **R. E. Tribble**, Workshop for future facilities at the LNS, Catania, Italy, (March 2003).

Tracing Charmonium Evolution at RHIC", International Workshop on Charm Production from Threshold via SPS to RHIC and LHC, **Che-Ming Ko, Invited Talk**, Trento, Italy (June 2002).

Predictions from AMPT, **Che-Ming Ko, Invited Talk**, INT/RHIC Winter Workshop on First Two Years of RHIC: Theory versus Experiments, Seattle, Washington (December 2002).

Searching for the Quark-Gluon Plasma at RHIC, **Che-Ming Ko, Invited Talk**, Seminar at University of Kentucky, Lexington, Kentucky (September 2002).

Intermediate Mass Fragments and Isospin Equilibration, **D. V. Shetty,** A. Keksis, E. Martin, A. Ruangma, G. A. Souliotis, M. Veselsky, E. M. Winchester, S. J. Yennello, R. Alfaro, J. Cibor, M. Cinausero, Y. El. Masri, D. Fabris, E. Fioretto, K. Hagel, T. Keutgen, M. Lunardon, Y. Ma, Z. Majka, A. Makeev, A. Martinez-Davalos, A. Menchaca-Rocha, M. Murray, J. B. Natowitz, G. Nebbia, L. Qin, G. Prete, V. Rizzi, P. Smith, P. Staszel, G. Viesti, R. Wada, and J. Wang, 2002 Fall meeting of the APS Division of Nuclear Physics, Michigan, U.S.A. (October 2002).

Isospin Dependence of Intermediate Mass Fragments in ^{124}Sn, ^{124}Xe + ^{124}Sn, ^{112}Sn, **D. V. Shetty,** A. Keksis, E. Martin, A. Ruangma, G. A. Souliotis, M. Veselsky, E. M. Winchester, S. J. Yennello, R. Alfaro, J. Cibor, M. Cinausero, Y.El. Masri, D. Fabris, E. Fioretto, K. Hagel, T. Keutgen, M. Lunardon, Y. Ma, Z. Majka, A. Makeev, A. Martinez-Davalos, A. Menchaca-Rocha, M. Murray, J. B. Natowitz, G. Nebbia, L. Qin, G. Prete, V. Rizzi, P. Smith, P. Staszel, G. Viesti, R. Wada, and J. Wang, 2003 Spring meeting of the APS Division of Nuclear Physics, Philadelphia, U.S.A. (April 2002).

Self Consistent HF-RPA and the Spurious Isoscalar Giant Dipole Resonance, **S. Shlomo, Invited Talk**, Workshop on Continuum Aspects of The Nuclear Shell Model, The European Center for Theoretical Studies in Nuclear Physics and Related Areas (ECT*), Trento, Italy (June 2002).

Isoscalar Giant Monopole and Dipole Resonances and the Nuclear Matter Incompressibility Coefficient, **S. Shlomo and B. K. Agrawal, Invited Talk**, Nuclear Physics in Astrophysics, 17th International Nuclear Physics Divisional Conference of The EPS (NPDC-17), ATOMKI, Debrecen, Hungary, (September - October 2002).

HF-RPA Theory for Giant Resonances and the Nuclear Matter Incompressibility Coefficient, **S. Shlomo, Invited Talk**, International Symposium on Frontiers of Collective Motion (CM2002), University of Aizu, Aizu, Japan (November 2002).

Current Status of the Nuclear Matter Incompressibility Coefficient as Deduced from Data on Compression Modes, **S. Shlomo and B. K. Agrawal, Invited Talk**, International Symposium on Physics of Unstable Nuclei (ISPUN02), Halong Bay, Veitnam (November 2002).

Self-Consistent Hartree-Fock Based Random Phase Approximation and the Spurious State Mixing, **S. Shlomo, Invited Talk**, RCNP, Osaka University, Japan (November 2002).

Superallowed Beta Decays, **J. C. Hardy, Invited Talk**, Workshop on Low Energy Precision Electroweak Measurements, LEPEM2002, Vancouver, Canada (April 2002).

Superallowed Nuclear Beta Decay and CKM Unitarity: Current Status and Future Prospects, **J. C. Hardy**, **Invited Talk,** Quark Mixing – CKM Unitarity, Heidelberg, Germany (September 2002).

Delimiting the Standard Model with Superallowed Nuclear Beta Decay, **J. C. Hardy, Invited Colloquium**, GSI, Darmstadt, Germany (November 2002).

Delimiting the Standard Model with Superallowed Nuclear Beta Decay, **J. C. Hardy, Invited Colloquium**, University of Jyvaskyla, Finland (November 2002).

Precise Half-life Measurement of the of Beta-Decays of ^{34}Cl and ^{34}Ar, **V. E. Iacob,** E. Mayes, J. C. Hardy, R. G. Neislon, M. Sanchez-Vega, A. Azhari, C. A. Gagliardi, L. Trache and R. E. Tribble, 2003 Spring Meeting of the APS Division of Nuclear Physics, Philadelphia, U.S.A. (April 2003).

RESEARCH PERSONNEL AND ENGINEERING STAFF

April 1, 2002 - March 31, 2003

Faculty and Research Group Leaders

Carl A. Gagliardi, Professor of Physics
John C. Hardy, Professor of Physics
Che Ming Ko, Professor of Physics
Akram Mukhamedzhanov, Research Scientist
J. B. Natowitz, Professor of Chemistry, Bright Chair - From 1/03
Richard P. Schmitt, Professor of Chemistry
Shalom Shlomo, Senior Scientist
Robert E. Tribble, Professor of Physics, Director - From 1/03
Rand L. Watson, Professor of Chemistry
Sherry J. Yennello, Prof. of Chemistry - From 9/1/02
Dave H. Youngblood, Professor of Physics

Research Staff

Henry Clark, Accelerator Physicist (50%)
Grigor Chubaryan, Research Scientist
John C. Hagel, Research Scientist (50%)
Vladimir Horvat, Research Scientist (50%)
Victor Iacob, Associate Research Scientist
Su Houng Lee, Research Scientist From 7/1/02
Yiu-Wing Lui, Research Scientist
Andrei Makeev, Research Assistant – To 3/11/03
Michael Murray, Asst. Ress Scientist - To 1/13/03
George Souliotis, Assistant Research Scientist
Livius Trache, Research Scientist
Maxim Vasilyev, Assistant Research Scientist (80%)
Ryoichi Wada, Research Scientist

Visiting Scientists

Naftauli Auerbach – From 1/23/03 To 2/14/03
Florin Carstoiu - To 12/13/02
Vladilen Goldberg - From 11/4/02
V. Kolomietz – From 1/1/03
Peter J. Levai - From 11/4/02 to 11/30/02
Ian Towner – From 6/7/02 To 8/20/02

Accelerator Physics And Radiation Line Staff

Henry Clark, Accelerator Physicist (50%)
Vladimir Horvat, Assoc. Res. Scientist (50%)
Bruce Hyman, Research Associate
George Kim, Accelerator Physicist
Don May, Chief Accelerator Physicist
Dennis Utley, Research Associate (25%)

Computer Systems Staff

Robert Burch, Jr., Research Associate
John C. Hagel, Assoc. Research Scientist (50%)
Maxim Vasilyev, Asst. Research Scientist (20%)

Engineering Staff

Walter Chapman, Mech. Engineer – To 9/30/02
Greg Derrig, Senior Mechanical Engineer
Lee Norris, Instr. Shop Supervisor – From 10/1/02
Robert Olsen, Mechanical Engineer

Postdoctoral Research Associates

Bijay Agrawal
Narayana P. Appathurai – From 6/11/02
Afshin Azhari
Lie-Wen Chen
Vicenzo Greco – From 9/1/02
Bency V. John – To 10/18/02
Ziwei Lin – To 9/30/02
Yu-Gang Ma
Ninel Nica – From 8/1/02
Subrata Pal – To 10/3/02
Vladimir Salamatin – From 6/26/02
Maria Sanchez-Vega – To 4/19/02
Dinesh Shetty
Gabriel Tabacaru – From 7/22/02
Xiaodong Tang – From 6/1/02
Yoshiaki Tokimoto
Martin Veselsky – To 4/5/02

STUDENTS

April 1, 2002 - March 31, 2003

Graduate Students

Tariq Al-Abdullah
Xinfeng Chen
Tiegang Di – To 11/1/02
Bogdan Dobrescu
Changbo Fu
Thomas Henry
August Keksis
Changhui Li – To 7/16/02
Wei Liu
Elizabeth Martin
Eric Mayes – To 5/31/02
James Musser
Yong Peng
Fakhriddin Pirlepesov
Oleksiy Pochivalov
Li Jun Qin
Ananya Ruangma – To 5/31/02
Au Kim Vuong
Eileen Winchester – To 8/31/02
Yuming Xiao
Yongjun Zhai – From 9/1/02

Undergraduates and Student Technicians

Anna Allred – To 5/31/02
Christopher J. Bemben – From 1/8/03
Rebecca Bierschenk – To 5/10/02
Joseph Brinkley – From 1/8/03
Christina M. Freeborn – From 1/8/03
Samuel Gooding – To 1/18/03
Stephen Hanssen – From 6/3/02
Chelsey Jones – From 9/2/02
Sarah Parketon - From 1/27/03
Barrett C. Parker – From 5/30/02
David Rosenfeld
Patrick Smith
Emily Squibb – To 9/7/02
Nicole Steiner
Patrick Tamain – From 6/24/02 To 8/2/02
William D. Wright – From 9/9/02
Erin P. Eurek – From 9/19/02

ORGANIZATIONAL CHART - CYCLOTRON INSTITUTE

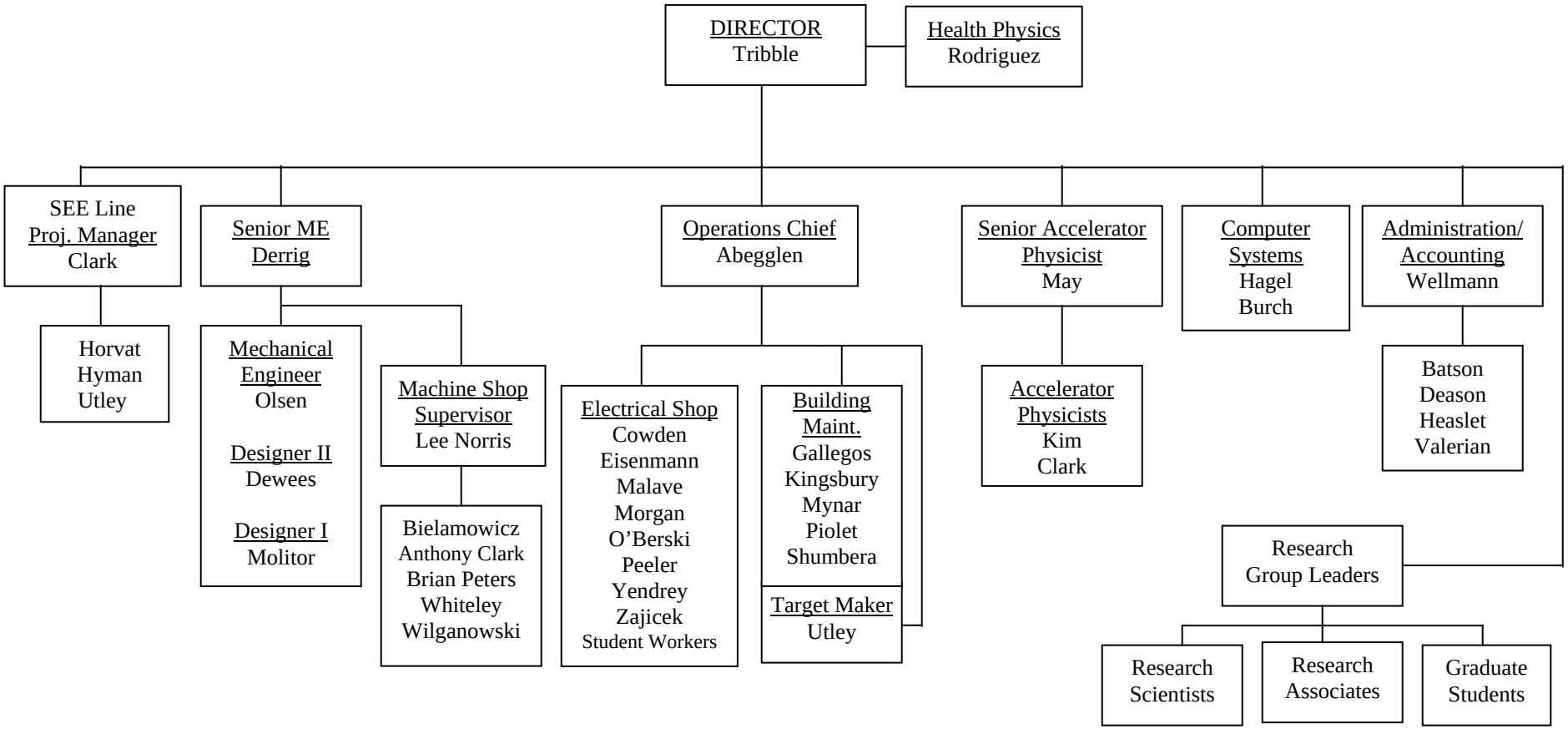

STUDENTS WHO RECEIVED GRADUATE DEGREES
FROM THESIS WORK CONDUCTED
AT
THE CYCLOTRON INSTITUTE

April 1, 2002 – March 31, 2003

Name	Year	Thesis Title	Advisor	First Position	Present Position
Tiegang Di	2002	*Charm Meson Interactions with Hadrons*	Che-Ming Ko	Graduate Research Assistant	Pursuing Ph.D. degree at Texas A&M University
Changhui Li	2002	*Multistrange Baryon Production from Strangeness-Exchange Reactions*	Che-Ming Ko	Graduate Research Assistant	Pursuing Ph.D. degree at Texas A&M University

INSTITUTE COLLOQUIA AND SEMINARS
April 1, 2002-March 31, 2003

2002

April 2	Dr. Bency John, Cyclotron Institute, Texas A&M University	*Isoscalar Giant Resonances in ^{12}C*
April 9	Professor J. Rapaport, Ohio University, Athens, Ohio	*Charge Exchange Reactions and Spin Transfer Measurements*
April 16	M. Sanchez-Vega and V. E. Jacob, Cyclotron Institute, Texas A&M University	*Test of the Unitarity of the CKM Matrix via Superallowed β^+ decay.*
April 23	Dr. Subrata Pal, Cyclotron Institute, Texas A&M University	*Strange Particle Production in Relativistic Heavy Ion Collisions*
April 30	Dr. Michael Murray, Cyclotron Institute, Texas A&M University	*Kaon Phase Space Density in Heavy Ion Collisions*
May 7	Dr. Livius Trache, Cyclotron Institute, Texas A&M University	*Determination of the S_{18} Astrophysical Factor for $^8B(p,\gamma)^9C$ from the Breakup of ^9C at Intermediate Energies*
May 21	Professor Gary Westfall, Cyclotron Laboratory, Michigan State University, East Lansing, Michigan	*The Study of Collective Flow in Nucleus-nucleus Collisions at Incident Energies Below 1 GeV/nucleon*
May 28	Dr. George Souliotis, Cyclotron Institute, Texas A&M University	*Neutron-Rich Rare Isotope Production*
June 4	Jinghua Fu (Lawrence Berkeley National Laboratory [LBNL] /Institute of Physics Publishing [IOPP]), Paul Sorensen (University of California at Los Angeles [UCLA]), Solenoidal Tracker at the Relativistic Heavy Ion Collider Collaboration [STAR] Collaboration	*K_0 and Λ Event Anisotropy Parameters from Au+Au Collisions at RHIC*
June 14	Professor Michael Hass, The Weizmann Institute, Rehovot, Israel	*A New Precision Measurement of the ^7Be (p,γ) ^8B Cross Section with an Implanted ^8Be Target*
June 11	Dr. Bao-An Li, Department of Chemistry and Physics, Arkansas State University, Jonesboro, Arkansas	*Probing the Equation of State of Neutron-Rich Matter*
July 16	Prof. F. Nunes, Universidede Fernando Pesoa, Porto, Portugal	*The Continuum in Reactions with Dripline Nuclei*

July 17	Prof. Jian-Ye Liu, Institute of Modern Physics, Chinese Academy of Sciences, Lanzhou, P.R. China	*Probing the Isospin Dependent in-Medium Nucleon-Nucleon Cross Sections*
August 20	Prof. Yigal Ronen, Ben Gurion University Beer-Sheva, Israel	*Space Travel: Science or Fiction?*
September 3	Prof. Su Houng Lee, Department of Physics and Institute of Physics and Applied Physics, Yonsei University, Seoul, Korea	*Hadrons in Nuclear Matter*
September 24	Dr. Gabriel Tabacaru, Cyclotron Institute, Texas A&M University	*Nuclear Astrophysics Experiments with Radioactive Beams at Centre de Recherche du Cyclotron Louvain-la-Neuve*
October 8	Dr. F. Carstoiu, Cyclotron Institute, Texas A&M University	*Breakup of ^{8}B from 28 to 1000 MeV/A Revisited*
November 11	Professor W. H. Trzaska, Department of Physics, University of Jyväskylä, Finland, and Helsinki Institute of Physics, Finland	*Manifestations of Clustering in Fission of Excited Actinides*
November 12	Dr. W. Catford, Department of Physics, University of Surrey, Guildford, United Kingdon	*Berylliums and other exotics via transfer*
November 13	Dr. Ralf Rapp*, Nordita, Denmark	*Open and Hidden Charm Production in High-Energy Nuclear Collisions*
November 15	Dr. G. Rogachev, Department of Physics, University of Notre Dame, Indiana	*Spectroscopy of Light Drip Line Nuclei by Means of Radioactive Beams*
November 19	Dr. Peter Levai, National Institute for Nuclear and Particle Physics, Budapest, Hungary	*Jet tomography: diagnostics of hot dense matter produced at RHIC*
December 3	Dr. Lie-Wen Chen, Cyclotron Institute, Texas A&M University	*Two-nucleon Correlation Functions as a Probe of the Nuclear Symmetry Potential*
December 5	Dr. Jerry Nolen, Argonne National Laboratory, Argonne, Illinois	*RIA Development at Argonne National Laboratory*
December 10	Dr. Takashi Nakatsukasa, Department of Physics, Tohoku University, Senda, Japan	*Continuum Response and Reaction of Weakly-bound Quantum Systems*

2003

January 14	Dr. A.M. Mukhamedzhanov, Cyclotron Institute, Texas A&M University	*Three-body Coulomb Effects in the ^{208}Pb(^{8}B, ^{7}Be p) ^{208}Pb Coulomb Breakup Reaction*
January 21	Dr. Y. Oh, Yonsei University, Seoul, Republic of South Korea and Cyclotron Institute, Texas A&M University	*Vector Meson Photoproduction Processes Near Threshold*
January 28	Dr. Konrad Gelbke, National SuperConducting Laboratory, Michigan State University, East Lansing, Michigan	*Rare Isotope Research Capabilities at the NSCL Today and at RIA in the Future*
February 4	Professor Naftali Auerbach, Tel-Aviv University, Tel-Aviv, Israel	*Tests of Time Reversal Violation in Radioactive Nuclei*
February 7	Dr. Oleg Tarasov, National Superconducting Laboratory, Michigan State University, East Lansing, Michigan	*LISE++ : new generation of the LISE code*
February 11	Professor Naftali Auerbach, Tel-Aviv University, Tel-Aviv, Israel	*Neutrino-Nucleus Interactions and Nuclear Structure*
February 25	Dr. Ninel Nica, Cyclotron Institute, Texas A&M University	*High-spin decay scheme of ^{155}Er nucleus*
March 4	Professor V.G. Zelevinsky, National Superconducting Cyclotron Laboratory (NSCL), Michigan State University, East Lansing, Michigan	*Nuclear Structure and Ideas of Quantum Chaos*
March 11	Dr. Vladilen Goldberg, Cyclotron Institute, Texas A&M University	*Let us Talk About ^{9}He*
March 18	Professor Jorge Piekarewicz, Florida State University, Tallahassee, Florida	*Impact of the neutron skin of ^{208}Pb on nuclear observables*